Broadband Wireless Communication Systems for High Mobility Scenarios

José Rodríguez-Piñeiro

Doctoral Thesis UDC / 2016

Advisors: Luis Castedo Ribas
José Antonio García Naya

Doutoramento en Tecnoloxías da Información e Comunicacións en Redes Móbiles

UNIVERSIDADE DA CORUÑA

D. Luis Castedo Ribas e D. José Antonio García Naya

CERTIFICAN

Que a memoria titulada "Broadband Wireless Communication Systems for High Mobility Scenarios" foi realizada por D. José Rodríguez-Piñeiro baixo a nosa dirección no Departamento de Electrónica e Sistemas da Universidade da Coruña e remata a Tese que presenta para optar ó grao de Doutor con mención internacional.

A Coruña, 26 de setembro de 2016.

Asdo.: Dr. Luis Castedo Ribas
Director da Tese Doutoral
Catedrático de Universidade
Departamento de
Electrónica e Sistemas
Universidade da Coruña

Asdo.: Dr. José A. García Naya
Director da Tese Doutoral
Profesor Contratado Doutor
Departamento de
Electrónica e Sistemas
Universidade da Coruña

Tese Doutoral: Broadband Wireless Communication Systems for High Mobility Scenarios

Autor: D. José Rodríguez-Piñeiro

Directores: Dr. Luis Castedo Ribas e Dr. José A. García Naya

Data de defensa: 26 de setembro de 2016

Tribunal

Presidente: Markus Rupp

Vogal: Ke Guan

Secretaria: Paula M. Castro Castro

此论文献给李秀艳，以感谢她予我完成它所需的灵感和幸福。

Tamén á miña nai, ao meu pai e ás miñas irmás, por todo o apoio delxs recibido.

Acknowledgements

When one decides to write a Ph.D. thesis, one must know that it will be difficult. However, more than difficult, it would be impossible without the valuable help and collaboration not only from colleagues, but also from friends, family and some special people. This is my short way to thank all those people who, in one way or another, helped me during the last few years to achieve this goal.

First of all I think that my two supervisors deserve to be thanked. I must thank Dr. Luis Castedo for having enough confidence to choose me for a project without knowing much about me at the beginning. During this path he always supported me and helped me in absolutely every detail. He supported absolutely all of my proposals, even some of them not directly related to this thesis, such as some collaborations with foreign groups. In fact, I may recognize that together with my other supervisor, Dr. José A., he showed me an important lesson from the beginning: I learned the difference between working *for* a project and working *in* a project. During the last few years I have always been working *in* projects, where my findings and ideas were taken into account and valued accordingly. With respect to José A... what can I say. Honestly speaking, I could write a full acknowledgments chapter for him. However, I guess that this thesis is long and boring enough to prevent me to do such a thing. I will negotiate with him to exchange such a chapter by some proper amount of cans of beer. José A. was always giving support, putting value on each single idea, and reviewing absolutely every detail of the performed work. He was not solely a supervisor, but also a work colleague, in many senses this thesis is authored by him as much as by me. It is absolutely clear to me that if it was not due to his aid I could not be writing these lines today. And, even much more than a supervisor or a colleague, José A. is, first of all, a good friend and an excellent person. Furthermore, his work capacity and effort is absolutely amazing, although this aspect is not different for the case of Luis. If this university still works is, without any doubt, thank to people like them. The other way around is not true, i.e., they are not responsible for how this university works...

After giving a special mention to both of my supervisors, I also have to sincerely thank the rest of my colleagues. The GTEC Team accepted me and treated me absolutely kindly from the beginning, even taking into account that I am an infiltrated Electrical Engineer in a group of Computer Engineers. I would like to thank specially to Dr. Miguel González, due to his support from the beginning and the nice and cordial talks we had many times. I must mention that he was the one who suggested me to apply for an FPU grant, which finally I obtained, and,

undoubtedly, absolutely changed my future opportunities and perspectives. I would also like to thank to Dr. Carlos J. Escudero. Together with José A. and Dr. Javier Rodas, he showed to me how to become a much more advanced person in the technological sense. I recognize the superiority of Computer Engineers with respect to the Electrical Engineers in this aspect. Javi, I also learned much from you. I know that, together with José A., we discussed a lot, but some positive knowledge could be extracted from each of our discussions. I also have to sincerely thank to the people I am working with at the GTEC Lab for the good moments that we enjoy daily. Among them, special thanks go to Dr. Pedro Suárez, who was my main reference book in relation to wireless channel modeling. I don't know if he knows as much as it seems, but at least he sounds convincing to me. I must also thank Mr. Tomás Domínguez, as I recognize that without his valuable help the source code of our GTEC Testbed would not have the same level of quality. I also recognize the superiority of Computer Engineers with respect to the Electrical Engineers in this other aspect. I may also not forget to thank our former colleague Mr. Ismael Rozas, who worked together with Dr. José A. and me in the development of our GTEC Testbed. We enjoyed good moments together with him, especially those involving food. Another person who deserves special mention is Ms. Paula (I am sorry but I will not write her horrible surname in my thesis). Paula helped us not to miss the theoretical part of railway transportation and, over all, she is a good friend who is there to assist whenever you may need her. We had several talks and undoubtedly she helped me a lot in many different senses. However, Paula, I am sorry to tell you that I still fully disagree with your ideas about politics. I want to spread my thankfulness among the rest of the GTEC group. Hence, I give my very sincere thanks to Dr. José P. González, Dr. Óscar Fresnedo, Mr. Ángel Carro, Mr. Valentín Barral, Mr. Diego Noceda, Ms. Fátima Armenteiros, Mr. Manuel Suárez, Dr. Adriana Dapena, Dr. Paula Castro, Dr. Daniel I. Iglesia, Dr. Francisco J. Araújo, Dr. Julio C. Brégains, Dr. Tiago Fernández, and Mr. José J. Lamas.

However, I have never walked alone along this path and it is time to thank all the people who gave me external support during these last few years. After being a total of six months working at the Telecommunications Institute of the Technische Universität Wien, I have to thank to all my colleagues there. Special thanks are deserved by Dr. Markus Rupp, who absolutely always supported me. From the personal point of view, I recognize that he is one of the most well organized and efficient people I have ever met, and also a very funny, friendly and enjoyable person. I should also thank Mr. Martin Lerch not only for being a great work colleague, but also for the good moments enjoyed together around Vienna. Sebastian Caban should be also thanked for his always very valuable contributions. I also want to thank to the rest of the MIMO Lab crew: Ronald Nissel and Martin Müller. I also want to explicitly mention Martin Taranetz for the good moments enjoyed together and the valuable concepts I have learned from him. Finally, I could not finish this paragraph without explicitly mentioning my cool friends Jelena Kaitovic and Giuseppe Papa, as well as the rest of the colleagues from the Telecommunications Institute.

However, the food is really bad in Vienna. That is why I prefer the research stays in

Paraguay. And I cannot start talking about Paraguay and the Paraguayan people without mentioning the one who made possible all the collaborations as well as the several research stays I performed there. In three days he will become also a Ph.D. I am talking about Mr. Jorge E. Rodas, who was the perfect companion during these years. With our mutual aid both of us obtained a huge benefit in different senses. We learned together from our errors and also sometimes from our successes. During the last few years our professional lives as well as our expectations and future plans, were absolutely parallel. But, much more important than this is that Jorge is one of my best friends. I would also like to mention his wife, Ingrid, and his son, Jordi Emmanuel. I would like to mention another baby... it seems that I cannot for the moment. However, all that we achieved in our collaborations with the National University of Paraguay would not be possible without the great assistance and support of Dr. Raúl Igmar Gregor Recalde. I think that both Jorge and me should thank him. He could deserve another acknowledgments chapter, but I know that he prefers that we go, together with Jorge, to O'Gaucho to have three or four kilograms of beef (per person). I also prefer this approach. I would like to extend my thankfulness among the rest of colleagues at the Facultad de Ingeniería and the CITEC of the National University of Asunción.

We have also collaborated with many other research groups and, over all, nice people. In this sense, I have to absolutely sincerely thank Dr. César Briso, not only for the good works performed together and the opportunities obtained thanks to him, but also for the great moments enjoyed together. We could mention specially the last conference in Switzerland, but it is better to not give so much details to the scientific readers. Also Dr. José I. Alonso must be thanked for his collaboration and dedication. I would also like to thank the people at Beijing Jiaotong University. I had the great opportunity to start collaborating with them some months ago. Among them, special mention should be given to Dr. Ke Guan as well as Mr. Dan Fei, both for the successful collaborations we are performing as well as for the good moments enjoyed together. In order to finish (in part) with the Chinese part of the acknowledgments, I would also like to thank Xuesong Cai and his advisor, Xuefeng, from the Tongji University, for the joint effort we are doing in finding new collaboration opportunities.

All the performed work would not be possible without the extra collaboration of the University of Málaga, Metro de Madrid and ADIF, so I would like to sincerely thank all of them.

Special mention should be also given to Dr. Bamrung Tau Sieskul, who always gave me his personal support. Much more than a colleague, he is a good friend of me and he knows that he is already a part of my family.

I also would not like to forget to mention my former colleagues and good friends Xurxo Cid, María Dolores Fernández, Daniel García, Iván Villasante, Adrián Canedo, José M. Fernández, Fran Campillo and other people that I cannot mention.

There is something that I have learned from my first measurement campaign together with

José A., which is that good results always start with a good meal. So, I would like to thank to our standard colleagues for the lunch time: Dr. Juan Ferreiro, Dr. Juan Cámara, Dr. Manuel Vázquez, and Dr. Julio Camiñas. We always have interesting talks during our lunch time and I learned a lot from all of them. And, that is true, there are no girls in our lunch group... Juan?

And, as usual, the last parts are the most important ones. Hence, the last part of my acknowledgments is for my family, specially my parents and sisters. All that I have done, and all that I am, would not be possible without their constant support and help. They are absolutely essential in all the steps I followed. They did not only support and encourage me to go along this path, but also bear with me in stressful moments. Finally, they even did not complain much due to the amount of weeks and months that I did not visit them for being working.

As I said, I left the most important part for the end. Hence, at the very end I want to thank Xiuyan Li, as I do every single day. She gave me the required support, optimism, hope and happiness not only to finish this path, but also to look for the next ones (together). There are some feelings that cannot be put into words, hence I would just thank her sincerely for them.

Resumo

Ao longo dos últimos anos o uso de servizos multimedia e, en xeral, baseados no acceso a información contida "na nube", experimentou un auxe sen precedentes. A diferencia respecto do pasado, os usuarios non soamente acceden aos servizos dende unha ubicación estática; pola contra, navegan libremente entre distintos lugares ao tempo que acceden, dende os seus dispositivos móbiles, a servizos na nube. Debido ao ritmo de vida actual, o tránsito entre zonas rurais e cidades tamén se incrementou de modo notable, ao ubicarse a maior parte dos lugares de traballo nas cidades ou nas súas respectivas contornas. Durante os períodos de transporte, cada vez máis, os pasaxeiros empregan os seus dispositivos móbiles para traballar, acceder a redes sociais ou como ferramenta de entretemento. O factor común da maior parte dos servizos típicamente empregados é a súa dependencia respecto do acceso á rede.

Na actualidade, GSM for Railways (GSM-R), baseado no xa vetusto GSM, é o sistema de comunicacións máis empregado entre os trens e o resto dos elementos involucrados na infraestrutura ferroviaria. Sen embargo, GSM-R non é axeitado para proporcionar servizos avanzados, tales como o control de piloto automático, así como para sustentar transmisións de banda ancha aos operadores ferroviarios ou proporcionar servizos de valor engadido aos pasaxeiros. Botando unha ollada ao mercado de dispositivos de comunicacións de ámbito xeral, a explosión de usuarios e servizos multimedia dos últimos anos motivou a migración, primeiro ás redes de terceira xeración e, seguidamente, ás de cuarta, con Long Term Evolution (LTE) á cabeza. Así, parece natural plantexar LTE como o candidato para a substitución de GSM-R.

No presente traballo lévase a cabo un completo estudo das prestacións de sistemas de comunicacións sen fíos de banda ancha en vehículos de alta velocidade baseado en campañas de medidas levadas a cabo en contornas reais de alta velocidade. Estudouse especialmente o caso de comunicacións LTE en trens de alta velocidade. Propóñense técnicas de redución de custo e complexidade en relación ás avaliacións en contornas de alta velocidade e valídase o seu funcionamento de xeito analítico, mediante simulación e empíricamente.

Os desenvolvementos presentados nesta tese foron validados para os sistemas de quinta xeración, aínda en fase de definición. Avaliáronse, mediante simulación e experimentalmente en contornas de alta velocidade, as prestacións brindadas polas propostas para sistemas de comunicacións de quinta xeración.

O código fonte do GTEC Testbed e do GTEC 5G Simulator está dispoñible públicamente baixo a licenza GPLv3 en https://bitbucket.org/tomas_bolano/gtec_testbed_public.git.

Resumen

A lo largo de los últimos años el uso de servicios multimedia y, en general, basados en el acceso a información "en la nube", experimentó un auge sin precedentes. A diferencia respecto del pasado, los usuarios no solamente acceden a los servicios desde una ubicación estática; por contra, navegan libremente entre distintos lugares al tiempo que acceden, desde sus dispositivos móviles, a servicios en la nube. Debido al ritmo de vida actual, el tránsito entre zonas rurales y ciudades también se incrementó de modo notable, al ubicarse la mayor parte de los lugares de trabajo en ciudades o en sus respectivos entornos. Durante los períodos de transporte, cada vez más, los pasajeros emplean sus dispositivos móviles para trabajar, acceder a redes sociales o como dispositivos de entretenimiento.

En la actualidad, GSM for Railways (GSM-R) es el sistema de comunicaciones más empleado entre los trenes y el resto de elementos involucrados en la infraestructura ferroviaria. Sin embargo, GSM-R no es adecuado para proporcionar servicios avanzados, tales como el control de piloto automático, así como para sustentar transmisiones de banda ancha a los operadores ferroviarios o proporcionar servicios de valor añadido a los pasajeros. Centrándonos en el mercado de dispositivos de comunicaciones de ámbito general, la explosión de usuarios y servicios multimedia de los últimos años motivó la migración, primero a las redes de tercera generación y, seguidamente, a las de cuarta, con Long Term Evolution (LTE) a la cabeza. Así, parece natural plantear a LTE como la tecnología candidata para la sustitución de GSM-R.

En el presente trabajo se lleva a cabo un completo estudio de las prestaciones de sistemas de comunicaciones inalámbricas de banda ancha en vehículos de alta velocidad basado en campañas de medidas llevadas a cabo en entornos reales. Se estudió especialmente el caso de comunicaciones LTE en trenes de alta velocidad. Se proponen técnicas de reducción del coste y complejidad en relación a las evaluaciones en entornos de alta velocidad y se prueba su funcionamiento de modo analítico, mediante simulación y empíricamente.

De cara a validar los desarrollos presentados en esta tesis en relación a los últimos avances en materia comunicaciones, se consideraron también las más novedosas propuestas para sistemas de quinta generación, actualmente aún en fase de definición. Es más, se evaluaron, tanto mediante simulación como vía medidas en entornos de alta velocidad, las prestaciones brindadas por las propuestas para sistemas de comunicaciones de quinta generación.

El código fuente del GTEC Testbed y del GTEC 5G Simulator está disponible públicamente bajo la licencia GPLv3 en https://bitbucket.org/tomas_bolano/gtec_testbed_public.git.

Abstract

Over the last few years multimedia and data-based services experienced a non-stopping growth. Unlike before, people do not use the services only from a static location, but they are continuously on the move between different scenarios, using their mobile devices to access data-based services. In parallel, commuter traffic from rural areas is also rising, since most of work places are in and around cities. During transportation, people intensively employ mobile devices to work, access to social networks, or as an entertainment means. Internet access is required for most of these services.

Currently, GSM for Railways (GSM-R), which is based on the Global System for Mobile Communications (GSM), is the most widely used communication system between trains and the elements involved in operation, control, and intercommunication within the railway infrastructure. However, GSM-R is not well suited for supporting advanced services such as automatic pilot applications or provisioning broadband services to the train staff and passengers. Besides trains, the increasing number of broadband services available for mobile devices motivated the migration from third-generation mobile networks to fourth generation ones, mainly Long Term Evolution (LTE). Therefore, LTE seems to be a good candidate to substitute the GSM as the fundamental technology for railway communications.

In this work a complete study on the performance of high capacity broadband wireless communication systems for high speed vehicles is presented, based on measurement campaigns in actual high speed environments. Special attention is devoted to the case of LTE in high speed trains. Techniques to greatly reduce the cost and complexity of measurement-based evaluations in high speed scenarios are proposed and proven to work analytically, by means of simulations and by measurements in actual high speed environments.

With the aim of checking the validity of the findings of this work for the latest advances in wireless communication systems, proposals for fifth generation (5G) communication systems, currently still under definition, were also considered. Moreover, the performance of the proposals for 5G communication systems was also evaluated by means of simulations as well as by measuring in high speed environments.

The source code of both the GTEC Testbed and the GTEC 5G Simulator is publicly available under the GPLv3 license at https://bitbucket.org/tomas_bolano/gtec_testbed_public.git.

Table of Contents

List of Figures

List of Tables

Chapter 1

Introduction

Over the last few years, multimedia and data-based services experienced a non-stopping growth. Unlike before, people do not use the services only from a static location, but they are continuously on the move between different scenarios, using their mobile devices to access data-based services for work-related purposes, entertainment or online socialization [SR16]. Moreover, people are not the only users of mobile communications, but more and more machines are provided with internet connection and continuously exchange information.

Commuter traffic from rural areas is also rising, since most work places are in and around cities. The European Environment Agency reported in 2013 that typical commuting times within larger cities are not unlikely to exceed one hour per trip; commuters from rural areas have to endure even longer trip durations [SR16]. During transportation, people intensively employ mobile devices to work, access to social networks, or as an entertainment means. Internet access is required for most of these services. Whereas sometimes the transmission of few bits is enough, continuous streaming of multimedia data is required in other cases. However, a significant portion of the mobile data is autonomously created by different types of machines. In the field of transportation, some examples are the communications for monitoring of the state of vehicles, serving connected entertainment systems, or the automated exchange of data between vehicles. Safety-related applications deserve special consideration since they impose stringent requirements on aspects such as reliability and low latency.

Trains are an efficient way of transportation for many applications [Dev89; AG84; Pro95]. Although the idea of moving carriages along rails was already found in ancient civilizations such as the Romans and the Greeks [AG84; Dev89; Pro95], railway transportation greatly evolved over the last few centuries. Its basis is the guided movement of metal wheels in direct contact with metal rails, which substantially reduces the rolling resistance [Pro95]. Taking also into account the capability of joining several transport units [Pro95], trains are well suited to transport several tons of freight or hundreds of passengers in a very efficient way in terms of energy consumption [AM84; UIC93] as well as environmental cost [UIC93;

Pro95]. However, when airplanes and private cars found their public in the society, trains had to modernize themselves in order to be competitive, mainly regarding speed, reduction of cost, and better organization and services provided [Pro95]. Hence, high speed trains, performing speeds higher than $500\,\text{km/h}$, appeared. This evolution of course also affected to railway communications. While the first communication system aimed to assist optical signaling was the telegraph in the XIX century [GFR98; AH11], primitive telephone lines [GFR98] appeared at the beginning of the XX century. Even wireless communication systems arose for non-critical communications, such as logistic management or maintenance tasks. It was years later, around the end of the 70s, when a wireless permanent communications channel between the train driver and a ground operator was established, which was the predecessor of the so-called GSM for Railways (GSM-R).

Currently, GSM-R is the most widely used communication system between trains and the elements involved in operation, control, and intercommunication within the railway infrastructure. GSM-R, which is based on the Global System for Mobile Communications (GSM), provides a continuous connection between the train driver and the ground controllers, allowing to perform emergency alarms, selective phone calls and data transmission. The communications are established between the train and the closest ground site, whereas all ground sites are connected by wires to a central controller. Since GSM-R is in charge of the train control signaling and safety-related communications, the Quality of Service (QoS) must be satisfied with testability, controllability, reliability, effectiveness, maintainability, safety and security [Lam+12; Fra+15; Rod+12; 10]. Operational and functional requirements for the railway environment impose stringent constraints on the underlying network technology such as reduced delay times or call setup times, as well as very reduced service interruptions.

However, GSM-R is not well-suited for supporting advanced services such as automatic pilot applications or provisioning broadband services to the train staff. Besides trains, the increasing number of broadband services available for mobile devices motivated the migration from third-generation mobile networks to fourth generation ones, mainly Long Term Evolution (LTE). Therefore, LTE seems to be a good candidate to substitute the GSM as the fundamental technology for railway communications. However, it is required to study if LTE is able to satisfy the operational and functional requirements imposed by the railway environment. Furthermore, the increasing demand for the use of mobile phones, laptops and other wireless devices by high-speed-train passengers has also attracted great interest from railway companies. New communications technologies are also interesting for metro transportation, where both train control and video surveillance can take advantage of the high throughput exhibited by fourth generation (4G) systems. It is also becoming more common to provide data access to users of buses, taxis or even particular cars. Simultaneously, the Mobile-Relay technique has been proposed in [3GP12] as a way to provide coverage to passengers based on a relaying scheme. All these factors motivate the increasing interest for the study of the radio propagation

characteristics for wireless communication systems in railways, with the aim of providing broadband communications in trains [Bri+14a; Ai+14].

Several radio channel models have been proposed for moving radio interfaces, such as [ITU97; Sie05; Kyo+07; ITU09a; Wei+10a; GZA11; Liu+12b; Par+08; Lua+13; HZA10; LZA10; He+11b; Liu+12a; Wei+10b; He+13e; Ai11; Ai+14; He+13a; He+13b; He+11a; LZB11; He+13c; BCA07; AGV98; CZW96; Zha+16b; HZB11; He+13d; Gua+12; Gua+13a; Gua+13b; Gua+14; He+12a; He+12b]. However, high speed train environments demand for specific scenarios such as rural macro cell, hilly terrain, viaducts, cuttings, tunnels or crossing bridges, among others. Moreover, for very high speeds (above $300\,\mathrm{km/h}$), non-stationary features of the channel arise [Ai+14] and the Wide-Sense Stationary Uncorrelated Scattering (WSSUS) assumption is no longer valid, whereas high Doppler frequency shifts and spreads are also introduced. This motivates the need for channel model characterizations based on measurement campaigns in realistic environments. However, measuring in the high speed train environment is complex, challenging and costly, whereas it usually demands for specific hardware and software solutions [Rod+13a].

In this work, a complete study on the performance of high capacity broadband wireless communication systems for high speed vehicles is presented, based on measurement campaigns in actual high speed environments. Special attention is devoted to the case of LTE in high speed trains. Techniques to greatly reduce the cost and complexity of measurement-based evaluations in high speed scenarios are proposed and proven to work. Also in the scope of this thesis, the so-called GTEC Testbed was designed, developed, and employed to perform several kinds of evaluations for different wireless communication techniques.

One must consider that the requirements and expectations regarding mobile communication systems continue growing day by day. In order to fulfill the increasing capacity demanded by users, the LTE standard evolved and new versions arose during the development of this thesis. Moreover, nowadays we are in the beginning of a new era for mobile communications, since the so-called fifth generation (5G) communication systems are currently under definition. Many of the current 5G proposals focus purely on quasi-static or nomadic users, hardly accounting for the impact of novel technological concepts on high-mobility users [SR16]. With the aim of checking the validity of the findings of this work for the latest advances in wireless communication systems, proposals for 5G communication systems were also considered. More specifically, Filter Bank Multicarrier (FBMC) modulation techniques were also evaluated in high speed environments. FBMC offers significant advantages with respect to Orthogonal Frequency-Division Multiplexing (OFDM) in the context of railway communications, such as higher bandwidth efficiency, improved multiple-access facilities in the uplink and its suitability for doubly dispersive channels. Bandwidth efficiency can become critical in railway environments due to the scarce spectrum available, and for facilitating the coexistence with the legacy systems such as GSM-R. The use of close-to-perfect subcarrier filters in FBMC

avoids multiple-access interference between different trains without requiring sophisticated synchronization methods, since the subcarriers are well frequency-localized. Regarding doubly dispersive channels, FBMC allows to achieve a compromise between the channel response spreading in time (multipath effect) and in frequency (due to the Doppler shift in different multipaths) by means of a proper prototype filter design [Far11; FAB95; Ala01; HB97; SB03; Ami+10].

1.1 Main Contributions of this Thesis

This work presents a complete study on the performance of high capacity broadband wireless communication systems (e.g., 4G and 5G ones) for high speed vehicles (e.g., high speed trains) based on measurement campaigns in actual high speed environments.

The main contributions of this thesis can be summarized as follows:

- Study of the specific characteristics of railway communications. More specifically, both the operational requirements and the typical services established for railway communications are introduced, as well as the feasibility of LTE to support such services. Wireless channel modeling particularities for the high speed train environment are also detailed.

- Proposal, theoretical analysis, and verification by means of measurements and simulations of a technique aimed to induce effects caused by highly-time varying channels on OFDM signals while conducting measurements at low speeds. Analysis of alternative methods to emulate high speed conditions while carrying measurements at low speeds.

- Design, development and use of the so-called GTEC Testbed, which represents an advanced set of hardware and software components which provide full flexibility to perform several kinds of evaluations for different wireless communication techniques.

- Performance assessment of both the outdoor-to-outdoor as well as the outdoor-to-indoor links in vehicle-to-infrastructure scenarios for 4G communication systems. The study was performed by means of several measurement campaigns using mobile receivers installed in cars, subways, and high speed trains.

- Theoretical study of the advantages that some proposals for 5G communication systems, such as FBMC modulations, provide for high speed train environments. Extension of the aforementioned high speed emulation technique to modulations proposed for 5G communication systems, and evaluation of its performance by means of simulations and

measurements. Finally, study of the performance of such modulation schemes for high speed train environments by means of simulations and measurements.

1.2 Structure of this Thesis

This thesis is structured in five chapters, in addition to the present one. A summary of the contents of each of the remaining chapters is presented below:

- Chapter 2 presents the evolution of railways in general and the railway communication systems in particular. Firstly, a brief introduction to the history of railways all over the world is presented. Some contents focus on the railway history in Spain and, more specifically, in Galicia. Evolution of the railways in the context of the telecommunications technologies is also considered, and a brief introduction to the current communication systems for railway environments is presented. The evolution of the general-purpose mobile communication systems and, in particular LTE, is also analyzed. Next, the particularities of the railway environment which should be taken into account when considering LTE as a candidate technology to support railway communications are presented. Finally, the advantages of the newest generation of communication systems, the so-called 5G, for the railway environment are analyzed.
- Chapter 3 proposes a technique to induce effects caused by highly-time varying channels on OFDM signals while conducting measurements at low speeds. This technique is aimed at considerably decreasing the cost and complexity of high speed measurement campaigns. It was evaluated by means of simulations and measurement campaigns in high speed scenarios in controlled and repeatable conditions. Finally, some other alternative methods to emulate high speeds are proposed and analyzed.
- Chapter 4 assesses the performance of 4G communication systems for both the outdoor-to-outdoor as well as the outdoor-to-indoor links in vehicle-to-infrastructure scenarios. On the one hand, the so-called GTEC Testbed, extensively used for the measurement campaigns, is introduced. On the other hand, the results of measurement campaigns in car-to-infrastructure, subway-to-infrastructure and high-speed-train-to-infrastructure scenarios are detailed.
- Chapter 5 checks the applicability of the previous findings regarding the proposals for 5G communication systems. First, the aforementioned high speed emulation technique is extended to the modulation schemes considered in 5G communications. Next, results of measurement campaigns for modulation techniques proposed for 5G communication systems, both in controlled measurement environments as well as in realistic ones, are presented. Also simulation results are provided.

- Chapter 6 concludes the study by presenting the main conclusions derived from this work and the proposed study lines to further continue it.

1.3 Co-authored Publications in the Scope of this Thesis

The study presented in this thesis led to the publication of several scientific co-authored contributions, including 5 journal papers (two of them under review) and 18 conference papers. Section 1.3.1 specifies the details of the journal papers, whereas Section 1.3.2 considers the conference ones.

1.3.1 Journal Papers

1. José Rodríguez-Piñeiro, Martin Lerch, José A. García-Naya, Sebastian Caban, Markus Rupp, and Luis Castedo. **Emulating Extreme Velocities of Mobile LTE Receivers in the Downlink**. In: *EURASIP Journal on Wireless Communications and Networking* 2015.106 (Apr. 2015). Special Issue on Experimental Evaluation in Wireless Communications. Online access: http://dx.doi.org/10.1186/s13638-015-0343-0

2. Pedro Suárez-Casal, José Rodríguez-Piñeiro, José A. García-Naya, and Luis Castedo. **Experimental Evaluation of the WiMAX Downlink Physical Layer in High-Mobility Scenarios**. In: *EURASIP Journal on Wireless Communications and Networking* 2015.109 (Dec. 2014). Special Issue on Experimental Evaluation in Wireless Communications. Online access: http://dx.doi.org/10.1186/s13638-015-0339-9

3. César Briso-Rodríguez, Carlos F. López, Jean R. Fernández, Sergio Pérez, Drasko Draskovic, Jaime Calle-Sánchez, Mariano Molina, José I. Alomso, Carlos Rodríguez, Carlos Hernández, Juan Moreno, José Rodríguez-Piñeiro, José A. García-Naya, and Luis Castedo. **Broadband Access in Complex Environment: LTE on Railway**. In: *IEICE Transactions on Communications* 97.8 (2014). Special Section on EU's FP7 R&D Project Activities on Future Broadband Access Technologies. Online access: http://dx.doi.org/10.1587/transcom.E97.B.1514, pp. 1514–1527

4. José Rodríguez-Piñeiro, Pedro Suárez-Casal, Tomás Domínguez-Bolaño, José A. García-Naya, and Luis Castedo. **Emulation of High Mobility Scenarios in Wireless Broadband OFDM Communications**. In: *Submitted to the IEEE Transactions on Vehicular Technology.* (2016)

5. Lei Zhang, José Rodríguez-Piñeiro, Jean R. Fernández, José A. García-Naya, David W. Matolak, César Briso, and Luis Castedo. **Propagation Modeling for Outdoor-to-**

Indoor and Indoor-to-Indoor Wireless Links in High-Speed Train. In: *Submitted to the Measurement journal.* (2016)

1.3.2 Conference Papers

1. José Rodríguez-Piñeiro, Tomás Domínguez-Bolaño, José A. García-Naya, and Luis Castedo. **Performance Assessment of 5G-Candidate Waveforms in High Speed Scenarios**. In: *27th Annual IEEE International Symposium on Personal, Indoor and Mobile Radio Communications (PIMRC 2016)*. Accepted for publication. Valencia, Spain, Sept. 2016

2. José Rodríguez-Piñeiro, Martin Lerch, Tomás Domínguez-Bolaño, José A. García-Naya, Sebastian Caban, and Luis Castedo. **Experimental Assessment of 5G-Candidate Modulation Schemes at Extreme Speeds**. In: *Ninth IEEE Sensor Array and Multichannel Signal Processing Workshop (SAM 2016)*. Río de Janeiro, Brazil, July 2016

3. José Rodríguez-Piñeiro, José A. García-Naya, Pedro Suárez-Casal, César Briso-Rodríguez, J. I. Alonso-Montes, and Luis Castedo. **Assessment of Channel Propagation Conditions for FDD LTE Transmissions in the Spanish High-Speed Railways**. In: *10th European Conference on Antennas and Propagation (EuCAP 2016)*. Davos, Switzerland, Apr. 2016

4. José Rodríguez-Piñeiro, Tomás Domínguez-Bolaño, Pedro Suárez-Casal, José A. García-Naya, and Luis Castedo. **Affordable Evaluation of 5G Modulation Schemes in High Speed Train Scenarios**. In: *ITG Workshop on Smart Antennas (WSA 2016)*. Munich, Germany, Mar. 2016

5. José Rodríguez-Piñeiro, Martin Lerch, Pedro Suárez-Casal, José A. García-Naya, Sebastian Caban, Markus Rupp, and Luis Castedo. **LTE Downlink Performance in High Speed Trains**. In: *2015 IEEE 81st Vehicular Technology Conference (VTC2015-Spring)*. Glasgow, United Kingdom, May 2015

6. José Rodríguez-Piñeiro, Pedro Suárez-Casal, José A. García-Naya, Luis Castedo, César Briso-Rodríguez, and J. Ignacio Alonso-Montes. **Experimental Validation of ICI-Aware OFDM Receivers under Time-Varying Conditions**. In: *Eighth IEEE Sensor Array and Multichannel Signal Processing Workshop*. Online access: http://dx.doi.org/10.1109/SAM.2014.6882411. A Coruña, Spain, June 2014, pp. 341–344

7. José Rodríguez-Piñeiro, José A. García-Naya, Pedro Suárez-Casal, and Luis Castedo. **LTE under the High-Speed-Train Channel Model**. In: *XXVIII Simposium Nacional de la Unión Científica Internacional de Radio (URSI 2013)*. Sept. 2013

8. José Rodríguez-Piñeiro, José A. García-Naya, Ángel Carro-Lagoa, and Luis Castedo. **A Testbed for Evaluating LTE in High-Speed Trains**. In: *16th Euromicro Conference on Digital System Design (DSD 2013)*. Online access: http://dx.doi.org/10.1109/DSD.2013.27. Sept. 2013, pp. 175–182

9. José Rodríguez-Piñeiro, Paula Fraga Lamas, José A. García-Naya, and Luis Castedo. **LTE security analysis for railway communications**. In: *IEEE Congreso de Ingeniería en Electro-Electrónica, Comunicaciones y Computación ARANDUCON 2012*. Nov. 2012

10. Tomás Domínguez-Bolaño, José Rodríguez-Piñeiro, José A. García-Naya, and Luis Castedo. **The GTEC 5G Link-Level Simulator**. In: *International Workshop on Link- and System Level Simulations (IWSLS2 2016)*. Vienna, Austria, July 2016

11. Martin Lerch, José Rodríguez-Piñeiro, José A. García-Naya, and Luis Castedo. **Methods to Perform High Velocity LTE Experiments at Low Velocities**. In: *2016 IEEE 83rd Vehicular Technology Conference (VTC2016-Spring)*. Nanjing, China, May 2016

12. Dan Fei, José Rodríguez-Piñeiro, José A. García-Naya, Luis Castedo, and Lei Xiong. **TD-LTE Downlink Performance Assessment in High Speed Scenarios**. In: *2016 IEEE 83rd Vehicular Technology Conference (VTC2016-Spring)*. Track "2nd International Workshop on Wireless Communications for High Speed Railways (HSRCom2016)". Nanjing, China, May 2016

13. Lei Zhang, Pedro Suárez-Casal, Jean Fernández, José Rodríguez-Piñeiro, Jaime Calle-Sánchez, José A. García-Naya, Luis Castedo, C. Rodríguez-Sánchez, J. Moreno, César Briso-Rodríguez, and J. I. Alonso-Montes. **Experimental Evaluation of 4G Technologies in Metro Tunnel Scenarios**. In: *10th European Conference on Antennas and Propagation (EuCAP 2016)*. Davos, Switzerland, Apr. 2016

14. Tomás Domínguez-Bolaño, José Rodríguez-Piñeiro, José A. García-Naya, and Luis Castedo. **Experimental Evaluation of 5G Modulation Schemes in Quasi-Static Scenarios**. In: *ITG Workshop on Smart Antennas (WSA 2016)*. Munich, Germany, Mar. 2016

15. Paula Fraga-Lamas, José Rodríguez-Piñeiro, José A. García-Naya, and Luis Castedo. **Unleashing the Potential of LTE for Next Generation Railway Communications**. In: *8th International Workshop on Communication Technologies for Vehicles (Nets4Cars / Nets4Trains / Nets4Aircraft 2015)*. Online access: http://dx.doi.org/10.1007/978-3-319-17765-6_14. Sousse, Tunisia, May 2015, pp. 153–164

16. Pedro Suárez-Casal, José Rodríguez-Piñeiro, José A. García-Naya, Luis Castedo, César Briso-Rodríguez, and J. Ignacio Alonso-Montes. **Experimental Assessment of WiMAX**

Transmissions under Highly Time-Varying Channels. In: *Eleventh International Symposium on Wireless Communication Systems (ISWCS)*. Online access: http://dx.doi.org/10.1109/ISWCS.2014.6933447. Barcelona, Spain, Aug. 2014, pp. 717–721

17. José A. García-Naya, José Rodríguez-Piñeiro, Ángel Carro-Lagoa, and Luis Castedo. **Demostrador para la Evaluación Experimental de LTE en Entornos Ferroviarios de Alta Velocidad**. In: *XXVIII Simposium Nacional de la Unión Científica Internacional de Radio (URSI 2013)*. Sept. 2013

18. Paula Fraga Lamas, José Rodríguez-Piñeiro, José A. García-Naya, and Luis Castedo. **A survey on LTE networks for railway services**. In: *IEEE Congreso de Ingeniería en Electro-Electrónica, Comunicaciones y Computación ARANDUCON 2012*. Nov. 2012

1.4 Co-authored Publications in Side Topics

Along the development of the performed study, some of the achievements and knowledge acquired allowed contributions to fields not directly related with the scope of this thesis. These contributions include both co-authored journal as well as conference papers. Section 1.4.1 specifies the details of the journal papers, whereas Section 1.4.2 considers the conference ones.

1.4.1 Journal Papers

1. Raúl Gregor, Guido Valenzano, Jorge Rodas, José Rodríguez-Piñeiro, and Derlis Gregor. **Design and Implementation of an FPGA-based Real-time Simulator for a Dual Three-Phase Induction Motor Drive**. In: 16.2 (Mar. 2016). Online access: http://dx.doi.org/10.6113/JPE.2016.16.2.553, pp. 553–563

1.4.2 Conference Papers

1. Raúl Gregor, Guido Valenzano, José Rodríguez-Piñeiro, and Jorge E. Rodas Benítez. **FPGA-based Real-Time Simulation of a Dual Three-Phase Induction Motor**. In: *16th European Conference on Power Electronics and Applications (EPE'14-ECCE)*. Online access: http://dx.doi.org/10.1109/EPE.2014.6911031. Lappeenranta, Finland, Aug. 2014, pp. 1–8

2. David Caballero, Federico Gavilán, Raúl Gregor, Jorge Rodas, Sergio Toledo, and José Rodríguez-Piñeiro. **MBPC Power Control in Three-phase Inverters for Grid-connected Applications**. In: *2015 IEEE PES Innovative Smart Grid Technologies Latin America (ISGT LATAM)*. Uruguay, Sept. 2015, pp. 817–821

Chapter 2

LTE Feasibility in Railway Scenarios

The railway history is strongly related with the general history of many countries over the last 200 years. In relation to the telecommunications history, this chapter will show that the evolution of the modern communication systems is closely related to the railway developments.

This chapter is mainly based on the following co-authored publications:

- José Rodríguez-Piñeiro, José A. García-Naya, Pedro Suárez-Casal, and Luis Castedo. **LTE under the High-Speed-Train Channel Model**. In: *XXVIII Simposium Nacional de la Unión Científica Internacional de Radio (URSI 2013)*. Sept. 2013

- José Rodríguez-Piñeiro, Paula Fraga Lamas, José A. García-Naya, and Luis Castedo. **LTE security analysis for railway communications**. In: *IEEE Congreso de Ingeniería en Electro-Electrónica, Comunicaciones y Computación ARANDUCON 2012*. Nov. 2012

- Paula Fraga-Lamas, José Rodríguez-Piñeiro, José A. García-Naya, and Luis Castedo. **Unleashing the Potential of LTE for Next Generation Railway Communications**. In: *8th International Workshop on Communication Technologies for Vehicles (Nets4Cars / Nets4Trains / Nets4Aircraft 2015)*. Online access: http://dx.doi.org/10.1007/978-3-319-17765-6_14. Sousse, Tunisia, May 2015, pp. 153–164

- Paula Fraga Lamas, José Rodríguez-Piñeiro, José A. García-Naya, and Luis Castedo. **A survey on LTE networks for railway services**. In: *IEEE Congreso de Ingeniería en Electro-Electrónica, Comunicaciones y Computación ARANDUCON 2012*. Nov. 2012

Firstly, Section 2.1 provides a brief introduction to the history of railways all over the world. Some contents are focused on the history of Spain and, more specifically, of Galicia. Section 2.2 details the evolution of the railways in the context of the telecommunications technologies, whereas Section 2.3 gives a brief introduction of the main systems used nowadays. Section 2.4 studies the evolution of the general-purpose mobile communications systems and, in particular, motivates the definition of Long Term Evolution (LTE), whereas Section 2.5

details the particularities of the railway environment which should be taken into account when considering LTE as a candidate technology to support railway communications. Finally, Section 2.6 introduces the advantages of the newest generation of communication systems, the so-called fifth generation (5G), for the railway environment.

2.1 Brief History of Railway Transportation

Every organized society along the history has been interested in the efficient transportation of people and goods. It is generally acknowledged [Dev89; AG84; Pro95] that the fundamental innovations regarding transportation include the discovery of the wheel as well as the invention of the railway and the plane.

One of the main characteristics of the railway transportation is its capability for joining several transport units [Pro95]. This enables trains to transport several tons of freight or hundreds of passengers. Other of their main characteristics constitutes also one of its main limitations, which is that they have a single degree of freedom for their movement, as opposed to cars, for example. This inflexibility, however, enables multiple tasks to be automatized.

Railway transportation is usually based on the guided movement of metal wheels in direct contact with metal rails. This reduces substantially the rolling resistance [Pro95], hence, for the same propulsion force, railways are able to carry much higher loads than road vehicles. Moreover, railways consume half as much energy as road transport for the same load [Pro95], whereas airplanes require 5 to 7 times more energy than railways [AM84; UIC93]. This also causes that the environmental cost in terms of pollution is much lower for trains with respect to their competitors [UIC93; Pro95].

The idea of moving carriages along rails was already found in ancient civilizations, such as the Romans and Greeks. Romans already carved grooves in the stone pavement to aid the movement of carriages [AG84] and we can still visit some of the deep grooves employed by the ancient Greeks to carry marble slabs at Mount Penteli, close to Athens [Dev89]. Movement of carriages on metal guides, however, is already illustrated in a 1550 gravure found in Basel, Switzerland, which shows transportation methods employed in the mines of Alsace [Pro95]. Railways in their present form are first documented at the beginning of the XIX century in British mines.

Years after the invention of the steam machine by Jacob Watt at the end of the XVIII century, attempts of using this technology for vehicles arose [Wai87]. Some examples are the steam carriage built by the French Cugnot or the approach of the engineers Cornonailles Trevithic and Vivian, established a steam-based stagecoach service in 1801. As the vehicles were not able to surpass the roughness of the roads at that time and they were difficult and dangerous to drive, they introduced the concept of metal rails to guide the vehicles. More or less successful

efforts based on this idea were later developed by Blekinsop, the Chapman brothers or Muntun. However, the first history of success was by J. Stephenson.

Stephenson was a son of a worker of the Killnigworth mines, close to Newcastle, at the north of England. At that time, carriages moved over rails were horse-powered. In 1813 the tenants of the mines supported Stephenson to built a so-called "traveler machine". Apart from the mining environment, there were some trials to introduce public tram systems powered by horses, most of them with few success. However, the initial success of the Stephenson's project motivated him to continue improving its machine, giving birth to the steam locomotive, which was used for the first time in the world, going from Stockton to Darlington. It was inaugurated in September 27th, 1825.

Three years afterwards, in USA, Horacio Allen acquired four European steam locomotives to study their technology and started to build his own machine. Also at that time, the Baltimore & Ohio Railroad built a 14 miles long line, whereas in 1934 Mathias W. Baldwin constructed a steam locomotive for a train line in Philadelphia. Jervis was the responsible of introducing the successful concept of "bogie", a modular subassembly of wheels and axles, which has been widely used later. Between 1836 and 1837, Baldwin built 80 steam locomotives. The railway lines in USA were growing and growing, and in 1855 the feasibility of joining the Atlantic Sea and the Pacific Sea by means of a railway line is studied.

Differences between the European and American trains were noticeable. The most remarkable one is that the American train carriages were much longer than their European counterparts and they did not have any partition indoors. Passengers were seated looking to the direction of the train movement. However, European carriages, clearly inspired in the former stagecoaches, were much shorter, and had plenty of divisions indoors. USA also introduced as soon as in 1839 berths and then full-sized beds inside train carriages, whereas this kind of advances lasted many years to appear in Europe.

News about the Stephenson developments arrived at Spain at a non-proper time for industrial investments. At that time, the roads in Spain were very underdeveloped. Their public construction started during the kingdom of Fernando VI (1746–1759). Although more effort was done during the Carlos III era (1759–1788). However, still at the beginning of the XIX century, the total length of the roads in Spain was less than 2300 km. Some public transportation services based on horse-powered stagecoaches were in operation, being the first one documented in 1771 [Wai87]. With the birth of the railway era, these horse-powered vehicles were condemned to disappear. Only for those areas where the railway did not arrive yet, transportation services based on horse-powered stagecoaches were maintained. It was the case, for example, of the itinerary between Santiago de Compostela and A Coruña, in Galicia, of about 70 km long, which still existed until the beginning of the XX century, when it was substituted by a railway line named "Compostelana".

However, the earliest trial to build a railway line in Spain was held by José Díaz Imbrechts

in Andalucía, who planned to build a train between Jerez and El Portal, close to the Guadalete river, to move the wine to be exported to England. The project was not accepted to be publicly funded. Another proposal was due to Mariano Calero y Portocarrero, who planned a train from Jerez to Sanlúcar de Barrameda, which was also rejected. Later, in 1834, Francisco Fasio proposed a line from Reus to Tarragona, which was also never built. Other proposal arose in the Basque Country in 1831, for the development of a train between Bilbao and Burgos, but it was discarded due to its high cost.

After the death of Fernando VII (1833), the so-called "Carlista" war started in Spain, lasting until 1840, which avoided industrial investments, and hence no railways were built at the Iberian Peninsula. However, Cuba was well-developed and, as a part of the plan to increase the quality of the Cuban roads and transportation means, a railway line between La Habana and Güines was built. Efficient transportation of sugar and tobacco justified the required investment and hence the first Spanish train was inaugurated on November 10th, 1837. Regarding the Iberian Peninsula, there were incipient railway trials in several areas where the private investment made sense. The well-industrialized Catalonia, the rich area of Valencia and the mining industry in Asturias were a good background for the starting of the railway era in Spain. Also Madrid, due to its importance for political and strategical reasons, was one of the first Spanish places where a train was built. Thus, the first railway lines in the Iberian Peninsula were *(a)* from Barcelona to Mataró, inaugurated in 1848 and having a length of 29 km, *(b)* from Madrid to Aranjuez (1851, 49 km), and *(c)* from Langreo to Gijón (1852).

Railways to Galicia were more delayed with respect to other peripheral areas of the Iberian Peninsula. Deployment of railways in Galicia was, in fact, motivated more by the needs of Spain with respect to Galicia than by the needs of the Galician people themselves. The railway arrived at Galicia 25 years later than at Alicante, the first city in the coast to have such a service, and more than 10 years later than at Santander, Bilbao, San Sebastián, Pamplona, Zaragoza, Barcelona, Valencia, Murcia, Málaga, Sevilla, Cádiz or Cáceres. There are three main reasons for the underdevelopment of the Galician railway lines, which are [Día06]:

- The region of Galicia is very far away from the center of the Iberian Peninsula. This also holds for other regions, such as Catalonia or Andalucía. However, in these cases, they serve as international connections with France and Africa, respectively;
- The obvious orographic difficulties inherent to Galicia. Although there are several mountain chains which have to be crossed to reach many peripheral areas from the center of the Iberian Peninsula (e.g. Cantabrian Mountains to the Basque Country, Cantabria or Asturias), there are many mountain chains and hundreds of rivers inside Galicia which make difficult and costly to build railway lines;
- The weak economy of Galicia with respect to other areas of the Iberian Peninsula. The lack of industry was a reason to avoid investments to reach Galicia by train.

Not only the railway in Galicia was delayed to a great extent with respect to other peripheral areas, but also its deployment was far from optimum. In fact, the railway lines were designed to be as cheap as possible and to minimize the deployment time. These factors caused that the most complicated areas from the orographic point of view were avoided by following alternative itineraries, which artificially increased the length of the lines to a great extent. This also introduced a lot of curves in the paths as well as prominent slopes, with the aim of avoiding building tunnels, bridges and viaducts. All these factors resulted on very long paths that could be only driven at slow speeds (both by the great slopes as well as the curves). Although these decisions allowed for building a cheaper train, they severely reduced its profitability in the long term [Día06].

Meanwhile, the performance of steam-powered locomotives was greatly improved. Speeds of 100 km/h were achieved in 1835 in Britain, whereas 144 km/h and 213 km/h in France (1890) and Germany (1903), respectively [Pro95]. Electric traction appeared in the early XX century and the advances in signaling and remote control achieved during the World War II decisively influenced the future railway communications.

However, time goes by and airplanes and private cars found their public in the society. Trains had to modernize themselves in order to be competitive, mainly regarding speed, reduction of cost, and better organization and services provided [Pro95]. Hence, the era of the high-speed trains (i.e., those that move faster than 200 km/h) approached. The two first examples were the Japanese high-speed line between Tokyo and Osaka, namely "Shinkansen", having a top speed of 210 km/h in 1964, as well as the "TGV" high-speed train between Paris and Lyon, having an initial top speed of 260 km/h in 1981, increased to 270 km/h in 1983 and to 300 km/h in 1989. More high-speed lines were deployed around 1980 in West Germany (Hannover–Wüzburg and Mannheim–Stuttgart), Italy (Rome–Florence), France (Paris–Bordeaux) and Spain (Madrid–Seville). Two main approaches to high-speed trains were followed [Pro95]:

- **Passenger-only trains**: the loads and tolerance to rail deficiencies are low. Of course this approach requires a high number of passengers to be cost-efficient. [Rou94];
- **Both passenger and freight trains**: they imply more maintenance costs and require lower values of longitudinal gradient [Pro85; Rou85]. Most of the current high-speed lines follow this approach.

Train technologies must be also mentioned which, although being based on guided vehicles, avoid contact of the moving vehicle with the rest of the railway infrastructure. There are two main technologies [Pro95]:

- **Aerotrain**: The propulsion is achieved by means of a compressed air cushion blown between the vehicle and the bearing substructure [Pro85]. Speeds as high as 422 km/h were achieved in 1969 in France. Finally, no aerotrain lines were deployed since the

construction cost as well as the energy consumption during aerotrain operation were very high. Furthermore, the aerotrain capacity was much lower than for conventional trains.

- **Maglev**: In this case, propulsion is ensured by magnetic phenomena. Forces required for levitation, propulsion and guidance are generated by means of properly set-up magnets and coils. The speed of 517 km/h was achieved in 1979 in Japan.

Finally, it must be noted that under the concept of railways not only the long distance trains are included, but also suburban trains, subways and even trams.

2.2 Evolution of the Railway Communications

The specific characteristics of the railway infrastructure and its way of operation convert the associated telecommunications into an strategic element not only for the safety, but also for the efficiency and capacity of the whole transportation system. Due to this fact, communications for railways were always much more advanced than for other environments. Moreover, railways decisively contributed to the development of many communication technologies that were further used by the general public, such as the telegraph or the telephone.

We can distinguish between two main types of communications, which are [GFR98] *(a)* simple signaling transmissions meant to be interpreted quickly (e.g., optical signals), and *(b)* complex communications which allow for transmitting more elaborated messages, such as the telephone. Regarding the first type of communications, typical devices are the so-called electronic bells. They were used for communication between the stations (e.g., the traffic controllers) and the operators along the rails (e.g., the switchmen). The electronic bells were installed at strategic points along the line. All the bells between two stations rang at the same time and they were used to code simple messages. The rest of this section is devoted to the second type of communications, i.e., the ones meant to transmit more complex messages.

The first communication system used to assist railway signaling was the telegraph and started in the United Kingdom. It was meant to provide a robust and fast signaling method against bad climatic conditions, since previous proposals were exclusively visual [AH11]. The first telegraph used in Spanish railways was inaugurated in 1851, on the railway line between Madrid and Aranjuez. Taking the United Kingdom case as a model, the use of the railway telegraph was soon extended to the general public. However, whereas the dense railway infrastructure of the United Kingdom allowed people to communicate fluently, it was necessary to define a telegraph system independent from the railway companies in Spain, altough it was mandatory for Spanish railway companies to allow for general telegraph traffic to operate under their telecommunication infrastructures. This way, a strong commercial cooperation between the railway companies and the telegraph national service started.

In relation to the train service of the XIX century, telegraphy was essential to establish

communications between train stations to learn the state and occupation of the tracks between them and to establish the so-called "blocking" of tracks between stations. The first electronic telegraph system was the breguet telegraph. It consisted on an apparatus capable of transmitting 25 different combinations of electric impulses, which served to code the characters of the alphabet. At the receiver, each received character was indicated by means of a clock hand. This kind of telegraphs were slow and the messages were not recorded in any physical medium. Due to this disadvantages, they were soon substituted by the Morse telegraphs, which used the Morse code to transmit symbols which were automatically written to paper at the receiver. Optionally, they could be decoded acoustically by an operator. The Morse telegraph significantly increased the message transmission speed. For both telegraph types, the physical medium used for the transmission of the electric signals was based on iron lines.

One of the first phone lines in Spain, only two years after the invention by Bell, was devoted to the railway infrastructure. It was in November 1877, when a phone line having a distance of 723 m and a phone manufactured by Edison at each of its extremes was installed by the telegraph staff of the Mataró Station [GFR98]. On December 31st 1877, phone calls between Barcelona and Tarragona (102 km) were established. With the beginning of the XX century, primitive voice phones were progressively incorporated to the railway signaling and controlling equipment, although it was only possible to establish calls between consecutive train stations. Telegraphy and voice calls were still the standard media to establish the "blockage" of the railway line between stations. Since 1922, a two-wire circuit was built along the whole railway lines, which connected the main train stations, so they could establish direct connections between them. When a message was sent from one station, all the others received it. This kind of communication was mainly used for messages related to the railway management (e.g., dispatching operations), but not for safety ones. In the latter case, the old lines between consecutive stations were still used. Later, another line which allowed for private point-to-point connections between different railway stations was introduced.

Besides to the communications systems related to safety and railway management, other schemes were introduced to assist in logistic management, maintenance tasks, etc. Bad maintenance of the communication lines for supporting large-distance communications motivated the introduction of a wireless system only for this kind of tasks (hence only intended for non-critical communications) based on shortwave transmissions for voice communications. At the same time, around the 50's, the classic telegraph was substituted by the teleprinter. In Spain, all teleprinters were connected to a common node. The main drawback at that time for wireless communications was the lack of security of the transmission medium, which caused more investment to be devoted to wired communication systems with respect to their wireless counterparts.

Other communication systems were also introduced, such as:

- **Portable telephones**: they might be plugged into metal plates available in some masts

close to the tracks, allowing the train driver, or the maintenance operators, to contact the management section, or some train stations;

- **Portable radio stations**: they were based on simple short-wave communications and they allowed for communications up to 25 km. In many cases they were used to aid in coordinating goods transportation;
- **Small Radio Frequency (RF) phones**: they enabled the establishment of communications up to 5 km. They were used to coordinate the two locomotives where applicable, indicate if the train was fully occupied, or to contact nearby train stations during maintenance tasks;
- **Public Address (PA) assistants**: mainly used to help or guide the passengers; and
- **Pannels in train garages**: they used to announce the identification number of each required worker for some task.

Other automation and control systems were introduced, such as those suited for detecting failures or malfunctions (falling objects, too hot wheels, etc.) or alarms.

Since 1967, with the electrification of the railways, the obsolete communication lines also started to be modernized. About 2000 km of wire were installed, with the aim of avoiding the electromagnetic interferences generated by the catenary and to increase the robustness. Moreover, several manual control systems were substituted by electronic ones, and a big effort on standardization and specification of the communication systems requirements started. An example is the specification number 751 [Che84] for communications between trains and ground stations, which defined an analog communications system working on the 460 MHz band.

Starting on 1975, several improvements in relation to the communications technologies started, such as the introduction of the fiber optic wire, teleprinters automation, fax introduction, and, the most important for our proposals, the introduction of the train-to-ground communications. It was at this time when the feasibility of joining the railway communications network and the public communications one was studied. Finally, it was decided to maintain both networks separated, although some cooperation between their infrastructures was established. Hence, investments for both network infrastructures were shared in some cases. The main reason to not combine both communication networks is that public network operators were only interested in general phone call services, as well as teleprinters and data transmission provision services, but not on specific services suited for the railway operators which would require a different network architecture and resources, as it will be seen. It is also remarkable that the Union Internationale des Chemins de Fer (UIC) recommends a dedicated communications network for the railway operators (from UIC meeting in Paris, 1966 [AH11]).

The main improvements between 1975 and 1985 regarding the railway communications

in Spain were the automation of switchboards, the installation of more fiber optic-based wires, deployment of automated Message Management Centers which routed messages to the recipient and a Telecommunications Control Center, the latter one still in use today. Other of the major advances was the automated ticket booking system. One of the remarkable facts was that the Spanish railway operator was able to install some automated ticket booking points in Paris, whereas the French railway operator, namely Société Nationale des Chemins de Fer Français (SNCF), installed its own automated booking points in Madrid. The network infrastructure was deployed by Red Nacional de los Ferrocarriles Españoles (RENFE) and SNCF, whereas some years later the first European data transmission network specific for the railway environment, namely HERMES, was deployed. Also between 1975 and 1985 a goods transportation management system based on computers was developed, which motivated the deployment of a fax service over the analog network for the railway environment. Finally, several automated control and alert systems were also developed and progressively installed, such as those aimed at measuring the temperature on wheels, catenary defects, detection of objects on the tracks, etc. In most cases, these systems sent reports to a controller by means of the railway communications network.

However, the main improvement regarding railway communications between 1975 and 1985 for our proposals was the establishment of a permanent communications channel between the train driver and a ground operator. The first analog communication system between the train and the ground operators was developed according to the UIC-751-3 [Che84] specification and deployed in 1982, allowing for voice calls and short teleprinter messages. A more advanced communication system, allowing also for data transmission, was deployed in some lines and started to be used in 1987. This was the predecessor of the GSM for Railways (GSM-R) deployments, still widely used today. In 1987, the train-to-ground communication system was available along 3500 km of the railway line and the required devices were installed in all locomotives, whereas in 1997 the coverage was extended to 6000 km along the rails [GFR98]. This train-to-ground system provided a continuous connection between the driver and the ground controllers, served to transmit emergency alarms and allowed for selective phone calls and data transmission. The network architecture was comprised by fixed ground sites as well as central controllers. Communication was established between the train driver and the closest ground site, whereas a wired connection between the central controller and the ground site was available.

On April 20th 1992, the first High-Speed Train (HST) Spanish line, between Madrid and Seville, was inaugurated, allowing for velocities up to 300 km/h. From the telecommunications point of view, the line was designed to be controlled in a centralized manner from a single control center. Hence, stringent requirements on availability, robustness and redundancy of the communication systems were established. From the physical point of view, two fiber optic wires were deployed in a redundant manner along the rails, whereas copper wires were deployed for

connections to the railway infrastructure. Three different network types were considered for the interconnection of the different elements (e.g., detectors of objects on the tracks, signaling devices...), which are:

- **Data network over a dedicated channel**: used only for signaling tasks;
- **Integrated data network**: used for data transmission, such as alarms about objects found on the tracks or high temperature on wheels; and
- **Voice transmission network**: management of the infrastructure. It included both fixed terminals as well as mobiles (train-to-ground connection).

At that time, many of the network resources used by the railway operator were rented to the public telecommunications operator in Spain. In order to decrease the operation costs, the railway operator made a great effort to extend its own network. Between 1995 and 1996 an Internet Protocol (IP)-based network was deployed and synchronous transmission systems substituted the former asynchronous ones. Circuit-Switching schemes were also progressively substituted by IP-based ones.

Another remarkable fact occurred in 1998, when the telecommunications in Spain were liberalized. The railway operator signed a contract with the European network HERMES and more than 10000 km of fiber optic wire were already installed in 2000.

Progressively, wireless proprietary communications systems used for the train-to-ground permanent channel were being migrated to GSM-R, a version of Global System for Mobile Communications (GSM) specifically suited for the railways, used both for management communications as well as signaling. This fact is really important since GSM-R poses as the first wireless communication system used for safety information transmission. A brief introduction to GSM-R will be provided in the ensuing section.

2.3 Brief Introduction to Current Railway Communication Systems

European advises on railway communications tend to promote maximization of interoperability between railway communication systems. This resulted on the definition of European Rail Traffic Management System (ERTMS), which includes three levels. Among them, levels 2 and 3 employ GSM-R as the basis technology to support communications. 4 MHz bandwidth is reserved in Europe for such communications. In theory, all railway lines in Spain are equipped with GSM-R, although dramatic recent events showed that this technology is not always ready to use [Wik].

Section 2.3.1 briefly introduces ERTMS, whereas Section 2.3.2 explains the basics of the GSM-R technology.

2.3.1 European Rail Traffic Management System (ERTMS)

ERTMS is devoted to provide an inter-operable railway management system. The main elements of ERTMS are:

- **European Train Control System (ETCS)**: allows for the automated train control. Consists of a Radio Block Center (RBCN) and a Lineside Electronic Units (LEU);
- **EURORADIO GSM-R**: radio infrastructure;
- **EUROBALISE**: balises[1] along the tracks allowing for precisely locating the trains; and
- **EUROCAB**: on-board management system, including European Vital Computer (EVC), Driver-Machine Interface (DMI) and measurement devices such as odometers.

ETCS can be divided into three levels, which are:

- **ETCS level 1**: location of the train is implemented by traditional means (i.e., no balises are used for locating the train), whereas communications between fixed safety infrastructure and trains is performed by means of balises;
- **ETCS level 2**: communication between trains and railway infrastructure is continuous and supported by the GSM-R technology. Location of the train is estimated by means of fixed balises; and
- **ETCS level 3**: checking of the integrity of the train elements is done at the train itself, so no devices at the track are required. Fixed balises are used to locate the train.

2.3.2 GSM for Railways (GSM-R)

GSM-R is a communications system for the railways which is based on the well-known GSM standard. It adds operative characteristics defined in the European Integrated Railway Radio Enhanced Network (EIRENE) (namely the Functional Requirement Specification (FRS) [UIC12a] and the System Requirement Specification (SRS) [UIC12b]) and the Mobile Radio for Railways Networks in Europe (MORANE), established jointly by the UIC as well as the European Telecommunications Standards Institute (ETSI). Currently, GSM-R is in operation in 38 countries across the world, including all member states of the European Union and countries in Asia, America and northern Africa.

Two frequency bands were reserved by the ETSI for railway communications in Europe in 1995, which are 876–880 MHz (uplink) and 921–925 MHz (downlink). It is possible to allocate 19 subcarriers of 200 kHz, including a single guard, for each band. Each subcarrier supports 8 data or voice channels.

The architecture of the GSM-R system is based on that of the GSM and can be subdivided into:

[1] Balise is a French word designating an electronic beacon or transponder placed between the reails of a railway track.

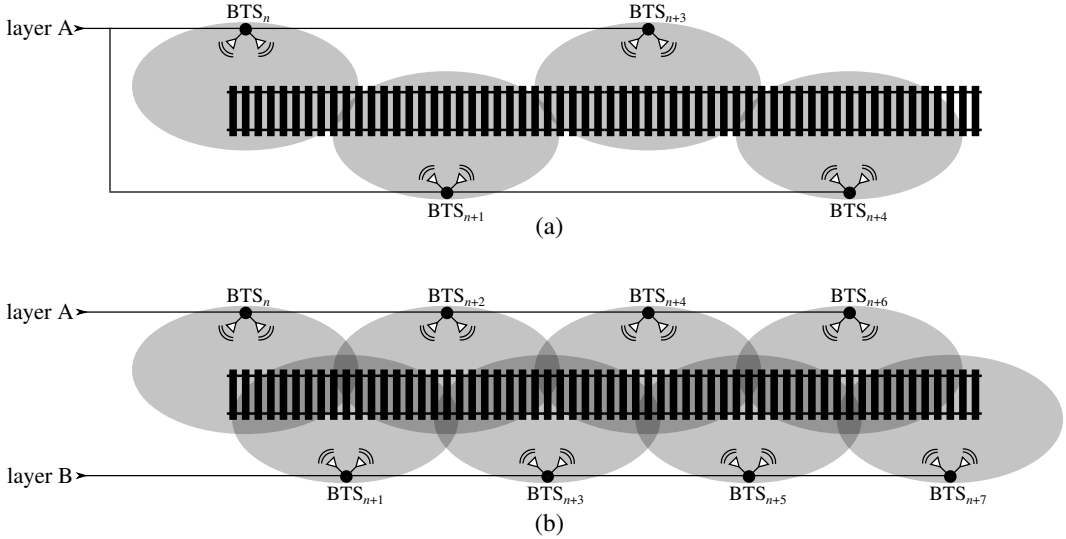

Figure 2.1: GSM-R deployment by means of elliptical cells. *(a)* non-redundant strategy, *(b)* redundant strategy.

- Mobile Station (MS) subsystem;
- Base Station Subsystem (BSS);
- Network Switching Subsystem (NSS); and
- Operation and management subsystem.

The MS subsystem enables the communication between trains, with the management team, or with the Radio Control Center (RCC). It includes Mobile Radio Centers (MRCNs), basically the on-board radio equipment, as well as Portable Radio Centers (PRCNs) which are mobile devices. Each device is provided with a Subscriber Identity Module (SIM) card, which is associated to a specific worker of the railway company.

The BSS is in charge of controlling the Base Transceiver Stations (BTSs), whereas the NSS deals with tasks regarding call routing and control. Finally, the operation and management subsystem manages and controls the access to resources and services provided by the network.

GSM-R network is deployed forming elliptical cells along the tracks. BTS antennas are pointed to the tracks. Each cell is serviced by a single BTS with one antenna per direction (see Fig. 2.1a). In case that more stringent robustness requirements are imposed, a redundant strategy may be adopted. In such a situation, two independent layers of cells completely overlapping are deployed (see Fig. 2.1b) [Tas06]. In principle, trains in one direction use one of the layers, whereas trains in the opposite direction use the other one. However, each layer is dimensioned to be able to transport all the traffic, hence if there is a problem regarding one of the layers, the other one would be used. Coverage for tunnels whose length is smaller than 2 km is provided by external antennas, whereas radiating cable or repeaters are installed indoors for longer tunnels.

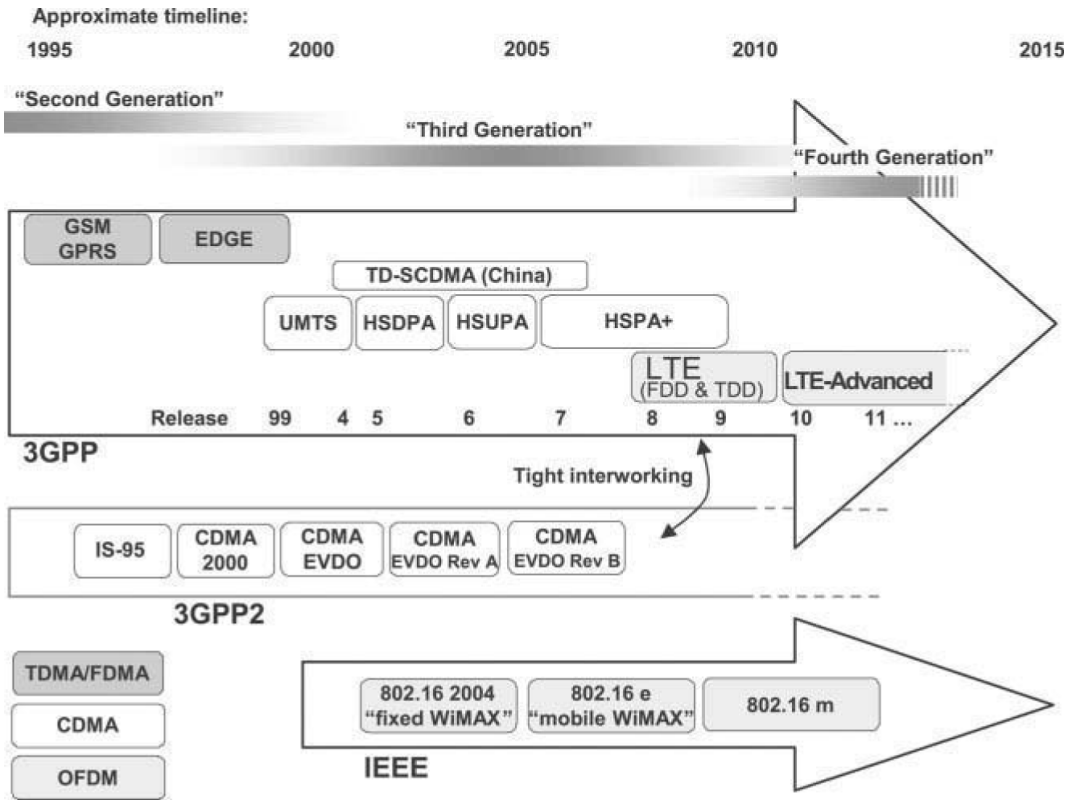

Figure 2.2: Approximate timeline of the mobile communications standards landscape [STB11].

2.4 Evolution of Public Mobile Communication Systems. LTE Communications

The concept of *cell* was introduced by the Bell Labs in 1947. This division of the coverage area into smaller areas, each one with its own base station operating at a different carrier frequency allowed for a substantial increase of the capacity of mobile networks. The first cellular-based mobile communication systems, namely first generation (1G), arrived in the 1980s. There were several independently developed systems based on analog technology, such as Analogue Mobile Phone System (AMPS) in America, Total Access Communication System (TACS) and Nordic Mobile Telephone (NMT) in some parts of Europe as well as Japanese Total Access Communication System (J-TACS) for Japan and Hong-Kong.

The second generation (2G) was inaugurated by the highly-successful technology Global System for Mobile Communications (GSM), which was digital. Being developed with a collaborative spirit, GSM soon became a robust, inter-operable and widely-adopted standard. The high penetration of GSM provided a revolution in personal communications, first by voice and text messaging, and later on by more advanced data services. This ubiquitous availability of mobile communications motivated the research and development of new mobile communications systems with increased capabilities.

Three main organizations have been developing standards according to the International

Mobile Telecommunications (IMT) requirements (see Fig. 2.2). The dominant standards development group, namely the 3rd Generation Partnership Project (3GPP), promoted technologies for three main generations: the family GSM/General Packet Radio Service (GPRS)/Enhanced Data Rates for Global system for mobile communications Evolution (EDGE) for the 2G; Universal Mobile Telecommunications System (UMTS) for the third generation (3G) and LTE for the fourth generation (4G). The radio access technology of LTE was designed with the aim of providing all services on a packet-switched basis for the first time. Furthermore, the non-radio aspects of the complete system were also noticeable evolved, under the term System Architecture Evolution (SAE), which includes the Evolved Packet Core (EPC) network. The combination of LTE and SAE form the Evolved Packet System (EPS), in which both the core network and the radio access are packet-switched.

On the other hand, CDMA2000 was developed taking the American IS-95 as a basis by the 3rd Generation Partnership Project 2 (3GPP2), constituting the first Code-Division Multiple Access (CDMA)-based mobile cellular communication system, and it was mainly deployed in USA, Japan and Korea. Extension to data-oriented systems was provided by means of EVolution-Data Optimized (EV-DO). Finally, the third organization developing standards was the Institute of Electrical and Electronics Engineers (IEEE), who standardized Worldwide Interoperability for Microwave Access (WiMAX), first as a technology for fixed access and then extended to the so-called Mobile WiMAX.

LTE requirements and targets for the Release 8 were established with the aim of ensuring competitiveness over a ten-year time-frame. Such requirements can be summarized as follows [STB11]:

- Reduced delays, in terms of both connection establishment and transmission latency;
- Increased user data rates;
- Inceased cell-edge bit-rate for uniformity of service provisioning;
- Reduced cost per bit by improving spectral efficiency;
- Greater flexibility of spectrum usage for both new and pre-existing frequency bands;
- Simplified network architecture;
- Seamless mobility between possibly different radio-access technologies; and
- Reasonable power consumption for the mobile terminals.

It is worth noting that network operator requirements for next generation mobile systems were also formulated by the Next Generation Mobile Networks (NGMN) alliance of network operators [NGM06]. Taking into account that LTE is designed from an all-IP basis, a particular challenge arises in relation to voice communications, due to their inherent tight delay constraints. On the other hand, according to the LTE specification, supporting communications with mobile units moving at speeds of up to $350\,$km/h, or even $500\,$km/h depending on the frequency band, is required. This requirement impacts not only on the physical layer, but

also on higher ones, as for example frequent handover between cells have to be feasible without interruption (i.e., with imperceptible delay and packet loss for voice calls and reliable transmission for data services).

Other relevant aspect of LTE is the flexibility regarding inter-operation with other radio access technologies. In particular, the EPC allows for inter-operation with GSM, EDGE, Universal mobile telecommunications system Terrestrial Radio Access Network (UTRAN), WiFi, CDMA2000 and WiMAX, among others.

In order to fulfill the aforementioned requirements, several advances regarding the radio technology were considered, being the most remarkable:

- Use of multicarrier technology;
- Employment of multiple antenna schemes; and
- Definition of a packet-switched radio interface.

Each of them will be briefly analyzed below.

2.4.1 Multicarrier technology

The choice of a multicarrier technology scheme was one of the major design decisions. A unified review of waveform design options for multicarrier schemes can be found in [SGA14]. Specifically, Orthogonal Frequency-Division Multiple Access (OFDMA) was selected for the LTE downlink, whereas Single Carrier Frequency-Division Multiple Access (SC-FDMA) was the final choice regarding the uplink.

The basis of Orthogonal Frequency-Division Multiplexing (OFDM) relies on splitting the full available bandwidth into different narrower and orthogonal subcarriers. OFDM has been extensively adopted by distinct technologies over the pass few years, due to several reasons:

- **Robustness against time-dispersive channels**: mainly due to the division of the full bandwidth into several narrow channels and the mitigation of Inter-Symbol Interference (ISI) by employing a Cyclic Prefix (CP);
- **Low complexity receivers**: equalization can be performed directly on the frequency domain; and
- **Convenient for broadcast networks**: signals from multiple transmitters can be easily combined.

OFDMA is a natural extension which exploits the flexibility brought by OFDM for sharing the spectrum among multiple users in several ways, such as:

- Configuration of the desired bandwidth without requiring to change any fundamental system parameter;
- Flexible-bandwidth resources can be allocated and scheduled freely in the frequency domain; and

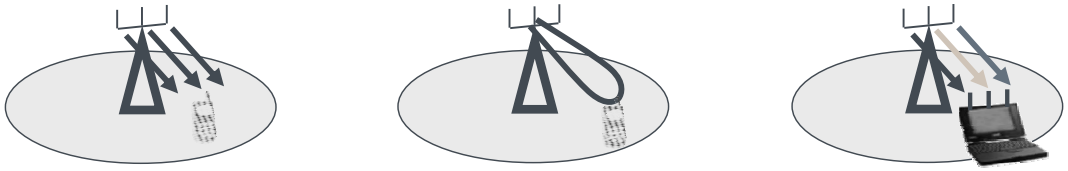

(a) (b) (c)

Figure 2.3: Three fundamental benefits of multiple antennas: *(a)* diversity gain, *(b)* array gain, and *(c)* spatial multiplexing gain. Adapted from [STB11].

- Simplified interference coordination schemes between cells are possible.

However, a well-known disadvantage of OFDM is a high Peak-to-Average Power Ratio (PAPR), which requires highly-linear (and hence costly) amplifiers. This was the main reason to avoid using OFDM for the LTE uplink, where the required power consumption and cost has to be kept under reasonable levels. In turn, SC-FDMA provides some of the main advantages of OFDMA, such as the flexibility in the frequency domain and mitigation of the ISI, whereas the PAPR is reduced significantly.

Furthermore, it is worth noting that the introduction of the CP, which allows for mitigating the ISI, is known to be a suboptimal solution under doubly dispersive channels since this approach does not treat the time and frequency dimensions equally [SGA14; KM98]. More appropriate proposals for doubly dispersive channels are described in Section 2.6.

2.4.2 Multiple Antenna Technologies

In theory, the achievable spectral efficiency scales linearly with the number of transmit and receive antennas being used in suitable radio propagation environments. The main fundamental ways to increase the spectral efficiency by means of Multiple-Input Multiple-Output (MIMO) techniques are:

- **Diversity gain**: improve the robustness against multipath fading channels by exploiting the spatial diversity provided by several antennas (see Fig. 2.3a);
- **Array gain**: serve users located at different positions by employing beamforming techniques (see Fig. 2.3b); and
- **Spatial multiplexing**: simultaneous transmission of different data streams to a single user on multiple spatial layers created by combinations of the available transmit and receive antennas (see Fig. 2.3c).

2.4.3 Packet-Switched Radio Interface

LTE has been designed from an all-IP basis. With the aim of improving the system latency, LTE considers packets having a time-duration of 1 ms. This is also convenient to cope with fast

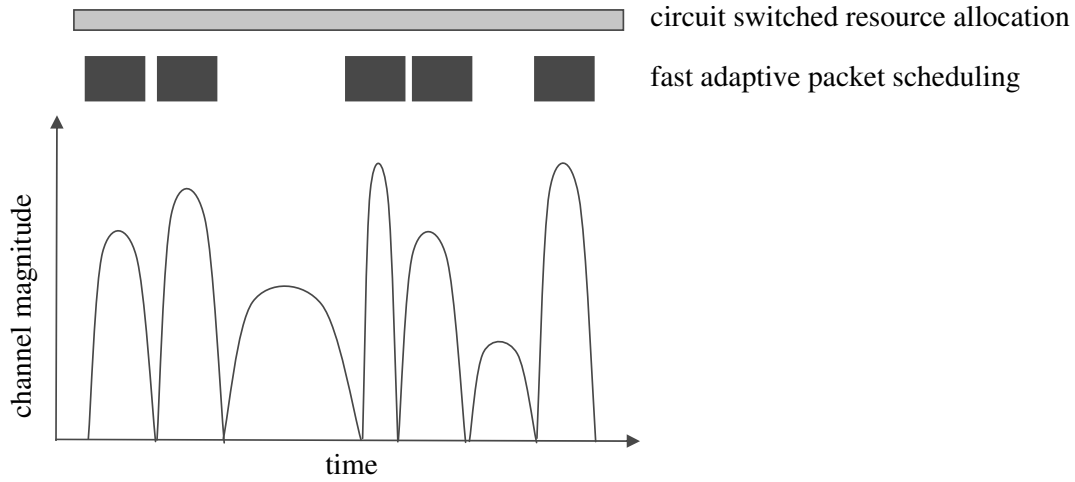

Figure 2.4: Fast scheduling and link adaptation. Adapted from [STB11].

fading channels, since the duration of the transmissions can be better adapted to the channel coherence time (see Fig. 2.4). Hence, Medium Access Control (MAC) and physical layers were jointly optimized in LTE, and the following techniques were considered:

- Adaptive scheduling in both the frequency and spatial dimensions;
- Adaptive MIMO configuration (e.g., selection of the number of spatial layers transmitted simultaneously);
- Adaptive modulation and coding schemes; and
- Fast channel state reporting.

Since LTE Rel. 10, all the requirements set by the ITU Radiocommunication Sector (ITU-R) for the IMT-Advanced designation [ITU09b] are fully satisfied and even exceeded in several aspects. This cause LTE-Advanced started to be envisaged. Some of the new characteristics with respect to previous versions of the specification are the carrier aggregation, which enables the total bandwidth to increase up to 100 MHz, as well as improved spectral efficiencies both for the downlink and the uplink. However, the most relevant features for our proposals are the support for relaying schemes and enhanced inter-cell interference coordination. This opens the door to introduce relaying schemes on trains where femtocells are deployed at the train and the passengers access to the network through them.

2.5 Specific characteristics of Railway Communications

When LTE is proposed as a basis technology for the support of train communications, both the specific operational and functional requirements for this environment, as well as the particularities of the signal propagation, must be taken into account.

In [Lam+12; Fra+15] we studied the operational requirements as well as the typical services established for railway communications and we analyzed the viability of LTE to support such

services. In [Rod+12] we analyze the security-related aspects of LTE for its application to the railway environment. Recall that GSM-R is in charge of the train control signaling and safety-related communications, hence the Quality of Service (QoS) must be satisfied with testability, controllability, reliability, effectiveness, maintainability, safety and security [10]. Operational and functional requirements impose stringent constraints on the underlying network technology such as reduced delay times or call setup times, as well as very reduced service interruptions.

On the other hand, knowledge of the wireless channel characteristics is the fundamental basis for the planning of wireless communication networks and the design of transceivers [Ai+14]. Several radio channel models have been proposed for moving radio interfaces, such as the International Telecommunication Union (ITU) channel models [ITU97], which include a vehicular radio environment (no high speed propagation conditions) and were used at the development of the Third Generation radio access systems, as well as the definition of the propagation conditions in the specifications of UMTS. The first channel model for high-speed train scenarios was proposed by Siemens in 2005 [Sie05]. More recent proposals are the WINNER Phase II model (high-speed moving networks were included in [Kyo+07]) and the radio channel models approved by the ITU-R for the evaluation of IMT-Advanced Technologies (high-speed train scenarios were explicitly considered in [ITU09a]), such as LTE-Advanced (LTE-A). However, only a few results based on empirically obtained data which can validate the aforementioned channel models are available. One example of high-speed train channel modeling contributions based on the results obtained by means of measurement campaigns is the propagation path-loss model proposed in [Wei+10a]. The same experimental results were also used for the definition of the large-scale model proposed in [GZA11]. An efficient channel sounding method for high-speed train scenarios using cellular communication systems is proposed in [Liu+12b] by considering Wideband Code-Division Multiple Access (WCDMA) signals.

However, HST communications demand for the evaluation of specific scenarios which are typical in most railway lines, such as:

- **Rural Macro Cell**: it happens when the train goes over an open space in a rural area with large cells and direct Line-of-Sight (LoS), whereas the height of the antennas is much larger than that of the surrounding elements. Several measurement campaigns were carried out to model such scenario [Kyo+07; Par+08].
- **Hilly Terrain**: a high density of scattering objects appears non-uniformly distributed, leading to more selective channels in the frequency domain than the previous scenario. Again, the LoS condition is dominant and the height of the antennas is much higher than that of the obstacles. Several measurement-based analyses have been carried out to characterize the hilly terrain scenario. Among them, in [Lua+13] the authors make use of the so-called high-resolution Subspace-Alternating Generalized Expectation-Maximization (SAGE) algorithm to analyze the statistical fading properties of the

wireless channel. Path loss, shadowing fading as well as the K-factor were modeled based on a measurement campaign in a passenger-dedicated line in China [Lua+13].

- **Viaducts**: this is the most common scenario for HST. On average, they make up 40% for a typical railway line [Ai+14; He+13e; Ai11]. The viaduct scenario features low-scattering from nearby elements, and the height of the viaduct and the base station help to get a very strong LoS component. Many papers in the literature the experimental modeling of this scenario [HZA10; LZA10; He+11b; Liu+12a]. The path loss, as well as the standard deviation of shadowing, have been analyzed in [Wei+10b] when the viaducts are located in different areas such as suburban, open, mountain or urban. The small-scale fading is studied in [He+11b], as well as the K-factor, Doppler frequency and delay spread. On average, typical height for a viaduct is between 10 and $30\,\mathrm{m}$, whereas the Base Station (BS) antennas are usually deployed at a distance between 10 or $20\,\mathrm{m}$ from the tracks, and about between 20 and $30\,\mathrm{m}$ higher than the train antennas [He+13e; Ai11; He+11b]. The propagation channel has been found to be greatly influenced by the viaduct height [He+11b]. Moreover, it has been found that the path loss increases with the height of the viaduct. This is because a higher viaduct leads to fewer reflected and scattered components, hence reducing the received power [He+13e; Ai+14]. Furthermore, path loss results predicted by the Hata model [Hat80] as well as the WINNER model (D2a scenario) [Kyo+07] are found to be not accurate with respect to the results obtained by measurements [He+13e].
- **Cuttings**: also known as a canyon or an U-shapped cutting, a cutting is the typical environment in which a train moves between high walls [He+13a], usually with similar heights and slopes [He+13b]. Even though the LoS component is still observed, it is not as dominant as in the previous scenarios. Furthermore, the steep walls at both sides affect the transmission of the signals, adding more scattering components. The propagation conditions as well as the fading characteristics of canyons are respectively analyzed in [He+11a; LZB11]. Lower and upper widths of the cutting, as well as its height, were found to be very influential on the radio wave propagation [He+13c; He+11a]. However, systematic research on the height dependence with sufficient number of samples to give statistically significant results is still a pending task [Ai+14].
- **Tunnels**: they exhibit a waveguide effect on the transmitted signals. Several measurements were carried out to analyze the behavior of the wireless channel in tunnels, e.g. [BCA07; AGV98; CZW96], as well as our contribution [Zha+16b]. Whereas the direct component is the main contribution to the received signal when the receiver is close to the transmitter. With the increase of the distance between the transmitter and the receiver, the influence of the direct ray becomes negligible and the most important contribution is that of the reflections. This leads to a special characteristic of delay

distribution named Far Line-of-Sight (FLoS) [HZB11]. Presence of stations also affect the delay characteristic inside the tunnel, as found in [He+13d], after a measurement campaign carried out at the subway of Madrid which shows the enlargement of the delay dispersion when the train is close to the station. Regarding the cases where the transmitter and receiver are close to each other, it has been found in [Gua+12] that for relatively small-sized users (pedestrian or small vehicles), the free-space propagation mechanism seems to be a good approximation, while the waveguide propagation model fits well at larger distances. However, for large-sized users (e.g., a train), short-distance communications fit well with the so-called near shadowing propagation mechanism [Gua+13a] followed by an area where the free-space propagation mechanism suits well under some assumptions, while the waveguide propagation model fits well for larger distances. It is also found that the near-region phenomenon inside tunnels lengthens considerably with the increase of working frequencies [Gua+13b]. As stated in [Ai+14], although electromagnetic wave transmission inside tunnels is a widely studied topic in the literature, there are still unsolved problems, such as *(1)* multimode waveguide propagation mechanisms and *(2)* determination of the breakpoint for different propagation mechanisms inside tunnels. Furthermore, almost all channel models derived from measurements are too specific for the actual considered tunnel and hence not applicable to others. Generic channel models for typical tunnels are still not available.

- **Crossing Bridges**: Crossing bridges are usually built over the cuttings to allow for pedestrian crossing. The crossing bridge leads to a Non-Line-of-Sight (NLoS) propagation within a short distance, which increases the path loss [Gua+14], whereas the small-scale fading is not severely affected by the presence of crossing bridges [He+12a].

Based on actual measurements [He+12b; Gua+14], it can be seen that these scenarios may cause deep fading of the signals being transmitted. Moreover, obstacles like railway auxiliary architectonic elements along the tracks (e.g. acoustic barriers or arched grids) and, more important, other train blockages, may increase the path loss level due to obstruction, reflection, diffraction or scattering of the signals.

Furthermore, very high speeds above 300 km/h bring new challenges for the channel modeling. Even for highway channel modeling with speeds up to 200 km/h, the transmission channel is usually assumed to be Wide-Sense Stationary Uncorrelated Scattering (WSSUS). However, for trains moving faster than 300 km/h, rapidly time-varying and non-stationary features of the wireless channel arise [Ai+14]. Moreover, most of the aforementioned HST scenarios have a strong LoS component, whereas the number of scatterers and obstacles is limited. Hence, the spatial correlation between different multipath elements can be large, resulting in the correlated scattering. Bo Ai *et al.* show this effect in [Ai+14] by means of simulations. Fig. 2.5 shows how the channel varies quickly and randomly within a LTE subframe (1 ms long).

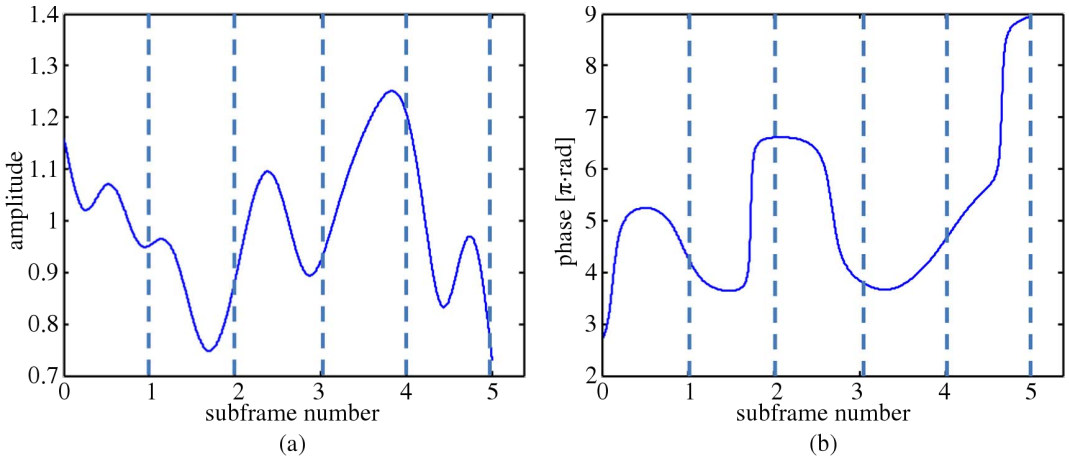

Figure 2.5: Channel variation versus LTE subframe (1 ms long) index. Adapted from [Ai+14].

High mobility also introduces high Doppler frequency shifts and spreads. Moreover, fast variation of the multipath structure occurs when the train moves between different typical HST environments, which can cause time-varying Doppler shifts superimposed on each multipath component [Ai+14].

Frequent handover may also happen, which could result in drop calls or the interruption of reliable transmission of the control signals.

2.6 Future communication networks. Extension to 5G

Communication systems have experienced a very remarkable growth over the past few decades. Day by day users become more demanding regarding the performance and services provided by means of wireless communication systems. More and more data rate and availability is required, and thus communication standards are continuously evolving to give the technological support to the users' wishes. Hence, from the beginning of this study until now, LTE standard evolved and new versions were released. Moreover, the new generation of communication systems, the so-called 5G, is currently under definition. With the aim of drastically increasing the value of this work and check the validity of the findings regarding the latest advances in communication systems, proposals for 5G communication systems have been also considered in this work.

One of the most remarkable proposals for the definition of 5G is the utilization of Filter Bank Multicarrier (FBMC) modulations instead of the well-known OFDM. In the ensuing paragraphs the most important advantages offered by FBMC with respect to OFDM for the railway environment are emphasized:

- FBMC offers a higher bandwidth efficiency, which is very beneficial since the simultaneous communications between different trains can be more efficiently allocated into the scarce spectrum available in railway environments.
- Co-existence between the current GSM-R and the new broadband systems is a major

concern in railway industry. OFDM-based systems usually exhibit a high co-channel interference, leading to a potential performance impact on current GSM-R systems. FBMC-based systems are much more efficient in this sense, thus allowing for better co-existence with current systems such as GSM-R.

- While OFDMA is adequate for efficiently allocating a subset of subcarriers per user in the downlink, the situation is different in the uplink because the users' signals must arrive at the Evolved NodeB (eNodeB) synchronously, both in terms of symbol timing and carrier frequency. For a practical deployment, a close-to-perfect carrier synchronization is necessary [Far11], which is affordable in an stationary network, but becomes a very difficult task –if not impossible– in a network including mobile nodes. Morelli *et al.* [MKP07] studied this in detail and concluded that the best way of facing this problem is through the use of a bank of filters to separate the users. However, due to the use of close-to-perfect subcarrier filters, FBMC avoids multiple-access interference without requiring sophisticated synchronization methods, since the subcarriers are well frequency-localized.
- Finally, one of the most important differences between OFDM and FBMC waveforms is their behavior under doubly dispersive channels, like the ones present in HST communications. The design of the prototype filter must achieve a compromise between the channel response spreading in time (multipath effect) and in frequency (due to the Doppler shift in different multipaths) [Far11]. In this sense, since OFDM is defined by means of a rectangular window in time, each OFDM symbol appears unbounded in the frequency domain, hence becoming a poor choice for doubly selective channels. According to several studies (see [FAB95; Ala01; HB97; SB03; Ami+10]), FBMC waveforms perform much better for doubly selective channels with respect to OFDM because such prototype filters can be designed specifically for minimizing both time and frequency dispersion.

However, it must be noticed that channel estimation is more challenging in most FBMC schemes with respect to FBMC. Whereas in OFDM the orthogonality of the symbols enables to estimate the channel in a simple way by inserting scattered pilots among the data, generally one can only assume real orthogonality (i.e., only the real part of the symbols fulfills the orthogonality condition) for FBMC schemes, preventing the channel to be estimated directly from a grid of pilots. To overcome this problem. several channel estimation methods are being proposed in the literature, such as [JLR03; Sti+10; Cui+15].

Finally, whereas OFDM offers full flexibility regarding MIMO structures, FBMC can only be used in certan MIMO schemes. Only schemes such as Filtered MultiTone (FMT) offer the same flexibility as OFDM, but FMT suffers from the same bandwidth loss as OFDM [Far11]. Alternatives to FBMC such as Generalized FDM (GFDM) [FKB09; al14] and Filtered OFDM (fOFDM) [Zha+15] are also being considered as candidates for 5G systems.

Chapter 3

High Speed Emulation

Long Term Evolution (LTE) is expected to substitute the Global System for Mobile Communications (GSM) as the radio access technology for railway communications. Recently, considerable attention has been devoted to high-speed trains since this particular environment poses challenging problems in terms of performance simulation and measurement. In order to considerably decrease the cost and complexity of high-speed measurement campaigns, a technique to induce effects caused by highly-time varying channels on Orthogonal Frequency-Division Multiplexing (OFDM) signals while conducting measurements at low speeds is proposed. In this chapter, the performance of this technique is illustrated by comparing the results of LTE measurements at different velocities in a controlled measurement environment. Additionally, the technique is validated by means of simulations considering one of the scenarios defined as part of the Winner Phase II Channel Models and specifically designed for high-speed train scenarios. The proposed technique is used to assess the performance of LTE for high-speed train scenarios up to 600 km/h. To accomplish this, we use both the controlled high-speed measurement setup as well as a channel model developed according to the guidelines of the ITU Radiocommunication Sector (ITU-R) for the evaluation of radio interface technologies for IMT-Advanced systems. Once the high-speed emulation technique is introduced and evaluated, as well as its main drawbacks pointed out, some alternative techniques under study are also presented.

Section 3.1 provides the motivation of this chapter, whereas Section 3.2 introduces the aforementioned technique for high speed emulation. Section 3.3 describes the evaluation environment and procedure both for measurements and simulations. Section 3.4 introduces the different figures of merit considered for the evaluations and Section 3.5 includes all the results of the performed experiments. Finally, Section 3.6 proposes and analyzes some alternatives to the technique of high speed emulation by interpolation and Section 3.7 is devoted to the conclusions of this chapter.

This chapter is mainly based on the following co-authored publications:

- José Rodríguez-Piñeiro, Martin Lerch, José A. García-Naya, Sebastian Caban, Markus Rupp, and Luis Castedo. **Emulating Extreme Velocities of Mobile LTE Receivers in the Downlink**. In: *EURASIP Journal on Wireless Communications and Networking* 2015.106 (Apr. 2015). Special Issue on Experimental Evaluation in Wireless Communications. Online access: http://dx.doi.org/10.1186/s13638-015-0343-0

- José Rodríguez-Piñeiro, Martin Lerch, Pedro Suárez-Casal, José A. García-Naya, Sebastian Caban, Markus Rupp, and Luis Castedo. **LTE Downlink Performance in High Speed Trains**. In: *2015 IEEE 81st Vehicular Technology Conference (VTC2015-Spring)*. Glasgow, United Kingdom, May 2015

- José Rodríguez-Piñeiro, Pedro Suárez-Casal, José A. García-Naya, Luis Castedo, César Briso-Rodríguez, and J. Ignacio Alonso-Montes. **Experimental Validation of ICI-Aware OFDM Receivers under Time-Varying Conditions**. In: *Eighth IEEE Sensor Array and Multichannel Signal Processing Workshop*. Online access: http://dx.doi.org/10.1109/SAM.2014.6882411. A Coruña, Spain, June 2014, pp. 341–344

- Martin Lerch, José Rodríguez-Piñeiro, José A. García-Naya, and Luis Castedo. **Methods to Perform High Velocity LTE Experiments at Low Velocities**. In: *2016 IEEE 83rd Vehicular Technology Conference (VTC2016-Spring)*. Nanjing, China, May 2016

- José Rodríguez-Piñeiro, Pedro Suárez-Casal, Tomás Domínguez-Bolaño, José A. García-Naya, and Luis Castedo. **Emulation of High Mobility Scenarios in Wireless Broadband OFDM Communications**. In: *Submitted to the IEEE Transactions on Vehicular Technology.* (2016)

3.1 Introduction

Over the last few years, broadband communication between nodes moving at high speeds has attracted special attention. One of the most relevant research topics in this field is the modeling of the High-Speed Train (HST) channel. Nowadays, the most widely used communication system between trains and the elements involved in operation, control, and intercommunication within the railway infrastructure is based on the GSM. This technology, namely the GSM for Railways (GSM-R), is not well-suited for supporting advanced services such as automatic pilot applications or provisioning broadband services to the train staff and passengers. Besides trains, the increasing number of broadband services available for mobile devices motivated the migration from third-generation mobile networks to fourth generation ones, mainly LTE. Therefore, LTE seems to be a good candidate to substitute the GSM as the fundamental technology for railway communications.

Several radio channel models have been proposed for moving radio interfaces and, more specifically, for the high speed train scenario. An overview of them can be found in Section 2.5. In such a section the need for more channel model research based on measurement campaigns in the real high speed train environment was also motivated. Moreover, only a few results based on empirically obtained data can actually validate most of the proposed channel models. One of the reasons that explains the low number of measurement campaigns in high-speed environments is their complexity and cost. Furthermore, it is not possible, in most cases, to measure at high speeds in controlled environments in a reproducible and repeatable way. In addition, measuring in high-speed trains demands for specific hardware and software solutions (see [Rod+13a]). In order to address those problems, a technique to induce the effects caused by highly time-varying channels in OFDM signals while conducting the measurements at much lower speeds [Rod+14] is proposed in this chapter. This technique consists basically in reducing the subcarrier spacing of the OFDM signal by scaling down the bandwidth of the whole OFDM signal. More specifically, we propose to interpolate the transmit OFDM signal in the time domain before its transmission. The time-interpolated signal still conveys exactly the same information as the original one but with a reduced subcarrier spacing, thus artificially increasing the sensitivity to the Inter-Carrier Interference (ICI). For example, if we time-interpolate the transmit OFDM signal by a factor I, the subcarrier spacing will be reduced by the same factor I, which is similar to what would happen if transmissions were conducted at I times the original speed.

This novel methodology was used for evaluating the performance of multicarrier transmissions in different real-world scenarios affected by large Doppler spreads while conducting the measurements at low speeds (see Section 4.3). Among these scenarios, we consider:

- Measurements carried out by using a car (see [Rod+14; Suá+14b; Suá+14a; Fei+16; Rod+16a]);
- Measurements carried out in a subway tunnel (see [Zha+16b]).

When conducting measurements with movement in realistic environments and using off-the-shelf vehicles (e.g. cars, trains) the repeatability of the results is basically lost because the following issues arise:

- It is extremely difficult to keep the vehicle speed constant during the measurements.
- Reaching high speed values with experimental user equipment is expensive and sometimes even not possible in realistic environments.
- Impacts from measurement control can always arise (e.g., another vehicle driving nearby) leading to non-repeatable results.
- Modifications in the measurement scenarios (e.g., the path of the road is modified, a huge vehicle is parked close to the measurement path) hinder fair comparisons with future measurements.

- It is quite challenging to drive several times along exactly the same path.

The assessment is performed employing a setup that allows for repeatable measurements at different speeds up to 200 km/h. This allows for validating the technique of high speed emulation while, at the same time, we overcome all the above-mentioned issues found when conducting non-repeatable measurements using off-the-shelf vehicles. LTE was considered as the wireless communication standard for the measurements. The setup consists in an antenna that is rotated around a central pivot at a constant speed [S C+14; CRG11a], allowing for validating our previously proposed technique under repeatable and controlled conditions.

The validation is completed by means of simulations considering a channel model suited for high speed train scenarios. More specifically, the channel model associated with the D2a link of the D2 scenario of the Winner Phase II Channel Models [Kyo+07] is considered. Notice that the aim is not to model the measurement environment using a channel model existing in the literature. Conversely, the main deal is to prove the validity of the results in a perfectly repeatable (and controlled) environment widely accepted for simulating high-speed train conditions. Therefore, measurement and simulation scenarios correspond to very different wireless communication environments since the simulations consider a rural macro-cell with Line-of-Sight (LoS) between the transmitter and the receiver, while an outdoor-to-indoor communication without LoS is considered for the measurements.

The presented results, obtained under repeatable conditions through measurements and simulations, show that the proposed technique induces highly time-varying channels with excellent agreement.

Finally, the high speed emulation technique is used to show the performance of LTE for high-speed train scenarios. To accomplish this, both the controlled high-speed measurement setup as well as a channel model developed according to the guidelines of the ITU-R for the evaluation of radio interface technologies for IMT-Advanced systems are considered.

3.2 Emulating High Speeds by Time Interpolation

Let us consider an OFDM modulation where N subcarriers are multiplexed to construct each OFDM symbol. OFDM symbols are cyclically extended by adding N_g samples, thus having a total length of $N_t = N + N_g$ samples. Accordingly, the k-th OFDM symbol can be represented as

$$\mathbf{s}_k = \mathbf{G}_1 \mathbf{F}^H \mathbf{x}_k, \tag{3.1}$$

where $\mathbf{x}_k$ is a $N \times 1$ vector containing the constellation symbols corresponding to the transmitted subcarriers in the k-th symbol, $\mathbf{F}$ is the standard $N \times N$ DFT matrix, $\mathbf{G}_1$ is a $N_t \times N$ matrix which cyclically extends the OFDM symbol, and $\mathbf{s}_k$ is a $N_t \times 1$ vector with the transmitted OFDM symbol in the time domain. This signal is transmitted at a sampling period T_s, hence

creating symbols with a duration $T_t = T_s N_t$ and a bandwidth $F_s = 1/T_s$. When transmitting $\mathbf{s}_k$ over a time-varying channel, and assuming a sufficiently long cyclic prefix, the received signal is [WG00]

$$\mathbf{r}_k = \mathbf{F}\mathbf{G}_2(\mathbf{H}_k^{(t)}\mathbf{G}_1\mathbf{F}^H\mathbf{x}_k + \mathbf{n}_k) = \mathbf{H}_k\mathbf{x}_k + \mathbf{w}_k, \tag{3.2}$$

where $\mathbf{H}_k^{(t)}$ is a $N_t \times N_t$ matrix with the time-varying channel impulse response experienced by $\mathbf{s}_k$, $\mathbf{G}_2$ is a $N \times N_t$ matrix to remove the cyclic prefix, $\mathbf{n}_k$ is a $N_t \times 1$ vector with uncorrelated complex-valued white Gaussian noise entries with power σ_n^2, $\mathbf{H}_k$ is a $N \times N$ matrix with the channel frequency response, and $\mathbf{w}_k$ is a $N \times 1$ vector containing uncorrelated complex-valued white Gaussian noise entries with variance σ_w^2.

If the channel is time invariant, $\mathbf{H}_k$ will be a diagonal matrix. In time-selective channels, however, non-zero entries will appear outside the main diagonal of $\mathbf{H}_k$ and ICI arises in the received signal. The amount of ICI relates to the normalized Doppler spread of the channel, which is given by $D_n = \nu T$, ν being the maximum Doppler frequency and $T = T_s N$ the duration of the OFDM symbol excluding the cyclic prefix. As proposed originally in [Rod+14], parameter T can be adjusted by time interpolation by a factor I, yielding an OFDM symbol duration $T^I = IT_sN$. Therefore, given the actual velocity v of the mobile receiver, the normalized Doppler spread, impacting the time-interpolated OFDM signal can be written as

$$D_n^I = \nu T^I = \nu I T_s N = \frac{T_s N I f_c v}{c_0} = \frac{T_s N f_c}{c_0} v^I, \tag{3.3}$$

with f_c the carrier frequency, $c_0 = 3 \cdot 10^8$ m/s the light speed in the open space, and $v^I = Iv$ the emulated speed as a result of an actual measurement speed v and an interpolation factor I. Consequently, enlarging the symbol length T^I by adjusting I allows for the emulation of a velocity v^I while conducting measurements at an actual speed v. Notice that this procedure is also valid for time decimation of the signal, simply taking $0 < I < 1$, leading to an emulated speed lower than the actual one. Finally, note also that I does not have to be an integer value. Fractional time interpolation and decimation factors are also possible, hence providing a great flexibility for adjusting v^I from v. Note that the statistical properties of the noise do not change by the decimation process regardless of the interpolation factor.

However, one may wonder what are the effects on the signal when it is interpolated. Fig. 3.1 shows a typical multicarrier architecture. For the case of OFDM, the pulse shaping filters at the transmitter and receiver are matched and rectangular (in time). On the other hand, the channel can be modeled as a set of M paths characterized by four parameters ν_m, a_m, α_m, and τ_m, with $m = 1, \ldots, M$, corresponding to the maximum Doppler frequency, the complex attenuation magnitude and phase, as well as the delay of the m-th channel path (see Fig. 3.2), respectively.

Based on the works of Robertson *et al.* (e.g., see [RK99b]) we can approximate the expression of the ICI energy seen by the b-th subcarrier due to the m-th path, namely $L_{b,m}$,

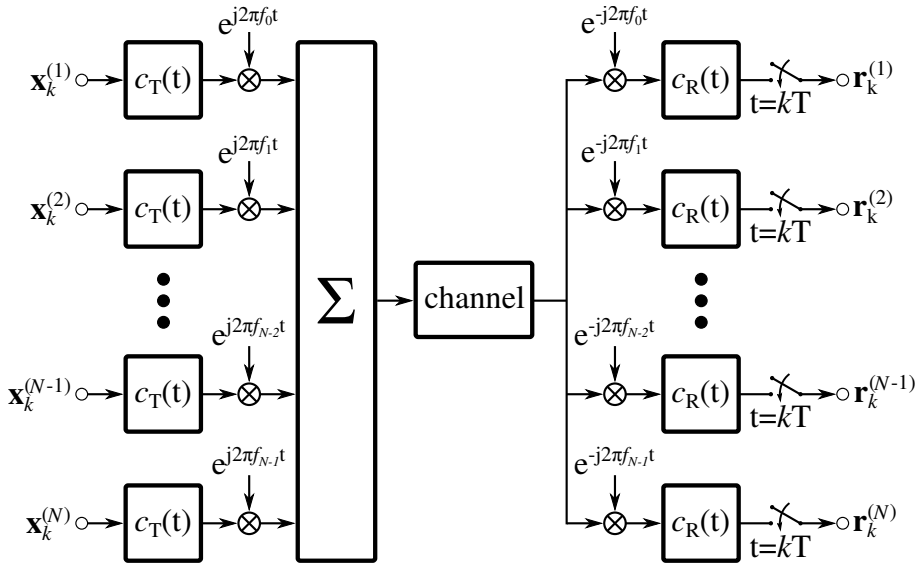

Figure 3.1: Baseband multicarrier transmission model with N subcarriers. For the OFDM case, both $c_{\mathrm{T}}(t)$ and $c_{\mathrm{R}}(t)$ are rectangular pulses.

as

$$L_{b,m}(T,v) = \sum_{\substack{i=0 \\ i\neq b}}^{N-1} a_m^2 \mathrm{sinc}^2\left(\pi T\left[f_i - f_b\right] + \pi T \nu_m(v)\right), \tag{3.4}$$

where it is clear that the second term inside the sinc $(\cdot)$ function is directly proportional to the maximum Doppler frequency of the m-th channel path, ν_m. Notice that the total ICI experienced is calculated as the sum of the individual contributions per path and per subcarrier:

$$L\left(T,v\right) = \sum_{m=1}^{M}\sum_{b=0}^{N-1} L_{b,m}\left(T,v\right). \tag{3.5}$$

Let us consider the effect of increasing the speed of the receiver in Eq. (3.4). Let us assume, without any loss of generality, that we have a static transmitter and a mobile receiver whose initial speed is v. Then

$$\nu_m\left(v\right) = \frac{v}{c_0} f_b \cos\left(\gamma_m\right) \propto \frac{v}{c_0} f_b \propto v, \tag{3.6}$$

where γ_m is the angle between the velocity vector of the mobile receiver and the direction of the incoming wave of the m-th path of the channel at the location of the mobile receiver [Mol05]. Thus, if we consider a change in the speed value so that the new speed of the receiver is $v^I = Iv$, the new maximum Doppler frequency, namely $\nu_m\left(v^I\right)$, becomes

$$\nu_m\left(v^I\right) = I\nu_m\left(v\right). \tag{3.7}$$

Applying Eq. (3.7) in Eq. (3.4), we can calculate the total ICI energy which results from all subcarriers onto the subcarrier with index b when the receiver increases its velocity by a factor

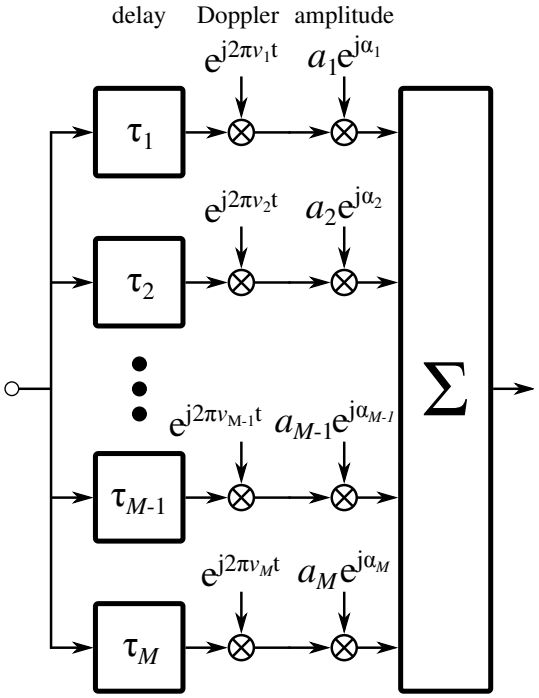

Figure 3.2: Channel model with M paths, each with a Doppler frequency ν_m, complex attenuation $a_m \exp(j\alpha_m)$ and delay τ_m, where $m = 1, \ldots, M$.

of I. Hence Eq. (3.4) becomes

$$L_{b,m}\big(T, v^I\big) = \sum_{\substack{i=0 \\ i\neq b}}^{N-1} a_m^2 \text{sinc}^2\left(\pi T\left[f_i - f_b\right] + \pi IT\nu_m\left(v\right)\right), \tag{3.8}$$

Now, if we consider the case in which the receiver speed is kept constant but the transmitted signal is time-interpolated by a factor I, we have that the new useful symbol duration for the interpolated signal is $T^I = IT$. In this case, the total ICI energy which results from all subcarriers onto the subcarrier with index b for the m-th path, namely $L_{b,m}\big(T^I, v\big)$, can be obtained from Eq. (3.4) as

$$\begin{aligned} L_{b,m}\big(T^I, v\big) &= \sum_{\substack{i=0 \\ i\neq b}}^{N-1} a_m^2 \text{sinc}^2\left(\pi T^I(f_i^I - f_b^I) + \pi T^I\nu_m\left(v\right)\right) \\ &= \sum_{\substack{i=0 \\ i\neq b}}^{N-1} a_m^2 \text{sinc}^2\left(\pi IT\frac{f_i - f_b}{I} + \pi IT\nu_m\left(v\right)\right) \\ &= \sum_{\substack{i=0 \\ i\neq b}}^{N-1} a_m^2 \text{sinc}^2\left(\pi T\left[f_i - f_b\right] + \pi IT\nu_m\left(v\right)\right), \end{aligned} \tag{3.9}$$

where $f_i^I = f_i/I$ and $f_b^I = f_b/I$ because when the signal is time-interpolated by a factor I, the subcarrier spacing is reduced by the same factor, since the total signal bandwidth also experiences such a reduction. Hence, Eq. (3.9) is equivalent to Eq. (3.8) and $L_{b,m}\big(T, v^I\big) =$

$L_{b,m}\left(T^I, v\right)$. This proves that, if the estimation of a_m, $m = 1, \ldots, M$ is accurate enough, it is feasible to recreate the ICI induced at high speeds by time-interpolation. However, although the statistical properties of the ICI hold after interpolation, this operation does affect the signal because the bandwidth is reduced by the same factor, so the experienced channel response is not the same as the original one. Indeed, the frequency response of the channel in the b-th subcarrier given a OFDM symbol period T can be expressed in terms of

$$M_b(T) \approx \sum_{m=1}^{M} a_m \mathrm{e}^{j(\alpha_m - 2\pi b \tau_m / T)}, \tag{3.10}$$

After evaluating $M_b(T^I) = M_b(IT)$, it is evident that for larger I values $M_b(TI) \approx \sum_{m=1}^{M} a_m \mathrm{e}^{j\alpha_m}$, which is a constant value independent of the subcarrier index. Hence, the frequency selectivity observed by the receiver when large I values are used will be lower, this is, the channel frequency response will be much more alike for all subcarriers. This feature must be taken into account when evaluating systems whose performance is affected by the frequency selectivity of the channel.

In order to illustrate the effects of the time-interpolation on the experienced channel response, let us take a realization of the IEEE Outdoor-to-Indoor and Pedestrian A Channel Model. Fig. 3.3(a) shows a realization of such a channel model for an LTE downlink signal having $10\,$MHz of bandwidth and $0.5\,$ms of time duration when the receiver is moving at $5\,$km/h. The same result is shown in Fig. 3.3(b) for a receiver moving at $10\,$km/h. It can be seen that the channel changes faster in the time dimension for the latter case. Note that the same seed was considered for the generation of both channels. If we time-interpolate the signal before the over-the-air transmissions, the bandwidth occupied is reduced. Fig. 3.3(c) shows the channel response when the receiver moves at $5\,$km/h and the interpolation factor is $I = 2$. It can be seen that the occupied bandwidth is halved while the transmission time is doubled. At the receiver, the signal is decimated, hence restoring the bandwidth of the original signal, as shown in Fig. 3.3(d). It can be seen that the channel varies faster in the time domain, similarly to the case of a receiver moving at $10\,$km/h (see Fig. 3.3(b)). However, the variation of the channel is reduced in the frequency dimension. More specifically, the channel seen by the receiver is similar to the central part of the channel shown in Fig. 3.3(b) stretched until it fulfills the original bandwidth. This reduces the frequency diversity of the channel whose speed is emulated through time-interpolation with respect to the channel measured at the actual speed.

According to Eq. (3.9), the results obtained by time-interpolation will be accurate as long as we are able to estimate the original Power Delay Profile (PDP) from the channel seen by the receiver. Since the frequency selectivity of the channel seen by the non-interpolated signal is increased, we may expect the proposed high speed emulation technique will lose accuracy.

Along the rest of this section we evaluate the accuracy of the technique for the ICI generation. The ICI level is measured by simulating the transmission of OFDM symbols over

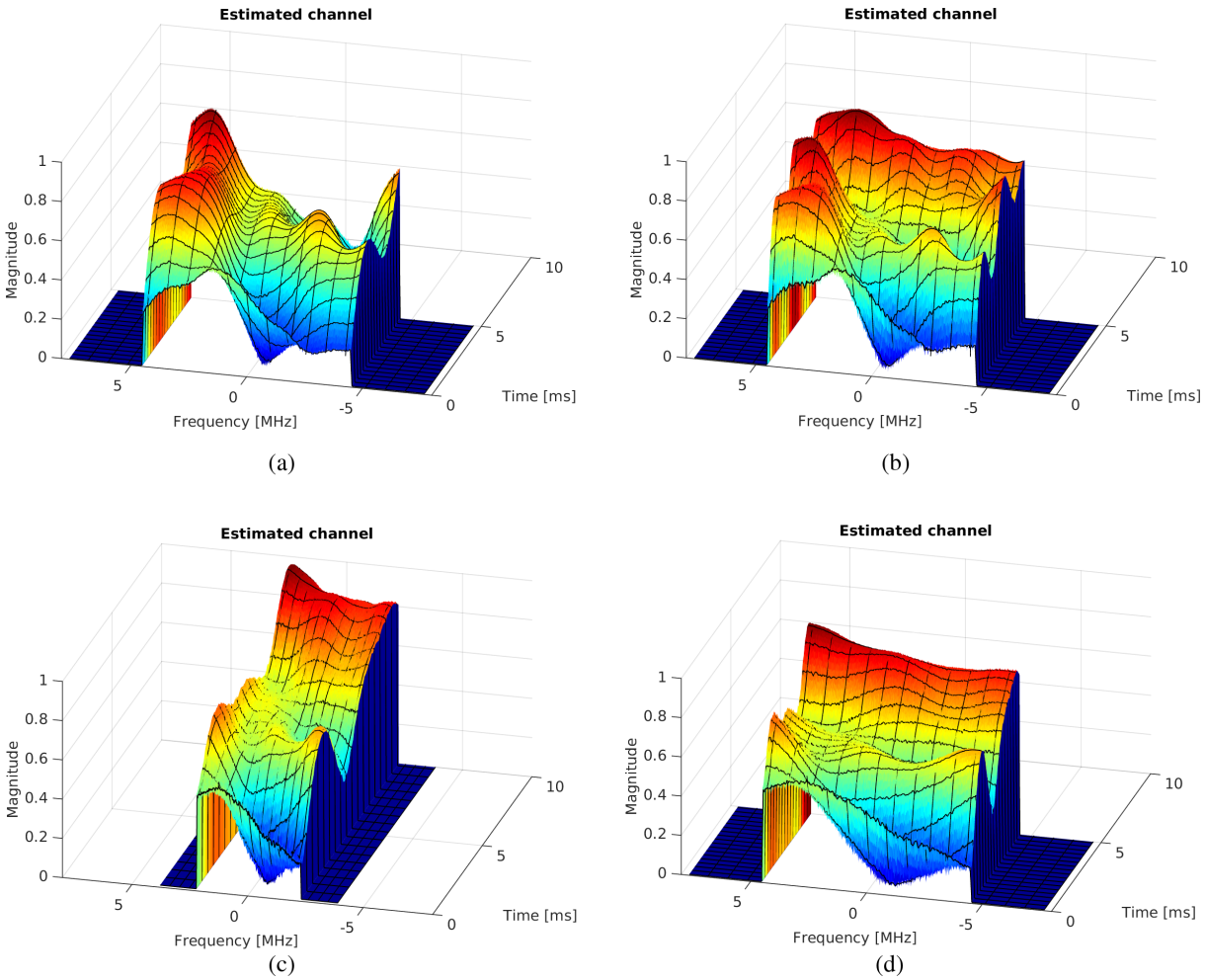

Figure 3.3: Channel response for an LTE downlink signal having 10 MHz of bandwidth and 5 ms of duration when: *(a)* the receiver moves at 5 km/h; *(b)* the receiver moves at 10 km/h; *(c)* the receiver moves at 5 km/h and the signal is interpolated by a factor $I = 2$ at the transmitter; and *(d)* the receiver moves at 5 km/h and the signal is interpolated by a factor $I = 2$ at the transmitter and decimated by the same factor at the receiver.

multipath fading channels. Then, the full frequency response matrix $\mathbf{H}_k$ from Eq. (3.2) is built, and the ICI is measured as

$$\text{ICI} = \frac{1}{N^2 - N}\left(\text{tr}\left(\mathbf{H}_k\mathbf{H}_k^H\right) - \sum_{n=1}^{N}\left|[\mathbf{H}_k]_{n,n}\right|^2\right), \tag{3.11}$$

where $[\cdot]_{i,j}$ denotes the i-th row and j-th column entry of a matrix. This expression measures the out of the main diagonal mean energy spread to neighbor subcarriers in the form of ICI.

The results were obtained using a configuration similar to that of the 10 MHz profile defined by the LTE standard. In this case, the number of subcarriers is $N = 1024$, the length of the cyclic prefix is $N_g = 72$ samples, and the carrier frequency is set to $f_c = 2.5$ GHz. Regarding the fading channels, three different standard channel models are used (exhibiting different levels of frequency selectivity): 3GPP Rural Area channel model (RAx), 3GPP Typical Urban channel

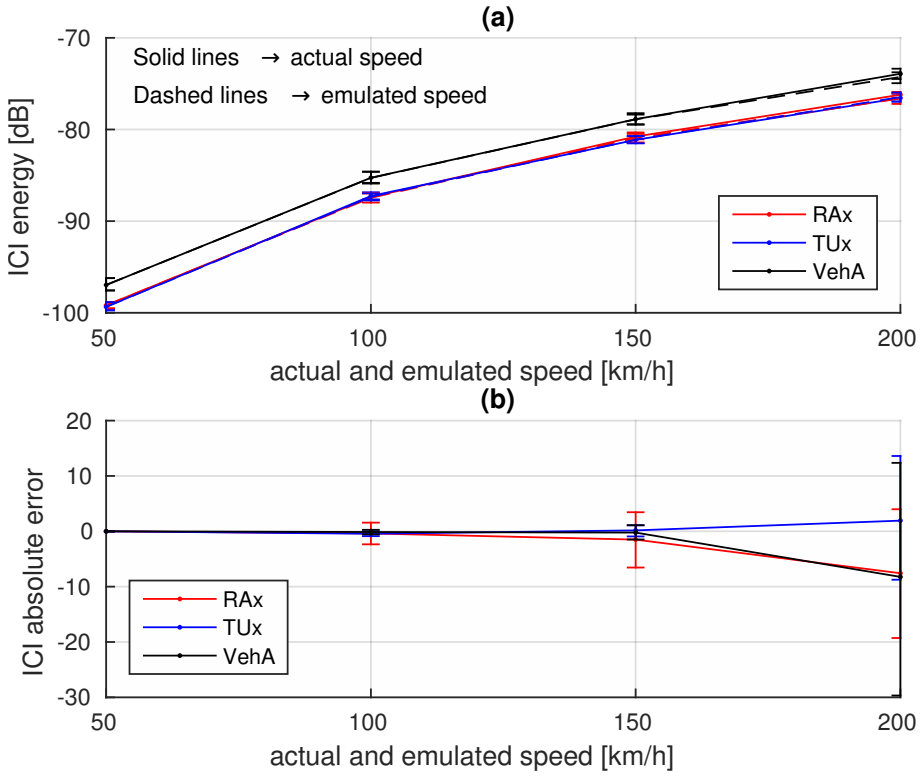

Figure 3.4: ICI values generated both by interpolating and without interpolating the signals: *(a)* Comparison of the actual ICI values with those induced by interpolating the signals; and *(b)* absolute error of the induced ICI values.

model (TUx), and Vehicular A (VehA).

Two types of results are obtained for each channel model. First, the maximum Doppler frequency ν is set to match the considered speeds $v \in \{50, 100, 150, 200\}$ km/h of the receiver by $\nu = v f_c/c$. Then, the same signal is transmitted over the same channel realization after its time interpolation by the integer factors $I \in \{1, 2, 3, 4\}$, but keeping ν as the one corresponding to the lowest speed $v = 50$ km/h.

Figure 3.4(a) shows the ICI energy versus the receiver speed calculated according to Eq. (3.11) for the three employed channel models, both considering the actual speed (solid curves) and the emulated one by time interpolation (dashed curves). The precision of the results is gauged by the 95% bootstrapping confidence intervals for the mean. It can be seen that the curves obtained using the actual speeds are well approximated by those employing time interpolation. Figure 3.4(b) shows the absolute error for the ICI energy obtained by time interpolation with respect to that of the non-interpolated case. The results show that the method is accurate enough for inducing ICI regardless of the channel frequency selectivity.

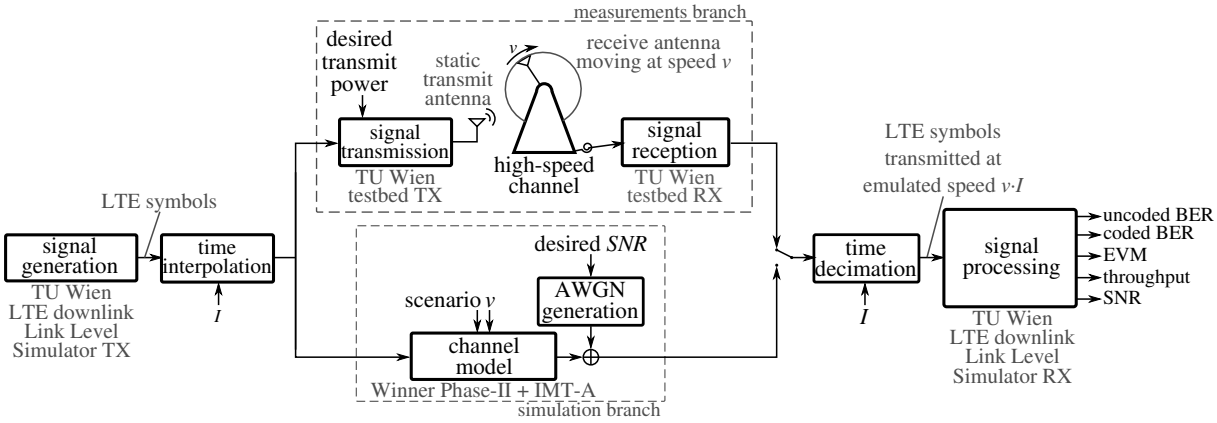

Figure 3.5: Block diagram of the considered setup.

3.3 Evaluation Setup and Procedure

Time-interpolation factors $I \geq 1$ are applied to standard-compliant downlink LTE OFDM signals before their over-the-air transmission to emulate situations with I times higher velocity than the actual receiver speed in a controlled measurement environment. The same principle is considered for the simulations.

In Section 3.3.1 the controlled measurement environment is introduced, whereas Section 3.3.2 describes the followed measurement procedure. Section 3.3.3 details the environment considered for the simulations and Section 3.3.4 the followed simulation procedure.

3.3.1 Measurement Setup

The measurement setup shown in Fig. 3.5 (measurements branch) is considered to test the proposed technique of emulating high speeds by time interpolation of OFDM signals. The setup consists of:

1. **Signal generation (transmitter side) and signal processing (receiver side)**: at the transmitter side, standard-compliant LTE subframes are generated using the LTE Downlink Link-Level Simulator developed at the Vienna University of Technology [RST16; Meh+11; tea]. At the receiver side, the same simulator is used to process the received signals and to estimate the considered figures of merit (see Section 3.4).
2. **Time interpolation and time decimation**: the signal is time-interpolated by a factor I at the transmitter and decimated by the same factor I at the receiver side. This way we emulate a Doppler spread similar to that obtained with a speed increase by a factor of I.
3. **Signal transmission and signal reception**: signals are transmitted over the air using a testbed developed at the TU Wien [Ler+14; CGR11]. The testbed transmitter is placed outdoors on a roof of a building in downtown Vienna, Austria. The receiver is placed

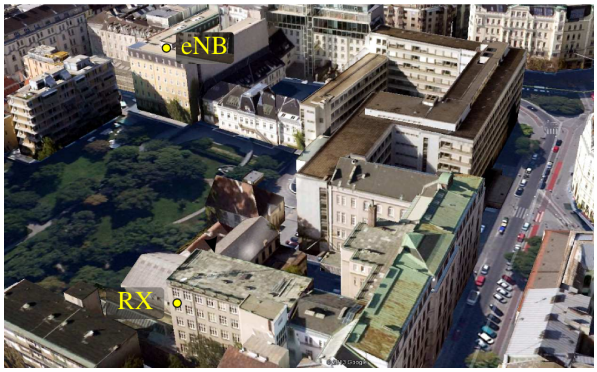

Figure 3.6: Location of the transmitter and the receiver. Note that the transmitter is installed outdoors on a roof of a building, while the receiver is placed indoors in the fifth floor of an adjacent building. The distance between transmitter and receiver is approximately 150 m.

indoors in the fifth floor of an adjacent building at a distance of 150 meters (see Fig. 3.6), hence recreating an infrastructure-to-vehicle scenario. Note that no feedback channel was used in the experiments. Consequently, no adaptive modulation and coding scheme was applied. Channel Quality Indicator (CQI) values were fixed in advance. Notice also that the testbed is equipped with a highly precise time and frequency synchronization system based on Global Positioning System (GPS)-disciplined rubidium oscillators and a custom made synchronization unit [Cab+11; S C+14]. As a result, we can assume close-to-perfect time and frequency synchronized measurements. Thus, time or frequency offsets due to imperfect synchronization can be ignored.

4. **Generation of high-speed conditions**: high-speed conditions are generated by transmitting from a static transmit antenna to a receive antenna that is rotated around a central pivot in a controlled and repeatable way [CRG11b] (see Fig. 3.7). Different channel realizations are obtained by measuring at different initial positions of the receive antenna. Note that the trajectory of the antenna is well approximated by a straight line since the diameter of the trajectory is two meters and each LTE subframe is 1 ms long (see Fig. 3.8).

In order to evaluate the impact of high-speed conditions on LTE transmissions, actual velocities ranging from 50 km/h to 200 km/h are considered. Furthermore, interpolation factors of $I = 1$ (no interpolation), $I = 2$, and $I = 3$ are used for generating Doppler spreads equivalent to those associated to velocities ranging from 50 km/h to 600 km/h. Note that it is possible to generate exactly the same Doppler spread value from different combinations of the actual velocity and the interpolation factor (see Table 3.1). This fact is considered to show that the high speed emulation technique allows for the evaluation of wireless communication systems at high speeds while measuring at much lower speeds. In order to do that, the same Doppler spread is generated by means of different velocities and interpolation factors, and the obtained results are compared. Table 3.1 shows the combinations of actual speeds and interpolation

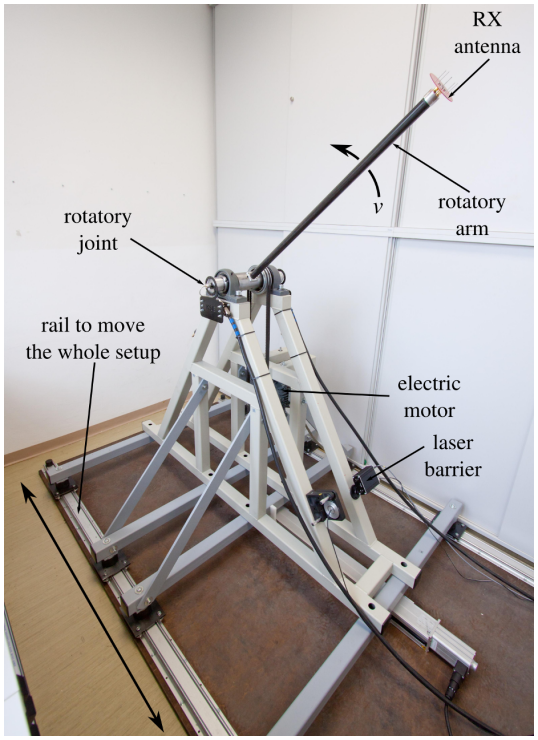

Figure 3.7: Setup used for generating high-speed conditions. The receive antenna is rotated around a central pivot, generating high-speed conditions in a controlled and repeatable way.

$I = 1 \Rightarrow$ subframe duration: 1 ms	trajectory length: 1 ms at 400 km/h $\approx$ 11 cm
$I = 2 \Rightarrow$ subframe duration: 2 ms	trajectory length: 2 ms at 200 km/h $\approx$ 11 cm
$I = 3 \Rightarrow$ subframe duration: 3 ms	trajectory length: 3 ms at 133.33 km/h $\approx$ 11 cm

Figure 3.8: Trajectory followed by the antenna during the acquisition of a single LTE subframe for the three interpolation factors $I = \{1, 2, 3\}$ at an emulated speed of 400 km/h. Evaluating the results at a speed value of 400 km/h can be done 1) by measuring at the actual velocity of 400 km/h without time interpolation ($I = 1$); 2) by measuring at half the speed with $I = 2$; 3) by measuring at $400/3 = 133.33$ km/h with $I = 3$. In all cases, the length of the trajectory described by the antenna is the same (close to 11 cm) and can be approximated by a straight line since the antenna describes a circle with a diameter of 2 m while rotating around the central pivot.

factors which lead to equal Doppler spreads (each row of the table corresponds to a different Doppler spread factor).

3.3.2 Measurement Procedure

Several measurements are conducted for each velocity and interpolation factor. More specifically, three different positions of the whole receiver (including the antenna rotation unit) along its rails (see Fig. 3.7) are considered. For each of these positions, 10 measurements per

Table 3.1: Emulated speed values (expressed in km/h) that can be obtained from more than an actual velocity v. Notice that these are the speed values considered in the error curves in Figs. 3.10 to 3.12 and 3.15 to 3.17.

emulated speed, $v^I = Iv$	$I = 1$	$I = 2$	$I = 3$
100	$v = 100$	$v = 50$	–
150	$v = 150$	$v = 75$	$v = 50$
200	$v = 200$	$v = 100$	$v = 66.6$
250	–	$v = 125$	$v = 83.3$
300	–	$v = 150$	$v = 100$

Table 3.2: Main parameters for measurements as well as for simulations. Although three CQI values were evaluated and considered throughout the text to validate the proposed technique, results in the figures only consider CQI = 12.

bandwidth, F_s [MHz]	15.36 (9 occupied)		
FFT size, N	1024		
used subcarriers	600 (excluding DC)		
velocities, v [km/h]	50, 66.6, 75, 83.3, 100, 125, 150, and 200		
carrier frequency, f_c [GHz]	2.5		
interpolation factors, I	1, 2, and 3		
SNR [dB]	38, 31, 21, 11, 1, and ∞ (simulations only)		
CQI values	1	8	12
modulation	4-QAM	16-QAM	64-QAM
code rate	0.076	0.48	0.65
efficiency	0.1523	1.9141	3.9023
source bits	1 192	15 288	31 192
coded bits	16 000	32 000	48 000
peak throughput [Mbit/s]	1.192	15.288	31.192

velocity and interpolation factor are carried out, each one starting at a given angular-shift on the circumference defined by the receive antenna rotating around a central pivot. Therefore, 30 different channel realizations are measured in total for each pair of velocity and interpolation

factor. Furthermore, the whole set of measurements is repeated for each Signal to Noise Ratio (SNR) value, among those specified in Table 3.2. The transmit power employed at the testbed transmitter is modified in order to achieve different average SNR values.

In order to be able to compare the results gathered from different interpolation factors, it is required to ensure that the receive antenna trajectory, spectrum usage and average OFDM symbol energy remain constant for each emulated velocity v^I:

1. **Equal receive antenna trajectory**: in order to maintain a constant Doppler spread, the rotation speed has to be divided by the interpolation factor (see Table 3.1). Therefore, as shown in Fig. 3.8, the trajectory of the receive antenna during the transmission of one LTE subframe does not vary when changing the interpolation factor and antenna velocity as long as the emulated speed is the same.
2. **Equal spectrum usage**: when a subframe is interpolated by a factor I, its bandwidth is decreased by the same factor, which in principle reduces the effect of the channel frequency diversity. In order to experience the same spectrum, I replicas of the interpolated signal are transmitted to ensure that the whole frequency range of the original signal is used. The results are then averaged. Fig. 3.9 shows an example of this procedure for $I = 2$, $I = 3$, and for an arbitrary interpolation factor. Section 3.6 studies in more detail the effects caused by the transmission of the replicas of the signal. However, the frequency diversity reduction inherent to the bandwidth decrease caused by the time interpolation does not seem to affect to the simulation or measurement results. Notice that it is expected to affect more in channels exhibiting a very high frequency selectivity, which is unlikely in high speed conditions in which the channel response changes fast.
3. **Equal average transmit energy per OFDM symbol**: in order to preserve the average energy per OFDM symbol, the interpolated signals are scaled in amplitude by a factor of $\sqrt{I}$ before being transmitted.

Notice that the main objective is to validate the proposed technique considering a realistic scenario while, at the same time, keeping its complexity under reasonable terms, hence simplifying the validation process and facilitating the results comprehension. Therefore, over-the-air standard-compliant LTE transmissions are considered as a good example of the state of the art in wireless communications. However, due to the above-mentioned simplicity reasons, the evaluation is restricted to a single-user scenario without feedback channel, so modulation and coding scheme values are fixed beforehand instead of being adapted according to the channel quality.

Each LTE frame in the Frequency Division Duplex (FDD) mode consists of ten subframes, each one following a different structure depending on the subframe index. For example, synchronization signals are always allocated in the first and sixth subframes, while broadcast channels are included, if necessary, in the first subframe. In order to make the comparison

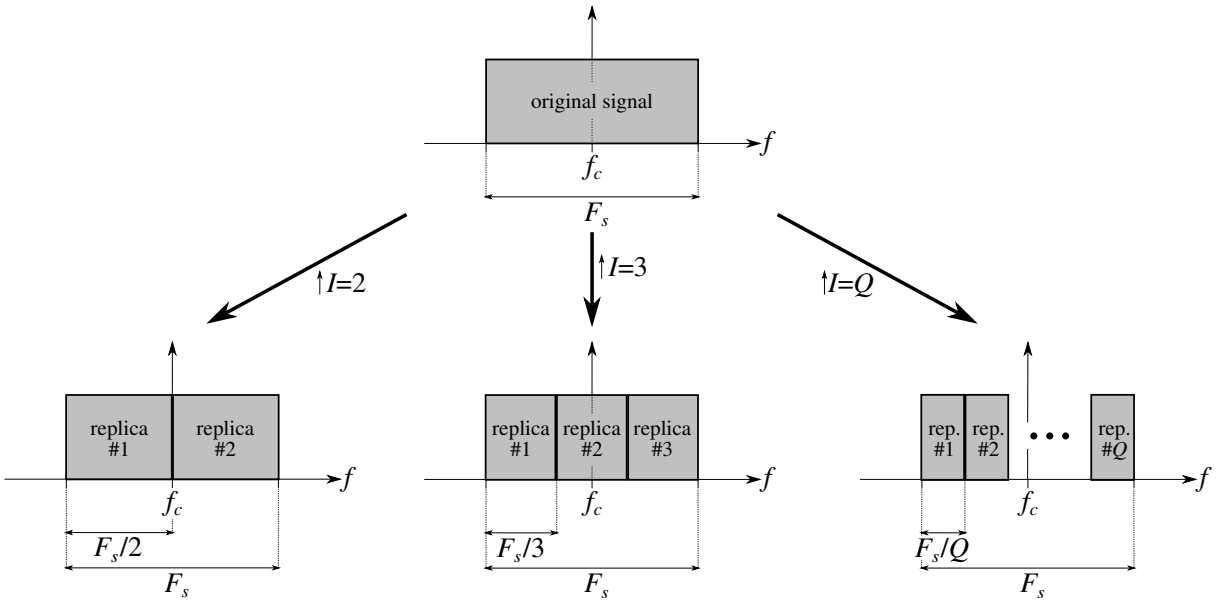

Figure 3.9: Ensuring equal spectrum usage for interpolation factors $I = 2$, $I = 3$, and for an arbitrary integer interpolation factor $I = Q$. I replicas of the interpolated signal are transmitted to ensure that the whole frequency range of the original signal (without interpolation) is used.

between channel realizations independent of the subframe structure, the seventh subframe was always transmitted, considering only pilot and data symbols in subsequent evaluations. Consequently, we ensure the same payload for each channel realization, which allows for fairly comparing the results of different measurements as the subframe structure is kept invariant all the time. More specifically, the number of data symbols that can be transported in the seventh subframe according to the system configuration is 8000, which leads to the number of coded bits, source bits, and peak throughput values specified in Table 3.2.

3.3.3 Simulation Environment

The setup shown in Fig. 3.5 (simulation branch) is employed to validate via simulations the technique of emulating high speeds by time interpolation. Noise variance values that lead to the same SNR values estimated from the measurements are set. A channel model suited for high-speed train scenarios was considered, namely the model defined by the D2a link of the D2 scenario of the Winner Phase II Channel Models [Kyo+07]. This scenario models the channel between an antenna placed at the roof of a train carriage and a network of fixed eNodeBs installed in a rural environment, which usually leads to LoS propagation conditions. Speeds up to 350 km/h can be considered for the train movement. In the following, we will name this channel model "Winner Phase II high speed train channel model".

Notice that the considered channel model does not intend to reproduce the wireless channel observed in the measurements. The aim is to complement the evaluation of the proposed technique in a simulation environment while, at the same time, avoiding the process of

characterizing the doubly selective wireless channel observed in the measurements. Finally, the aforementioned channel model is specifically designed to model an outdoor-to-outdoor high-speed scenario with LoS between transmitter and receiver, while the measurement environment corresponds to an outdoor-to-indoor scenario with Non-Line-of-Sight (NLoS) between them.

Finally, a channel model better suited for high-speed train scenarios was defined in order to evaluate the performance of LTE for high speed scenarios up to $600\,\text{km/h}$. To accomplish this, the model defined by the D2a link of the D2 scenario of the Winner Phase II Channel Models [Kyo+07] was tuned according to the guidelines of the ITU-R for evaluation of radio interface technologies for IMT-Advanced systems [ITU09a]. More specifically, parameters such as delay spread distribution, arrival and departure angle distributions, shadow fading, K-factor, cross-correlations, delay scaling parameters, number of clusters, rays per cluster, etc. were adjusted according to [ITU09a, Table A1-7]. In the following, we will name this channel model "IMT-A high speed train". This scenario models the channel between an antenna placed at the roof of a train carriage and a network of fixed eNodeBs installed in a rural environment, which usually leads to LoS propagation conditions. The key characteristic of this scenario is a continuous wide area coverage by large cells, leading to noise-limited and/or interference-limited conditions. The building density is expected to be low and the height of the antennas much higher than the average building height.

3.3.4 Simulation Procedure

The number of evaluated subframes by simulation was the same considered when measuring, i.e., 30 channel realizations for each velocity and interpolation factor pair. The SNR, velocity and interpolation factors were also kept unchanged. We also guarantee an equal spectrum usage as well as equal average transmit energy per OFDM symbol. Furthermore, to fairly compare the results, the channel model was fed with identical initial conditions (e.g., delays and mean power per path) for each evaluated interpolation factor. This way, a situation in which the receiver moves along the same path for each interpolation factor is modeled.

Table 3.2 details the most relevant parameters for the experimental evaluations as well as for the simulations.

3.4 Figures of Merit

Four different figures of merit to evaluate the quality of the signal at different points in the receive signal processing chain were selected: 1) Error Vector Magnitude (EVM) calculated without knowing the transmitted symbols; 2) uncoded Bit Error Ratio (BER), which is the BER after the symbol decision; 3) coded BER, which corresponds to the BER at the output of the

channel decoder; and 4) throughput for a fixed CQI value for the evaluation of LTE performance in high speed environments.

Recall that the main objective is to determine the level of agreement between the results obtained from those figures of merit when the wireless system is evaluated at actual speed conditions with respect to those obtained when the system is evaluated (under similar conditions) using emulated speeds by time interpolation. Given that the testbed employed for the measurements guarantees excellent time and frequency synchronization between transmitter and receiver, the results of the four figures of merit enumerated above greatly depend on the channel equalizer, which is strongly affected by ICI.

EVM was chosen because it is an unbounded and continuous metric. EVM is particularly valuable when the SNR is high and saturates the BER to its minimum value of zero. On the other hand, considering uncoded BER in the evaluation is very convenient since it is one of the most used performance metrics in wireless communications, but also because the EVM is calculated only from the received symbols. Hence, EVM results loose accuracy since the corresponding SNR value decreases. Coded BER is specially relevant in our evaluation since the proposed technique causes a signal bandwidth reduction proportional to the time interpolation factor, hence reducing the frequency diversity and potentially degrading the channel decoder performance. Consequently, one could expect that, in terms of coded BER, the wireless system would perform differently when actual speeds are considered in comparison to emulated ones. Finally, the achievable throughout is the most important performance metric for many applications, so it was considered for evaluating the performance of LTE in high speed environments.

With the aim of assessing the level of agreement between the results obtained by means of actual speeds with respect to emulated ones, we also included curves for the relative error values computed for those emulated speed values that can be obtained from more than one actual velocity (see Section 4.5.2). We evaluated the emulated speed values that can be obtained from at least two of the three interpolation factors considered (see Table 3.1).

The procedure followed to evaluate the different figures of merit is detailed below:

SNR: The SNR is estimated considering exclusively the data subcarriers. Thus, the guard subcarriers, Direct Current (DC) subcarrier as well as the pilots are discarded. SNR is estimated by performing the following steps:

1. Noise samples for a given velocity v and interpolation factor I are captured directly (measurement case) or generated (simulation case). In the measurement case, noise samples in the time domain are captured with the transmitter switched off (hence not transmitting any signal).
2. The captured noise samples in the time domain are then processed as if they were actual data samples, i.e., they are downsampled by the corresponding interpolation factor (if

required), the cyclic prefix is removed, a Fast Fourier Transform (FFT) is performed and both guard subcarriers, pilots and also the DC subcarrier are discarded.

3. As a result, $w^{(b,k,q)}$ noise samples are obtained in the frequency domain, each one corresponding to the b-th subcarrier of the k-th OFDM symbol of the q-th subframe, where $b \in \mathcal{D}^{(k,q)}$, being $\mathcal{D}^{(k,q)}$ the set of the indexes of the data subcarriers for the k-th OFDM symbol of the q-th subframe.
4. All previous steps are repeated when the transmitter is switched on, so $r^{(b,k,q)}$ data samples are obtained in the frequency domain.
5. The average SNR for a given velocity v and interpolation factor I is then estimated by averaging out the SNR values corresponding to each channel realization. Defining

$$\bar{r} = \frac{1}{KQ} \sum_{k=1}^{K} \sum_{q=1}^{Q} \sum_{b \in \mathcal{D}^{(k,q)}} \frac{1}{\left|\mathcal{D}^{(k,q)}\right|} \left| r^{(l,k,s)} \right|^2, \tag{3.12}$$

and

$$\bar{w} = \frac{1}{KQ} \sum_{k=1}^{K} \sum_{q=1}^{Q} \sum_{b \in \mathcal{D}^{(k,q)}} \frac{1}{\left|\mathcal{D}^{(k,q)}\right|} \left| w^{(l,k,s)} \right|^2, \tag{3.13}$$

the SNR is calculated as follows

$$\text{SNR} = \frac{\bar{r} - \bar{w}}{\bar{w}}, \tag{3.14}$$

with $\left|\mathcal{D}^{(k,q)}\right|$, the total number of data subcarriers for the k-th symbol of the q-th subframe, K the total number of OFDM symbols, and Q the total number of subframes, respectively.

EVM: The EVM is obtained based on the equalized symbols which feed the receiver decision. The following steps are considered for the EVM estimation:

1. The dynamic range of the equalized symbols is bounded. This is realistic in a practical receiver. In this sense, real and imaginary parts of the symbols are clipped to a maximum value. This avoids symbols having extremely large modulus (e.g., due to imperfect zero-forcing channel equalization), hence distorting the EVM estimation. Clipping values were selected, taking into account the mean power of the equalized symbols in perfect conditions (flat channel in absence of noise).
2. A hard decision unit is fed with the clipped symbols. Let $\mathbf{s}_c = \left(s_c^1, s_c^2, \ldots, s_c^S\right)^T$ be the vector of S clipped symbols in a subframe and $\mathbf{s}_d = \left(s_d^1, s_d^2, \ldots, s_d^S\right)^T$ the vector of decided symbols.
3. The EVM per subframe, expressed in decibels, is obtained as

$$\text{EVM} = 10 \log_{10} \left(\frac{P_r}{P_c} \right), \tag{3.15}$$

with $P_c = \frac{1}{S}\left|\left|\mathbf{s}_c\right|\right|^2$, $P_r = \frac{1}{S}\left|\left|\mathbf{s}_c\right|\right|^2$ and $\mathbf{s}_r = \left|\left|\mathbf{s}_c - \mathbf{s}_d\right|\right|^2$, where $\left|\left|\cdot\right|\right|^2$ denotes the squared norm-2 operation. Notice that the aforementioned procedure for calculating the EVM does not require knowing the transmitted symbols. However, the higher the uncoded BER, the more underestimated the EVM is.

Throughput: Since no feedback channel is considered for the experiments, no adaptive modulation and coding schemes are applied, being the CQI values fixed in advance. Results regarding different CQI values are provided.

Besides the performance results in terms of EVM as well as uncoded and coded BER, BER and EVM relative error values are also provided, being computed from the results obtained when the same emulated speed is obtained by using different interpolation factors. The relative error values are calculated differently for EVM and for BER (coded and uncoded):

- **Relative error for uncoded and coded BER**: given W_A and W_B the number of received bits estimated without errors, corresponding to a channel realization and obtained for the interpolation factors $I = A$ and $I = B$, respectively, the instantaneous relative error for the BER is defined as

$$E_{\text{BER}}(A, B) = 100 \cdot \frac{W_A - W_B}{W_B} \quad [\%]. \tag{3.16}$$

- **Relative error for EVM**: given EVM_A and EVM_B the instantaneous EVM values corresponding to a channel realization and obtained for the interpolation factors $I = A$ and $I = B$, respectively, the instantaneous relative error is defined as

$$E_{\text{EVM}}(A, B) = 100 \cdot \frac{\text{EVM}_A - \text{EVM}_B}{\text{EVM}_B} \quad [\%]. \tag{3.17}$$

Mean relative error values for both error types are calculated by averaging instantaneous relative error values for all channel realizations. These mean relative error values are plotted together with their corresponding 95% Bias-Corrected and accelerated (BCa) bootstrap confidence intervals for the mean [EH94]. The precision of the result curves is also evaluated by calculating the 95% confidence intervals for the mean.

3.5 Results

This section presents both the measurements and simulation results obtained by employing the high speed emulation technique. Firstly, Section 3.5.1 shows the results obtained by means of measurements in a controlled scenario. Next, Section 3.5.2 shows the results obtained by simulation.

Three types of performance curves are included in the results graphs:

- **Red solid lines**: they correspond to the cases with no interpolation ($I = 1$). According to the speed values considered for the measurements as well as for the simulations, the red solid curves range from 50 km/h to 200 km/h.
- **Green dashed lines**: they correspond to the cases with $I = 2$, so the emulated velocity is twice the measured or simulated speed. Therefore, the green curves range from 100 km/h to 400 km/h.
- **Pink dotted lines**: they correspond to the cases where $I = 3$. In this case, the emulated velocity is three times the measured or simulated speed, and the curves range from 150 km/h to 600 km/h.

Besides the performance curves, we also included the relative error curves for most figures although in some cases not all error curves are plotted. Three types of relative error curves are included (see Table 3.1):

- **Green dashed lines**: they correspond to the relative difference between the results obtained when the interpolation factor $I = 2$ is employed and when actual speeds are used.
- **Blue dashed lines**: they correspond to the relative difference of the results between the interpolation factors $I = 3$ and $I = 2$.
- **Pink dotted lines**: they correspond to the relative difference of the results between the interpolation factors $I = 3$ and $I = 1$ (actual speeds).

Note that the confidence intervals both for the results and the error graphs are plotted as an area around each curve and in the same color as the corresponding curve.

Due to limitations of the inverter driving the motor used to rotate the receive antenna (see Fig. 3.7), the actual velocity range considered for the measurements (and also for the simulations) starts at 50 km/h, while the maximum actual speed value is set to 200 km/h. Given that we consider interpolation factors $I = 1, 2, 3$, in the speed range from 50 km/h to 300 km/h, at least two curves overlap, thus allowing for evaluating the level of agreement of the results between different interpolation factors.

3.5.1 Measurement Results

Fig. 3.10 shows the measured EVM for CQI=12 (64-QAM) for SNR values ranging from 11 dB to 38 dB. For high SNR values, it can be seen that the higher the emulated speed is, the worse the EVM becomes, as expected. However, it can be seen that the curves for different interpolation factors (as well as their associated confidence regions) overlap, which demonstrates that the proposed technique of emulating high speeds by time interpolation performs adequately. Results for CQI=1 (4-QAM) and CQI=8 (16-QAM) were not included, but they have been also evaluated and they show that the achieved performance is very similar

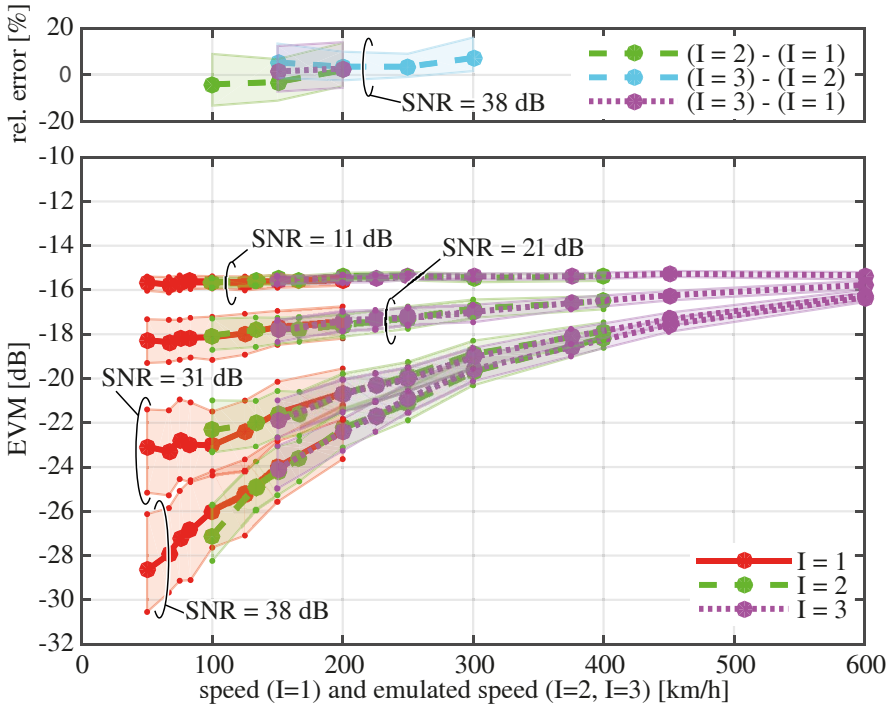

Figure 3.10: Measured EVM for different SNR values. EVM results obtained by measuring when CQI=12 and SNR ranges from 11 dB to 38 dB for the interpolation factors $I = 1, 2, 3$. 95% confidence regions are provided. We have also evaluated the EVM for CQI = 1 (4-QAM) and CQI = 8 (16-QAM) and the results are almost indistinguishable. Corresponding relative error curves are plotted when the SNR is set to 38 dB, showing an excellent agreement.

despite the considered modulation scheme. Fig. 3.10 also shows that the quality of the received signal, in terms of EVM, is significantly affected by the speed for high SNR values, showing that the main source contributing to the signal distortion is the ICI. As the SNR decreases, however, the performance is less affected by the emulated speed because the noise is the main contributor to the signal distortion.

The relative error curves in Fig. 3.10 also demonstrate the excellent agreement of the results independently from the source of the Doppler spread: actual speed or emulated velocity from time interpolation. Note that the confidence intervals for the relative error values are mainly influenced by the number of realizations averaged. Hence, these confidence intervals could be decreased by increasing the number of realizations measured. However, as the receive antenna trajectory is kept constant between different interpolation factors, the relative error is mainly influenced by the repeatability of the setup, the noise, and the interpolation itself. For this reason, we can achieve relative agreements with mean error values below 10% in the worst case (i.e., the highest SNR value of 38 dB) without increasing the number of channel realizations.

Figs. 3.11 and 3.12 show the measured uncoded BER and coded BER, respectively, for different SNR values when CQI=12. Both uncoded BER and coded BER are strongly dependent on the emulated speed for high SNR values, while the noise is the main source

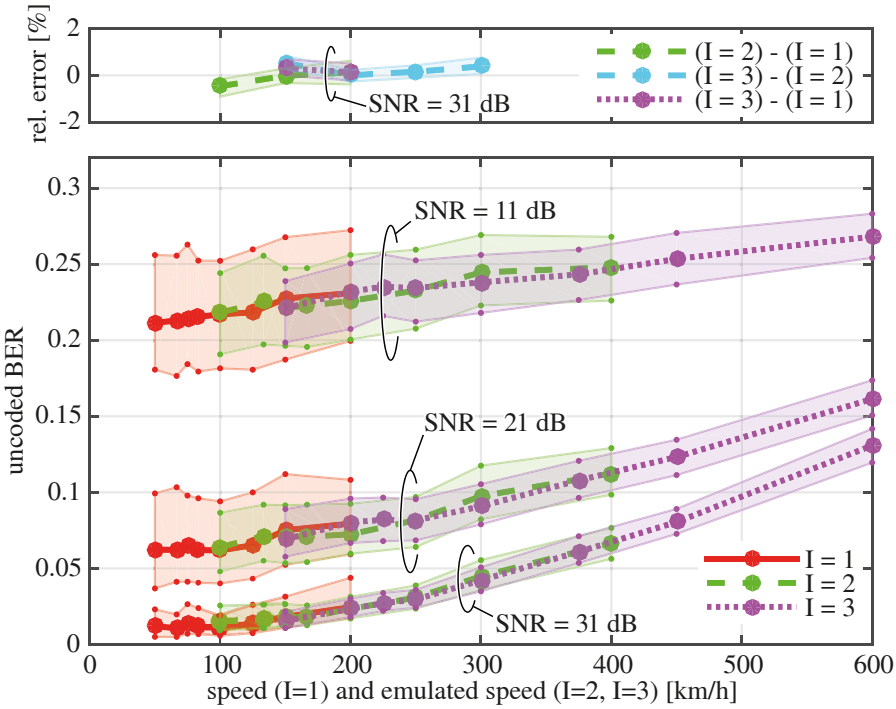

Figure 3.11: Measured uncoded BER for different SNR values. Uncoded BER results obtained by measuring when CQI=12 and SNR ranges from 11 dB to 31 dB for the interpolation factors $I = 1, 2, 3$. 95% confidence regions are provided. Corresponding relative error curves are plotted when the SNR is set to 31 dB, showing an excellent agreement.

of signal distortion when the SNR decreases. It can also be observed that curves for different interpolation factors overlap both for uncoded BER and coded BER, demonstrating again the excellent results of the proposed technique. Notice also that, as shown in the corresponding relative error curves in Figs. 3.11 and 3.12, the agreement of the proposed technique is below 2 %, both in terms of uncoded BER and coded BER. Therefore, such a proposed technique can be effectively used for emulating high speed effects at any point of the receive signal processing chain.

As a sample of the effect of the CQI choice, Fig. 3.13 shows the measured uncoded BER for different CQIs and SNR values. As shown in previous graphs, it can be seen that the higher the emulated speed is, the worse the uncoded BER becomes, as expected. However, it can be also seen that the higher the CQI, the higher the dependency level with the emulated velocity. Finally, note that the curves for different interpolation factors (as well as their associated confidence regions) overlap despite of the CQI and SNR values, which demonstrates that the proposed technique of emulating high speeds by time interpolation performs adequately also regardless of the CQI value.

Fig. 3.14 shows the measured throughput for different CQIs as well as SNR values. Since no feedback channel was used in our experiments, no adaptive modulation and coding schemes were applied, being the CQI values fixed in advance. Take also into account that the maximum

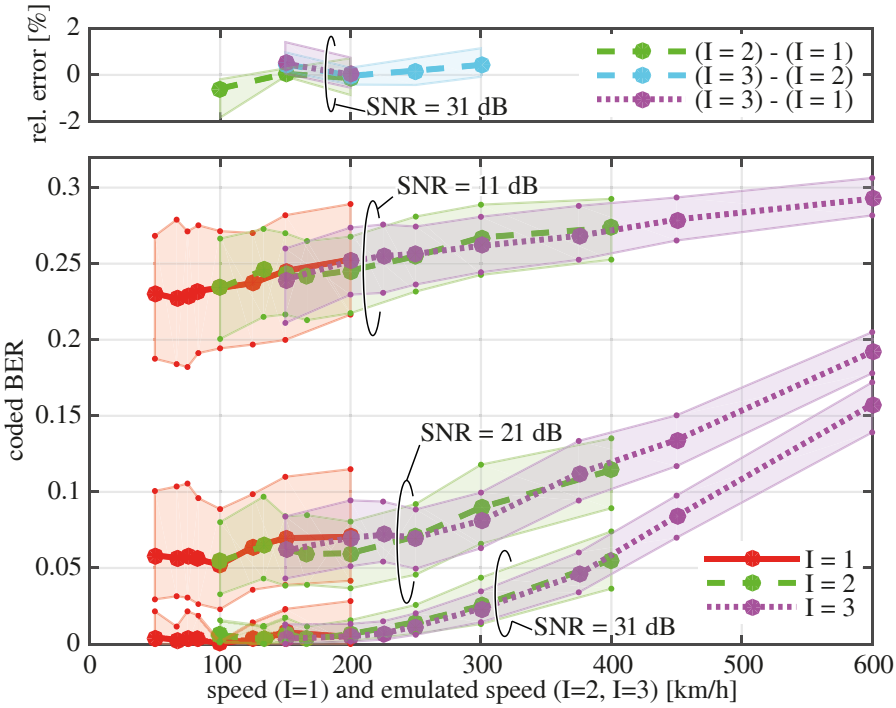

Figure 3.12: Measured coded BER for different SNR values. Coded BER results obtained by measuring when CQI=12 and SNR ranges from 11 dB to 31 dB for the interpolation factors $I = 1, 2, 3$. 95% confidence regions are provided. Corresponding relative error curves are plotted when the SNR is set to 31 dB, showing an excellent agreement.

throughput values are 1.192 Mbit/s, 15.288 Mbit/s, and 31.192 Mbit/s for CQI $= 1$, CQI $= 8$ and CQI $= 12$, respectively. The considered CQI not only determines the maximum throughput available but also limits the system robustness. Thus, it can be seen that for not so high SNR values, a better throughput can be achieved by reducing the CQI. In fact, the system works in absence of errors even for SNR $= 11$ dB when CQI $= 1$ and despite of the velocity.

3.5.2 Simulation results

Fig. 3.15 shows the simulated EVM for CQI=12 (64-QAM) for SNR values ranging from 11 dB to 38 dB and for the Winner Phase-II high speed train channel model. Additionally, we have also evaluated the results in absence of noise (infinite SNR). Note that the slopes of the curves are similar to those obtained by measurements as shown in Fig. 3.10, while the obtained EVM values are always lower for the same SNR value. This result is expected because the channel model considered for the simulations is easier to equalize due to the lower variability of the simulated channel. However, when the SNR decreases (SNR = 11 dB and SNR = 21 dB in our case), the above-mentioned effect vanishes as the noise becomes the main contribution to the signal distortion and the corresponding curves approach each other for simulations and for measurements.

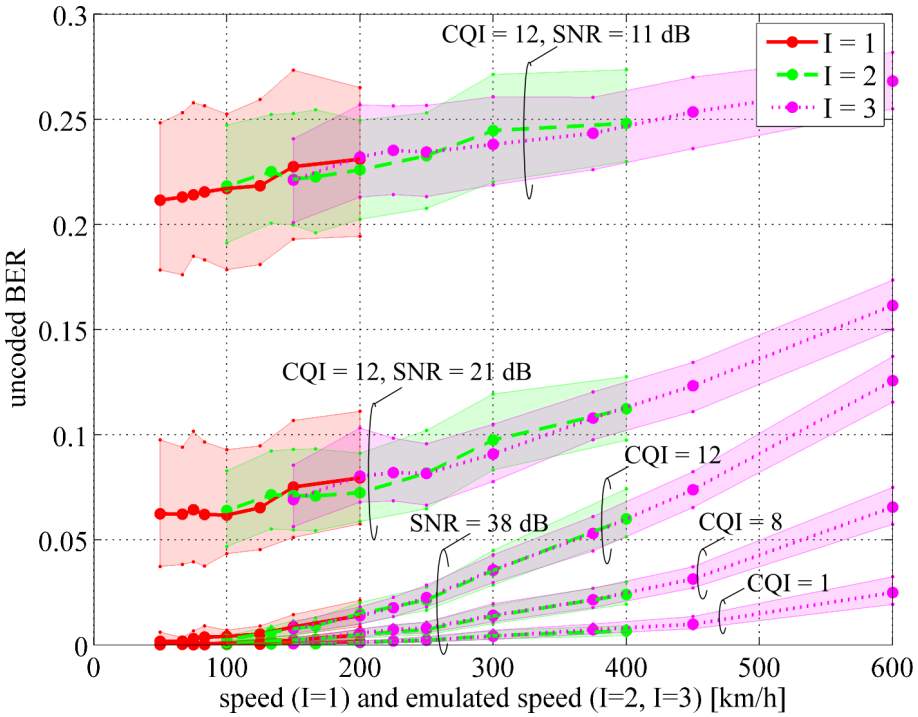

Figure 3.13: Measured uncoded BER for CQIs and different SNR values. The dependency level of the uncoded BER with respect to the emulated speed increases for higher CQI values. The technique of high speed emulation by time interpolation is accurate regardless of the considered CQI value.

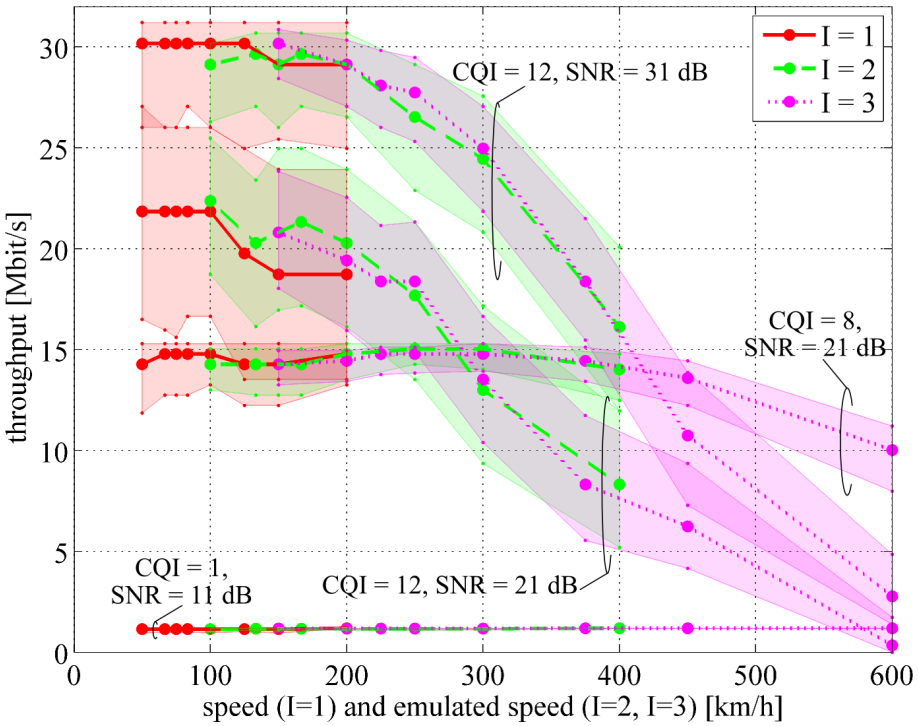

Figure 3.14: Measured throughput for different CQIs and SNR values. Increasing the CQI increases the maximum achievable throughput. However, for low SNR values a higher throughput can be achieved by reducing the CQI, as this will result in an increase of the robustness of the system.

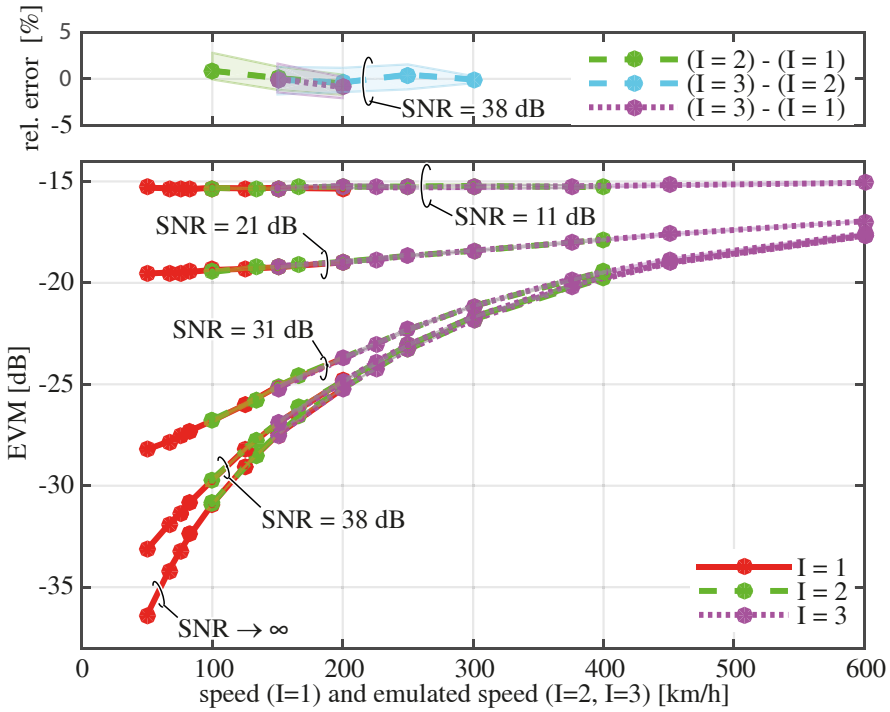

Figure 3.15: Simulated EVM for different SNR values when the Winner Phase-II high speed train channel model is considered. EVM results obtained by simulation when CQI=12 and SNR ranges from 11 dB to infinity for the interpolation factors $I = 1, 2, 3$. Note that the channel model associated to the D2a link of the D2 scenario of the Winner Phase II Channel Models was applied. 95% confidence regions are provided. We have also evaluated the EVM for CQI = 1 (4-QAM) and CQI = 8 (16-QAM) and the results are almost indistinguishable. Corresponding relative error curves are plotted when the SNR is set to 38 dB, showing an excellent agreement.

The variability of the results obtained by simulations is much lower than that of the measurements because, on the one hand, the simulated channel is less variable than that observed in the measurements. On the other hand, exactly the same initial channel conditions are applied in the simulations for each interpolation factor and velocity pair, thus ensuring much less variability between the different channel realizations generated for each interpolation factor and velocity pair. In fact, the confidence region of each simulated curve completely overlaps the curve itself, which causes that the confidence regions cannot be appreciated although they are included. Additionally, curves simulated for different interpolation factors almost completely overlap, hence showing the good behavior of the proposed technique also in this case. This precise behavior is also confirmed by the corresponding relative error curves in Fig. 3.15.

Figs. 3.16 and 3.17 show the simulated uncoded BER and coded BER, respectively, for different SNR values when CQI=12 and the Winner Phase-II high speed train channel model was considered. Some level of dependency on the emulated speed for high SNR values can be still appreciated for the uncoded BER, while the coded BER is always zero for SNR values greater than or equal to 21 dB since the channel decoder is able to correct all errors. Notice

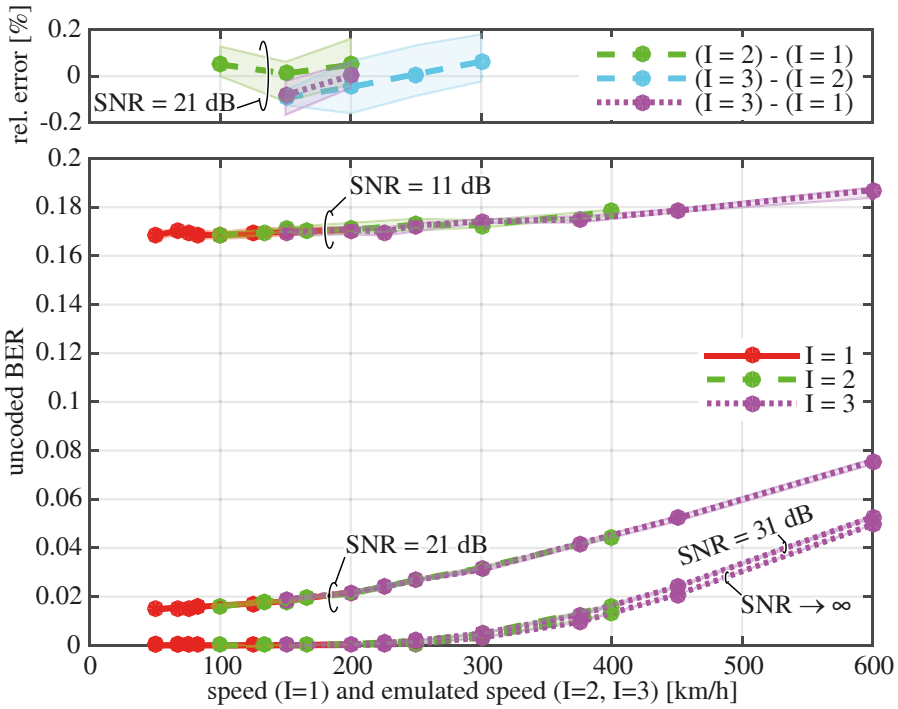

Figure 3.16: Simulated uncoded BER for different SNR values when the Winner Phase-II high speed train channel model is considered. Uncoded BER results obtained by simulation when CQI=12 and SNR ranges from 11 dB to 31 dB for the interpolation factors $I = 1, 2, 3$. Note that the channel model associated to the D2a link of the D2 scenario of the Winner Phase II Channel Models was applied. 95% confidence regions are provided. Corresponding relative error curves are plotted when the SNR is set to 21 dB, showing an excellent agreement. Note that for SNR values greater or equal than 31 dB the BER curves are close to zero for speeds below 250 km/h, hence the relative error curves do not provide much information.

that this is not the case for the measurements as the channel is much more difficult to equalize. Curves for different interpolation factors overlap both for uncoded BER and coded BER, thus showing the good behavior of the proposed interpolation technique. This is also confirmed by the corresponding error curves.

Fig. 3.18 shows the simulated uncoded BER for different CQIs and SNR values for the IMT-A high speed train channel model. One can see that the results when CQI $= 12$ are almost indistinguishable from the results obtained for the Winner Phase-II high speed train channel model (see Fig. 3.16). Regarding the results for CQI $= 1, 8$, it can be seen that the uncoded BER is always zero regardless of the SNR. Again, curves simulated for different interpolation factors completely overlap, showing the good behavior of the proposed technique also in this case.

Fig. 3.19 shows the simulated coded BER results obtained for the IMT-A high speed train channel model when CQI $= 12$. The obtained results are almost indistinguishable from those corresponding to the Winner Phase-II high speed train channel model (see Fig. 3.17). The coded

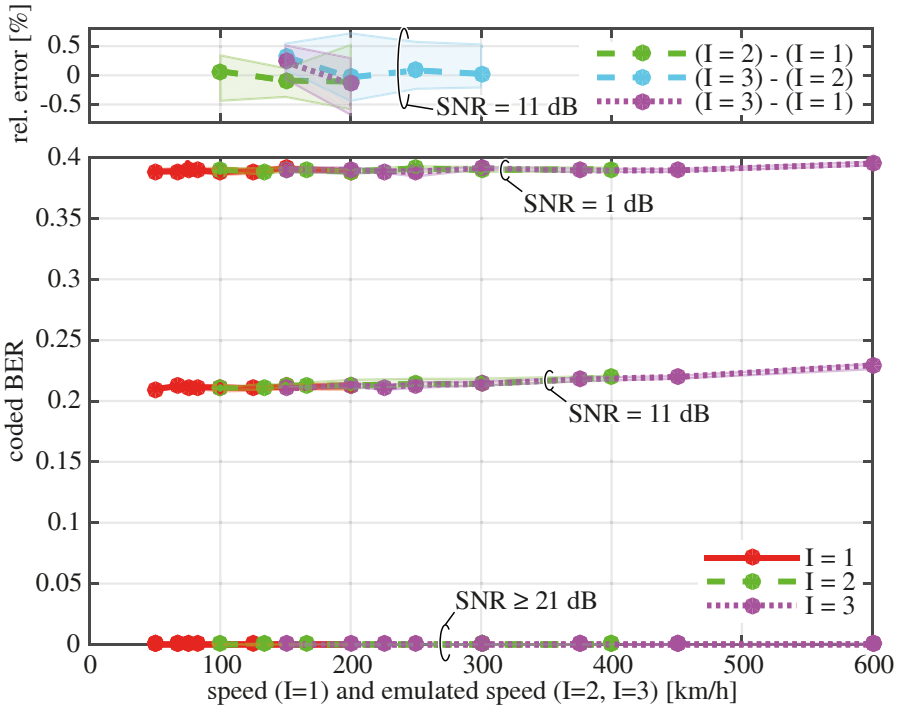

Figure 3.17: Simulated coded BER for different SNR values when the Winner Phase-II high speed train channel model is considered. Uncoded BER results obtained by simulation when CQI=12 and SNR ranges from 1 dB to infinity for the interpolation factors $I = 1, 2, 3$. Note that the channel model associated to the D2a link of the D2 scenario of the Winner Phase II Channel Models was applied. 95% confidence regions are provided. Corresponding relative error curves are plotted when the SNR is set to 11 dB, showing an excellent agreement. Note that for SNR values greater or equal than 21 dB the BER curves are close to zero for all considered speeds, hence the relative error curves do not provide much information.

BER is always zero for SNR $\geq$ 21 dB, since the channel decoder is able to correct all errors. Few level of dependence of the coded BER results with respect to the receiver velocity can be appreciated regardless of the SNR value. Again, the curves for different interpolation factors overlap both for uncoded BER and coded BER, thus showing the good behavior of the proposed interpolation technique. This is also confirmed by the corresponding error curves.

Fig. 3.20 shows the simulated throughput results for different CQIs as well as SNR values, for the IMT-A high speed train channel model. Since no feedback channel was used in our experiments, no adaptive modulation and coding schemes were applied, being the CQI values fixed in advance. The obtained results are coherent with those shown in Fig. 3.19. Moreover, since channel coding succeeds in correcting all the errors introduced by the channel when SNR $\geq$ 1 dB (CQI $=$ 1), SNR $\geq$ 11 dB (CQI $=$ 8) and SNR $\geq$ 31 dB (CQI $=$ 12), being the reached throughput values the maximum ones (1.192 Mbit/s, 15.288 Mbit/s, and 31.192 Mbit/s for CQI $=$ 1, CQI $=$ 8 and CQI $=$ 12, respectively). When the SNR is equal or below 11 dB the maximum CQI value provides the worst performance. Hence the use of a more robust CQI

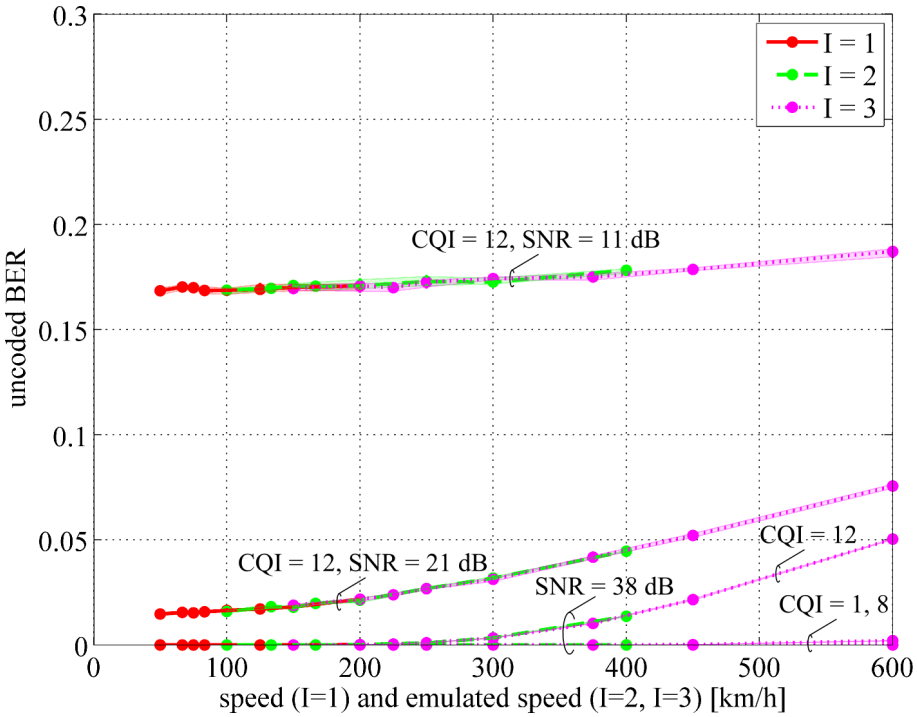

Figure 3.18: Simulated uncoded BER for different CQIs and SNR values when the IMT-A high speed train channel model is considered. Obtained results when CQI $=$ 12 are almost indistinguishable from those obtained for the Winner Phase-II high speed train channel model. For lower CQI values, the uncoded BER is zero regardless of the SNR.

is beneficial for low SNR values.

3.6 Alternatives to Time Interpolation

In previous sections a method to emulate high speed conditions whereas performing the measurements at much lower speeds was studied in detail. While the proposed method preserves the spatial properties of the mobile radio channel, it performs a spectral compression (see Section 3.2). This spectral compression also changes other spectral parameters of the transmit signal. In case of LTE [ETSb] downlink transmissions, where OFDM is used as the modulation scheme, these parameters are the transmit bandwidth and the spectral spacing of the reference symbols (pilots). In this section, a new set of alternative methods that preserve the spectral properties by inserting additional subcarriers is proposed. Instead of time interpolating the symbols, the new methods proposed increase the FFT length in the frequency domain by inserting additional subcarriers between the original ones. Next, the technique based on the time interpolation is compared to the new set of methods by simulations based on standard-compliant LTE signals. Finally, practical aspects to be considered when implementing the proposed high speed emulation techniques are highlighted.

Section 3.6.1 gives a detailed description of the different methods considered. In

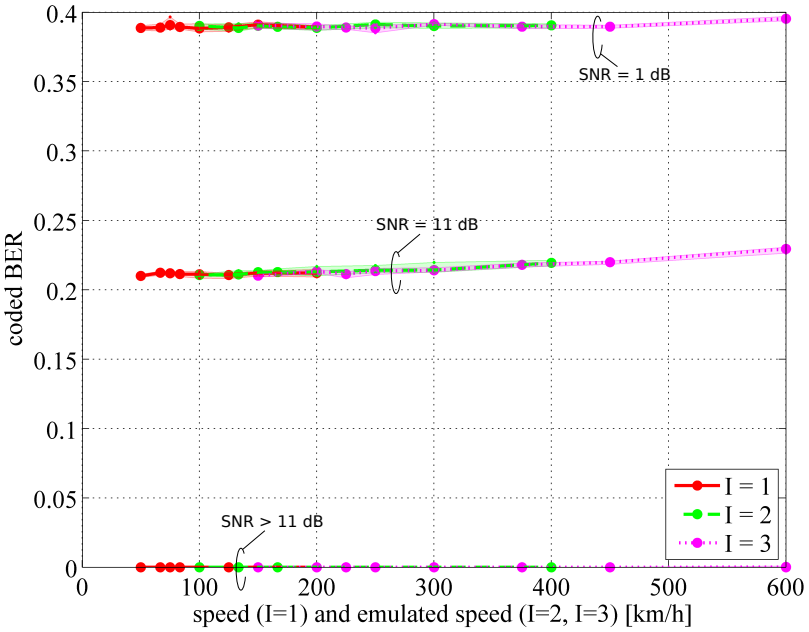

Figure 3.19: Coded BER for CQI $=$ 12 and different SNR values when the IMT-A high speed train channel model is considered. The coded BER is always zero for SNR $\geq$ 21 dB, since the channel decoder is able to correct all errors. Few level of dependence of the coded BER results with respect to the receiver velocity can be appreciated regardless of the SNR value.

Section 3.6.2 the applicability and the limitations of the different methods are shown by simulations before practical aspects are discussed in Section 3.6.3. In Section 3.6.4, all findings of this section are summarized.

3.6.1 Methods

The considered high speed emulation methods are divided into two different sets, as illustrated in Fig. 3.21. On the one hand we have the methods based on time interpolation, while on the other hand we have the methods based on inserting subcarriers.

Time-Interpolating the Signals

The simplest method to change the length of a given OFDM signal to any value higher or lower than the initial length by a factor I is to time-interpolate the signal, i.e., change the sampling rate at both the transmitter and the receiver by the same factor $\frac{1}{I}$. In its basic implementation (*method 1*) this method is completely transparent to the communication system so there is no need for any modifications in the implementation of the actual system except for a change in the sampling rate. In order to validate this method by measurements, a modified method was introduced (the so-called *method 2*), which was the one used for our experiments in previous sections. As explained in Section 3.3.2, under the constraint of an integer factor I>1, the resampled

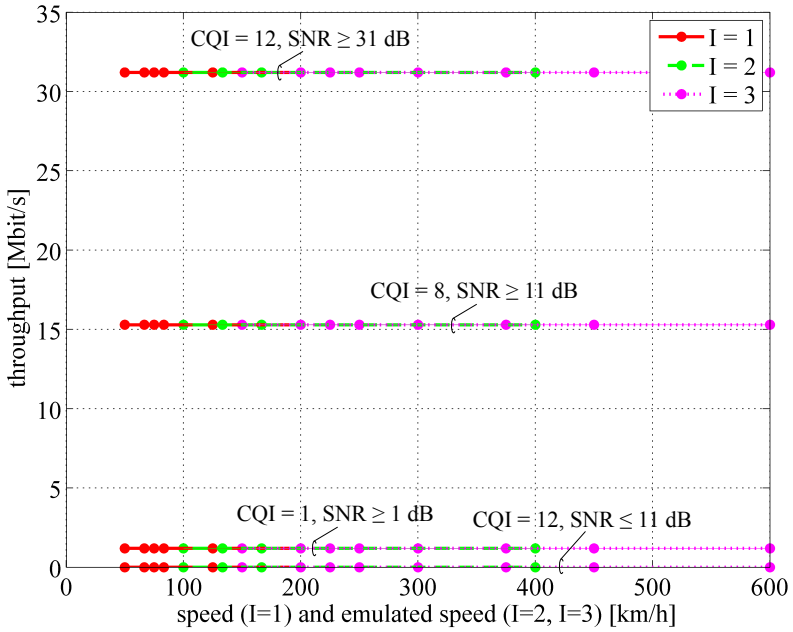

Figure 3.20: Simulated throughput for different CQIs and SNR values when the IMT-A high speed train channel model is considered. The obtained results show that channel coding succeeds in correcting all the errors introduced by the channel when SNR $\geq$ 1 dB (CQI $=$ 1), SNR $\geq$ 11 dB (CQI $=$ 8) and SNR $\geq$ 31 dB (CQI $=$ 12). For lower SNR values it is shown that increasing the CQI can decrease the achieved throughput.

signal is repeated I times in order to occupy the same total bandwidth as the original signal. Measurement results for all signals are then averaged preserving the SNR. However, repeating exactly the same signal results in an increase of the Peak-to-Average Power Ratio (PAPR) as shown in Section 3.6.3[1]. Therefore, we also considered the so-called *method 3*, in which different realizations of the same signal are repeated.

Inserting Additional Subcarriers

In order to preserve the bandwidth and the pilot spacing, the OFDM signal can be time-stretched in a different fashion. As illustrated in Fig. 3.21b, the FFT length, which is the total number of subcarriers (including guard subcarriers at the edges) passed to the Inverse Fast Fourier Transform (IFFT) in the OFDM modulator, is increased by an integer factor I>1 by inserting $(I-1)$ additional subcarriers between the original ones. By keeping the initial sampling frequency, the symbol length is thereby increased by the factor I and the subcarrier spacing is decreased by the same factor. At the receiver side, the additional subcarriers are discarded after the FFT in the OFDM demodulator. The choice of the symbols being modulated

[1]Note that this effect can be avoided when using the measurement setup described in Section 3.3 since it is possible to transmit each signal replica separately, as the measurement setup ensured repeatable conditions.

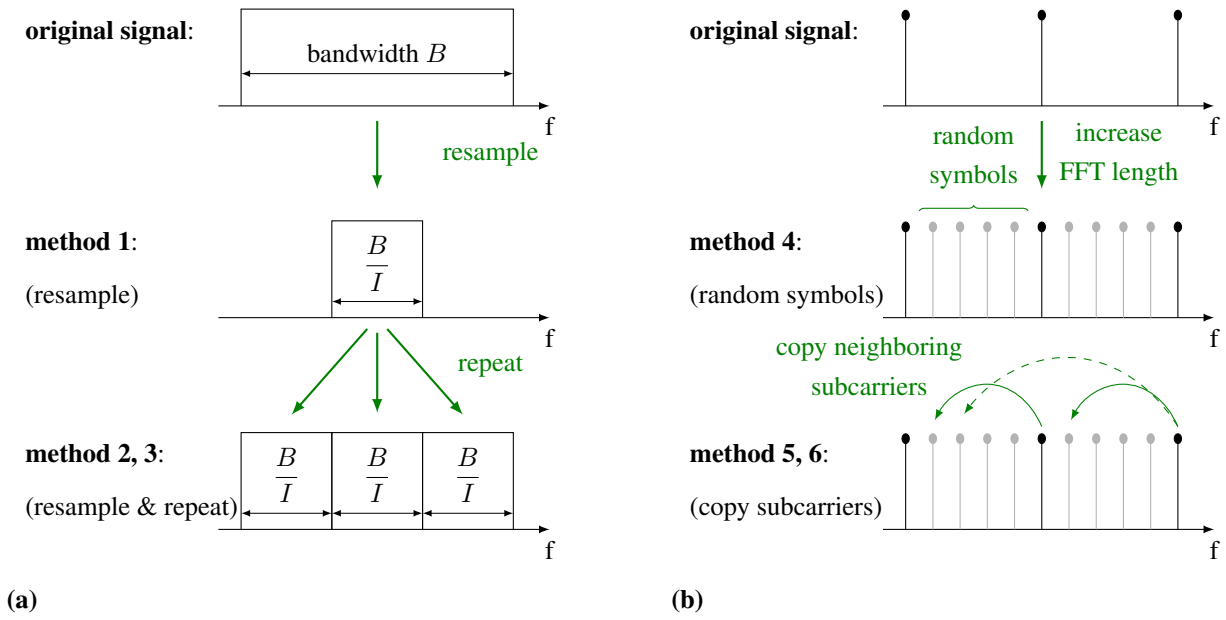

Figure 3.21: Methods to decrease the subcarrier spacing of an OFDM signal: (a) Resampling. (b) Increasing the FFT length and inserting additional subcarriers.

onto the additional subcarriers depends on the application. If only the average ICI level is to be emulated, random symbols from the symbol alphabet used for the actual data symbols are used (*method 4*). ICI cancellation algorithms cannot perform correctly in this case since the interference is not caused by the original neighboring subcarriers. This drawback is considered in *method 5*, where the initial neighboring subcarriers are copied to the appropriate positions in order to generate the ICI in a more natural way. The number of "correct" neighbors is then limited to $\left\lfloor \frac{I}{2} \right\rfloor$[2]. The drawback of this method is its increased PAPR since the subcarriers are not independent anymore (see Section 3.6.3). Therefore, *method 6* is considered into our comparison, where only the adjacent neighbor is copied and random symbols are used for the remaining subcarriers.

3.6.2 Comparison Based on Simulations

In order to show the applicability and the limitations of the different methods discussed in this section, simulations using a modified version of the Vienna LTE Downlink Link Level Simulator [RST16; Meh+11; tea] were performed. First, the original signal is transmitted at receiver velocities of v=50, 100, 200 and 400 km/h. Then, the modified signals are transmitted at 50 km/h to emulate transmissions at v=100 km/h (I=2), 200 km/h (I=4) and 400 km/h (I=8). Two different channel models, both based on a modified version [ZM05a] of the Zheng

[2]For even I it is possible to randomly choose one of the two possible subcarriers for the center position.

model [ZX03] for time-variant channels are considered. Thereby, the *Pedestrian B* (PedB) channel model [Tec02] implements frequency selective channels while *flat Rayleigh* channels consist of a single channel tap and are therefore frequency flat. The channel estimation in the receiver used is performed using least squares channel estimation with linear interpolation.

Signal to interference ratio

The Signal-to-Interference Ratio (SIR) is obtained by setting subcarriers that are not too close to each other and not too close to the spectral edges of the signal to zero. The SIR is then calculated by obtaining the signal plus interference power P_{SI} at the non-zero data subcarrier positions $\mathcal{D}^{(k)}$ and the interference power P_I at the zero subcarrier positions $\mathcal{Z}^{(k)}$ as

$$\text{SIR}\,(v,I) = \frac{\overline{P}_{SI} - \overline{P}_I}{\overline{P}_I} = \frac{\overline{P}_{SI}}{\overline{P}_I} - 1 \tag{3.18}$$

$$= \frac{\sum_{u=1}^{U}\sum_{k=1}^{K} \frac{1}{|\mathcal{D}^{(k)}|} \sum_{b\in\mathcal{D}^{(k)}} \left|r^{(l,k,u)}\,(v,I)\right|^2}{\sum_{u=1}^{U}\sum_{k=1}^{K} \frac{1}{|\mathcal{Z}^{(k)}|} \sum_{b\in\mathcal{Z}^{(k)}} \left|r^{(l,k,u)}\,(v,I)\right|^2} - 1, \tag{3.19}$$

whereas $r^{(l,k,u)}$ is the received symbol after the FFT in the demodulator at subcarrier b, time symbol k and channel realization u. K is the number of considered time symbols and U the total number of channel realizations. In Fig. 3.22 shows a comparison between the simulation results and the analytical ones [RK99a]. Notice that the Jakes' spectrum is considered in both cases. The results for all methods that resample the original signal agree with the desired result for the original signal and the analytical result. For the second set of methods, where additional subcarriers are inserted, only the method that inserts random symbols properly emulates the average SIR. We observe higher interference power for the case where data symbols are repeated and are therefore not independent anymore.

Channel estimation error

All methods investigated here have in common that signals are stretched in time to emulate higher receiver velocities and therefore the spatial lengths of the resulting signals are exactly the same as for the original signal at the velocity to be emulated. This is also valid for the spatial pilot spacing and therefore for the resulting spatial channel interpolation errors. However, differences arise in the frequency domain. While the original pilot spacing is preserved for the methods that insert additional subcarriers, the pilot spacing decreases with I when time interpolating the original signal by the factor I (see Fig. 3.3). In order to analyze this effect, simulations at v=0 km/h were performed and the mean squared channel estimation and

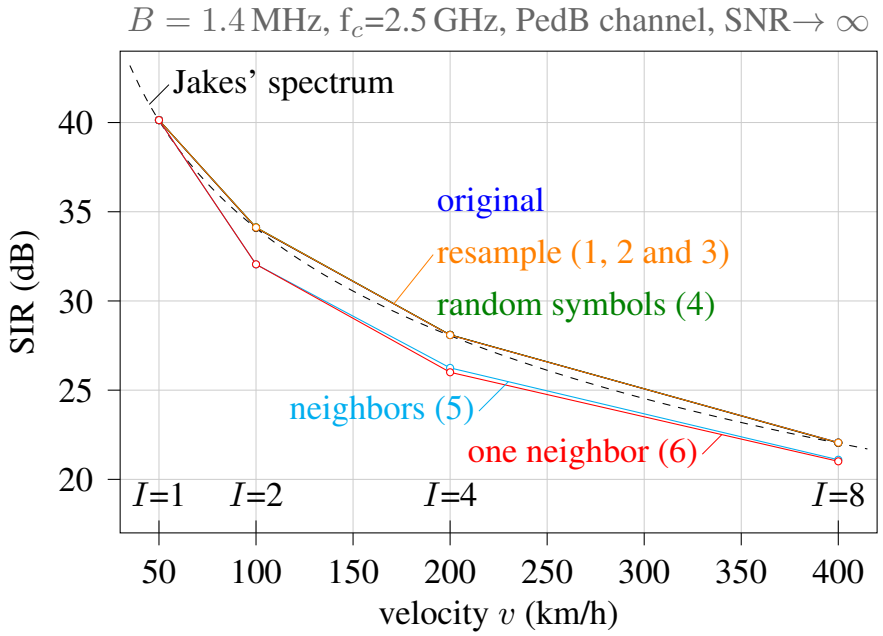

Figure 3.22: All methods that keep data symbols independent emulate the SIR correctly. Repeating data symbols increases the interference power.

interpolation error

$$\mathrm{MSE} = \frac{1}{U}\frac{1}{K}\frac{1}{N}\sum_{u=1}^{U}\sum_{k=1}^{K}\sum_{b=1}^{N}\left|\widehat{H}^{(l,k,u)} - H^{(l,k,u)}\right|^2 \tag{3.20}$$

was evaluated. In the former expression, $\widehat{H}^{(l,k,u)}$ denotes the estimated channel coefficient and $H^{(l,k,u)}$ is the actual channel coefficient at subcarrier b, time symbol k and channel realization u. Fig. 3.23 shows the increased channel estimation error due to the frequency selectivity of the PedB channel compared to the frequency flat channel. Since the absolute pilot spacing decreases with increasing I, the channel estimation error decreases and converges to the error for the frequency flat channel for the methods based on time interpolation.

Physical layer throughput

The physical layer throughput combines all the aforementioned effects. Hence it can be used as a metric for the applicability of the different methods to emulate higher velocities at lower velocities. In order to avoid the impact of feedback, necessary for link adaption, a brute-force approach is followed where all possible Modulation and Coding Schemes (MCSs) are transmitted over the same channel realizations and the best performing MCS is chosen as the one an ideal feedback function would have chosen. The average physical layer throughput is then calculated as the average over all channel realizations r of the data rate of the respectively

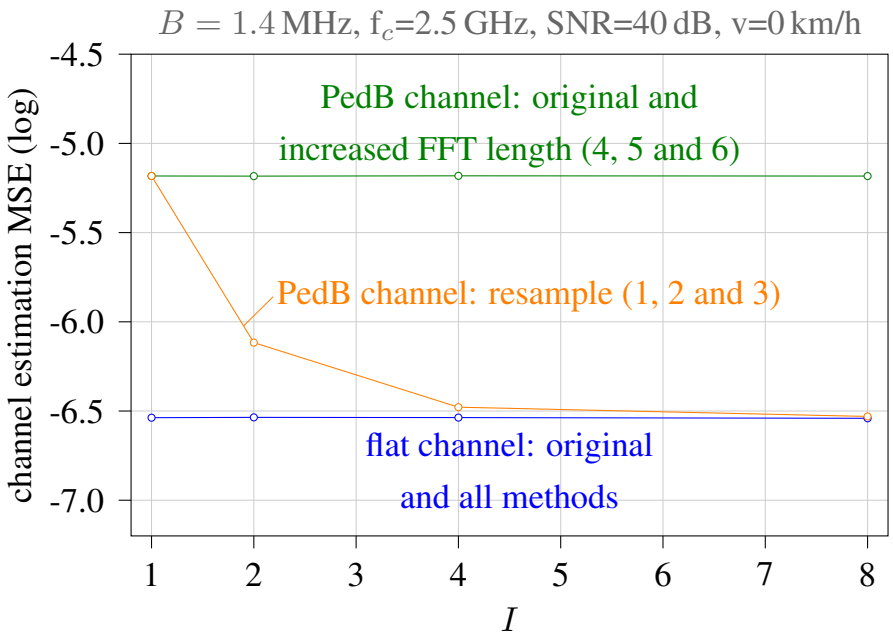

Figure 3.23: The spectral channel estimation error decreases with decreasing pilot spacing in frequency selective channels. For a fixed pilot spacing the channel interpolation error is emulated correctly.

best performing MCS to

$$D\left(v, I\right) = \frac{I}{R} \sum_{r=1}^{R} \max_{\text{MCS}} D_r\left(v, I, \text{MCS}\right). \tag{3.21}$$

In order to compare the emulated throughput rather than the actual throughput, the actual throughput is scaled with I as the symbol length increases with I and therefore the emulated throughput decreases. Fig. 3.24 shows the results in terms of throughput as well as the relative error in relation to the results for the original signal. For the frequency flat channel (Fig. 3.24a) the methods that repeat subcarriers have a lower throughput due to a lower SIR. All other methods emulate the higher velocities accurately in terms of throughput. That is different for the frequency selective PedB channel as shown in Fig. 3.24b. Only the method that inserts random symbols emulates the higher velocities correctly. For the time-interpolation based methods the throughput is higher than it should be since the pilot spacing decreases and therefore the channel estimation errors decrease with I.

3.6.3 Practical aspects

While simulations are a proper and convenient way to evaluate and compare the different methods proposed, their intended use are in real world experiments where one has to cope with hardware limitations and impairments. In order to evaluate the impact of the effects of time varying mobile channels like channel interpolation errors and ICI, the impact of other

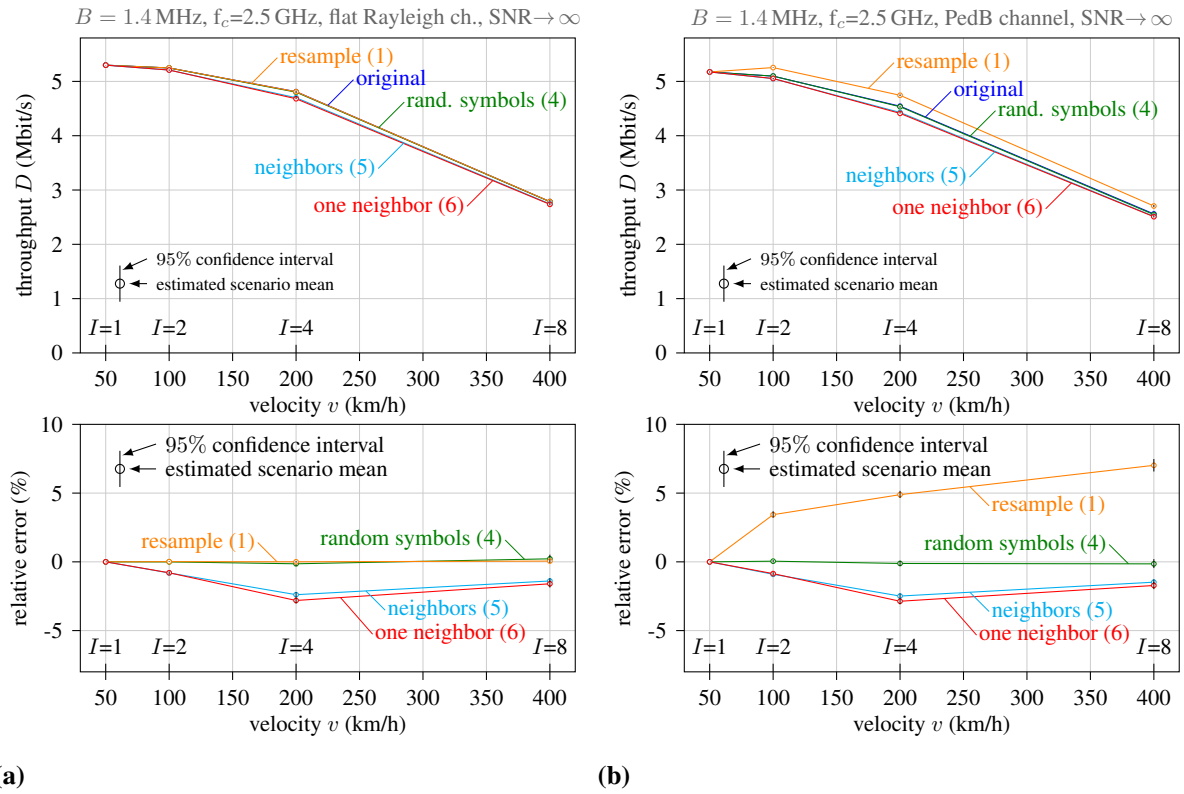

Figure 3.24: (a) For a frequency flat channel the throughput for the methods that repeat data symbols is lower due to the lower SIR while all other methods perform well. (b) For the frequency selective PedB channel the throughput for the resample methods is too high due to the lower channel estimation errors.

Table 3.3: Comparison of the different methods considered. '+' indicates that the method is fair regarding each of the considered aspects, while − indicates that it is not the case. '(+)' indicates that the method can be fair under some assumptions.

method		$I \in$	bandwidth	SNR	SIR	pilot spacing	neighboring subcarriers	PAPR	scenarios	ICI canc.
1	interpolation	$\mathbb{R}_{>0}$	-	$\propto I$	+	-	+	+	low del. spread	+
2	int. & repeat same	$\mathbb{N}_{>1}$	(+)	= const.	+	-	+	-	low del. spread	+
3	int. & repeat	$\mathbb{N}_{>1}$	(+)	= const.	+	-	+	+	low del. spread	+
4	insert random symbols	$\mathbb{N}_{>1}$	+	≈ const.	+	+	-	+	all	-
5	repeat neighbors	$\mathbb{N}_{>1}$	+	≈ const.	-	+	(+)	-	all	(+)
6	repeat one neighbor	$\mathbb{N}_{>1}$	+	≈ const.	-	+	(+)	(+)	all	(+)

effects should be kept small compared to the effects under investigation. Effects on SNR and PAPR can result of special interest as they can severely impact on the obtained results. For a given maximum transmit power the PAPR limits the maximum average transmit power and therefore also the SNR. On the other hand, for a given average transmit power, the ICI caused by nonlinearities in the transmission chain increases with increasing PAPR.

Signal-to-noise ratio

For the analysis of the SNR the powers of the signal and the noise are evaluated after the FFT in the OFDM demodulator. Considering a transmission system with a fixed transmit power and zero-mean noise with fixed spectral density at the receiver, all methods have in common that the average per-subcarrier noise variance after the FFT[3] is independent of I and independent of the FFT length. That is different for the received signal power. For all methods except *method 1* the number of subcarriers increases with I and therefore the per-subcarrier transmit power decreases as the fixed total transmit power is equally allocated to all subcarriers. On the other hand, the symbol energy increases by I with increasing I for a fixed per-subcarrier transmit power as the symbol duration increases by I. Therefore an SNR gain $g = \frac{I \cdot L}{L_t}$ is achieved whereas L denotes the initial number of subcarriers and L_t the number of subcarriers transmitted. For the methods that insert additional subcarriers we achieve a very small[4] gain of $g = \frac{I \cdot L}{I \cdot (L-1)+1} > 1$. For the methods that resample and repeat, where $L_t = I \cdot L$, it holds g=1, while the time-interpolation method achieves a gain of I since the number of subcarriers is not increased.

Peak to average power ratio

A per-symbol search for the peak power with oversampling factor $J = 4$ [JW08] is performed for the evaluation of the PAPR. Different signals can then be compared by plotting the statistics

[3] When using a $\frac{1}{\sqrt{N}}$ scaling, i.e.: $X[k] = \frac{1}{\sqrt{N}} \sum_{n=0}^{N-1} e^{-j2\pi \frac{kn}{N}} \cdot x[n]$

[4] For L=72 subcarriers and I=8, g=0.0531 dB .

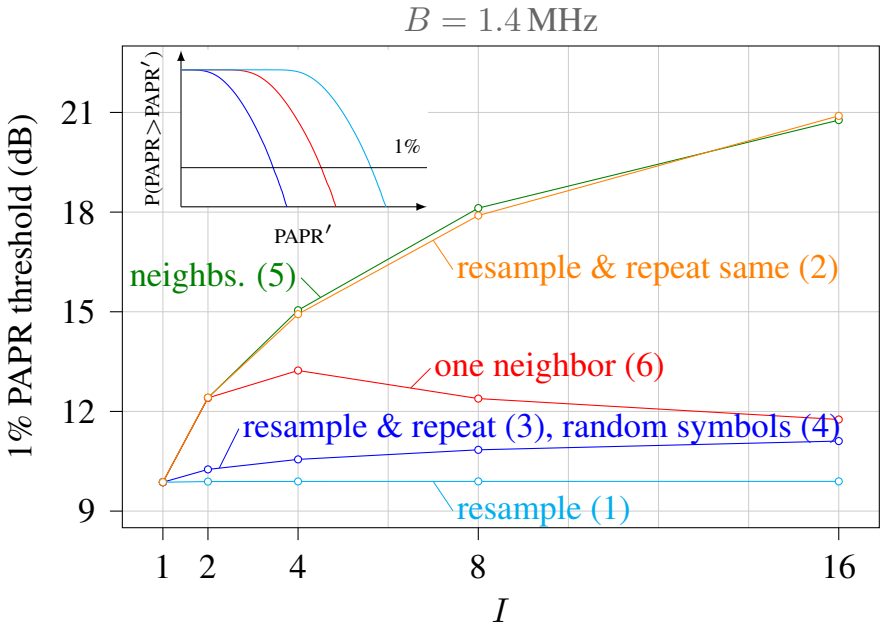

Figure 3.25: Repeating subcarriers causes a strong increase of PAPR while when increasing the number of subcarriers and keeping the symbols random only a slight increase of PAPR is observed.

of the peak powers in terms of a Complementary Cumulative Distribution Function (CCDF) as illustrated for three different signals in the embedded subplot of Fig. 3.25. In order to compare all different methods for different values of I, the value of PAPR that is exceeded by 1 % of the OFDM symbols is obtained. Fig. 3.25 shows the thereby obtained results. While resampling does not change the PAPR, repeating the same resampled signal results in a strong increase of the PAPR as data symbols are repeated. This effect vanishes when different signal realizations[5] are used for the copies. The effect that the PAPR increases with increasing number of subcarriers remains as for the method where random symbols are inserted. Copying neighboring subcarriers yields similar results as copying the same signal. The PAPR is reduced by copying just the next neighbor and filling the remaining subcarriers with random symbols.

3.6.4 Summary of the Comparison

Table 3.3 shows that there is no perfect technique to emulate high speed velocities while measuring at low speeds among the considered methods. The choice of the method to use depends on the scenario, the application and the intended implementation effort. Simply time-interpolating the transmit signal is very easy to implement and allows for measurements at higher effective SNRs. In order to transmit with the correct bandwidth, the time-interpolated signal can be repeated over frequency. However, time-interpolation based methods reduce the

[5]If we consider different data symbols and different values for the pilots by using different LTE Cell IDs the subcarriers are completely independent.

pilot spacing with respect to the original signal. Transmissions with correct spectral properties are achieved by inserting random subcarriers. With this method, the average ICI is emulated correctly but not the actual one. The methods that emulate the correct ICI by inserting the correct subcarriers generate ICI levels higher than the intended one.

Note that all the considerations and findings found are not limited to the LTE downlink. However, LTE was used as an exemplary signal for convenience.

3.7 Conclusions

In this chapter we showed that time interpolating OFDM signals prior to their transmission followed by the corresponding decimation at the receiver is a suitable technique for inducing high speed effects (mainly ICI) while actually measuring at much lower speeds. The key idea behind the proposed technique is that the ICI level experienced by the received signals after OFDM demodulation and before channel equalization depends on the relative factor between subcarrier spacing and Doppler spread. Hence, instead of changing the Doppler spread, one can change the subcarrier spacing by the same factor to obtain similar results. Moreover, we showed analytically and by simulations that the same level of ICI can be generated both by increasing the actual speed of the mobile receiver or by time interpolating the transmitted OFDM signals. The main advantage of the proposed technique is its feature to offer experimental evaluation of OFDM-based wireless communication systems at very high velocities while conducting measurements at much lower speeds. The price to be paid is that the signal bandwidth is reduced proportionally to the time interpolation factor, therefore potential inaccuracies could arise due to the loss of frequency diversity. However, to combat this loss in diversity, we proposed to transmit different replicas of the interpolated signal to cover the same bandwidth as in the non-interpolated case. Moreover, the frequency diversity reduction inherent to the bandwidth decrease caused by the time interpolation does not seem to affect to the simulation or measurement results. It is expected to affect more in channels exhibiting a very high frequency selectivity, which is unlikely in high speed conditions in which the channel response changes fast.

A measurement methodology for validating our technique in a controlled environment and under repeatable conditions was designed. The basic idea consists in evaluating different figures of merit for a certain range of actual speed values and to compare them with emulated speeds of the same magnitude under the same conditions. For example, when the figures of merit considered are evaluated at 150 km/h, three different cases are evaluated under the same conditions: 1) the receive antenna moves at the actual speed of 150 km/h; 2) the receive antenna moves at the actual speed of 75 km/h and a time interpolation factor $I = 2$ is used, hence the emulated speed is $75 \times 2 = 150$ km/h; and 3) the receive antenna moves at 50 km/h and $I = 3$

is applied. Besides the measurement results, we have also evaluated the proposed technique through simulations based on channel models specifically designed for modeling high speed scenarios. We selected EVM, uncoded BER, coded BER and throughput as figures of merit, all being evaluated for different SNR, CQI, and speed values. All results based on the four figures of merit have shown an excellent agreement between actual and emulated speeds for all the interpolation factors considered, hence validating the proposed technique as a good candidate to be considered not only for physical layer performance evaluations, but also for higher layer ones.

Besides validating the proposed technique, we have also shed light on the effects caused by high and even extremely high speeds on OFDM signals. More specifically, we have selected LTE as a waveform example of the state of the art of current mobile wireless systems. As expected beforehand, received signals suffer a similar degradation (in terms of EVM, uncoded and coded BER) when the SNR decreases or when the speed (and correspondingly the ICI level) increases. However, low SNR values can conceal the effects due to high speeds as the noise becomes the main contributor of the signal distortion. It was also shown that lower CQIs provide more robustness at high speeds, although reducing the maximum achievable throughput. Even for not so low SNR levels, the performance can be increased by considering lower CQI values for the high speed train environment. Notice that, as expected, the higher the constellation size, the higher the sensitivity it exhibits with respect to the speed. Moreover, a reliable and low-latency link at very high speeds demands for small-size constellations like 4-QAM, making adaptive modulation and coding schemes less attractive in these scenarios since a potential throughput increment when increasing the constellation size yields a high-BER with a very high probability, thus requiring retransmissions and impacting on both the delay and the jitter of the link.

It has been also shown that the proposed technique performs excellent not only in outdoor-to-indoor measurement scenarios, but also in simulations for a channel model specifically designed for outdoor-to-outdoor high speed scenarios. In both cases, the level of agreement between the results for actual speed and for emulated speeds is at the level of possible measurement accuracy, as the corresponding relative error curves have shown.

Finally, in the light of the excellent agreement of the results obtained under repeatable conditions for the figures of merit considered and regardless actual or emulated speeds are considered, it can be concluded that the proposed technique is valid for inducing high speed effects at any point in the signal processing chain at the receiver. Moreover, the technique for high speed emulation based on time-interpolating the signal has proven to be much simpler than other alternatives proposed. More specifically, this technique is transparent for the transmitter and receiver processing chains, apart from the interpolation and subsequent decimation processes. Although some of the other alternative proposals have the main advantage of not changing the spectral properties of the signal, most of them require to perform

changes on the processing chain of both transmitter and receiver.

Chapter 4

Experimental Results

Over the past few years, railway and telecommunication companies have shown a great interest in deploying broadband mobile wireless networks in high-speed-trains with the aim of supporting both the provision of passenger services and automatic train control and signaling. In this context, the Mobile-Relay technique has been proposed by the 3rd Generation Partnership Project (3GPP) as a way to provide coverage inside the train carriages. This motivates the study of the outdoor-to-indoor and outdoor-to-outdoor radio propagation characteristics for broadband wireless communications in high-speed railways, which is the main contribution of this chapter. Performance of the fourth generation (4G) communication systems for both the outdoor-to-outdoor as well as the outdoor-to-indoor links in vehicle-to-infrastructure scenarios was experimentally assessed by means of several measurement campaigns using mobile receivers installed in cars, subways and high speed trains.

This chapter is mainly based on the following co-authored publications:

- Pedro Suárez-Casal, José Rodríguez-Piñeiro, José A. García-Naya, and Luis Castedo. **Experimental Evaluation of the WiMAX Downlink Physical Layer in High-Mobility Scenarios**. In: *EURASIP Journal on Wireless Communications and Networking* 2015.109 (Dec. 2014). Special Issue on Experimental Evaluation in Wireless Communications. Online access: http://dx.doi.org/10.1186/s13638-015-0339-9

- César Briso-Rodríguez, Carlos F. López, Jean R. Fernández, Sergio Pérez, Drasko Draskovic, Jaime Calle-Sánchez, Mariano Molina, José I. Alomso, Carlos Rodríguez, Carlos Hernández, Juan Moreno, José Rodríguez-Piñeiro, José A. García-Naya, and Luis Castedo. **Broadband Access in Complex Environment: LTE on Railway**. In: *IEICE Transactions on Communications* 97.8 (2014). Special Section on EU's FP7 R&D Project Activities on Future Broadband Access Technologies. Online access: http://dx.doi.org/10.1587/transcom.E97.B.1514, pp. 1514–1527

- José Rodríguez-Piñeiro, José A. García-Naya, Pedro Suárez-Casal, César Briso-

Rodríguez, J. I. Alonso-Montes, and Luis Castedo. **Assessment of Channel Propagation Conditions for FDD LTE Transmissions in the Spanish High-Speed Railways**. In: *10th European Conference on Antennas and Propagation (EuCAP 2016)*. Davos, Switzerland, Apr. 2016

- José Rodríguez-Piñeiro, Pedro Suárez-Casal, José A. García-Naya, Luis Castedo, César Briso-Rodríguez, and J. Ignacio Alonso-Montes. **Experimental Validation of ICI-Aware OFDM Receivers under Time-Varying Conditions**. In: *Eighth IEEE Sensor Array and Multichannel Signal Processing Workshop*. Online access: http://dx.doi.org/10.1109/SAM.2014.6882411. A Coruña, Spain, June 2014, pp. 341–344

- José Rodríguez-Piñeiro, José A. García-Naya, Ángel Carro-Lagoa, and Luis Castedo. **A Testbed for Evaluating LTE in High-Speed Trains**. In: *16th Euromicro Conference on Digital System Design (DSD 2013)*. Online access: http://dx.doi.org/10.1109/DSD.2013.27. Sept. 2013, pp. 175–182

- Dan Fei, José Rodríguez-Piñeiro, José A. García-Naya, Luis Castedo, and Lei Xiong. **TD-LTE Downlink Performance Assessment in High Speed Scenarios**. In: *2016 IEEE 83rd Vehicular Technology Conference (VTC2016-Spring)*. Track "2nd International Workshop on Wireless Communications for High Speed Railways (HSRCom2016)". Nanjing, China, May 2016

- Lei Zhang, Pedro Suárez-Casal, Jean Fernández, José Rodríguez-Piñeiro, Jaime Calle-Sánchez, José A. García-Naya, Luis Castedo, C. Rodríguez-Sánchez, J. Moreno, César Briso-Rodríguez, and J. I. Alonso-Montes. **Experimental Evaluation of 4G Technologies in Metro Tunnel Scenarios**. In: *10th European Conference on Antennas and Propagation (EuCAP 2016)*. Davos, Switzerland, Apr. 2016

- José A. García-Naya, José Rodríguez-Piñeiro, Ángel Carro-Lagoa, and Luis Castedo. **Demostrador para la Evaluación Experimental de LTE en Entornos Ferroviarios de Alta Velocidad**. In: *XXVIII Simposium Nacional de la Unión Científica Internacional de Radio (URSI 2013)*. Sept. 2013

- Lei Zhang, José Rodríguez-Piñeiro, Jean R. Fernández, José A. García-Naya, David W. Matolak, César Briso, and Luis Castedo. **Propagation Modeling for Outdoor-to-Indoor and Indoor-to-Indoor Wireless Links in High-Speed Train**. In: *Submitted to the Measurement journal.* (2016)

In Section 4.1 the motivation of this chapter is provided, whereas Section 4.2 describes the so-called GTEC Testbed, extensively used for the measurement campaigns. Section 4.3 presents the results obtained for car-to-infrastructure evaluations, whereas Section 4.4 and

Section 4.5 introduce the results obtained for subway-to-infrastructure and high-speed-train-to-infrastructure evaluations. Finally, Section 4.6 summarizes the main findings of this chapter.

4.1 Motivation

Over the past few years, the increasing demand for the use of mobile phones, laptops and other wireless devices by high-speed-train passengers has attracted great interest from railway companies. Simultaneously, the Mobile-Relay technique has been proposed in [3GP12] as a way to provide coverage to passengers based on a relaying scheme. These factors motivate the increasing interest for the study of the radio propagation characteristics for wireless communication systems in railways, with the aim of providing broadband communications in trains [Bri+14a]. Not only high speed trains are the scenarios of interest, but also metro transportation, in which both train control and video surveillance can take advantage of the high throughput exhibited by 4G systems. Moreover, Long Term Evolution (LTE) is already being deployed in metro systems [Co] due to the aforementioned reasons. Finally, it is also becoming more common to provide data access to users of buses, taxis or even particular cars by means of relaying schemes.

In Section 2.5, several of the most typical environments for high speed train scenarios were studied in detail. Propagation properties for different scenarios involving outdoor-to-indoor transmission with movement, such as elevator shafts [SM13], cars [Har+13] or aircrafts [Mor+09; And+12], have also been studied. Propagation characteristics of intra-car and inter-car links for carrier frequencies close to $2\,\text{GHz}$ are studied in [Mar+13] and [Shi+14], respectively. Measurements in [Ito+11] show the influence of the signal entering through the windows of the train in inter-car links when the carrier frequency is $5\,\text{GHz}$. Propagation losses inside the train at $2.35\,\text{GHz}$ and $2.15\,\text{GHz}$ have been also studied by wideband measurements at the high-speed railway environment in [Don+10].

In general, wireless network access systems for the railway environment can be classified into four types:

- **Intra-car link**: the link between a mobile device and an Access Point (AP), both located inside the same car;
- **Inter-car link**: the link between a mobile device and an AP located inside different cars;
- **Base Transceiver Station (BTS)-train link**: the outdoor-to-outdoor link between a BTS and the outdoor antennas of a train; and
- **BTS-mobile link**: the outdoor-to-indoor link between a BTS and a mobile inside of a train (e.g., a passenger using a mobile device directly attached to the commercial cellular network).

The main contribution of this chapter is to present a performance study for the BTS-train as

well as BTS-mobile links in different environments by means of actual measurements using 4G waveforms (Worldwide Interoperability for Microwave Access (WiMAX) and LTE). Note that no coordination between links is considered. In a practical deployment of a relaying scheme, several possibilities could be implemented, such as *(i)* a simple amplify&forward scheme or *(ii)* that each AP on the train acts as a femtocell to the network (e.g., see [Che+13] for the LTE case). Whereas the first approach is probably the simplest one, some interference management mechanism must be required in case the same frequency bands are used for both links in Frequency Division Duplex (FDD). Regarding the second approach, it may be more efficient in terms of resources sharing , although it would probably require to install a different femtocell per network operator. On the other hand, alternatives which employ non-4G waveforms inside the moving vehicle could be also considered, such as Wi-Fi APs.

4.2 The GTEC Testbed

In this section the testbed developed at the Group of Electronic Technology and Communications (GTEC) is briefly described. This testbed was extensively used for experimental evaluations of WiMAX signals in high speed environments (see [Suá+14a; Rod+14; Suá+14b]), and LTE signals in subways, railway scenarios and high speed environments (see [Zha+16a; Rod+16c; Zha+16b; Fei+16]). Finally, it has been used also for experimental evaluations of the new waveform proposals for the fifth generation (5G) systems both in static environments (see [Dom+16a]) and high speed ones (see [Rod+16a]). The GTEC testbed allows for converting previously generated data into electromagnetic waveforms that are transmitted over-the-air (TX side), as well as receive and store the acquired samples for further processing (RX side). The testbed consists of several nodes which are evolved versions of the one described in [Rod+13a]. The hardware and the software parts of the nodes are described in Section 4.2.1 and Section 4.2.2, respectively. Figure 4.1 shows a typical configuration of the testbed, in which one of the nodes is used in transmit-only mode while the other is set up in receive-only mode.

4.2.1 Hardware

The heart of each node (see Fig. 4.2) is an Universal Software Radio Peripheral (USRP) B210 board [Resa] built from the AD9361 chip [Dev] by Analog Devices, which supports a continuous frequency coverage from 70 MHz to 6 GHz; full-duplex Multiple-Input Multiple-Output (MIMO) operation with up to two antennas, and a maximum bandwidth of 56 MHz; USB 3.0 connectivity; on-chip 12 bit Analog-to-Digital Converters (ADCs) and Digital-to-Analog Converters (DACs) up to 61.44 Msample/s; and configurable transmit and receive gain values.

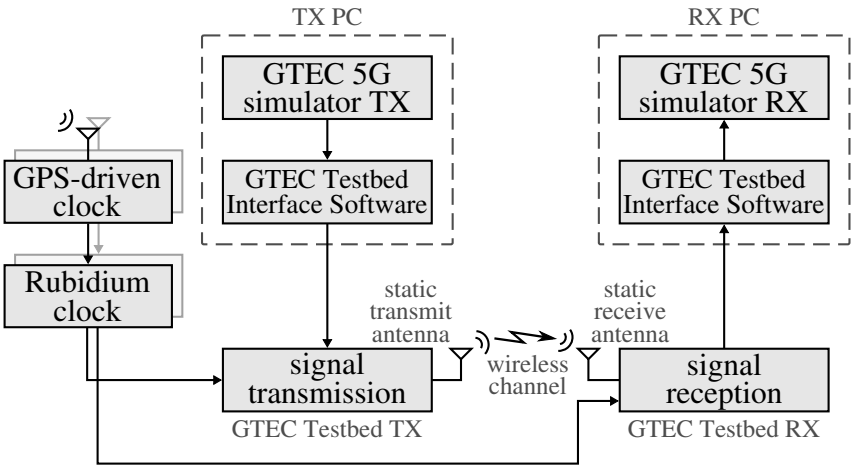

Figure 4.1: The GTEC Testbed architecture. Typical configuration in which one node is used in transmit-only mode while the other is set up in receive-only mode.

A Rubidium oscillator, optionally driven by a Global Positioning System (GPS)-disciplined clock, may also be used at each node to provide very accurate time and frequency synchronization.

4.2.2 Software

For each node, its corresponding USRP board is connected to a computer (usually a laptop for convenience) equipped with two solid-state drives: one containing a GNU/Linux operating system and the custom-developed measurement software, whereas the other is dedicated to store the transmit/acquired signals. The laptops are labeled in Fig. 4.1 as "TX PC" (transmitter) and "RX PC" (receiver).

There are two main software components used in both nodes, as shown in Fig. 4.1, the GTEC Testbed Interface Software (GTIS) and the "GTEC 5G Simulator TX/RX".

GTEC Testbed Interface Software

This software component communicates directly with the USRP and is used to set up or change the configuration, read the signals to be transmitted from disk and store the acquired samples. We use a custom-developed multi-threaded software implemented in C++ with Boost [DA] and based on the Ettus USRP Hardware Driver (UHD) [Resb]. The main thread of the receiver is responsible for retrieving the samples coming from the USRP through the USB 3.0 bus and store them in a set of buffers in the main memory of the host laptop. The second thread reads the samples from such buffers and saves them persistently in a dedicated solid-state drive. Finally, there is a low-priority thread for logging important information for documenting the measurement campaign. On the other hand, the transmitter is a single-thread process since the same signals are cyclically transmitted over-the-air. Therefore, the signals to be radiated are

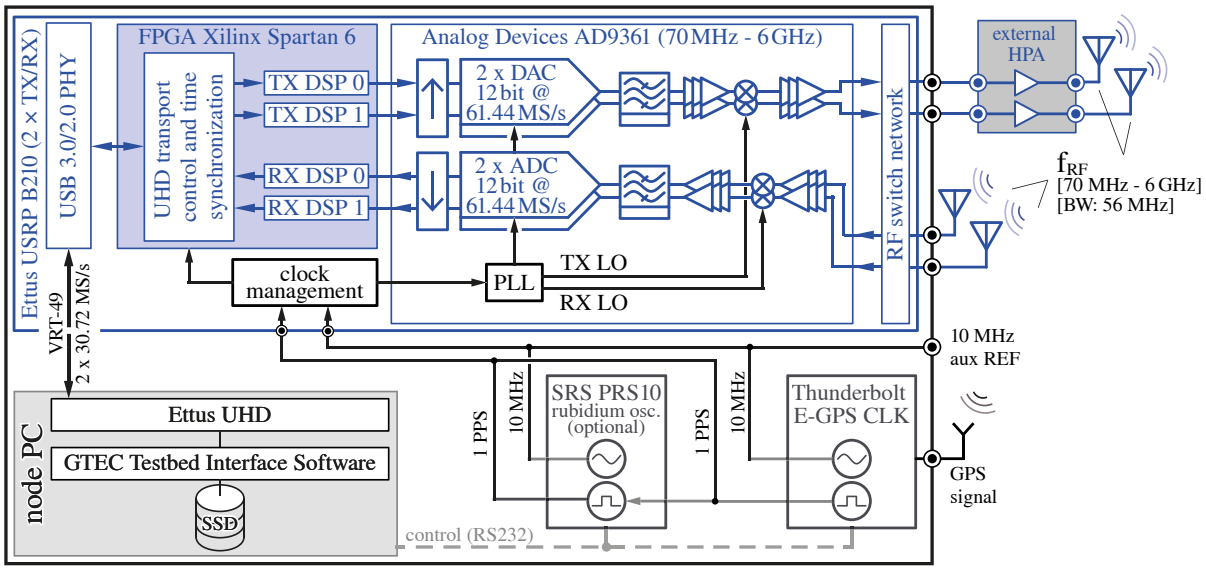

Figure 4.2: Block diagram of a node of the GTEC Testbed. Trimble Thunderbolt E-GPS and Standford Research Systems PRS10 are optional. A GPSDO available from Ettus can be also used as a GPS-disciplined oscillator. The advantage of the latter is that allows for capturing NMEA records to get the position and velocity among other.

first stored in a temporary buffer and next transmitted in a loop to the USRP through the USB 3.0. Several wrapper calls were also developed in Matlab™ to allow for controlling the testbed directly from Matlab™.

GTEC 5G Simulator

This software component is used to generate and process the signals of interest and is fully integrated with the GTIS part. This software could be easily replaced by other software implementations of any desired communication system that meets the constraints of the testbed. For example, the Vienna LTE Simulator [RST16] was integrated with the GTEC testbed. Currently, the software allows for generating and processing WiMAX and LTE signals, as well as signals that consider the new modulation schemes proposed for 5G systems. Moreover, the GTEC 5G Simulator can be used jointly with the GTEC testbed to perform measurements or in a standalone fashion to perform simulations.

The code of both the GTIS and the GTEC 5G Simulator is publicly available under the GPLv3 license at [Tea]. More information on the GTEC Testbed, both for the hardware and the software part, can be found in [Dom+16b] and in Section 5.3.1.

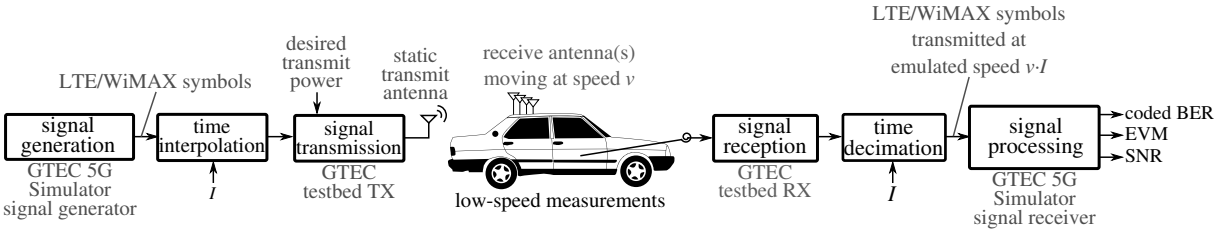

Figure 4.3: Block diagram of the considered setup for the Car-to-Infrastructure measurements.

4.3 Car-to-Infrastructure Measurements

In this section, the performance of 4G communication systems in a vehicle-to-infrastructure link is assessed by analyzing the results of measurement campaigns where the receiver nodes are installed in a car. More specifically, performance results both for WiMAX and LTE signals are provided for receive antennas placed outdoors (on the roof of the car) and a single base station. Measurements are carried out at a speed of 20 km/h and the technique introduced in Section 3.2 is used to emulate much higher speeds.

In Section 4.3.1 the measurement setup and procedure followed for both the WiMAX and LTE evaluations is introduced, whereas the obtained results are included in Section 4.3.2. Finally, brief conclusions are provided in Section 4.3.3.

4.3.1 Measurement Setup and Procedure

This section describes the considered measurement setup as well as the followed procedure for assessing the performance of 4G signals (WiMAX and LTE) in realistic environments by using the high speed emulation technique presented in Section 3.2. For both cases, the evaluation setup shown in Fig. 4.3 is considered. It allows for assessing the performance in a typical outdoor-to-outdoor high-speed scenario, where the base station remains static and very high velocities are considered for the mobile unit, whereas the measurements are carried out at a much more convenient speed, such as 20 km/h.

Firstly, the details of the setup for WiMAX assessment are introduced. Next, the LTE case is considered.

Experimental Setup (WiMAX Evaluations)

For the case of the WiMAX evaluations, the receiver is provided with an Inter-Carrier Interference (ICI) cancellation scheme. Although ICI estimation and elimination in Orthogonal Frequency-Division Multiplexing (OFDM) is a well studied topic in the literature, few works have addressed the problem under real conditions [RL11] except for underwater acoustic communications [PS09]. Most ICI cancellation techniques are based on the use of Basis Expansion Models (BEMs) to account for the channel time variations. Some works focus on the

estimation of time-varying channel impulse responses from the pilots of a single OFDM symbol [Tan+07], while others rely on multiple OFDM blocks to perform such estimation [TLB06; HR09; Sim+11; Suá+13; Cas15]. For the case of these measurements, once each WiMAX frame is detected and its frequency offset corrected based on the repetition properties of the WiMAX preamble [Rod+14], an ICI estimation algorithm based on the output of a frequency response estimator is applied. The output of this frequency response estimator is denoted as $\hat{\mathbf{h}}_k$, which is a $N \times 1$ vector containing the frequency response estimation of the k-th OFDM symbol. To model the channel time variations, a P-order BEM is used. It is represented by $\mathbf{B}$, a $MN \times P$ matrix whose columns are the BEM vectors corresponding to a group of M consecutive symbols. ICI can be estimated from the frequency response estimations in such a group as

$$\hat{\mathbf{c}}_i = (\mathbf{L}^H\mathbf{L})^{-1}\mathbf{L}^H\mathbf{J}_i, \tag{4.1}$$

where $\mathbf{J}_i = [\hat{\mathbf{h}}_i, \hat{\mathbf{h}}_{i+1}, \cdots, \hat{\mathbf{h}}_{i+M-1}]^T, i = 1, \ldots, (K - M + 1)$ is a $M \times N$ matrix containing the frequency response of the M symbols of the i-th group of OFDM symbols; $\mathbf{L} = [\mathbf{b}_{N/2}, \mathbf{b}_{N+N/2}, ..., \mathbf{b}_{(M-1)N+N/2}]^T$ is a $M \times P$ matrix, with $\mathbf{b}_k$ the k-th column of $\mathbf{B}^T$; and $\hat{\mathbf{c}}_i$ a $P \times N$ matrix with the ICI estimation coefficients for the i-th group of OFDM symbols. From $\hat{\mathbf{c}}_i$ and $\mathbf{B}$, the $\mathbf{H}_k$ matrices for each of the M consecutive symbols of the group can be computed [Sim+11].

The receiver first estimates the frequency response of each OFDM symbol with a time-domain Least Squares (LS) estimator assuming that all subcarriers are known. With this estimation, groups of $M = 6$ OFDM symbols are defined to apply the ICI estimator using a DPS-BEM [ZM05b] with order $P = 5$ designed for the Doppler spreads to be expected during the experiments ($D_n = 0.2$). The algorithm to remove the ICI works as follows:

- **Initialization**. ICI is estimated from the first group ($i = 1$) of 6 OFDM symbols and removed from the first to the fourth OFDM symbols of the group;
- **Loop**. For $i = 2$ to $i = K - M$, the ICI is estimated from each group and removed from the fourth OFDM symbol of each group;
- **Termination**. For $i = K - M + 1$, the ICI is removed from the fourth to the sixth OFDM symbols.

The aim of the scheme above is to use the central OFDM symbols of each group where the lowest estimation error is achieved with the proposed method [Suá+13]. Once the ICI is removed from the symbols using a successive interference cancellation equalizer, the time-domain LS estimator is used again to equalize the subcarriers. Notice that if not all subcarriers are assumed to be known at the receiver, the initial frequency response estimation would be worse, the overall ICI estimation would be also degraded, and at least part of the induced ICI would not be revealed in the results.

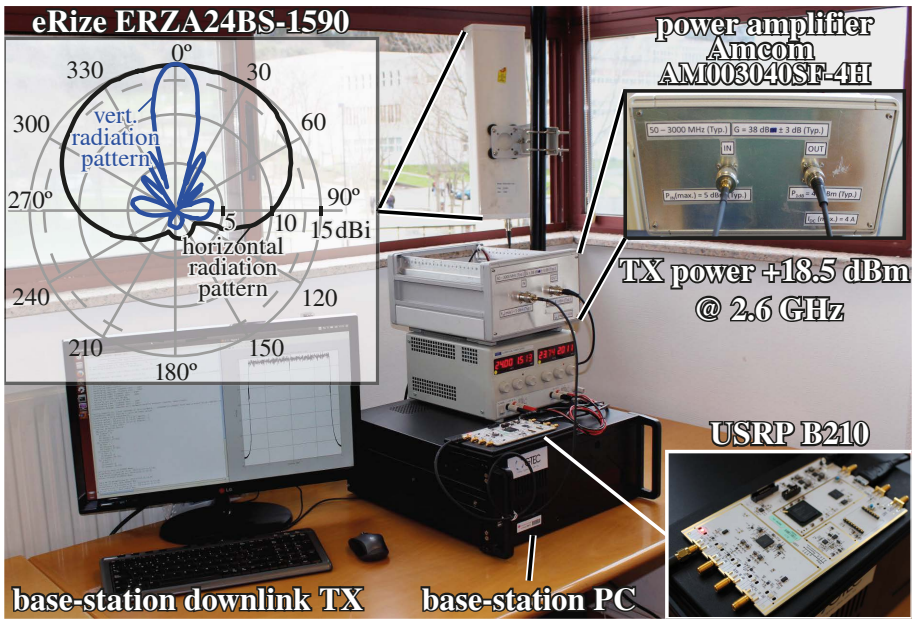

Figure 4.4: GTEC Testbed node acting as a transmitter placed in a room inside the building of the Faculty of Informatics at the University of A Coruña. Note that in this case the software of the testbed was installed in a Personal Computer instead of a laptop, since no mobility was required at the transmitter side.

The WiMAX profile considered for the measurements corresponds to that of 7 MHz of bandwidth, whereas the sampling rate is $F_b = 8$ Msample/s. $N = 1024$ subcarriers and a cyclic prefix of $1/8$ ($N_g = 128$ samples) are employed. The transmit frame consists of 6 bursts of 4 OFDM symbols per burst ($K = 24$ OFDM symbols per frame). The first two bursts use 4-QAM, the next two use 16-QAM, and finally, the last two employ 64-QAM symbols. At the base-station, once the OFDM signals are generated, they are interpolated by a factor $I \in \{21, 32\}$ using an interpolation FIR filter, yielding a signal bandwidth of 360 kHz for $I = 21$, and 240 kHz for $I = 32$. Next, the signals are shifted 1 MHz in frequency to avoid the DC leakage at both the transmitter and the receiver, thus the DC subcarrier is shifted 1 MHz to avoid the distortion caused by the DC leakage to the subcarriers around the DC since the subcarrier spacing is reduced.

The base station reads the file containing the previously generated signals to be transmitted cyclically. First, such signals are transferred to the USRP where they are again interpolated in the FPGA by a factor of 6 before reaching the DACs, which are configured at 48 Msample/s. Next, the signals are up-converted to $f_c = 2.6$ GHz, pre-amplified inside the USRP (configured with a gain value of 70 dB out of 89.5 dB), amplified by the Amcom AM003040SF-4H power amplifier (38 dB gain), and finally radiated by the antenna. The power value measured at the antenna input is +18.5 dBm. Table 4.1 shows the main parameters considered for the experiments.

Fig. 4.4 shows the base-station placed in a room with the antenna pointing outdoors. It also

Table 4.1: Main parameters used in the experiments.

Signal bandwidth, F_s	7 MHz
Sampling rate, F_b	8 Msamples/s
Number of subcarriers, N	1024
Symbols per frame, K	24
Cyclic prefix length, N_g	128
Actual velocities, v	20 km/h
Carrier frequency, f_c	2.6 GHz
Transmit power	+18.5 dBm (at antenna port)
Interpolation factors, I	21 and 32 (to emulate 640 km/h)

shows the power amplifier, the USRP B210, and the antenna radiation pattern. Note that in this case the software of the testbed was installed in a personal computer instead of a laptop, as no mobility was required from the transmitter side.

During the measurements, the acquired signals are persistently stored in a dedicated drive, but they are not processed using the WiMAX receiver. As shown in Fig. 4.5, a single receive antenna is sticked on the roof of a car and connected directly to the USRP B210, which is powered by the aforementioned laptop. The gain of the USRP is set to 34 dB out of 73 dB to ensure a linear operation. With this configuration, the peak Signal to Noise Ratio (SNR) at the starting point (see Fig. 4.6) exceeds 35 dB.

Figure 4.6 shows the measurement scenario, including the position of the base-station and the path followed by the mobile receiver. From the starting to the end points there is a distance of 240 m, which is completed in 43.2 seconds at a speed of 20 km/h. At the beginning of the path, Line-of-Sight (LoS) propagation conditions between the transmitter and the receiver occur, but as the link distance increases, more obstacles appear in between, hence reducing the relevance of the LoS component.

Experimental Setup (Time-Division LTE Evaluations)

Three testbed nodes, a single transmitter and two receivers, are used for the evaluations. They are configured to work in a Time Division Duplex (TDD) fashion, as it is the case of many LTE networks in several countries, such as China. Speeds as high as 500 km/h are considered, since they are typical for high speed train environments.

The scenario shown in Fig. 4.7 is considered: a car equipped with the mobile unit downlink receiver (see Fig. 4.8) moves along the path (161 m long) at a constant (and convenient) speed of 20 km/h, completing each pass in 29 seconds. The eNodeB downlink transmitter is placed on the corner of a building adjacent to the measurement path (see Fig. 4.9), with the starting

Figure 4.5: GTEC Testbed node acting as a mobile receiver mounted on a car.

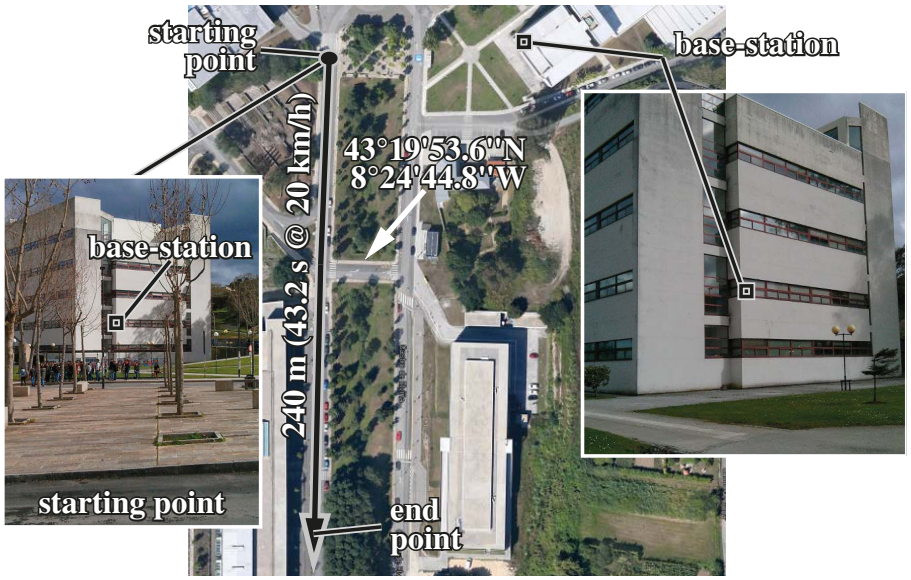

Figure 4.6: Measurement scenario considered for the WiMAX measurements in A Coruña, at the University of A Coruña. The path followed by the mobile receiver, as well as the location of the transmitter, are indicated in the figure.

point of the path being the farthest from the eNodeB. Some trees in the vicinity of the path produce shadowing effects about 100 m away from the starting point, while the building in front of the eNodeB, although lower, partially blocks the signal for the last 20 m of the path (see the estimated SNR along the trajectory plotted in Fig. 4.10).

The configuration parameters changed during the experimental evaluation are, on the one hand, the time interpolation factor $I \in \{10, 15, 21, 25\}$ to obtain the corresponding emulated speed values of 200, 300, 420, and 500 km/h and, on the other, the constellation size, selected from 4-, 16-, or 64-QAM. A different TD-LTE frame is generated for each combination of

Figure 4.7: Measurement scenario considered for the Time-Division LTE (TD-LTE) measurements in A Coruña, at the University of A Coruña. The path followed by the receiver as well as the location of the transmitter are indicated in the figure.

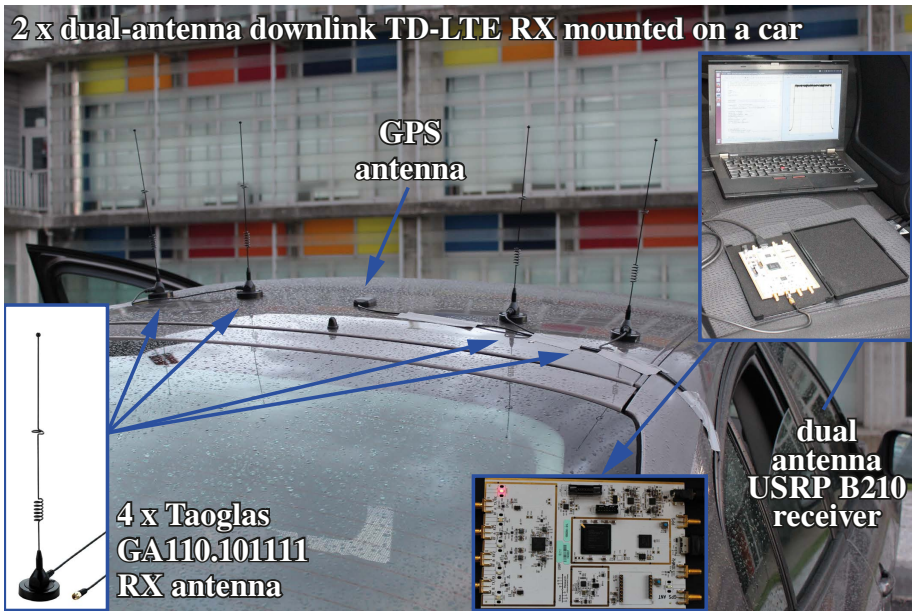

Figure 4.8: Two GTEC Testbed nodes configured as TD-LTE dual-antenna receivers were mounted on a car for the experiments performed.

interpolation factor and constellation size (12 combinations in total). During the measurements, a single frame is transmitted over the air in a cyclical fashion by the eNodeB while, at the same time, the receiver mounted on the car completes the trajectory shown in Fig. 4.7 twice at the constant speed of 20 km/h. The measurement is repeated again without modifying any parameter. Thus, two measurements are obtained for each time-interpolation and constellation-size pair.

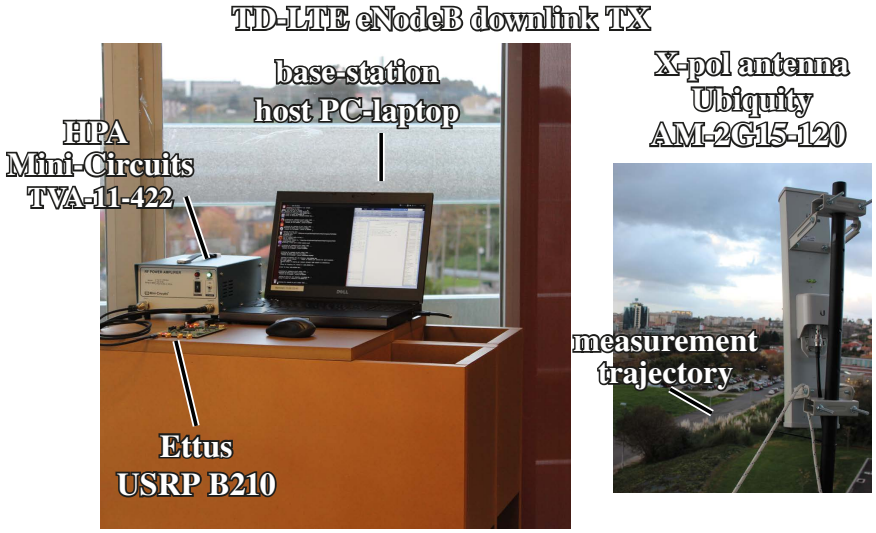

Figure 4.9: GTEC Testbed node acting as a TD-LTE single-antenna downlink transmitter. The vertically polarized antenna element of the X-pol Ubiquity AM-2G-15-120 is used.

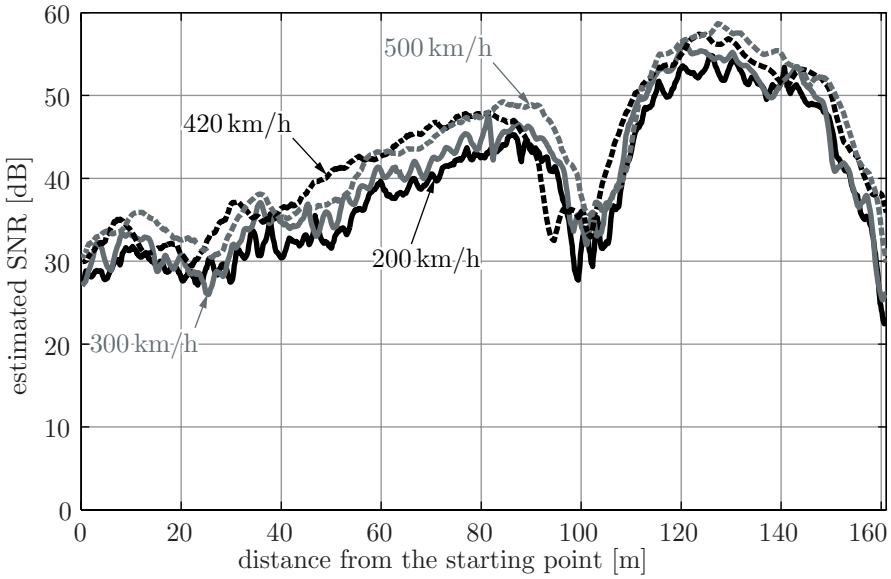

Figure 4.10: Measured SNR along the path followed by the car for the four emulated speeds. Shadowing effects at about 100 m away from the starting point are caused by some trains in the vicinity, whereas a building placed in front of the Evolved NodeB (eNodeB) partially blocks the signal for the last 20 m of the path. As expected, the SNR does not vary significantly with a change on the speed.

TD-LTE Signal Generation and Processing: Standard-compliant TD-LTE [ETSa] subframes corresponding to the uplink-downlink configuration pattern shown in Fig. 4.11 are generated using the LTE System Toolbox for Matlab™.

At the receiver side, a custom software solution developed using the LTE System Toolbox is employed to process the acquired signals and to estimate the following metrics: SNR, coded Bit Error Ratio (BER), and Root Mean Square (RMS) Error Vector Magnitude (EVM). More specifically, a zero-forcing channel equalizer available in the LTE System Toolbox is used

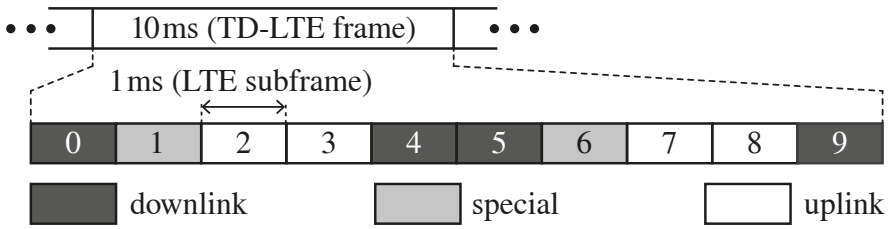

Figure 4.11: TD-LTE uplink-downlink configuration pattern considered in the measurements for the 10 LTE subframes composing a 10 ms LTE frame.

together with time and frequency synchronization algorithms developed from those provided by the aforementioned LTE System Toolbox. Note that since no feedback channel is used in our experiments, no adaptive modulation and coding schemes are applied. Thus, the achievable throughput is fixed all the time and only depends on the constellation size. The main parameters involved in the measurements are summarized in Table 4.2.

Time Interpolation and Time Decimation: The signal is time-interpolated by a factor $I \in \{10, 15, 21, 25\}$ at the transmitter and decimated by the same factor I at the receiver side (see Fig. 3.5). This way, we emulate a Doppler spread similar to that obtained with a speed increase by the factor of I. In order to preserve the average energy per OFDM symbol –and keeping a constant transmit power value independent of the interpolation factor– the interpolated signals are scaled in amplitude by a factor of $\sqrt{I}$ before being transmitted. Given that the actual speed of the car is fixed at 20 km/h, the four interpolation factors considered yield the emulated speed values of 200, 300, 420, and 500 km/h, correspondingly.

Different Channel Realizations: As commented above, two car passes are performed for each interpolation-factor and constellation-size pair. In other words, for each interpolation factor (emulated speed), the car moves twice along the measurement path while keeping constant the constellation size. Actually, two identical dual-antenna receivers are mounted on the car. Hence, four antennas acquire simultaneously, thus yielding eight measurement records for each interpolation-factor and constellation-size pair.

On the other hand, given that each TD-LTE frame is $T_F = 10$ ms long, the total duration of each time-interpolated frame is $T_F \cdot I$. Considering $I = 25$, the duration of the TD-LTE time-interpolated frame is 250 ms. Thus, 1160 frames can be acquired by each of the four antennas during the 29 s of a single measurement pass, yielding 9280 acquired frames in total (4 antennas times 2 passes) for each constellation size with $I = 25$. For lower values of I, more frames are acquired since the duration of each time-interpolated frame is shorter although the actual speed of the car is the same.

Table 4.2: Main parameters used in for the TD-LTE measurements. RMC stands for Reference Measurement Channel according to [ETSa].

Signal bandwidth, F_s	10 MHz (9 MHz used)
FFT size, N	1024
Number of used subcarriers	600 (excluding DC)
Actual velocity, v	20 km/h
Carrier frequency, f_c	2.6 GHz
Transmit power	+18.5 dBm (at antenna port)
Interpolation factors, I	10 (200 km/h), 15 (300 km/h), 21 (420 km/h), and 25 (500 km/h)
RMC number	R.2 (4-QAM), R.3 (16-QAM), and R.7 (64-QAM)
TDD	configuration mode #1 (see Fig. 4.11)
Max. throughput [Mbit/s]	1.966 (4-QAM), 6.408 (16-QAM), 13.910 (64-QAM)

4.3.2 Measurement Results

In this section, the results obtained by measuring using the setups described in the previous section are analyzed. First, the case of WiMAX transmissions is considered. Next, the analysis of LTE signals is introduced.

WiMAX Measurement Results

Figure 4.12 shows the obtained results in terms of SNR and EVM for the measurements carried out at 20 km/h and with an interpolation factor $I = 32$. This corresponds to a normalized Doppler spread $D_n = 0.2$ at $f_c = 2.6$ GHz, which agrees with that obtained if the signal is not interpolated at all and the car moves at 640 km/h. Also some exemplary simulation results are included. More specifically, the following assumptions were considered during the simulations: 1) a single-tap Ricean channel model with a $K_{\text{Rice}} = 4$ factor estimated according to [TAG03] (given that the measured channel is almost frequency flat due to the interpolation factors considered in the measurements); 2) a Jakes Doppler spectrum corresponding to a mobile moving at 640 km/h, yielding a normalized Doppler spread $D_n = 0.2$ at $f_c = 2.6$ GHz; and 3) the SNR values estimated from the measurements using the ratio between the power of data subcarriers and the noise level of the guard subcarriers. Such SNR values are shown at the top of Fig. 4.12.

Figure 4.12 shows the EVM values (multiplied by -1 to be included in the same figure together with positive SNR values and EVM gain values) obtained both from measurements and also by simulation.

Notice that when the SNR decreases, a degradation of the EVM in the received signal

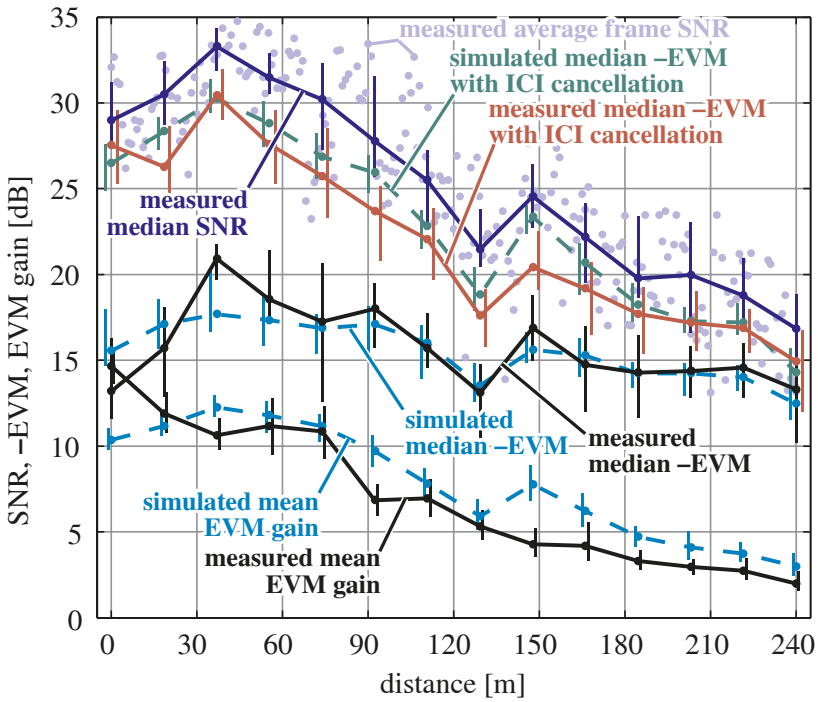

Figure 4.12: SNR and EVM results both obtained by means simulations and measurements carried out at an actual speed of 20 km/h. As expected, a reduction of SNR causes a decrease of the performance in terms of EVM (note that the EVM values are multiplied by -1). However, it can be seen that the performance is improved when the ICI cancellation is considered, showing that the technique of high speed emulation effectively introduces ICI on the signal. Moreover, the measurement results are well correlated with those obtained by simulations.

occurs. This effect can be observed both in the simulated and real scenarios, whether the ICI cancellation algorithm is considered or not. Nevertheless, it can be seen that the performance improves for any SNR value when the ICI cancellation method is used, allowing us to conclude that the received signal is affected by ICI. On the other hand, the empirical results are well correlated with those obtained by means of simulations, which do not consider frequency offsets. The performance gain in terms of EVM for both the simulated and the empirical results is also included at the bottom of Fig. 4.12. Notice that the SNR does not monotonically decrease due to the specific propagation conditions of the measurement scenario.

TD-LTE Measurement Results

Fig. 4.10 plots the coded BER and the EVM with respect to the estimated SNR, which ranges from 20 to almost 60 dB in the measurements. Firstly, the instantaneous values for each figure of merit are grouped into intervals according to their instantaneous SNR. Next, the averaged values for each figure of merit –together with their corresponding 95 % confidence intervals for the mean– are plotted with respect to the average SNR for each group. Finally, four curves corresponding to the emulated velocities of 200, 300, 420, and 500 km/h are plotted in coded

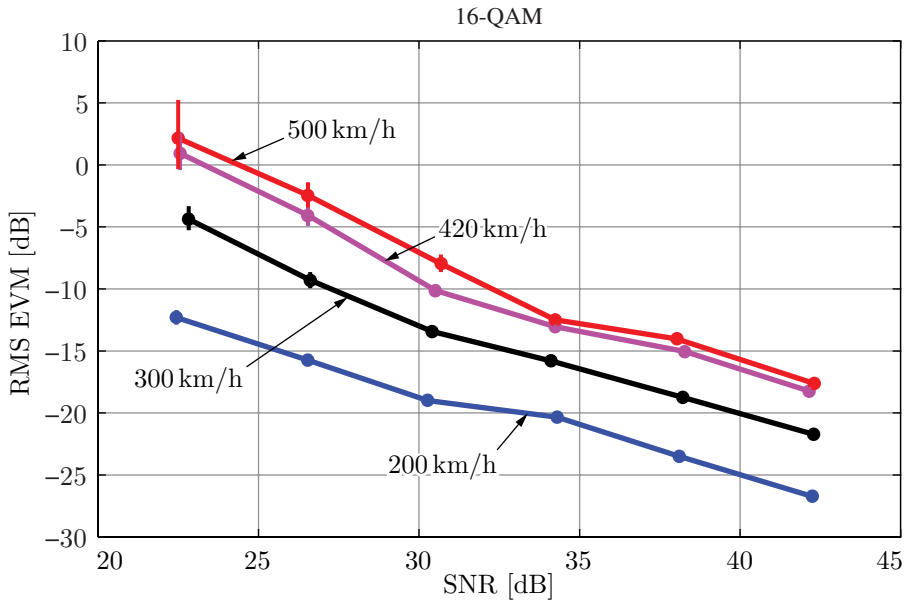

Figure 4.13: Measured RMS EVM versus the SNR for a 16-QAM constellation. As expected, the higher the emulated speed and the lower the SNR, the worse the RMS EVM. The high precision of the results is ensured by the reduced magnitude of the condifence intervals.

BER and EVM figures.

Figure 4.13 plots the EVM when 16-QAM is considered (the corresponding curves for 4-QAM and 64-QAM are not included because they do not provide any additional knowledge). The lengths of the confidence intervals are very short for most of the points, thus revealing a very good precision exhibited by the results. As expected, the higher the emulated speed and the lower the SNR, the worse the RMS EVM. Additionally, the RMS EVM degradation due to the increase of the speed ranges between 10 and 13 dB over the considered SNR range, thus revealing two independent sources of performance degradation: the link SNR and the receiver speed.

Figures 4.14 to 4.16 show the coded BER with respect to the SNR for the three constellation sizes. Again, the higher the constellation size, the higher the BER. Considering a threshold BER value of 10^{-2}, it is clear that 64-QAM requires an SNR above 33 dB for 200 km/h, while more than 42 dB are needed for 300 km/h. If the constellation size is reduced to 16-QAM, then the minimum SNR values are 25, 32, and 38 dB depending on the speed. Finally, when 4-QAM is used, less than 20 dB of SNR are required for 200 km/h; less than 25 dB for 300 km/h; less than 28 dB for 420 km/h; and less than 33 dB for 500 km/h. In view of the results, it is clear that higher constellation sizes exhibit large BER values and more variability, whereas 4-QAM is very robust even for a very high speed of 500 km/h.

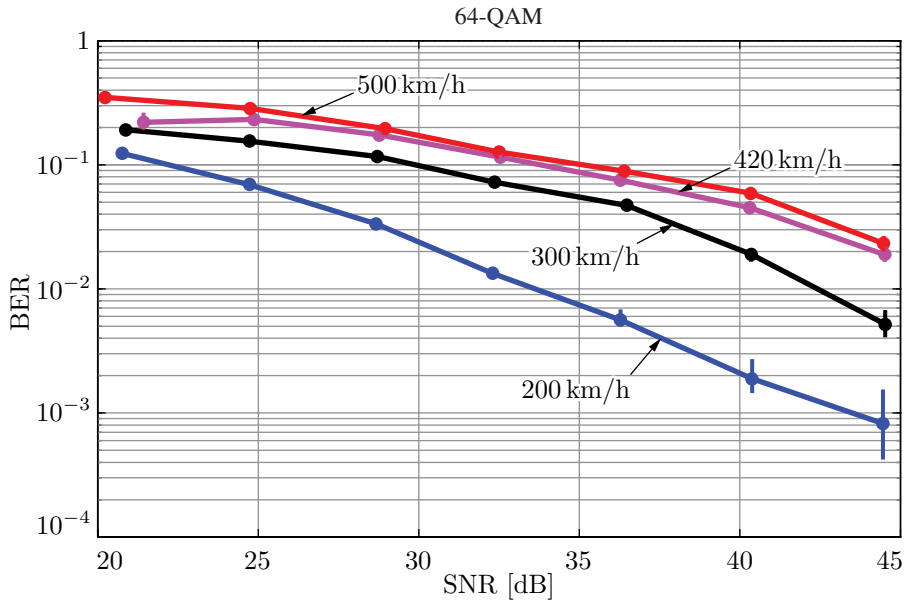

Figure 4.14: Measured Coded BER with respect to the SNR for a 64-QAM constellation. The lower the SNR, the worse the coded BER results, as expected. If a coded BER threshold of 10^{-2} is considered, more than 33 dB of SNR are required for 200 km/h and more than 42 dB for 300 km/h.

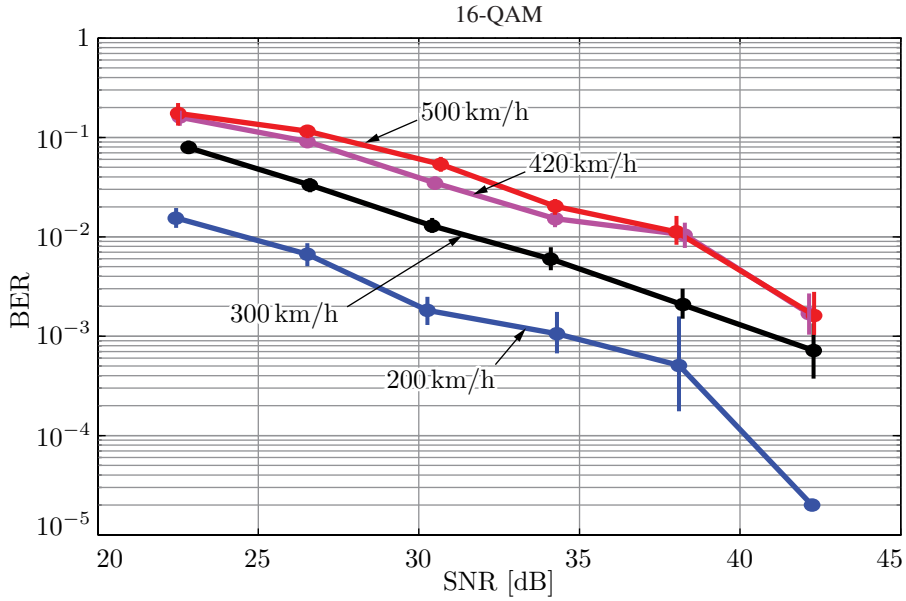

Figure 4.15: Measured Coded BER with respect to the SNR for a 16-QAM constellation. The lower the SNR, the worse the coded BER results, as expected. If a coded BER threshold of 10^{-2} is considered, more than 25 dB of SNR are required for 200 km/h; more than 32 dB for 300 km/h; and more than 38 dB for 420 km/h.

4.3.3 Conclusions

Performance results obtained by measuring 4G signals (WiMAX and LTE) in car-to-infrastructure scenarios were provided in this section. The technique of high speed emulation presented in Section 3.2 was used to carry out the measurements at low speeds for convenience.

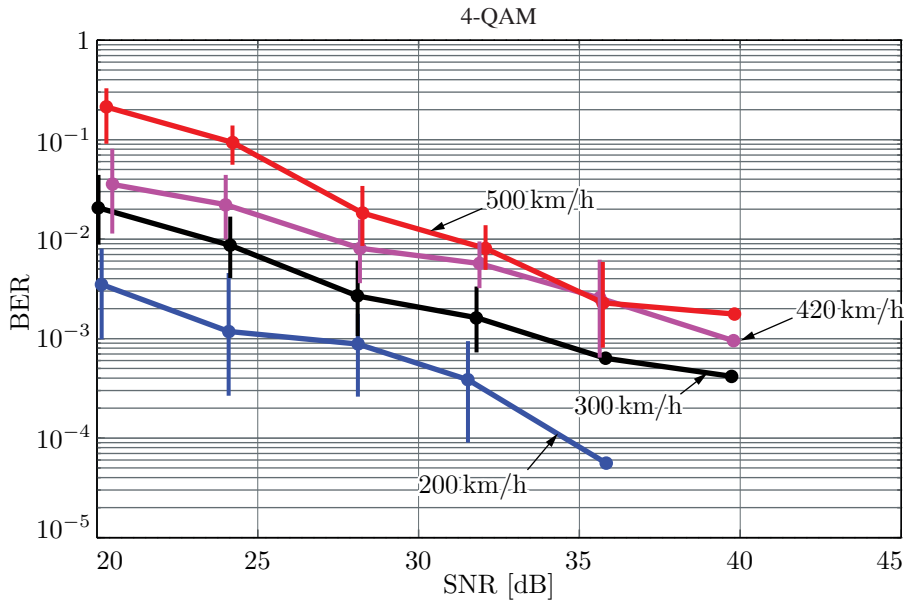

Figure 4.16: Measured Coded BER with respect to the SNR for a 4-QAM constellation. The lower the SNR, the worse the coded BER results, as expected. By comparing the results with the ones correspondent to higher order modulations, it is clear that higher constellation sizes exhibit large BER values and more variability, whereas 4-QAM is very robust even for a very high speed of 500 km/h.

The performance of an ICI cancellation algorithm with measured and simulated WiMAX symbols was confronted, and similar results were obtained, thus showing that the technique of high speeds emulation by time interpolation can be applied to actual evaluations in high speed environments. The technique was even employed for assessing the TD-LTE downlink performance in a typical outdoor scenario. The emulated speeds range from 200 to 500 km/h, being typical in high-speed train scenarios. The obtained results show, on the one hand, that the main performance degradation sources are the SNR of the link and the speed of the mobile receiver. On the other, a reliable and low-latency link at very high speeds demands for small-size constellations like 4-QAM, making adaptive modulation and coding schemes less attractive in these scenarios since a potential throughput increment when increasing the constellation size yields a high BER with very high probability, thus requiring retransmissions and impacting on both the delay and the jitter of the link.

4.4 Subway-to-Infrastructure Measurements in Tunnels

In this section, the performance of 4G communication systems in a vehicle-to-infrastructure link is assessed by analyzing the results of measurement campaigns for which the receiver nodes are installed in an underground train. More specifically, the performance results for WiMAX signals are provided for receiver antennas placed outdoors (attached to the subway structure) and indoors (inside one of the train carriages), considering a single base station equipped with a

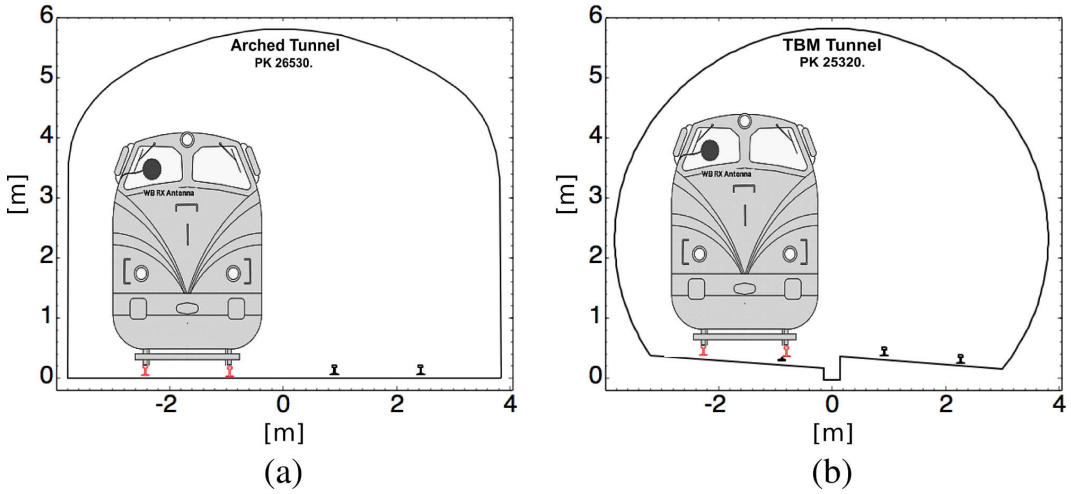

Figure 4.17: Exemplary tunnel cross sections: *(a)* arched tunnel; *(b)* TBM tunnel.

single transmit antenna. The main objective is to evaluate the performance when the subway is approaching, leaving, and inside a train station, so the base station position is fixed at the station, whereas the subway crosses the station at 18 km/h, which is the maximum allowed speed at that track segment.

Section 4.4.1 introduces the measurement setup and followed procedure for carrying out the measurements, whereas Section 4.4.2 presents the obtained results. Finally, Section 4.4.3 details the main conclusions derived from the measurements.

4.4.1 Measurement Setup and Procedure

The evaluation of 4G technologies in the metro environment requires to carry out measurements in tunnels with different types of sections, curves and stations. The two most common cross sections in metro tunnels are the circular (excavated by Tunnel Boring Machine (TBM)), and the arched ones (see Fig. 4.17). The radius of curves in a tunnel are also relevant, since the propagation losses increase in tunnels with small radius of curvature. The curvature radius range in metro tunnels is typically from 90 m to 1000 m, while the slope of the tunnels is always less than $5.5\,\%$. Another essential aspect is the presence of stations, which are usually very different in size and shape from tunnels. Old metro stations used to be very narrow, while modern stations are wide and pit-shaped with a high ceiling. Thus, the narrow stations can be considered as wide tunnels, but modern large stations are different.

A set of measurements was carried out at the *Ciudad de los Ángeles* station (Line 3 of *Metro de Madrid*) in order to assess the performance of a 4G physical layer by means of over-the-air transmissions. Note that metro infrastructures require access permissions and specific security requirements must be complied to carry out this kind of measurements. Furthermore, measurements must be carried out during maintenance periods in a short time-window during night, requiring easy-to-deploy testbeds. In this sense, the use of the GTEC Testbed, described

Figure 4.18: Deployment of the base station at the subway station as well as the outdoors receive antennas. The considered transmit antenna is labeled as "Tx_1", while the outdoors receive antennas are "Rx_1" and "Rx_2_2".

in Section 4.2, was found to be very beneficial. A single-antenna transmitter is placed on the platform of the station (see antenna "Tx_1" in Fig. 4.18), while two different nodes acting as receivers are employed simultaneously. The first one is installed inside the cabin (see Fig. 4.19a), with the antennas fixed on the windshield of the front car (see antennas "Rx_1" and "Rx_2" in Fig. 4.18). The second receiver is placed inside the train and its two antennas are also installed indoors (see Fig. 4.19b). The approximate distance between the two receivers is 50 m. The antennas installed outdoors model the rail operator communications infrastructure, while the indoor antennas are aimed to model the signal received by the mobile device of a train passenger. Notice that no multiple-antenna transmission scheme has been considered and that the carrier frequency was set to 2400 MHz as it is one of the most common values found in this type of applications.

WiMAX signal transmission is considered in this case. The frames transmitted convey six data bursts, each one allocated with four consecutive OFDM symbols and all the available subcarriers, adding up to a total of 24 OFDM symbols per frame. Each burst carry information symbols with different profiles of modulation and channel coding rates, namely, 4-QAM 1/2, 4-QAM 3/4, 16-QAM 1/2, 16-QAM 3/4, 64-QAM 1/2 and 64-QAM 3/4. Channel coding algorithm in all bursts is a tail-biting terminated convolutional code.

The samples captured by the testbed during the measurement stage are batch-processed with a receiver consisting of frame detection, time and carrier frequency offset synchronization,

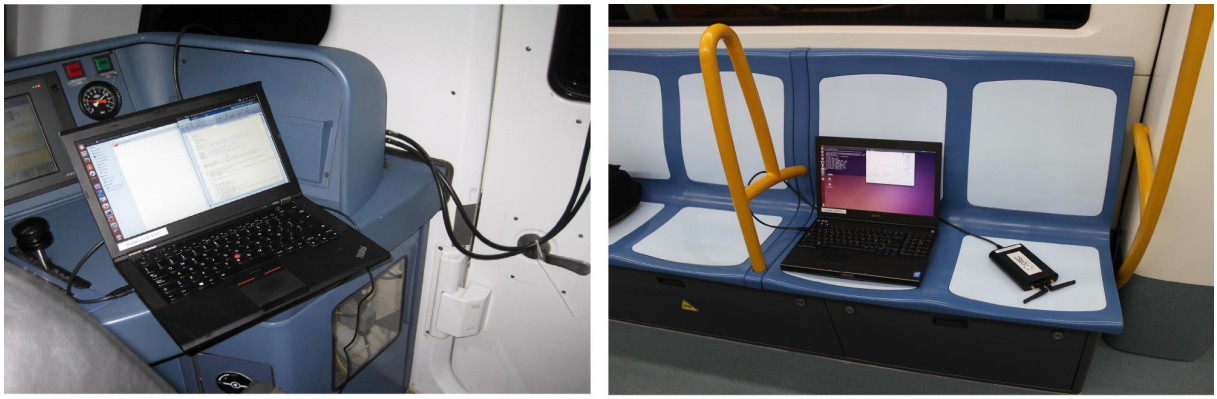

(a) (b)

Figure 4.19: GTEC Testbed receiver nodes: *(a)* node connected to the outdoors antennas; *(b)* node provided with its own indoors antennas.

Table 4.3: Parameters used for the WiMAX measurements.

Sampling frequency	8 MHz
Useful bandwidth	7 MHz
Number of subcarriers	1024
Number of data subcarriers	720
Number of pilot subcarriers	120
Subcarrier spacing	7.81 kHz
Cyclic prefix length	128 samples
Permutation zone	PUSC

channel estimation, equalization, and channel decoding. Frame detection and synchronization is computed from the preamble symbol which precedes each frame. This symbol has a three-fold repetition structure in the time domain, which can be exploited to detect its arrival, and obtaining synchronization parameters estimation. For channel estimation and equalization, linear Minimum Mean Squared Error (MMSE) algorithms have been implemented, after estimating the channel and noise covariance from the received signal. The main parameters used to generate the transmit signal are provided in Table 4.3.

4.4.2 Experimental results

The results presented in this section are obtained when the train approaches the station at a constant speed of 18 km/h. The recording of the signals starts when the whole train is still inside the entrance tunnel of the station and finishes when the front cabin enters in the exit tunnel of the station.

All acquired frames are processed to estimate the strength of the received signal and the physical layer throughput, both for the antennas outside and inside the train. First, SNR and

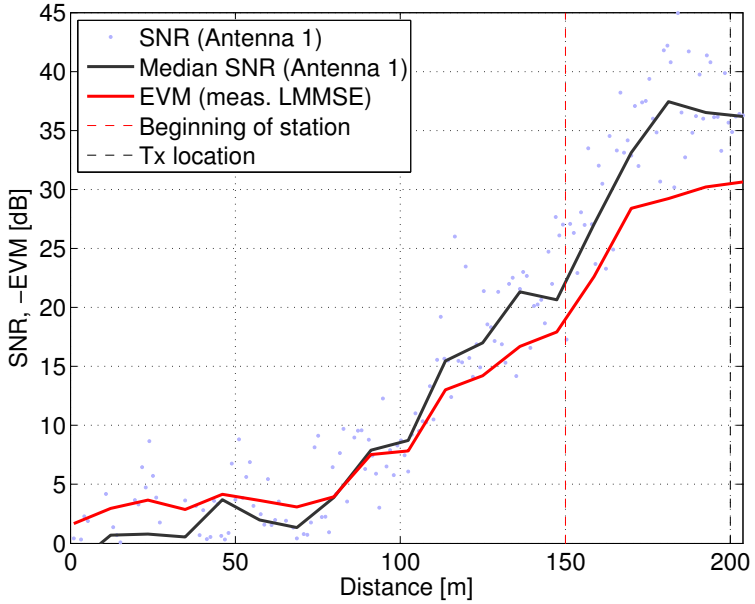

Figure 4.20: EVM and SNR measured for indoor antennas at the subway station. During the first part of the path, the receiver is still inside the tunnel, which results in a strong attenuation of the signal due to the signal blockage by the train. When the antennas reach the station the SNR increases, achieving its maximum value at the end of the path, where the receiver antennas are in front of the transmitter one.

EVM values are estimated for each frame. After frame detection, the strength of the received signal before the frame, which it is assumed to be a silent period, is used as a reference to obtain mean SNR estimations. Also, after channel equalization, the mean squared error of the received symbols compared to the transmitted ones is used to estimate the EVM.

Figures 4.20 and 4.21 show the results for the indoor and the outdoor antennas, respectively, where the dots represent the mean SNR detected for each received frame. The solid lines are computed by dividing the course of the train in 15 equal sectors, and by obtaining the median SNR and EVM for each sector. A large difference between the SNR levels observed from the indoor and outdoor antennas is appreciated. In the first part of the course of the train, the indoor receiver is still inside the entrance tunnel, and a strong attenuation of the signal (the train blocks the signal path) can be appreciated compared to the outdoor front antennas. Once the indoor antennas are inside the station (the train does not block the signal path anymore) the SNR increases and reaches its maximum when the indoor antennas are in front of the transmit antenna, which happens at the end of the measurement path. At this point, the outdoor antennas approach the exit tunnel, and the SNR for such outdoor antennas decreases with respect to its maximum due to the signal blockage caused by the train structure.

Throughput estimations are also obtained. In this case, the transmitted bits are decoded, and for each burst, the ratio of erroneous bits received is measured. Then, the throughput is estimated by two methods, which are:

- **Ideal Throughput**: it is assumed that the bursts with the highest rate and no errors for

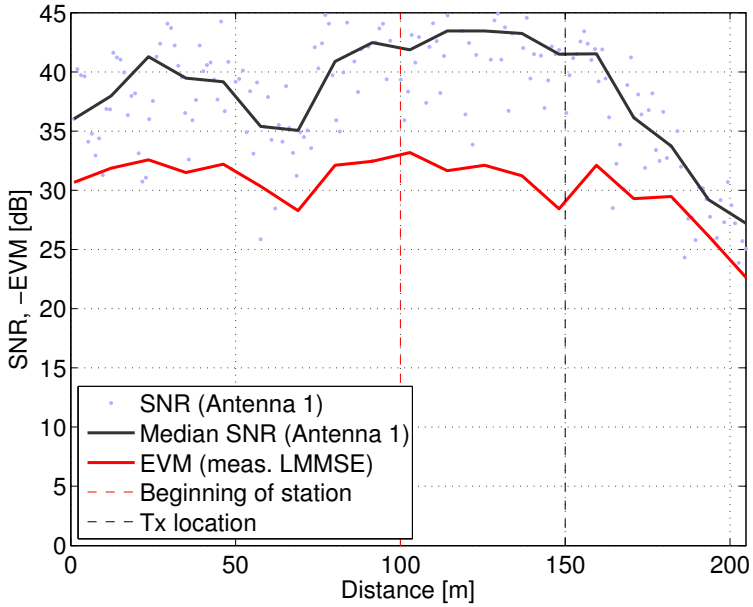

Figure 4.21: EVM and SNR measured for outdoors antennas at the subway station. Much higher SNR values are obtained with respect to the case of the antennas placed indoors. A slight decrease of the performance can be appreciated at the end of the path as the antennas reach the exit tunnel of the station and the train structure blocks the signal transmission.

each frame were transmitted; and

- **Feedback Throughput**: the transmitted burst is picked by means of the mean EVM level detected at the receiver, choosing higher burst profiles for high EVM values, and vice versa.

Figures 4.22 and 4.23 show the results corresponding to these throughput estimations, both for antennas inside and outside the train. The behavior of throughput is very similar to that of the SNR, and similar conclusions can be drawn. Throughput when the indoor receiver is inside the tunnel is close to zero, and as long as the train enters in the station, these values increase. Regarding the outdoor antennas, the throughput is stable around the maximum achievable. As expected, the results are a bit better when the so-called ideal throughput profile selection method is considered, which serves to determine an upper bound of the achievable throughput.

4.4.3 Conclusions

In this section, the performance of 4G waveforms in a metro environment has been experimentally evaluated. More specifically, the SNR, the EVM, and the throughput exhibited by WiMAX signals in a subway station were evaluated. The measurement results show that wireless communications directly with passengers inside the train are still a challenge due to the strong attenuation of the train structure. In relation with the results for the outdoors antennas, the importance of choosing an adequate placement of the receiver antennas to minimize the

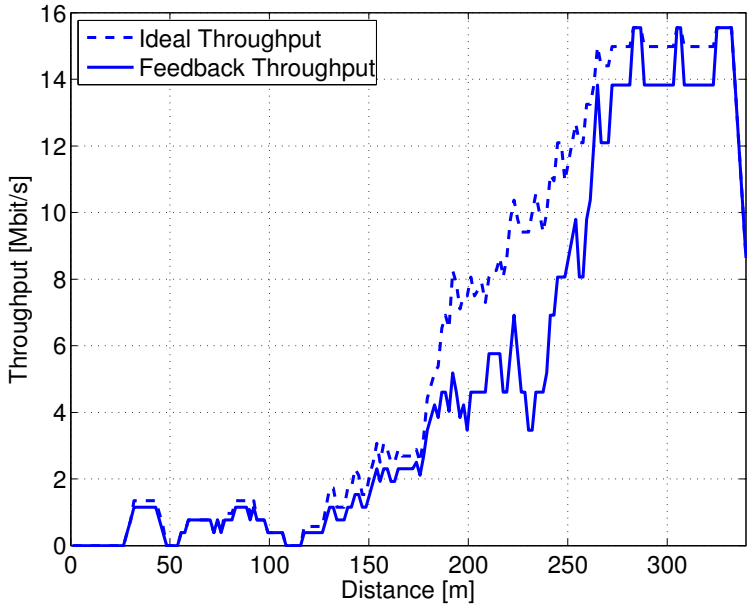

Figure 4.22: Throughput obtained for indoor antennas at the subway station. During the first part of the path, the receiver is still inside the tunnel, which results in a strong decrease of the obtained throughput due to the signal blockage by the train. When the antennas reach the station the throughput increases noticeably, achieving its maximum value at the end of the path, where the receiver antennas are in front of the transmitter one.

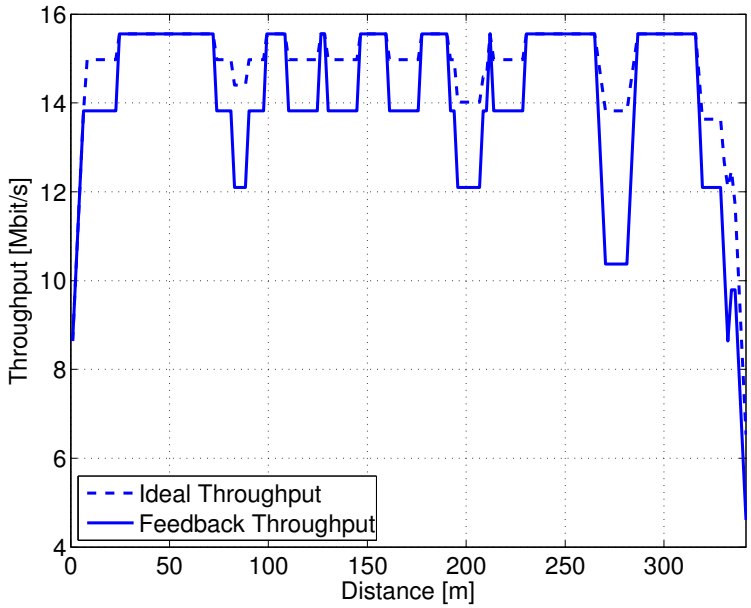

Figure 4.23: Throughput obtained for outdoor antennas at the subway station. Much higher throughput values are obtained with respect to the case of the antennas placed indoors, as the signal is not blocked by the train. A noticeable throughput decrease can be appreciated at the end of the path as the antennas reach the exit tunnel of the station and the train structure blocks the signal transmission.

blockage of the signal by the train structure must be remarked.

4.5 High-Speed-Train-to-Infrastructure Measurements

The performance of 4G communication systems in a vehicle-to-infrastructure link is assessed in this section by analyzing the results of a measurement campaign[1] where the mobile receivers are installed in a high-speed train. More specifically, the performance results for LTE transmissions are provided for receiver antennas placed outdoors (on the roof of a train carriage) and indoors (inside one of the train carriages). A single eNodeB is considered, being its placement the same of a base station currently in operation by the railway administrator. The performance achieved both for the indoor and the outdoor antennas is evaluated when the train moves at high speeds.

Section 4.5.1 introduces the measurement setup and followed procedure for carrying out the measurements, whereas Section 4.5.2 presents the obtained results. Finally, Section 4.5.3 details the main conclusions derived from the measurements.

4.5.1 Experimental Setup

This section describes the considered measurement setup as well as the followed procedure for assessing the performance of LTE signals in an actual high-speed train environment. First, the characteristics of the measurement environment are detailed. Next, the considered measurement setup is described.

Measurement Environment

A measurement campaign has been conducted at the high-speed train line between Córdoba and Málaga (Spain), currently in commercial operation up to 330 km/h. The test track is a segment in the vicinity of Antequera-Santa Ana station (Kilometric Point (KP) 96.800). This track section includes a GSM for Railways (GSM-R) site located at KP 97.075[2] consisting of two cabins for GSM-R and commercial equipment and a tower of 40 meters height with antennas for different wireless technologies (see Figs. 4.24 and 4.25). The measurements are carried out with the train moving along the track at a constrant speed between KPs 93.4 and 102.0, passing in front of the tower where the eNodeB antennas are installed at KP 97.075.

The test train is the *Séneca* laboratory train (Talgo A-330) provided by the ADIF. It is an electric train mainly intended for infrastructure inspections and it was extensively used in testing activities for implantation of European Rail Traffic Management System/European

[1]This measurement campaign was possible thanks to the project entitled "Radiocommunication technologies for trains autopilot and railway controlling" (TECRAIL). This project was funded by the Ministry of Science and Innovation (INNPACTO program, 2011 call) of the Government of Spain. Members of the project team are Alcatel-Lucent, the Spanish Railway Infrastructure Administrator (ADIF), AT4 Wireless, Metro de Madrid, the University of Málaga, the Politechnical University of Madrid and the University of A Coruña.

[2]The exact GPS coordinates of the site are $37^\circ\ 4'\ 3.14''$ N, $4^\circ\ 43'\ 12.52''$ W.

(a) (b)

Figure 4.24: Test track used for the evaluations: *(a)* detailed view of the closest area to the eNodeB; and *(b)* path considered for the evaluations.

Train Control System (ERTMS/ETCS) standard in Spanish high-speed lines. The *Séneca* train is 80.92 m long and can reach a maximum speed of 363 km/h (see Fig. 4.26).

Measurement Equipment

At the transmitter side, a commercial LTE eNodeB is set up. Two sectors are deployed. Hence, the eNodeB is installed in one of the cabins (see Fig. 4.27) and two remote radio heads (each one connected to two antenna elements in the same antenna panel) are mounted at the tower structure at a height of 20 meters (see Fig. 4.25). Both transmit antenna panels (Moyano MY-DTBSBS17276518) have the same orientation as the commercial GSM-R antennas already installed in the same tower. At the carrier frequency considered in the measurements, these cross-polarized antennas feature a gain of 18 dBi and half-power beam width of $62°$ (horizontal) and $5°$ (vertical). The antenna panel which serves the north sector has an azimuth orientation of $355°$ and a tilt of $0°$ (both electrical and mechanical), whereas the one radiating for the south sector has an azimuth orientation of $175°$ but a total tilt of $-1.4°$ ($0°$ mechanical and $-1.4°$ electrical).

At the receiver side, two nodes of the GTEC Testbed are used in receive-only mode. Both receivers are installed inside the train (see Fig. 4.28). One of them is connected to two of the four antennas available on the roof of the train carriage (see Fig. 4.29), which corresponds to the BTS-train link (see Section 4.1). The other receiver is connected to two of the four omni-directional antennas installed inside the carriage, emulating a passenger mobile terminal directly attached to the LTE network (BTS-mobile link), thus allowing for comparing the signals captured by indoor and outdoor receivers. The GPS receiver included at each node is used for

Figure 4.25: Tower structure with the eNodeB antennas installed at a height of 20 m. Two cabins are deployed, one for the GSM-R infrastructure and the other one for commercial telecommunication operators.

geo-referencing (time and position) the measurements. For the case of the BTS-train link, an external GPS antenna is used, whereas an internal GPS antenna is installed for the receiver corresponding to the BTS-mobile link. Note that measurements involving LTE BTS-train and BTS-mobile links are carried out simultaneously, thus the same transmitted LTE signals are acquired at the same time by the two indoor and the two outdoor antennas.

4.5.2 Obtained Results

One of the key requirements of high-speed train network deployments (at least those intended for supporting services like automatic train control and signaling) is to ensure continuous coverage along the tracks to avoid the interruption of safety-related critical services. Using the aforementioned LTE testbed, we provide in this section an empirical study of the estimated SNR along the track surrounding the eNodeB when transmitting an LTE signal. The eNodeB (LTE testbed transmitter) provides coverage for two different sectors while both LTE testbed receivers perform a handover approximately when the train passes in front of the tower where

Figure 4.26: *Séneca* train at the Antequera-Santa Ana train station.

(a) (b)

Figure 4.27: Transmitter installation: *(a)* detail of the inner part of the GSM-R cabin; and *(b)* actual eNodeB and Evolved Packet Core (EPC) emulated in a Personal Computer (PC).

the eNodeB antennas are installed. Additionally, In order to characterize the channel, especially its time and frequency selectivity, the Power Delay Profile (PDP) of the BTS-to-train channel is estimated from the measurements. Finally, capacity bounds for such a channel are also obtained. The main configuration parameters considered for the experiments are shown in Table 4.4.

SNR Estimation

The SNR is estimated considering exclusively the data subcarriers. Thus, guard subcarriers, Direct Current (DC) subcarrier as well as pilot subcarriers are discarded *a priori*. However, for some cases the receiver is not able to correctly detect an acquired LTE frame. In these cases the procedure is identical but the pilot subcarriers are not discarded since their positions on the time-frequency grid are not known. This fact should not impact on the results significantly since

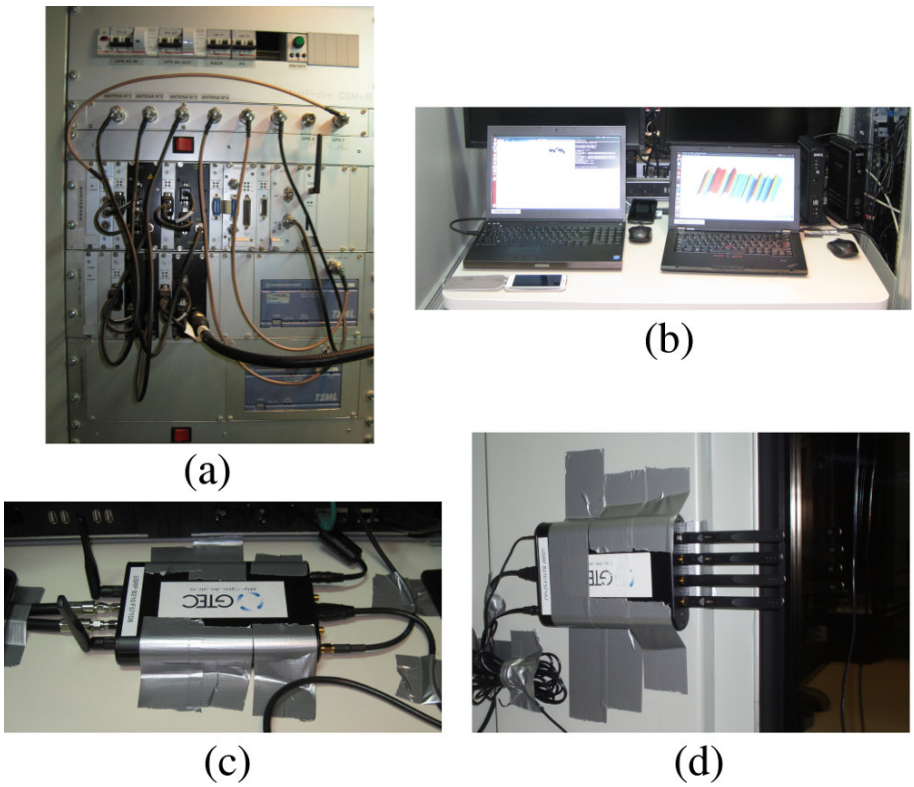

Figure 4.28: GTEC Tesbed nodes installed inside the train carriage: *(a)* connection panel for the external antennas; *(b)* laptops of the testbed receiver nodes; *(c)* receiver node connected to the outdoor antennas (the additional attached antennas are just meant for test purposes); and *(d)* receiver node with its own indoor antennas (only two of them are used).

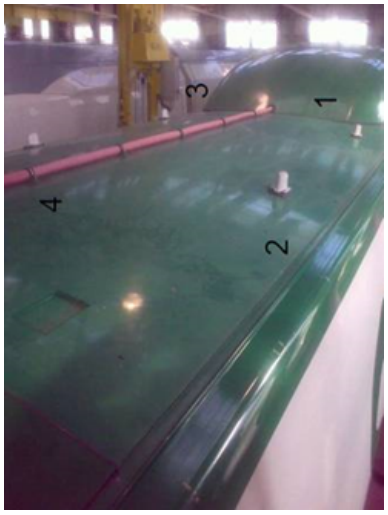

Figure 4.29: Outdoor antennas on the roof of the train carriage. Only two of them are used for the measurements.

no pilot power boosting was considered[3]. The SNR estimation is performed by considering the following steps:

1. Noise samples in the time domain are captured with the transmitter switched off (hence

[3]In other words, the energy per symbol of the data symbols and the pilots is the same.

Table 4.4: Configuration parameters considered for the experiments.

Transmitted power	46 dBm
Carrier frequency	2.6 GHz
Bandwidth	10 MHz (9 MHz occupied)
Number of subcarriers	1024 (600 used)
Transmitter scheme	Transmit diversity
Cyclic prefix length	Normal

not transmitting any signal).

2. The captured noise samples in the time domain are then processed as if they were actual data samples, i.e., the cyclic prefix is removed, a Fast Fourier Transform (FFT) is performed and both guard and DC subcarriers are removed. Note that the noise samples corresponding to pilot subcarriers are only used when an LTE frame is not detected.
3. As a result, $w^{(b,k)}$ noise samples are obtained in the frequency domain, each one corresponding to the b-th subcarrier of the k-th OFDM symbol, where $b \in \mathcal{D}^{(k)}$, being $\mathcal{D}^{(k)}$ the set of indexes of the data subcarriers (or the set of indexes of the data subcarriers plus the pilot subcarriers when the corresponding LTE frame is not detected) for the k-th symbol.
4. All previous steps are repeated when the transmitter is switched on, so $r^{(b,k)}$ data samples (of course also affected by noise) are obtained in the frequency domain.
5. The average SNR for each OFDM symbol is then estimated by averaging out the instantaneous SNR values for the different data subcarriers. Defining

$$\bar{r}^{(k)} = \frac{1}{\left|\mathcal{D}^{(k)}\right|} \sum_{b \in \mathcal{D}^{(k)}} \left|r^{(b,k)}\right|^2, \tag{4.2}$$

and

$$\bar{w}^{(k)} = \frac{1}{\left|\mathcal{D}^{(k)}\right|} \sum_{b \in \mathcal{D}^{(k)}} \left|w^{(b,k)}\right|^2, \tag{4.3}$$

where $\left|\mathcal{D}^{(k)}\right|$ is the number of data subcarriers (or the number of data and pilot subcarriers when the corresponding LTE frame is not detected) for the k-th symbol. Then, the SNR for each OFDM symbol is calculated as

$$\text{SNR}^{(k)} = \frac{\bar{r}^{(k)} - \bar{w}^{(k)}}{\bar{w}^{(k)}}. \tag{4.4}$$

Figure 4.30 shows the estimated SNR values when the train moves between KPs 93.4 and 102.0 at 50 km/h. Four curves are included, two of them corresponding to two outdoor antennas located on the roof of the train carriage (namely “ant #1 (outd.)” and “ant #2 (outd.)”,

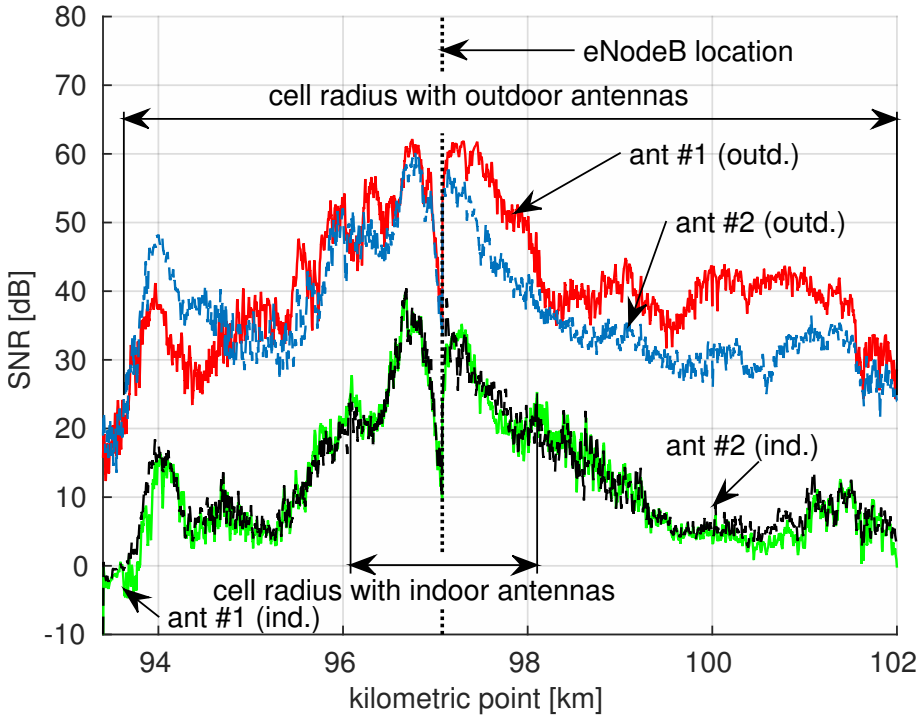

Figure 4.30: Estimated SNR values by means of measurements corresponding to both BTS-train and BTS-mobile links. The SNR value is maximum when the receiver passes in front of the tower where the antennas are installed. Shapes of SNR curves for indoor and outdoor antennas are similar. However, the SNR is reduced by approximately 26 dB for the indoor antennas due to the attenuation introduced by the train carriage structure, which causes that the cell radius is much larger for outdoor antennas than for indoor ones.

respectively) and the other two corresponding to the two indoor antennas (namely "ant #1 (ind.)" and "ant #2 (ind.)", respectively). The horizontal axis in Fig. 4.30 shows the kilometric point, while the vertical one shows the estimated SNR values in dB. The train carriage, where the receivers are installed, passes in front of the tower where the eNodeB antennas are installed at approximately KP 97.075 km. At this point, the handover between the two deployed sectors occurs. In order to avoid interference effects, the two sectors are not used simultaneously. Thus, when the train moves between KPs 93.4 and 97.075, only the first sector is active. Conversely, when the train moves between KPs 97.075 and 102.0, the first sector is not active while the second one is active.

In Fig. 4.30 it can be seen that the obtained results are very similar for both outdoor antennas. The shape of the SNR curves corresponding to the indoor ones is also similar, but the SNR is reduced approximately by 26 dB due to the attenuation introduced by the train carriage structure. It can also be seen that the SNR values for the antennas placed outdoors are above 10 dB for all the considered measurement points, while the maximum values are obtained when the train is in the vicinity of the eNodeB antennas. Finally, the so-called cell radius is defined both for the outdoors as well as the indoors antennas. We define the cell radius as the zone limited by the

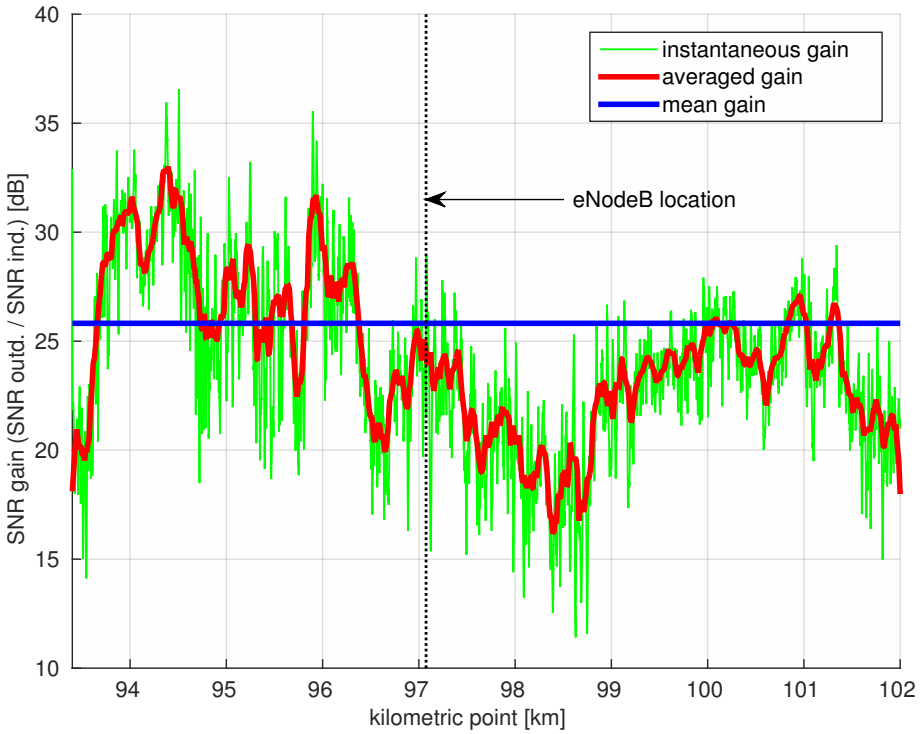

Figure 4.31: Estimated SNR difference between the BTS-train and BTS-mobile links operating simultaneously. During most of the time, the SNR gain is between 20 dB and 35 dB for the outdoor antennas with respect to the indoor ones. The average gain for the whole path is about 26 dB.

first kilometric point where the SNR is higher than 25 dB and the latest kilometric point where this condition is still fulfilled. It can be observed that the cell radius is much larger for outdoor antennas than for indoor ones, as expected.

Figure 4.31 shows more clearly the SNR gain between one of the outdoor antennas (namely "ant #1 (outd.)") and one of the indoor ones (namely "ant #1 (ind.)"). A curve obtained by averaging the instantaneous values by using a sliding-window of 6.5 ms duration is also included. It can be seen that the SNR gain is between 20 dB and 35 dB during most of the time. The average SNR gain for the whole path is also indicated in Fig. 4.31 and it is about 26 dB.

PDP Estimation

Apart from ensuring an acceptable strength of the received signal and a continuous coverage, the characterization of the channel, especially its time and frequency selectivity, is also addressed. In order to achieve this goal, the estimation of the channel PDP is performed for different train speeds.

Figure 4.32 illustrates the behavior of the channel response both in the frequency as well as in the time domains for different speeds and antenna configurations. Firstly, Fig. 4.32a presents the spectrum of an OFDM symbol received by one of the outdoor antennas when the train approaches the KP 96.0 at 50 km/h. Figure 4.32b shows the magnitude of the time-frequency

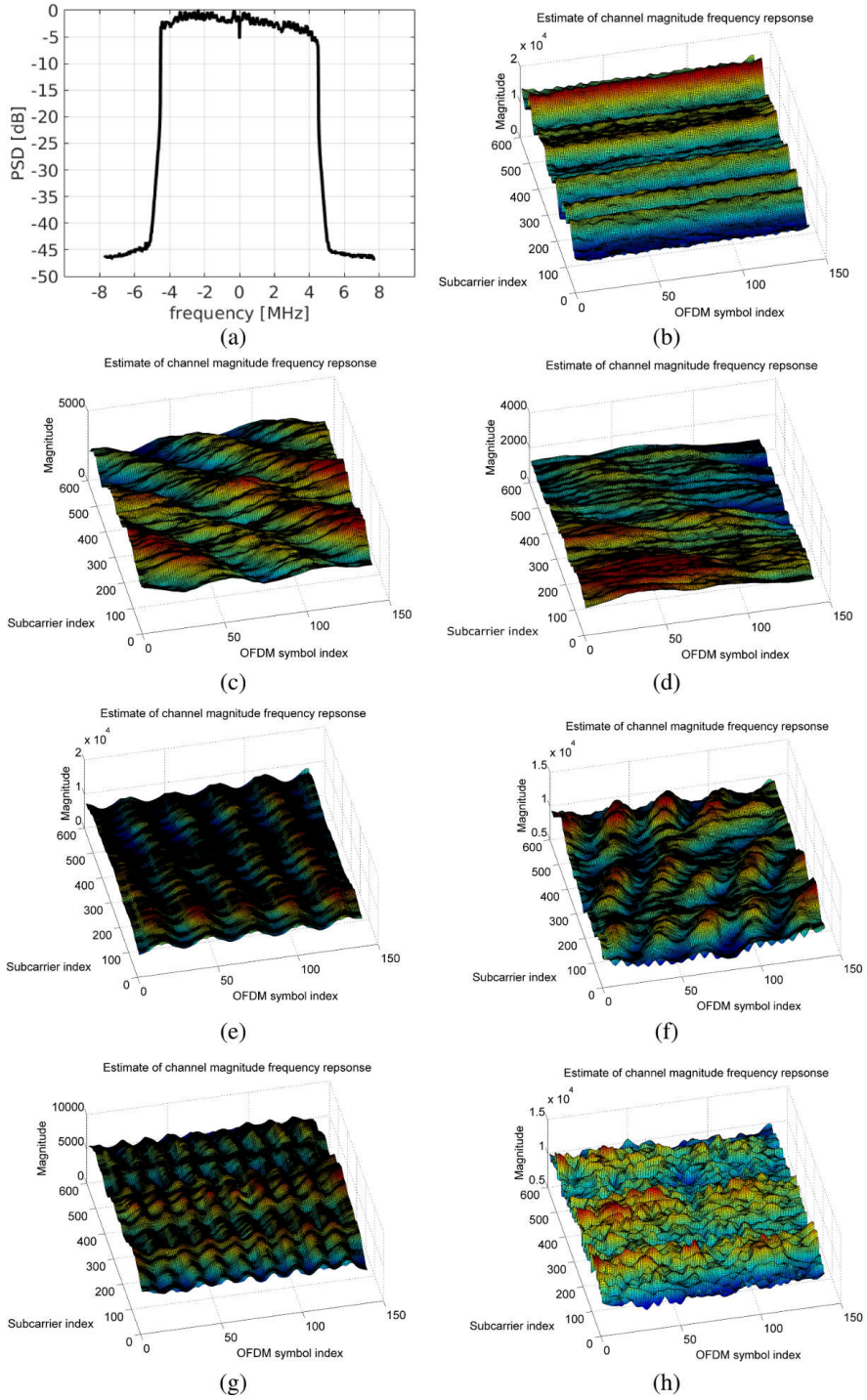

Figure 4.32: Exemplary channel response plots: *(a)* received Spectrum; *(b)* time-frequency response of the channel when the train is parked at the train station; *(c)* time-frequency response of the channel seen by one of the outdoor antennas when the train moves at 50 km/h; *(d)* time-frequency response of the channel seen by one of the indoor antennas when the train moves at 50 km/h; *(e)* time-frequency response of the channel seen by one of the outdoor antennas when the train moves at 100 km/h; and *(f)* time-frequency response of the channel seen by one of the indoor antennas when the train moves at 100 km/h; *(g)* time-frequency response of the channel seen by one of the outdoor antennas when the train moves at 200 km/h; and *(h)* time-frequency response of the channel seen by one of the indoor antennas when the train moves at 200 km/h.

channel response for one of the outdoor antennas when the train is parked at the train station. This time-frequency channel response is obtained from the received pilots and it corresponds to a complete LTE frame. As expected, the channel response does not vary in the time dimension since the train is not moving. Figure 4.32c shows the magnitude of the channel time-frequency response for one of the outdoor antennas when the train approaches the KP 96.0 at 50 km/h, whereas Fig. 4.32d shows the same result for one of the indoor antennas. In these cases, the variation of the channel response in the time dimension due to the train movement can be observed. However, note that the measurement scenario can be modeled as rural macro-cell when the train is far away from the train station. Hence, we can assume that the power of the Non-Line-of-Sight (NLoS) components is negligible with respect to the LoS component for the measurements obtained with the antennas placed on the roof of the train carriage. However, this is not the case for the antennas placed indoors, as the signal reflections on the train structure may cause non-negligible NLoS components (i.e., multipath). Hence, much more irregular channel responses are observed for the indoor antennas. Figure 4.32e and Figure 4.32g show the magnitude of the channel responses obtained for one of the antennas placed outdoors at the same evaluation point when the train speed values are 100 km/h and 200 km/h, respectively. It can be seen that the variation of the channel response on the time dimension is faster when the train speed increases. Fig. 4.32f and Fig. 4.32h show similar results when one of the indoor antennas is employed. Again, it can be seen that the channel responses corresponding to the indoor antennas are much more irregular than those of the outdoor antennas.

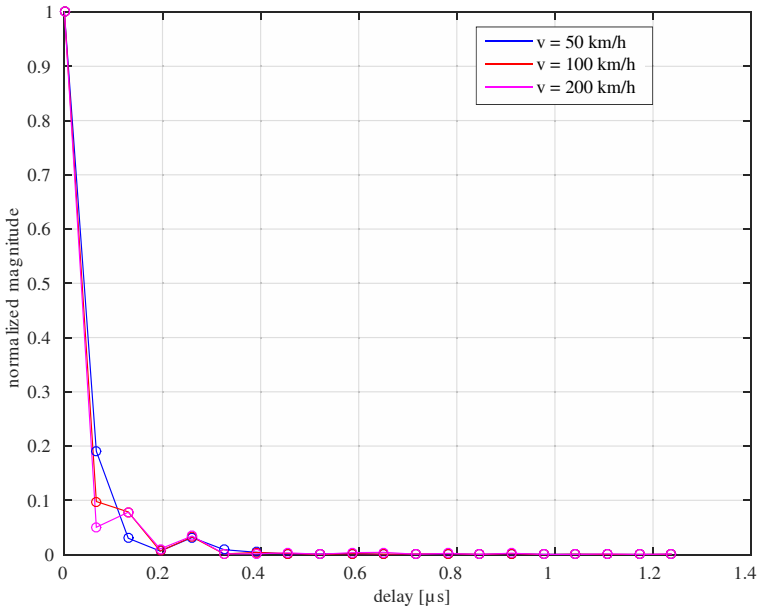

Figure 4.33: Estimations of the PDP of the BTS-train link for different speeds. No meaningful differences are observed for the results at different speeds, which corresponds to a rural area with strong line of sight between transmit and receive antennas.

With the aim of further characterizing the BTS-train link, PDP estimations are measured by

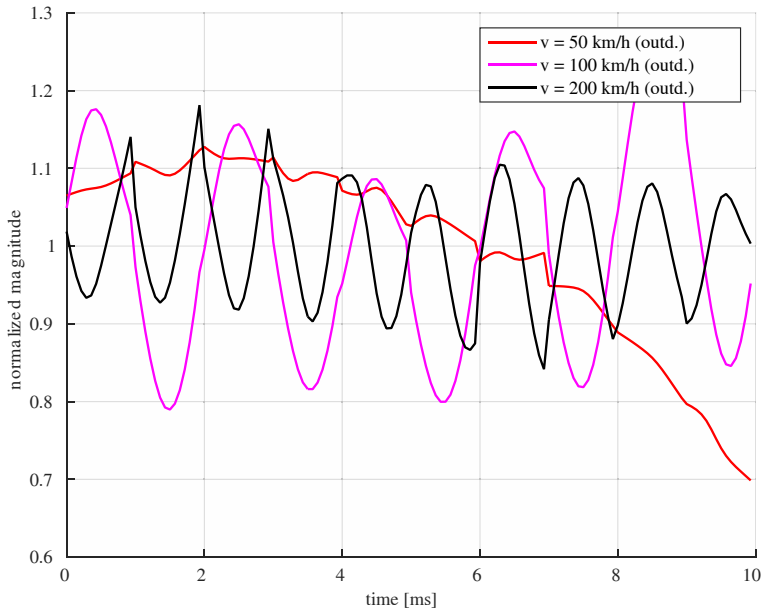

Figure 4.34: Evolution of the magnitude of the first tap of the BTS-train channel for different speeds. As expected, the time-selectivity increases with the speed of the train.

computing the channel impulse response for each OFDM symbol in each acquired frame, and then the power per tap is obtained. Figure 4.33 shows the normalized PDPs at different speeds, while no meaningful differences are observed between the PDPs obtained, which corresponds to a rural area with strong line of sight between transmit and receive antennas. Note that 20 taps are considered for these results.

In Fig. 4.34 the evolution of the magnitude of the first channel tap is shown for different speeds and, as expected, the time-selectivity increases with the speed of the train. It can be concluded that the scenario presents a very low delay spread, and that time-selectivity would determine the overall system performance of the system as long as the speed of the train increases.

Capacity Bounds Estimation

One of the most interesting properties of the channel is the so-called channel capacity, which represents the amount of data that can be transmitted per channel use. The channel capacity is usually plotted with respect to the SNR at the receiver. However, it is still unknown how to compute the channel capacity from channel estimates obtained after processing the signals acquired during a measurement campaign. Fortunately, theoretical bounds for the capacity under channel estimation errors are available in the literature [YG06; HH03].

From now on, the mathematical expressions used for calculating the channel capacity bounds assuming the best possible receiver in absence of channel state information are introduced. An ideal transmitter in which the transmitted signals are Gaussian distributed is assumed. The MMSE channel estimator is considered, whereas time and frequency

synchronization errors are also ignored. On the other hand, Jakes model is assumed to model the variation of the channel over time.

The following received signal model is assumed for the transmission of OFDM symbols with N subcarriers in subframes of K symbols

$$\mathbf{y}_k = \mathbf{H}_k \mathbf{x}_k + \mathbf{n}_k, \tag{4.5}$$

where $\mathbf{x}_k = \mathbf{P}_k \mathbf{p}_k + \mathbf{D}_k \mathbf{d}_k$ is a $N \times 1$ vector with the transmitted subcarriers, with $\mathbf{p}_k$ and $\mathbf{d}_k$ the vectors with the pilot and data subcarriers, and $\mathbf{P}_k$ and $\mathbf{D}_k$ permutation matrices that assign each symbol to its final position in the OFDM symbol; $\mathbf{H}_k$ is a $N \times N$ MIMO channel frequency response matrix, $\mathbf{n}$ is a $N \times 1$ vector of additive Gaussian noise with $\mathbf{n}_k \sim \mathcal{N}(\mathbf{0}, \sigma_n^2 \mathbf{I}_N)$, $\mathbf{y}_k$ is the $N \times 1$ vector with the received signal after the FFT, and where subindex k denotes the number of the k-th OFDM symbol in an LTE subframe. We will also assume that $\mathbb{E}(\mathbf{x}_k \mathbf{x}_k^H) = \sigma_x^2 \mathbf{I}$, as it is the case in typical LTE configurations.

Under time-selectivity conditions, the channel matrix will have a banded structure. Thus, the previous model can be further decomposed to consider the impairments caused by time selectivity of the channel as

$$\mathbf{y}_k = \left(\bar{\mathbf{H}}_k + \mathbf{G}_k\right) \mathbf{x}_k + \mathbf{n}_k = \bar{\mathbf{H}}_k \mathbf{x}_k + \mathbf{g}_k + \mathbf{n}_k, \tag{4.6}$$

where $\bar{\mathbf{H}}_k = \operatorname{diag}(\mathbf{H}_k)$ is a diagonal matrix with the elements of the main diagonal of $\mathbf{H}_k$, $\mathbf{G}_k = \mathbf{H}_k - \bar{\mathbf{H}}_k$, and $\mathbf{g}_k = \mathbf{G}_k \mathbf{x}_k$ represents the ICI. The ICI vector $\mathbf{g}_k$ is approximated as Gaussian noise $\mathbf{g}_k \sim \mathcal{N}(\mathbf{0}, \sigma_{\text{ICI}}^2 \mathbf{I}_N)$, where σ_{ICI}^2 is the variance of the ICI, and it is approximated assuming that the channel time-selectivity follows the Jakes model [LC01]

$$\sigma_{\text{ICI}}^2 \approx \sigma_x^2 \int_{-1}^{1} (1 - |x|) J_0(2\pi f_D N x / f_s) dx, \tag{4.7}$$

where J_0 is the Bessel function of the first kind, f_D is the maximum Doppler frequency and f_s is the baseband sampling frequency.

If we also consider channel estimation errors on the matrix $\bar{\mathbf{H}}_k$, we then obtain

$$\mathbf{y}_k = \left(\hat{\mathbf{H}}_k + \tilde{\mathbf{H}}_k\right) \mathbf{x}_k + \mathbf{g}_k + \mathbf{n}_k = \hat{\mathbf{H}}_k \mathbf{x}_k + \tilde{\mathbf{x}}_k + \mathbf{g}_k + \mathbf{n}_k, \tag{4.8}$$

where $\hat{\mathbf{H}}_k$ is an estimation of $\bar{\mathbf{H}}_k$, and $\tilde{\mathbf{H}}_k = \bar{\mathbf{H}}_k - \hat{\mathbf{H}}_k$ is the estimation error. To derive bounds of the capacity from the measurements, only $\tilde{\mathbf{n}}_k = \tilde{\mathbf{x}}_k + \mathbf{g}_k + \mathbf{n}_k$ is assumed as interference, whereas other sources of interference (e.g. synchronization errors) are ignored. All these interference sources will be assumed to follow a Gaussian distribution, which is the worst case scenario in terms of capacity when compared to any other distribution with equivalent variance. In case any of these interference vectors follow a different distribution from Gaussian, the actual capacity of the system will be higher [HH03].

Regarding the estimation error, the MMSE estimator covariance matrix is used, considering the pilot structure of LTE for $N = 1024$ subcarriers (corresponding to the 10 MHz profile), and $K = 14$ symbols per subframe (cyclic prefix with normal length), yielding the following channel estimation model

$$\mathbf{Py} = \mathbf{X}_p\mathbf{P}\bar{\mathbf{h}} + \mathbf{Pg} + \mathbf{Pn}, \tag{4.9}$$

where the vectors $\mathbf{y}$, $\mathbf{g}$, and $\mathbf{n}$ are the result of stacking the elements composing a subframe, e.g. $\mathbf{y} = [\mathbf{y}_1^T, \ldots, \mathbf{y}_K^T]^T$. The permutation matrix is built as $\mathbf{P} = \text{blockdiag}(\mathbf{P}_1^T, \ldots, \mathbf{P}_K^T)$, and $\mathbf{X}_p = \text{diag}(\mathbf{p}_1, \ldots, \mathbf{p}_K)$ is a diagonal matrix with the pilot symbols. Finally, the vector $\bar{\mathbf{h}} = [\mathbf{h}_1, \ldots, \mathbf{h}_k]$ is defined, with $\bar{\mathbf{h}}_k = \text{diag}(\bar{\mathbf{H}}_k)$, and $\mathbf{C}_h = E(\mathbf{hh}^H) = \mathbf{C}_t \otimes \mathbf{C}_f$, where $\mathbf{C}_t$ and $\mathbf{C}_f$ are the time and frequency channel covariance matrices. The frequency covariance matrix is assumed to be $\mathbf{C}_f = \mathbf{F}_L \,\text{diag}(\mathbf{p})\mathbf{F}_L^H$, with $\mathbf{p}$ a $L \times 1$ vector with the PDPs estimated above, and $\mathbf{F}_L$ is a $N \times L$ matrix with the first L columns of the standard Discrete Fourier Transform (DFT) matrix. Regarding the time covariance matrix $\mathbf{C}_t$, the Jakes model is assumed again, whose autocorrelation function is $E(h(t_1, \tau)h^*(t_2, \tau)) = J_0(2\pi f_D(t1 - t2))$.

If we also assume that $\mathbf{g}$ and $\mathbf{n}$ are interferences, and also that $E(\mathbf{X}_p\mathbf{X}_p^H) = \mathbf{I}$, the channel estimation error is given by

$$\sigma_e^2 = \frac{1}{NK}\,\text{tr}\left(\mathbf{C}_h - \mathbf{C}_h\mathbf{P}^T\left(\mathbf{PC}_h\mathbf{P}^T + (\sigma_{\text{ICI}}^2 + \sigma_n^2)\mathbf{I}_{NK}\right)^{-1}\mathbf{PC}_h\right). \tag{4.10}$$

Finally, theoretical bounds for the capacity under channel estimation errors are available in the literature [YG06; HH03]. The lower bound of the capacity is

$$C_{\text{l}} = \frac{Df_s}{T}\frac{1}{10KN}\sum_{i=1}^{N}\sum_{j=1}^{10K}\log_2\left(1 + \frac{|\hat{h}_{ij}|^2}{\sigma_n^2 + \sigma_{\text{ICI}}^2 + \sigma_e^2}\right), \tag{4.11}$$

where:

- D denotes the number of data subcarriers allocated in an LTE subframe;
- $f_s = 15.36$ Msample/s is the sampling rate;
- $T = 10N(K + G_S(K - 2) + 2G_L)$ is the number of samples in an LTE frame (which consists of 10 subframes), whereas $G_S = 72$ and $G_L = 80$ are the lengths of the short and long cyclic prefixes, respectively. Notice that these values correspond to the so-called normal cyclic prefix length defined in the standard;
- Finally, $\hat{h}_{ij}$ are the estimates of the channel frequency response corresponding to the i-th subcarrier of each OFDM symbol and the j-th OFDM symbol within the LTE frame. Such channel frequency response estimations are obtained from the measured LTE frames.

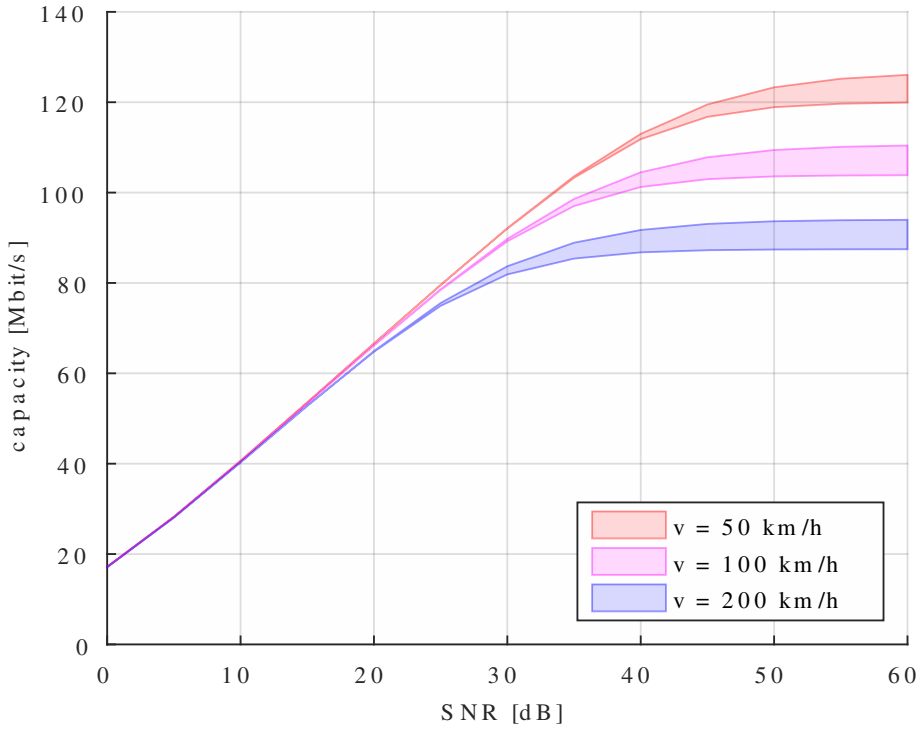

Figure 4.35: Capacity bounds for different speeds with respect to the SNR. The colored areas fill the gap between the lower and the upper capacity bounds for each scenario. Higher capacity values are achieved for the low.speed scenarios, where the ICI is weaker. For the low SNR regime, the lower and the upper bounds almost overlap, since the error due to the MMSE channel estimation and the ICI is in the same order of magnitude than the noise variance. However, for high SNR values the contribution of the ICI is much larger than those of other sources of interference, and a larger difference is observed between the upper and the lower bounds of the capacity.

Analogously, the upper bound of the capacity is defined as follows:

$$C_{\mathrm{u}} = C_{\mathrm{l}} + \frac{D f_s}{T} E_x \left(\log_2 \left(\frac{\sigma_n^2 + \sigma_{\mathrm{ICI}}^2 + \sigma_e^2}{\sigma_n^2 + (\sigma_{\mathrm{ICI}}^2 + \sigma_e^2) x^2} \right) \right), \tag{4.12}$$

where x represents the constellation mapping –which we assume to follow a Gaussian distribution– and $\mathrm{E}[\cdot]$ denotes the expectation operator.

Figure 4.35 plots both capacity bounds for different speeds of the train with respect to the $\mathrm{SNR} = 1/\sigma_n^2$ and considering a system with imperfect channel state information. The colored areas fill the gap between the lower and upper capacity bounds for each scenario. Since the capacity estimations are done under the assumption that the ICI is treated as an interference, higher capacity values are achieved for the low speed scenarios, where the ICI is weaker.

Also, the difference between the lower and upper bound of the capacity is about 0.1 Mbit/s for low SNR values, because the error due to the MMSE channel estimation and the ICI is in the same order of magnitude than the noise variance. This behavior changes for high SNR values, were the ICI is much larger than the other sources of interference.

4.5.3 Conclusions

The main conclusions of this section are summarized below:

- The GTEC Testbed was successfully used to experimentally evaluate broadband communications in the High-Speed Train (HST) environment. Such a testbed allows for evaluating channel properties directly from the transmitted commercial LTE signals. eNodeB antennas were installed at the same locations as the antennas used for the GSM-R deployment and a commercial LTE eNodeB was set up. The testbed receivers were connected to two antennas placed on the roof of the train carriage as well as to two indoor antennas placed inside the train carriage.
- The SNR was estimated for the link between the eNodeB and the on board testbed receiver. The results show that the SNR at the receiver is always above 10 dB for the considered cell sectors, while the SNR lies between 30 dB and 50 dB during most of the trajectory. The maximum SNR values are achieved when the train passes in front of the eNodeB antennas. Note that the SNR was also evaluated at different train velocities (more specifically, 50 km/hm, 100 km/h, and 200 km/h) yielding very similar results, as expected.
- There is a strong signal penetration loss caused by the train carriage structure. For the case of LTE broadband signals at a carrier frequency of 2600 MHz, the SNR loss is about 26 dB when the indoor antennas are used. As expected, this results in a noticeable reduction of the cell radius when indoor antennas are used with respect to the cases where the outdoor antennas are used, which definitely motivates the study of communication architectures based on relay schemes.
- Estimations of the PDP for the BTS-train link were also obtained at different speeds. It could be observed that the channel exhibited a low delay spread regardless of the train speed, as expected in a rural scenario with a strong line of sight between the transmitter and the receiver. Therefore, the time selectivity of the channel due to the high speeds achieved by the trains is the limiting factor for the system performance.
- Channel capacity bounds for the BTS-train link have been computed considering the frame structure of LTE and the estimated PDPs. The obtained results proved that, in the high SNR regime, the time-selectivity due to the train speed is again the main limiting factor for the system performance.

4.6 Conclusions

The main conclusions derived from this chapter can be summarized as follows:

- The GTEC Testbed was successfully used to experimentally evaluate broadband communications in different vehicle-to-infrastructure scenarios and with different 4G

signals. More specifically, high-speed car-to-infrastructure scenarios (high speed conditions emulated by time interpolation), subway-to-infrastructure in tunnel scenarios and high-speed-train-to-infrastructure scenarios were considered, whereas both WiMAX and LTE standard-compliant signals were transmitted.

- From the results obtained after the measurements in car-to-infrastructure scenarios, it can be concluded that the high speed emulation technique by time interpolation introduced in Section 3.2 can be effectively used for measurements in real world scenarios.
- The obtained results from high-speed vehicle-to-infrastructure measurements show, on the one hand, that the main performance degradation sources are the link SNR and the mobile receiver speed. On the other hand, a reliable and low-latency link at very high speeds demands for small-size constellations like 4-QAM, making adaptive modulation and coding schemes less attractive in these scenarios. A potential throughput increment when increasing the constellation size yields a high BER with very high probability, thus requiring retransmissions and impacting on both the delay and the jitter of the link.
- From the comparison of the results for BTS-train and BTS-mobile links in different environments (e.g., subway stations or high-speed trains crossing rural areas), it can be concluded that wireless communications directly with passengers inside the train are still a challenge due to the strong attenuation of the train structure. Attenuation values greater than 25 dB were observed. This results in a noticeable reduction of the cell radius when indoor antennas are used with respect to the cases where the outdoor antennas are used. This definitely motivates the study of communication architectures based on relay schemes.
- The results obtained from the measurements for subway-to-infrastructure scenarios in train stations showed the importance of choosing an adequate placement of the receiving antennas at the train to minimize the blockage of the signal by the train structure.
- From the PDP estimates for the high-speed-train-to-infrastructure scenario, a low delay spread channel was observed regardless of the train speed, when a rural area environment was considered. This shows that the time selectivity of the channel due to the high speeds achieved by the trains is the limiting factor for the system performance.
- Channel capacity bounds of the BTS-train link were computed from the high-speed-train-to-infrastructure measurements. The obtained results corroborated that, for the high SNR regime, the time-selectivity due to the train speed is the main limiting factor for the system performance.

Chapter 5

5G Architectures

Requirements and expectations regarding mobile communication systems grow day by day. In order to fulfill the increasing capacity demanded by users, the Long Term Evolution (LTE) standard evolved and new versions arose. Moreover, nowadays we are in the beginning of a new era for mobile communications, since the so-called fifth generation (5G) communication systems are currently under definition.

With the aim of drastically increasing the value of this work and to check the validity of the findings regarding the latest advances in wireless communication systems, proposals for 5G communication systems are considered in this chapter.

Section 5.1 reviews the most relevant advantages of 5G communications systems for the high speed train environment. Section 5.2 extends the high speed emulation technique presented in Section 3.2 to 5G systems, whereas Section 5.3 introduces the setup and procedure followed to validate such a technique. Section 5.4 includes the obtained results and Section 5.5 is devoted to the chapter conclusions.

This chapter is mainly based on the following co-authored publications:

- José Rodríguez-Piñeiro, Tomás Domínguez-Bolaño, José A. García-Naya, and Luis Castedo. **Performance Assessment of 5G-Candidate Waveforms in High Speed Scenarios**. In: *27th Annual IEEE International Symposium on Personal, Indoor and Mobile Radio Communications (PIMRC 2016)*. Accepted for publication. Valencia, Spain, Sept. 2016

- José Rodríguez-Piñeiro, Martin Lerch, Tomás Domínguez-Bolaño, José A. García-Naya, Sebastian Caban, and Luis Castedo. **Experimental Assessment of 5G-Candidate Modulation Schemes at Extreme Speeds**. In: *Ninth IEEE Sensor Array and Multichannel Signal Processing Workshop (SAM 2016)*. Río de Janeiro, Brazil, July 2016

- José Rodríguez-Piñeiro, Tomás Domínguez-Bolaño, Pedro Suárez-Casal, José A. García-Naya, and Luis Castedo. **Affordable Evaluation of 5G Modulation Schemes in High**

Speed Train Scenarios. In: *ITG Workshop on Smart Antennas (WSA 2016)*. Munich, Germany, Mar. 2016

- Tomás Domínguez-Bolaño, José Rodríguez-Piñeiro, José A. García-Naya, and Luis Castedo. **The GTEC 5G Link-Level Simulator**. In: *International Workshop on Link- and System Level Simulations (IWSLS2 2016)*. Vienna, Austria, July 2016

- Tomás Domínguez-Bolaño, José Rodríguez-Piñeiro, José A. García-Naya, and Luis Castedo. **Experimental Evaluation of 5G Modulation Schemes in Quasi-Static Scenarios**. In: *ITG Workshop on Smart Antennas (WSA 2016)*. Munich, Germany, Mar. 2016

5.1 Introduction

One of the most remarkable proposals for the definition of 5G is the utilization of Filter Bank Multicarrier (FBMC) modulation techniques instead of the well-known Orthogonal Frequency-Division Multiplexing (OFDM). In Section 2.6 the most important advantages offered by FBMC with respect to OFDM as well as other alternative modulation schemes are described. As a brief reminder, the most remarkable advantages offered by FBMC with respect to OFDM in the context of railway communications are summarized below:

- **Higher bandwidth efficiency**: allowing for a more efficient utilization of the scarce spectrum available in railway environments, while facilitating the coexistence with legacy systems, such as GSM for Railways (GSM-R).
- **Improved multiple-access facilities in the uplink**: due to the use of close-to-perfect subcarrier filters which ensure well frequency-localized subcarriers, FBMC does not require sophisticated synchronization methods for avoiding multiple-access interference.
- **Suitability for doubly dispersive channels**: the waveforms used in FBMC can be optimized for doubly dispersive channels like the ones present in High-Speed Train (HST) communications, hence allowing for a compromise between the time and frequency channel response [Far11].

5.2 Emulating High Speeds in FBMC

A technique to induce the effects caused by highly time-varying channels in OFDM signals while conducting the measurements at low speeds was introduced in Section 3.2 [Rod+14]. This technique consists in reducing the subcarrier spacing by means of time-interpolation of the transmit OFDM signal, hence scaling down the bandwidth of the transmitted signal.

The time-interpolated signal conveys exactly the same information as the original one but with a reduced subcarrier spacing, thus artificially increasing the sensitivity to Inter-Carrier Interference (ICI). For example, if we time-interpolate the transmit OFDM signal by a factor I, the subcarrier spacing will be reduced by the same factor I, which is similar to what would happen if transmissions were conducted at I times the original speed. This technique performs accurately for both standard-compliant WiMAX Mobile (IEEE 802.16e) waveforms [Rod+14; Suá+14b; Suá+14a] (see Section 4.3.2) as well as LTE ones [Rod+15a; Rod+15b; Fei+16] (see Sections 3.5 and 4.3.2). In this chapter, the application of the aforementioned high-speed emulation technique to FBMC signals is addressed.

Let us consider an FBMC modulation where N_c subcarriers are multiplexed to construct each FBMC symbol, yielding a total length of N_t samples per FBMC symbol that are transmitted at a rate $F_s = 1/T_s$. Therefore, each FBMC symbol has a time duration $T_t = T_s N_t$. When an FBMC signal is transmitted, the discrete-time representation of the received signal after passing a doubly-selective channel is

$$r(n) = \sum_{\tau} h(n, \tau) s(n - \tau) + w(n), \tag{5.1}$$

where $s(n)$ contains the transmitted FBMC signal, $h(n, \tau)$ is the linear time-variant discrete-time channel impulse response, and $w(n)$ corresponds to uncorrelated complex-valued white Gaussian noise with variance σ_w^2.

When multicarrier systems are used in time-selective channels, ICI arises in the received signal. The amount of ICI relates to the normalized Doppler spread of the channel, which is given by $D_n = f_d T$, f_d being the maximum Doppler frequency and T the FBMC symbol period, which depends on the FBMC scheme. For example, for Staggered Multitone (SMT) such a symbol period is $T_{\text{SMT}} = T_s N_c/2$.

Recall that the parameter T can be modified by time interpolation by a factor I, yielding an FBMC symbol period $T^{(I)} = IT$, and consequently an I times narrower signal bandwidth (see Section 3.2). Given the actual velocity of the mobile receiver v, the normalized Doppler spread value impacting the time-interpolated FBMC signal is

$$D_n^{(I)} = f_d T^{(I)} = f_d IT = \frac{IT f_c v}{c} = \frac{T f_c}{c} v^{(I)}, \tag{5.2}$$

with f_c the carrier frequency, c the speed of light, and $v^{(I)} = Iv$ the emulated speed as a result of an actual measurement speed v and an interpolation factor I. Consequently, enlarging the symbol period $T^{(I)}$ by adjusting I allows for the emulation of a velocity $v^{(I)}$ while conducting measurements at a (presumably much lower) speed v. Note that the statistical properties of the noise are not changed by the decimation process regardless of the interpolation factor.

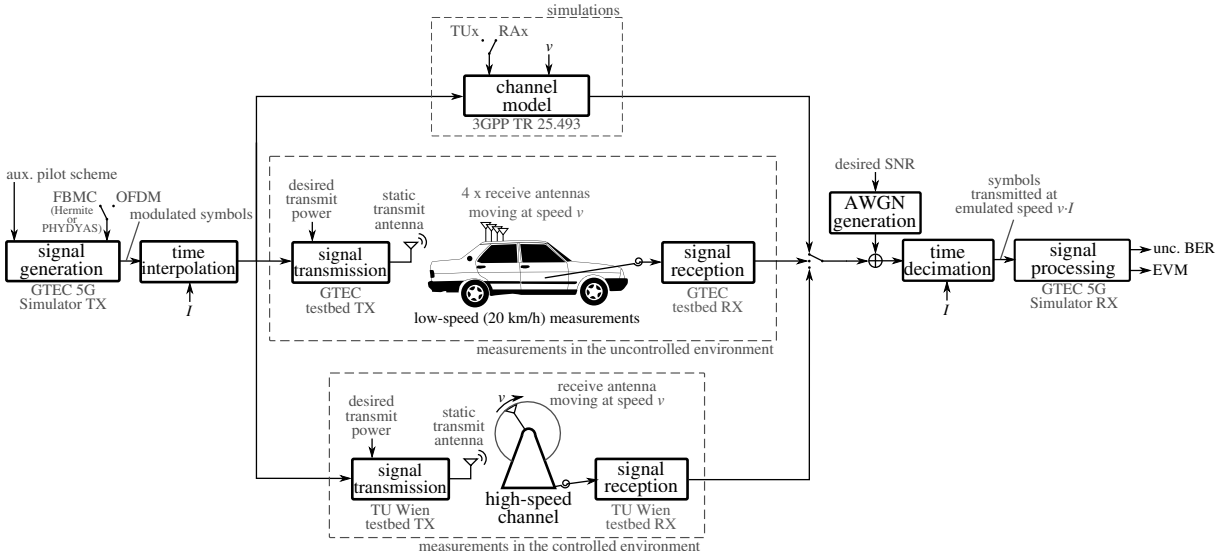

Figure 5.1: Block diagram of the setup used for the evaluations, both by means of measurements and simulations.

5.3 Evaluation Setup and Procedure

Three different performance evaluation strategies will be considered regarding FBMC signals:

- **Evaluation by means of simulations**: the accuracy of the technique of high speed emulation through time interpolation is tested by using different channel models.
- **Evaluation by measuring in a controlled environment**: the measurement setup and environment described in Sections 3.3.1 and 3.3.2 are considered for the assessment, hence empirically corroborating the results obtained by simulations.
- **Evaluation by measuring in a non-controlled environment**: the technique of high speed emulation through time interpolation is used to assess the performance of FBMC-based transmission in a typical outdoor-to-outdoor high-speed scenario for velocities up to 500 km/h.

Section 5.3.1 describes in detail the considered evaluation setup, whereas Section 5.3.2 is devoted to the description of the evaluation procedure used for the different experiments considered.

5.3.1 Evaluation Setup

Figure 5.1 shows the setup used to test the technique of high speed emulation by time interpolation for FBMC signals. The setup consists of the following blocks:

Signal Generation and Signal Processing

FBMC signals are generated and processed by means of the so-called GTEC 5G Link-Level Simulator (see [Dom+16b]), whose source code is publicly available under the GPLv3 license

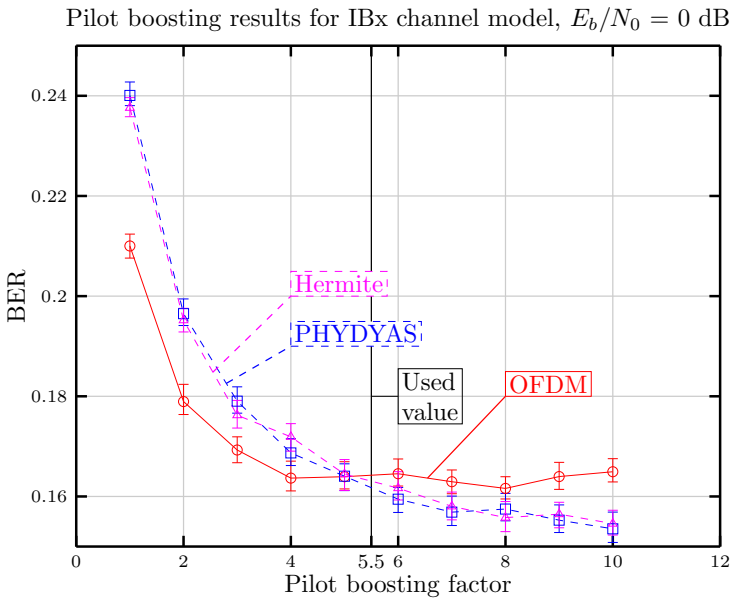

Figure 5.2: Bit Error Ratio (BER) versus pilot boosting factor for E_b/N_0 = 0 and the Indoor Office B (IBx) channel model. For low pilot boosting factors OFDM performs better than FBMC, while the contrary effect occurs for higher pilot boosting factors.

in [Tea].

At the transmitter side, FBMC-modulated signals are generated by using a custom-developed FBMC signal generator. Two different prototype filters were implemented, namely the one defined by the PHYDYAS project [Bel+10] and the so-called Hermite pulse [HB97]. It is worth noting that the latter one is specially suited for multicarrier transmissions over doubly dispersive channels since it minimizes both the ICI and Inter-Symbol Interference (ISI) by means of a good localization in time and in frequency [HB97]. The signal generator also supports OFDM signals (which correspond to the use of a rectangular filter in the time domain). At the receiver side, a custom-developed FBMC receiver is used. Such a receiver includes:

- **Basic channel estimation**: the channel response is estimated by means of a rectangular grid of pilots. For the case of FBMC signals, the receiver has to deal with the interference caused by the lack of orthogonality of the received signal, since only orthogonality in the real-valued part is ensured [Far11]. Several methods that minimize the effect of the interference based on the so-called auxiliary pilot schemes were implemented [JLR03; Sti+10; Cui+15]. For the results shown in this work, the so-called Coded Auxiliary Pilot (CAP) method [Cui+15] (using 8 symbols around each pilot) is considered. Notice that pilot boosting is used, i.e., the energy of the pilots is higher than that of the data symbols. Since the pulses are different, the energy allocated for each pilot may be different and the system performance may be different. Figure 5.2 shows the BER versus pilot boosting factor for OFDM and FBMC when $E_b/N_0 = 0$ dB. The results are obtained by means of simulations and considering the Indoor Office B (IBx) scenario from the

ITU Radiocommunication Sector (ITU-R) third generation (3G) channel models [ITU97]. The obtained results show that for low pilot boosting factors the performance of OFDM is better than the one of FBMC, whereas this changes then the pilot boosting factor is increased. According to the obtained results, a pilot boosting factor of 5.5 (7.4 dB) was used both for OFDM and FBMC.

- **Basic channel interpolation**: the channel response at the non-pilot time-frequency positions is obtained with two-dimensional interpolation using cubic splines.
- **Basic channel equalization**: a basic Zero-Forcing (ZF) equalizer is considered.

Time and frequency synchronization algorithms were also implemented. Time and frequency offsets are estimated and corrected by means of preambles inserted by the transmitter [Dom+16b]. For OFDM, a synchronization algorithm based on the Schmidl & Cox method [SC97] is employed, whereas a method based on the one defined in [ZC14] is considered for FBMC. It is worth noting that the results from both simulations and measurements in the controlled scenario were obtained under perfect time and frequency synchronization conditions. On the contrary, the aforementioned synchronization algorithms were employed when evaluating the measurements from the non-controlled scenario.

Time Interpolation and Time Decimation

The signal is time-interpolated by a factor I at the transmitter and decimated by the same factor I at the receiver side. A Doppler spread value similar to that obtained with a speed increase by a factor of I is emulated (see Section 5.2).

Channel Model (Simulations Branch)

Two channel models are considered in order to evaluate the performance of the velocity emulation technique for various scenarios. More specifically, the profiles Rural Area channel model (RAx) and Typical Urban channel model (TUx) of the 3rd Generation Partnership Project (3GPP) channel models for deployment evaluation [3GP04] are considered. The Doppler spread parameter of the channel was set according to the desired speed and carrier frequency values. While the profile RAx models the typical scenario in which a train moves across a rural area covered by macro-cells, the TUx environment is more suitable for situations in which the train moves through urban areas.

The Power Delay Profiles (PDPs) of the considered channel models are shown in Fig. 5.3, whereas Fig. 5.4 shows a sample of the estimated time-frequency response of a realization of the TUx channel.

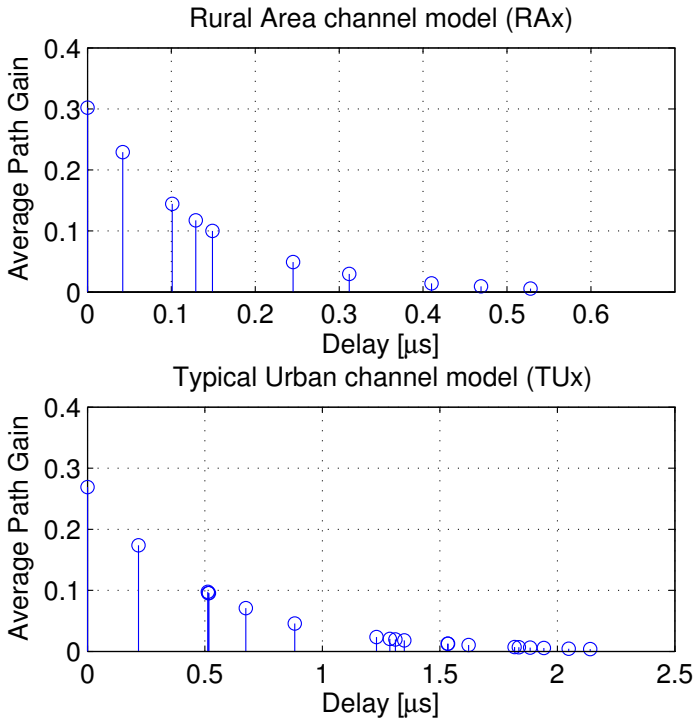

Figure 5.3: Simulations. Power Delay Profile of the considered channel models: Rural Area channel model and Typical Urban channel model.

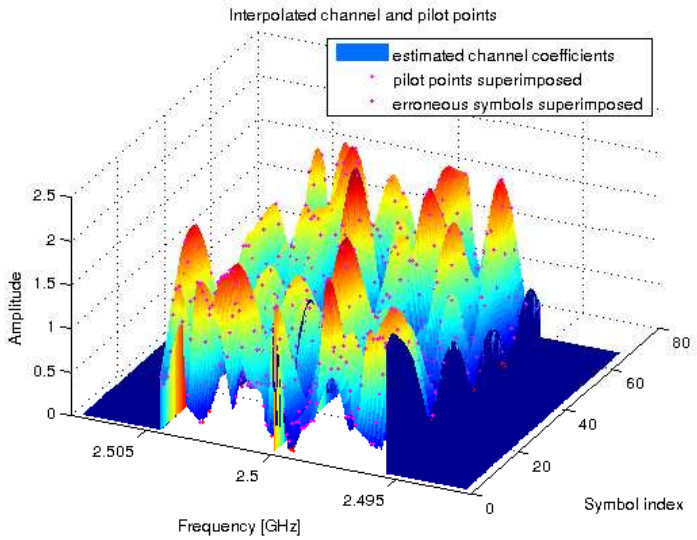

Figure 5.4: Simulations. Sample of the estimated time-frequency response for the TUx channel model.

Noise Addition

Noise variances that lead to the desired Signal to Noise Ratio (SNR) values are selected for the evaluations.

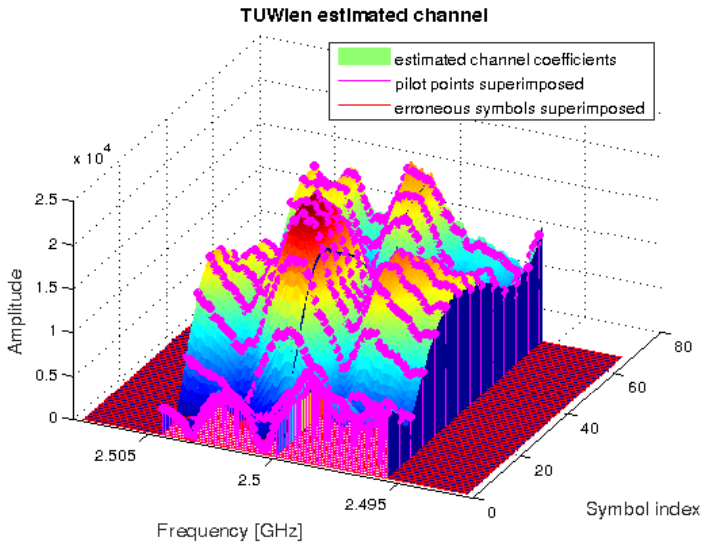

Figure 5.5: Measurements in the controlled environment. Sample of the estimated time-frequency response of the measured channel.

Signal Transmission and Reception under Actual High-Speed Conditions (Controlled Measurements Branch)

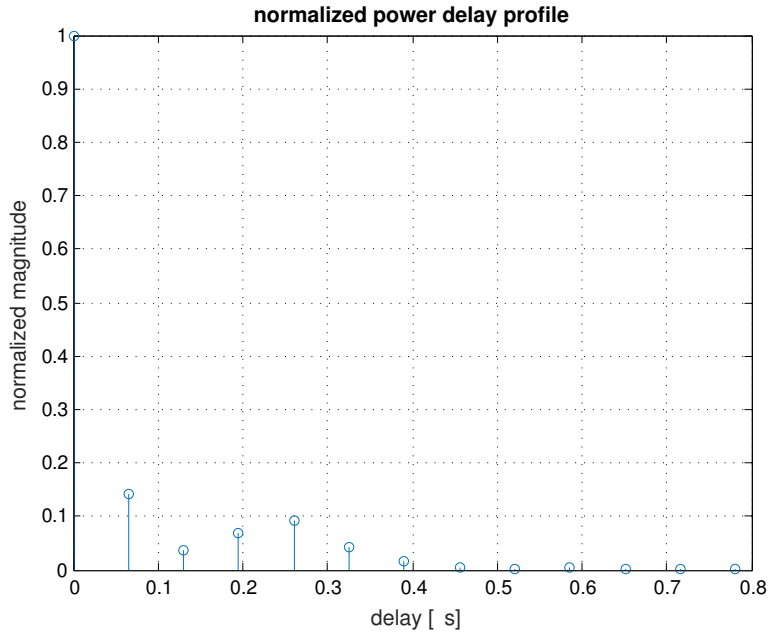

Figure 5.6: Measurements in the controlled environment. Estimated PDP of the measured channel.

Signals are transmitted over the air using a testbed developed at the TU Wien [Ler+14]. The measurement procedure described in Section 3.3 was considered, although the maximum speed for the rotation of the receiving antenna was increased up to $400\,\text{km/h}$.

A sample of an estimate of the time-frequency measured channel response is shown in Fig. 5.5, whereas the PDP estimation is provided in Fig. 5.6.

Signal Transmission and Reception under Uncontrolled Realistic Scenario (Uncontrolled Measurements Branch)

Signals are transmitted over the air using the testbed developed at the University of A Coruña, which is described in detail in Section 4.2 (see also [Suá+14a]). More specifically, three testbed nodes, including a single static transmitter and two receivers installed inside a car, were used.

5.3.2 Evaluation Procedure

In this section, the procedure followed for evaluating the impact of high-speed conditions on FBMC transmissions and for validating the technique of high speed emulation by time interpolation is described. First, the procedure for the simulations, as well as the measurements in the controlled measurement scenario, is detailed. Secondly, the evaluation procedure for the uncontrolled realistic scenario is described. The following subsection explains the different aspects considered for ensuring a fair comparison between the results for different modulations. This section concludes specifying the considered figures of merit for the evaluations.

Simulations and Measurements in the Controlled Measurement Scenario

In order to evaluate the impact of high-speed conditions on FBMC transmissions and to validate the technique of high speed emulation by time interpolation, actual velocities ranging from 50 km/h to 400 km/h were considered both for the channel models (simulations case) as well as the receive antenna (measurements in the controlled environment). Furthermore, interpolation factors of $I = 1$ (no interpolation), $I = 2$, and $I = 3$ were used for generating Doppler spreads equivalent to those associated to velocities ranging from 50 km/h to 1200 km/h. Note that it is possible to generate exactly the same Doppler spread value from different combinations of the actual velocity (the one used to configure the channel model or the rotation speed of the receive antenna) and the interpolation factor (see Table 5.1). This fact is helpful to show that our technique allows for the evaluation of wireless communication systems at high speeds while measuring at much lower speeds. In order to do that, we generated the same Doppler spread values by means of different velocities and interpolation factors and then we compared the obtained results. Table 5.1 shows the combinations of actual speeds and interpolation factors which lead to equal Doppler spreads (each row of the table corresponds to a different Doppler spread factor).

When conducting over-the-air measurements, the signals were transmitted several times for each velocity and interpolation factor. More specifically, the whole receiver (including the antenna rotation unit) was moved in two dimensions between 16 different positions on the floor. For each receiver position, 6 measurements per velocity and interpolation factor were carried out, each one starting at a given angular-shift on the circumference defined by the receive

Table 5.1: Measurements in the controlled environment. Combinations of actual velocities and interpolation factors employed.

	interpolation factors $I \in \{1 \text{ (no interpolation)}, 2, 3\}$													
	emulated velocity [km/h]													
actual velocity [km/h]	50	66.6	100	133.3	150	200	266.6	300	400	450	600	800	900	1200
50	1	–	2	–	3	–	–	–	–	–	–	–	–	–
66.6	–	1	–	2	–	3	–	–	–	–	–	–	–	–
100	–	–	1	–	–	2	–	3	–	–	–	–	–	–
133.3	–	–	–	1	–	–	2	–	3	–	–	–	–	–
150	–	–	–	–	1	–	–	2	–	3	–	–	–	–
200	–	–	–	–	–	1	–	–	2	–	3	–	–	–
300	–	–	–	–	–	–	–	1	–	–	2	–	3	–
400	–	–	–	–	–	–	–	–	1	–	–	2	–	3

rotating antenna. The same set of symbols (including data and pilots) was always transmitted for each modulation scheme, hence enabling a fair comparison of the results from different measurement configurations.

Measurements in the Uncontrolled Realistic Scenario

After validating the high speed emulation technique by time interpolation for FBMC signals, it was used to assess the performance of FBMC-based transmissions in a typical outdoor-to-outdoor high-speed scenario. The base station transmitter remains static and very high velocities up to 500 km/h are considered for the mobile unit, whereas the measurements are carried out at a much more convenient speed of 20 km/h. Such high speed values are considered because they are typically found in high-speed train scenarios. More specifically, the interpolation factors $I \in \{10, 15, 21, 25\}$ are considered. Given that the actual speed of the car is fixed at 20 km/h, the four interpolation factors considered yield the emulated speed values of 200, 300, 420, and 500 km/h, correspondingly.

We consider the scenario shown in Fig. 5.7, where a car equipped with the mobile unit downlink receiver (see Fig. 5.8) moves along the path (161 m long) at a constant (and convenient) speed of 20 km/h, completing each pass in 29 seconds. The base station downlink transmitter is placed on the corner of a building adjacent to the measurement path (see Fig. 5.9), with the starting point of the path being the farthest from the base station. Some trees in the vicinity of the path produce shadowing effects about 100 m away from the starting point, while the building in front of the base station, although lower, partially blocks the signal for the last 20 m of the path (see the estimated SNR along the trajectory plotted in Fig. 4.10 and [Fei+16, Fig. 7], which corresponds to the same measurement scenario). With the aim of extending the range of SNR values under evaluation, we simply add the required Additive White Gaussian Noise (AWGN) to the received signals before processing them.

Figure 5.7: Measurements in the uncontrolled environment. Scenario with the trajectory followed by the car and the location of the base station.

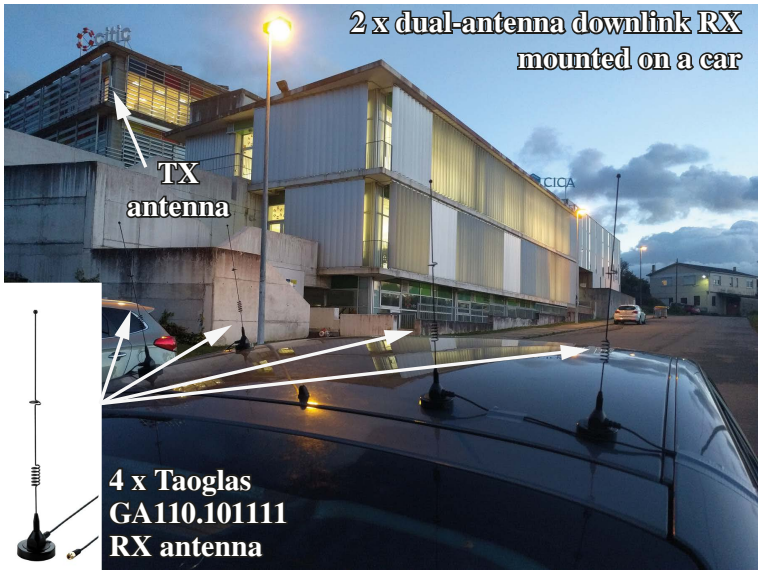

Figure 5.8: FBMC/OFDM dual-antenna receiver nodes mounted on a car.

Fairly Comparing Different Signals

To be able to compare the results gathered from different interpolation factors and the distinct modulations considered, the following aspects are taken into account:

Equal Mobile Simulated Trajectory (Simulations). The channel model was generated with identical initial conditions and the same seed (for the pseudo-random numbers generator) for each evaluated velocity and interpolation factor values. This way, we model a situation in which the receiver moves along the same path for each interpolation factor and speed value.

Equal Receive Antenna Trajectory (Controlled Measurements Environment). The trajectory of the receive antenna during the transmission of each signal does not vary if the emulated speed is kept constant. The arc length defined by the antenna during the transmission

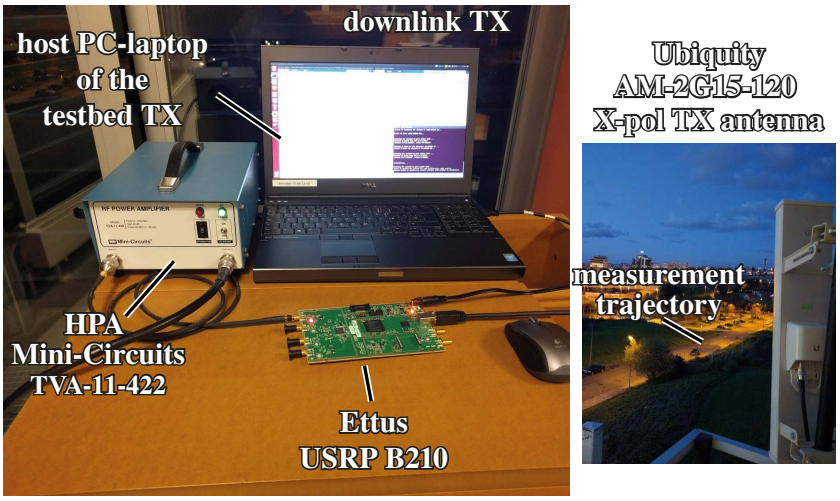

Figure 5.9: Measurements in the uncontrolled environment. Single-antenna base station. The vertically polarized antenna element of the X-pol Ubiquity AM-2G-15-120 is used.

of a single FBMC symbol, namely ΔZ, can be expressed as $\Delta Z = \left(v^{(I)}/I\right) T_t I$, where $v = v^{(I)}/I$ is the actual rotation speed and $T_t I$ is the time required for transmitting an FBMC symbol after being interpolated by a factor of I. It can be seen that ΔZ does not vary regardless of the interpolation factor I.

Equal Mobile Trajectory (Uncontrolled Measurements Environment). During the measurements, signals are transmitted over the air in a cyclical fashion while, at the same time, the two receiver nodes mounted on the car acquire the signals from the four available antennas in total while the car completes the trajectory shown in Fig. 5.7 at the constant speed of 20 km/h. The trajectory is followed by the car for two times without modifying any parameter. Thus, two measurements (each one consisting of four acquired records, one per each of the four available receive antennas) are obtained for each time interpolation factor.

Equal Spectrum Usage. When the signal is interpolated by a factor of I, its bandwidth is decreased by the same factor, which in principle reduces the channel frequency selectivity. In Section 3.3.2 it was proposed to transmit I replicas of the interpolated signal to ensure that the whole frequency range of the original signal is used. However, as mentioned in Section 3.3.2, the frequency selectivity reduction inherent to the bandwidth decrease caused by the time interpolation does not seem to affect the simulation nor the measurement results. It is expected to affect more in channels exhibiting a very high frequency selectivity, which is unlikely in high speed conditions in which the channel response changes fast. Taking this into account, a single replica of the signal was transmitted for the measurements considered in this chapter. Notice that the effects caused by the transmission of several replicas of the signal are studied in Section 3.6 in more detail.

Equal Average Transmit Energy per Symbol. In order to preserve the average energy per symbol, the interpolated signals are scaled in amplitude by a factor of $\sqrt{I}$ before being

transmitted.

Ensuring a Fair OFDM vs FBMC Comparison. In order to fairly compare the results for OFDM and FBMC (with Hermite and PHYDYAS pulses), the following aspects are also considered:

- The number of data subcarriers, as well as the subcarrier spacing, are the same in all cases. More specifically, 600 subcarriers were used, while the subcarrier spacing was set to 15 kHz (for the OFDM case, 600 subcarriers are used for a 1024-point Fast Fourier Transform (FFT)). These parameters correspond to the typical configuration for the 10 MHz downlink LTE profile.
- The pilot density considered for the channel estimation is equivalent in all cases. Note that in the case of FBMC some additional symbols, namely the Auxiliary Pilots (APs), are required to minimize the interference caused by the lack of orthogonality of the received pilots [Far11]. More specifically, a rectangular grid of pilots was used. Such pilot spacing in the time-frequency grid is of 8 subcarriers in the frequency dimension and of 10 symbols in the time dimension for FBMC signals (5 symbols in the case of OFDM given that consecutive symbols do not overlap).
- The same algorithms for channel estimation, interpolation and equalization are considered for each modulation (see Section 5.3.1).
- A 2-PAM constellation is used for the FBMC transmissions, while 4-QAM is considered for OFDM, since the symbols are complex-valued in the latter case.
- Approximately the same number of user data bits is considered per transmission. Taking into account that real-valued symbols are used in FBMC, whereas complex-valued ones are used for OFDM, more time-positions in the time-frequency grid are required for FBMC with respect to OFDM for the same number of transmitted bits. However, provided that consecutive FBMC symbols partially overlap in the time domain (because a SMT scheme is considered), this does not mean that, in order to transmit the same amount of data bits, twice the time-positions for FBMC with respect to OFDM are required. With the model considered, the user bit rate is approximately equivalent for both OFDM and FBMC, with slight differences caused by the length of the OFDM cyclic prefix and the time dispersion of the prototype filters in FBMC. More specifically, the obtained data rates for OFDM and FBMC signals are approximately 16372 kbit/s and 16653 kbit/s, respectively. If the signals being transmitted are long enough the differences in data rate due to the time dispersion of the prototype filters in FBMC become negligible.
- The signals are scaled to ensure that the transmitted energy per bit is equivalent for both OFDM and FBMC.

Note that the number of used subcarrriers could be increased in FBMC with respect to OFDM for a common spectral mask, since the subcarriers are better frequency-localized.

Table 5.2: Main parameters used in the experiments.

parameter	value
Sampling frequency, F_s	15.36 MHz
FFT size	1024 points
Number of used subcarriers	600 (excluding DC)
CP length (OFDM)	72 samples
Constellations	2-PAM (FBMC) 4-QAM (OFDM)
Pilot spacing	8 subcarriers (frequency dimension) 10 symbols (time dimension, FBMC) 5 symbols (time dimension, OFDM)
Auxiliary Pilot scheme	CAP (8 surrounding symbols)
Pulse overlapping	3 symbols (Hermite) 4 symbols (PHYDYAS)
Actual velocities, v	20, 50, 66.6, 100, 133.3, 150, 200, 300, and 400 km/h
Carrier frequency, f_c	2.6 GHz
Interpolation factors, I	1, 2, 3, 10, 15, 21, and 25
SNR	from 0 to 30 dB
Transmit power (measurements in the uncontrolled environment)	+18.5 dBm (at antenna port)

Furthermore, the bandwidth per subcarrier could be also increased for FBMC by decreasing the number of subcarriers while keeping the total used bandwidth constant. Although this would require more advanced equalizers, it will be beneficial in terms of Peak-to-Average Power Ratio (PAPR) and robustness against ICI. However, the number of subcarriers as well as the subcarrier spacing were kept constant to perform a fair comparison, although this would imply not to take advantage of all the potential benefits of FBMC systems. This leads to approximately the same number of user data bits per transmission for the FBMC and for the OFDM cases, whereas the same algorithms for channel estimation, interpolation and equalization are employed.

Considered Figures of Merit

Table 5.2 shows the most relevant parameters considered during the experiments, both for the simulations as well as the measurements. From the obtained results, we consider two figures of merit, which are:

- **Error Vector Magnitude (EVM)**: it is calculated assuming the transmitted symbols are

known beforehand. It is an unbounded and continuous metric particularly valuable when the SNR is high enough to saturate the BER to its minimum value of zero. In order to compute the EVM, the dynamic range of the equalized symbols is bounded. This is realistic in a practical receiver. In this sense, real and imaginary parts of the symbols are clipped to a maximum value. This avoids symbols having extremely large modulus (e.g., due to imperfect ZF channel equalization), hence distorting the EVM estimation. It is worth mentioning that, for the case of FBMC, only the real part of the symbols is considered to compute the EVM, since the imaginary part contains the interference generated by the lack of orthogonality of the signals [Far11] and it is ignored at the receiver.

- **Uncoded BER**: calculated as the BER after the hard symbol decision. It is one of the most used performance metrics in wireless communications.

Besides the performance results in terms of EVM and uncoded BER, coded BER and EVM relative error values are also provided. Such figures of merit are computed from the results obtained when the same speed is emulated from different interpolation factors. For the case of the BER, the relative error is computed by averaging (by computing the median value) the instantaneous BER relative error values E_{BER}, which are defined as

$$E_{\text{BER}}\left(A,B\right) = 100 \cdot \frac{W_A - W_B}{W_B}\ [\%]\,,$$

where W_A and W_B denote the number of received bits estimated without errors, corresponding to a channel realization and obtained for the interpolation factors $I = A$ and $I = B$, respectively. EVM relative error values are computed by averaging (by computing the median value) the instantaneous EVM relative error values, i.e.

$$E_{\text{EVM}}\left(A,B\right) = 100 \cdot \frac{\text{EVM}_A - \text{EVM}_B}{\text{EVM}_B}\ [\%]\,,$$

where EVM_A and EVM_B are the instantaneous EVM values for the interpolation factors $I = A$ and $I = B$, respectively.

5.4 Obtained Results

All the results included in this section are expressed in terms of BER and EVM with respect to the SNR, and with respect to the so-called "emulated speed", which means that the speed can correspond to the actual velocity ($I = 1$) or a velocity obtained by time-interpolating the transmit signal. With the objective of illustrating the accuracy of the results, 95 % confidence intervals obtained from bootstrapping (see [EH94]) are also included in most figures.

The results obtained by means of simulations are shown in Section 5.4.1, whereas the results obtained by means of measurements in the controlled environment are included in

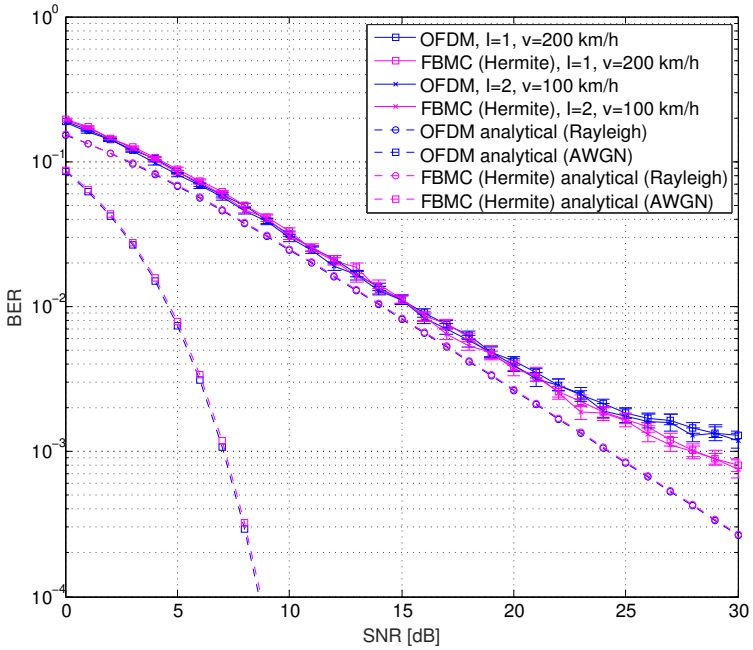

Figure 5.10: BER versus SNR for the RAx channel model, OFDM and FBMC (Hermite) modulations, $I = 1, 2$ and for an emulated speed of 200 km/h. Curves corresponding to different interpolation factors almost overlap, showing the accuracy of the proposed technique. FBMC with Hermite prototype filter performs a slightly better than OFDM in the high SNR regime.

Section 5.4.2. Finally, Section 5.4.3 is devoted to the results obtained in the uncontrolled measurement environment.

5.4.1 Simulation Results

Figure 5.10 shows the BER versus the SNR for the RAx channel model when an emulated speed of 200 km/h is obtained considering $I = 1$ (no interpolation) and $I = 2$, for the cases of OFDM and FBMC (Hermite prototype filter). Analytic curves for both AWGN and Rayleigh channels for OFDM and FBMC are also included. It can be seen that such analytic curves almost overlap, ensuring that a fair comparison is performed. With respect to the simulation results, the curves corresponding to OFDM for the emulated speed $v = 200$ km/h obtained by considering the interpolations factors $I = 1$ and $I = 2$ almost overlap, hence showing that our technique performs adequately, being the same effect appreciated for the curves corresponding to FBMC. Moreover, there is an excellent agreement between the OFDM and FBMC results for most SNR values. This shows that the performance of both modulation schemes is very similar for $v = 200$ km/h and the RAx channel model. Only slight differences are appreciated for the maximum SNR value of 30 dB, since the random effects due to the noise are minimized and hence do not hide the other sources of disagreement in the results. Therefore, SNR $= 30$ dB will be considered for the results of BER versus emulated speed which are shown below, as it is the worst case for the proposed high speed emulation technique.

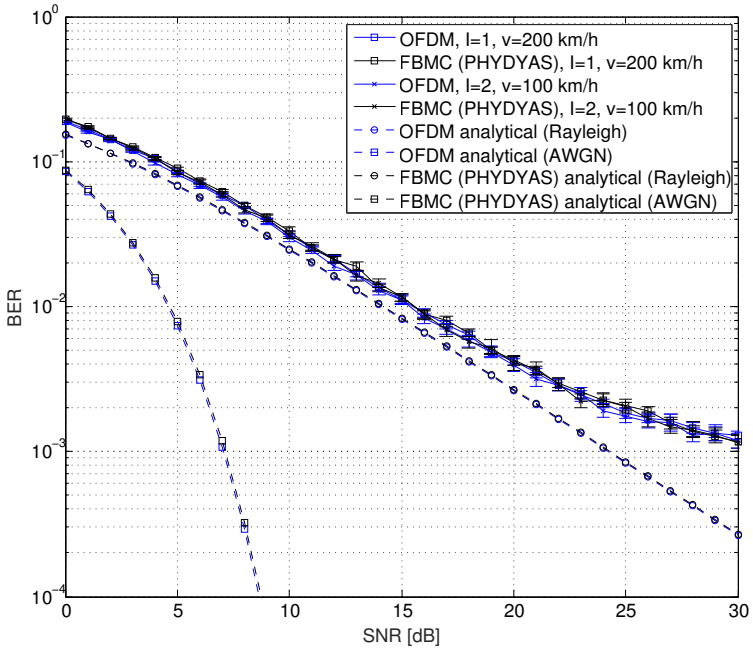

Figure 5.11: BER versus SNR for the RAx channel model, OFDM and FBMC (PHYDYAS) modulations, $I = 1, 2$, and for an emulated speed of $200\,\text{km/h}$. Curves corresponding to different interpolation factors almost overlap, showing the accuracy of the proposed technique. No differences in the performance achieved by OFDM and FBMC with the PHYDYAS prototype filter are appreciated.

Figure 5.11 is similar to the previous figure, but it includes the results for OFDM and FBMC with the PHYDYAS prototype filter. The plot shows again the good behavior of the proposed technique, since the curves corresponding to the same modulation and emulated speed almost overlap regardless of the considered interpolation factor. However, in this case no noticeable performance differences between OFDM and FBMC with the PHYDYAS prototype filter can be appreciated, regardless of the considered SNR value.

The performance in terms of EVM versus SNR is shown in Fig. 5.12 for the RAx channel model and the three modulation schemes, for an emulated velocity of $200\,\text{km/h}$. These results are in accordance with those obtained for the BER. Again, an excellent level of agreement between the curves obtained for different interpolation factors can be observed, thus validating the proposed technique for inducing high-speed effects while evaluating the system under test at much lower velocities. Moreover, it can be seen that FBMC with the Hermite prototype filter performs better in terms of EVM for the high SNR regime.

Figure 5.13 shows the BER versus the emulated speed for the RAx channel model and considering OFDM and FBMC with the PHYDYAS prototype filter. Interpolation factors $I = 1, 2, 3$ are considered. On the one hand, the three OFDM curves corresponding to the three interpolation factors show an excellent level of agreement. The same effect is observed for the FBMC (PHYDYAS) curves. On the other hand, a significant performance difference between OFDM and FBMC (PHYDYAS) is appreciated for speeds above $300\,\text{km/h}$. This is because the PHYDYAS prototype filter is much better localized in frequency than the OFDM one, and

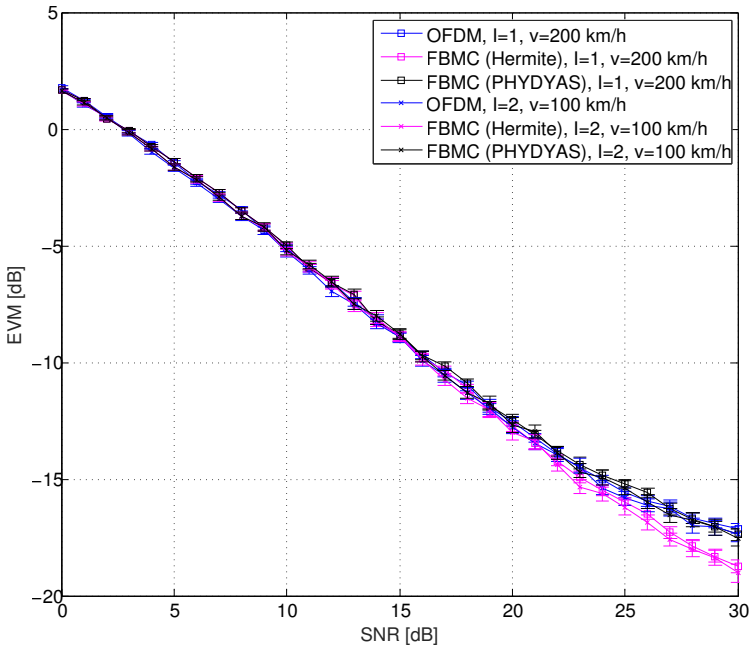

Figure 5.12: EVM versus SNR for the RAx channel model, OFDM and FBMC (Hermite and PHYDYAS) modulations, $I = 1, 2$ and for an emulated speed of $200\,$km/h. Curves corresponding to different interpolation factors almost overlap, showing the accuracy of the proposed technique. FBMC with Hermite prototype filter performs slightly better than the other modulation schemes for the high SNR regime.

hence it accounts better for the channel time dispersion. In other words, the FBMC PHYDYAS prototype filter helps in combating the effect of the ICI better than OFDM. However, for practical HST velocities (below $350\,$km/h) the performance difference is not very significant. Figure 5.14 shows also the BER versus the emulated speed for the RAx channel model but for the two FBMC prototype filters considered (Hermite and PHYDYAS). Again, an excellent agreement is shown between the results for emulated speeds obtained by means of different interpolation factors regardless of the considered modulation scheme. Figure 5.14 also shows that the performance obtained for the Hermite prototype filter is better than that exhibited by the PHYDYAS one, specially for those speeds which are more practical in the HST environment. The reason for this behavior is that the Hermite prototype filter is slightly worse localized in frequency than the PHYDYAS one, but it is better localized in time, thus simultaneously minimizing both ICI and ISI.

Figures 5.15 and 5.16 show the BER versus the emulated speed for the TUx channel model and considering OFDM and FBMC (PHYDYAS prototype filter) modulation schemes in the first case, and both FBMC schemes (PHYDYAS and Hermite prototype filters) in the latter. Given that the TUx channel model is more frequency selective than the RAx one, the BER results are worse than those obtained for the RAx channel model. On the other hand, the level of agreement between the curves corresponding to the three interpolation factors is also slightly worse than in the RAx case. Besides the performance curves, BER relative error curves are

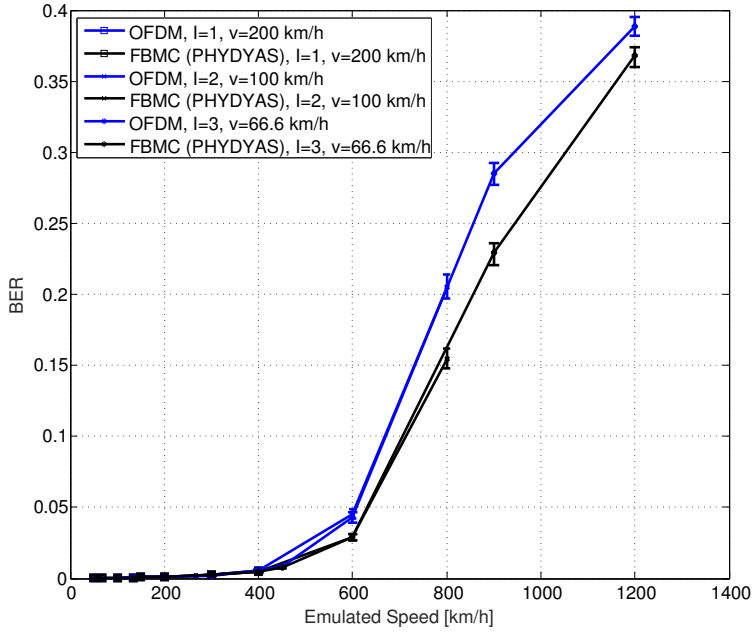

Figure 5.13: BER versus emulated speed for the RAx channel model, OFDM and FBMC (PHYDYAS) modulations and $I = 1, 2, 3$. Curves corresponding to different interpolation factors almost overlap, showing the accuracy of the proposed technique. FBMC with PHYDYAS prototype filter performs better than OFDM for speeds above 300 km/h, whereas negligible performance differences are appreciated for lower speeds.

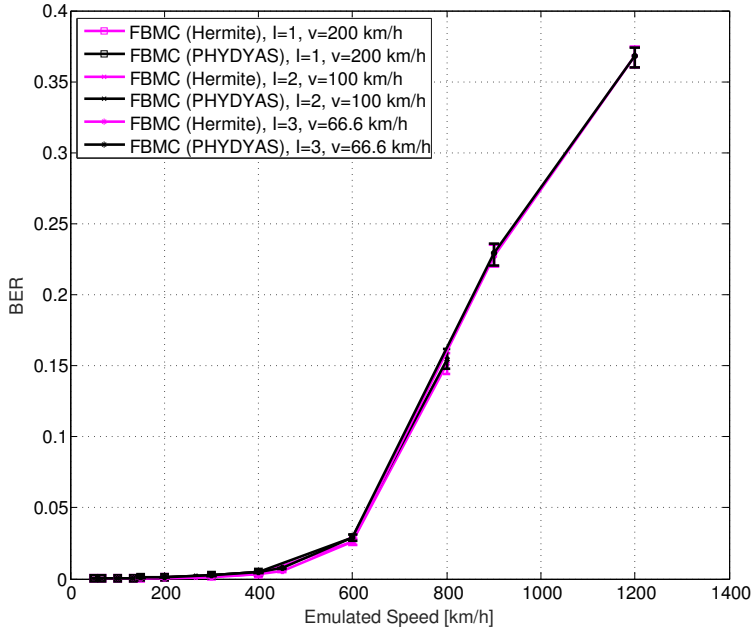

Figure 5.14: BER versus emulated speed for the RAx channel model, FBMC (Hermite and Phydyas) modulation and $I = 1, 2, 3$. Curves corresponding to different interpolation factors almost overlap, showing the accuracy of the proposed technique. The Hermite prototype filter provides a better performance than the PHYDYAS one for practical HST speeds.

also included in Fig. 5.17 for the worst case (TUx channel model). Three types of relative error curves are included, which are *(a)* relative difference between the results obtained when

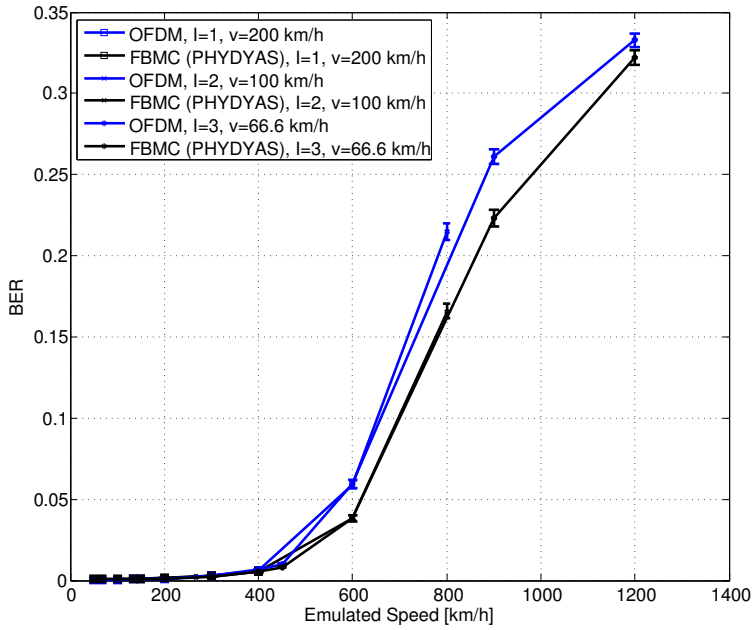

Figure 5.15: BER versus emulated speed for the TUx channel model, OFDM and FBMC (PHYDYAS) modulations and $I = 1, 2, 3$. The performance is lower than that for the RAx channel model, since the frequency selectivity of the channel is higher. This also causes that the level of agreement between the curves corresponding to the three interpolation factors is also slightly worse than in the RAx case.

the interpolation factor $I = 2$ is employed and actual speeds are used; *(b)* relative difference between the results obtained when the interpolation factor $I = 3$ and the actual speeds are considered; and *(c)* relative difference between the results obtained for the interpolation factors $I = 3$ and $I = 2$. These curves are computed as explained in Section 5.3.2. It can be seen that the obtained error values are below $0.2\,\%$ in any case.

The performance in terms of EVM versus emulated speed is shown in Fig. 5.18 for the RAx channel model, and in Fig. 5.19 for the TUx channel model. These results are in accordance with those obtained for the BER. Again, an excellent level of agreement between the curves obtained for different interpolation factors can be appreciated, thus validating the proposed technique for inducing high-speed effects while evaluating the system under test at much lower velocities.

5.4.2 Measurement Results in the Controlled Environment

Fig. 5.20 shows the BER versus SNR when the emulated speed is 200 km/h for the interpolation factors $I = 1$ (i.e., no interpolation) as well as $I = 2$ and all the modulation schemes considered. It can be seen that the curves for each modulation almost overlap regardless of the interpolation factor. In accordance with the results obtained by simulation (see Section 5.4.1), the performance is very similar when $v = 200$ km/h for all modulation schemes. Only slight differences can be observed for very high SNR values, since the random effects due to noise

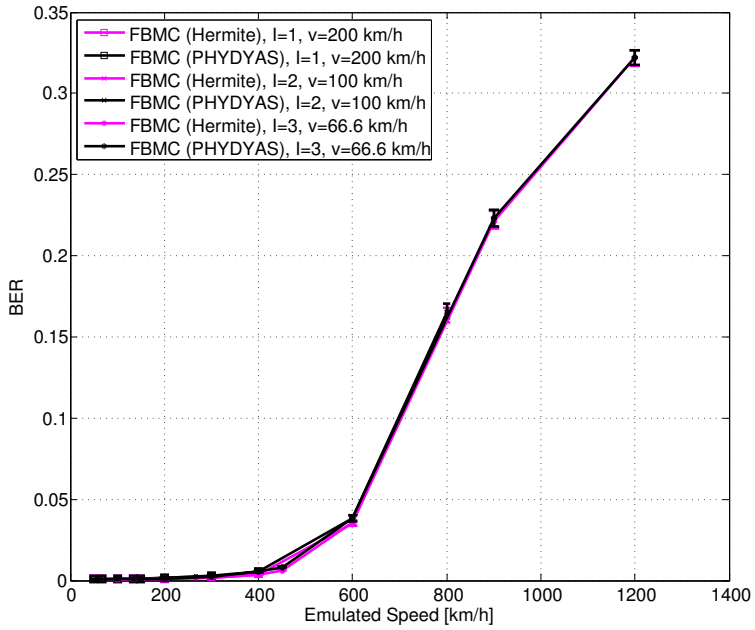

Figure 5.16: BER versus emulated speed for the TUx channel model, FBMC (Hermite and PHYDYAS) modulation and $I = 1, 2, 3$. The performance is lower than that for the RAx channel model, since the frequency selectivity of the channel is higher. This also causes that the level of agreement between the curves corresponding to the three interpolation factors is also slightly worse than in the RAx case.

are minimized and hence do not hide other sources of disagreement in the results. Note that, in these cases, FBMC with the Hermite prototype filter performs slightly better than the other alternatives. Figure 5.21 shows the performance in terms of EVM for an emulated speed of 200 km/h and $I = 1, 2$. It can be seen that the obtained results are strongly correlated with those corresponding to the BER. Moreover, curves corresponding to the same emulated speed also overlap regardless of the interpolation factor, showing that the proposed technique is also well suited to emulate the distortion suffered by the received constellations due to the receiver movement. In the remaining of this section we consider SNR $= 30$ dB as the worst case for the proposed technique.

Fig. 5.22 shows the BER versus the emulated speed for $I = 1, 2, 3$ and all the modulation schemes being considered. On the one hand, curves corresponding to the same emulated speed obtained by different interpolation factors show an excellent level of agreement for each of the modulation schemes. A significant difference on the performance between OFDM and FBMC (for both considered prototype filters) can be observed for speeds higher than 300 km/h, which is in accordance with the simulation results. As mentioned in the previous section, the reason for the observed behavior is that both prototype filters considered for FBMC are much better localized in frequency than the OFDM waveform, and hence they account better for the channel time dispersion. In other words, they are better suited to combat the ICI. However, for practical HST speeds (less than 350 km/h), the difference is not very significant. Similarly to the results obtained by simulations, a slight difference in the results obtained for the PHYDYAS

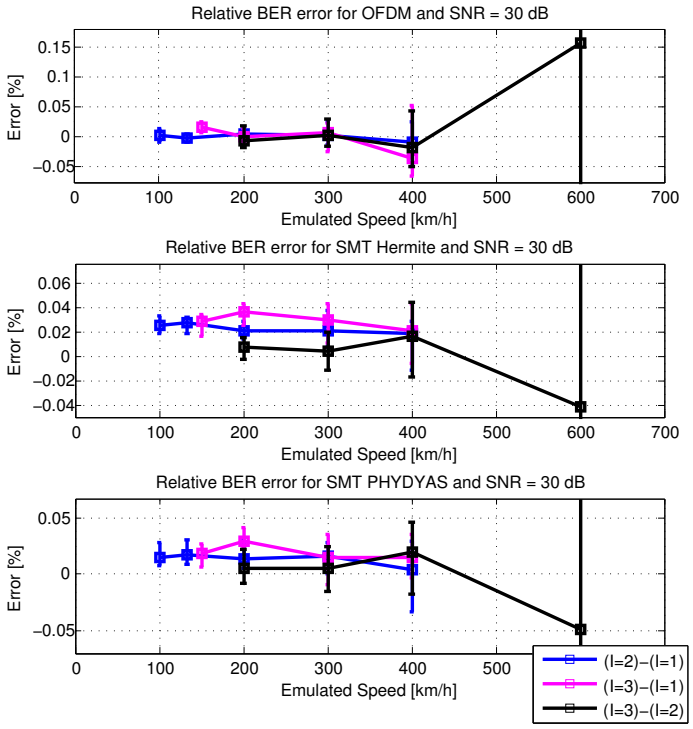

Figure 5.17: Relative error curves for BER evaluations over the TUx channel model. An excellent agreement can be appreciated. Notice that the confidence interval for the case labeled as "$(I = 3)$ - $(I = 2)$" is not completely shown in the graphs. The lower bounds of such an interval are approximately $-0.55\,\%$, $-0.33\,\%$ and -0.45% for the OFDM, FBMC (Hermite) and FBMC (PHYDYAS) cases, respectively. The respective upper bounds of the confidence interval are approximately $0.46\,\%$, $0.22\,\%$ and $0.16\,\%$.

and Hermite prototype filters can be observed, being better the results obtained for the latter one. The reason for this behavior is that the Hermite prototype filter is slightly worse localized in frequency than the PHYDYAS one, but it is better localized in time.

BER relative error curves for the measurements are included in Fig. 5.23. Similarly to the simulation results, three types of relative error curves are provided, which are *(a)* relative difference between the results obtained when the interpolation factor $I = 2$ is employed and actual speeds are used; *(b)* relative difference between the results obtained when the interpolation factor $I = 3$ and the actual speeds are considered; and *(c)* relative difference between the results obtained for the interpolation factors $I = 3$ and $I = 2$. These curves are computed as explained in Section 5.3.2. It can be seen that the obtained error values are below $0.2\,\%$ in any case.

5.4.3 Measurement Results in the Uncontrolled Environment

Fig. 5.24 shows the BER vs SNR results obtained after measurements in the uncontrolled environment. Three different curves are plotted for each of the four different emulated speeds:

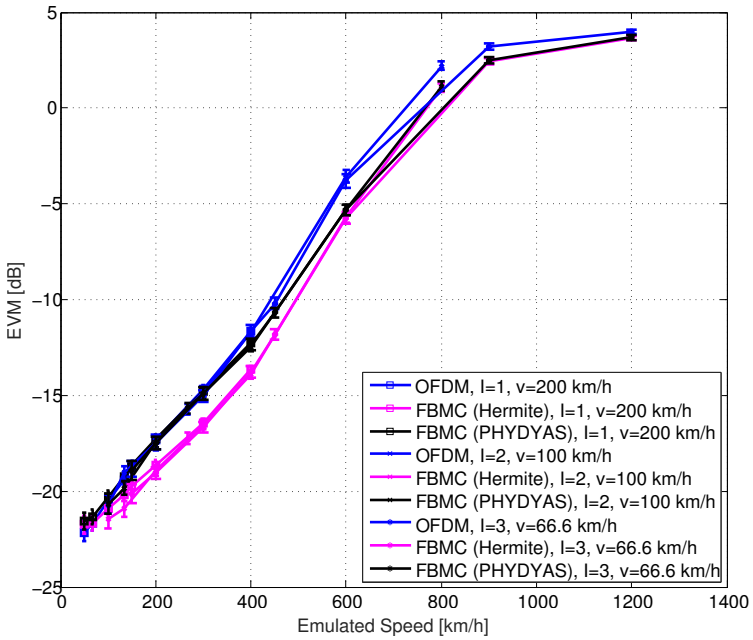

Figure 5.18: EVM versus emulated speed for the RAx channel model, OFDM and FBMC (Hermite and PHYDYAS) modulations and $I = 1, 2, 3$. The results are in accordance with those obtained for the BER and an excellent level of agreement between the curves obtained for different interpolation factors can be appreciated.

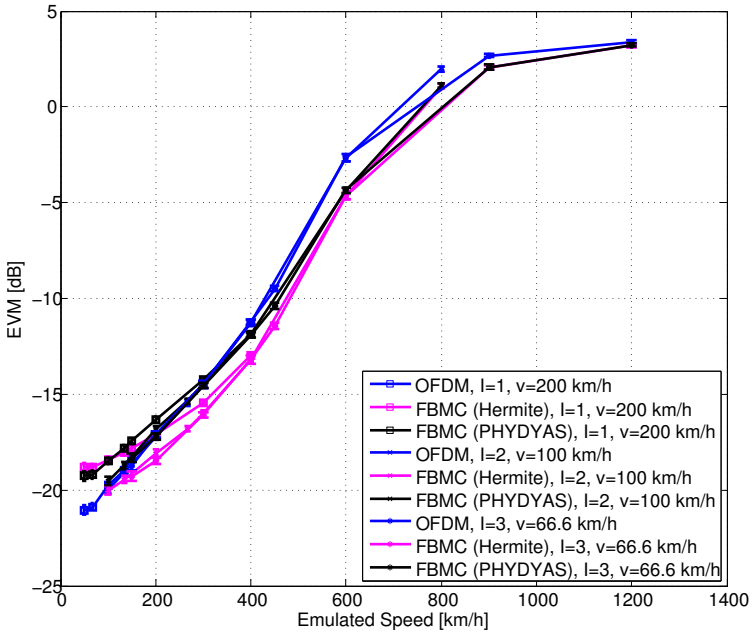

Figure 5.19: EVM versus emulated speed for the TUx channel model, OFDM and FBMC (Hermite and PHYDYAS) modulations and $I = 1, 2, 3$. The results are in accordance with those obtained for the BER and an excellent level of agreement between the curves obtained for different interpolation factors can be appreciated.

the one corresponding to OFDM in black color, the one corresponding to FBMC with the Hermite prototype filter in blue color, and finally, the one corresponding to the PHYDYAS prototype filter in red color. For 200 and 300 km/h the performance does not change significantly

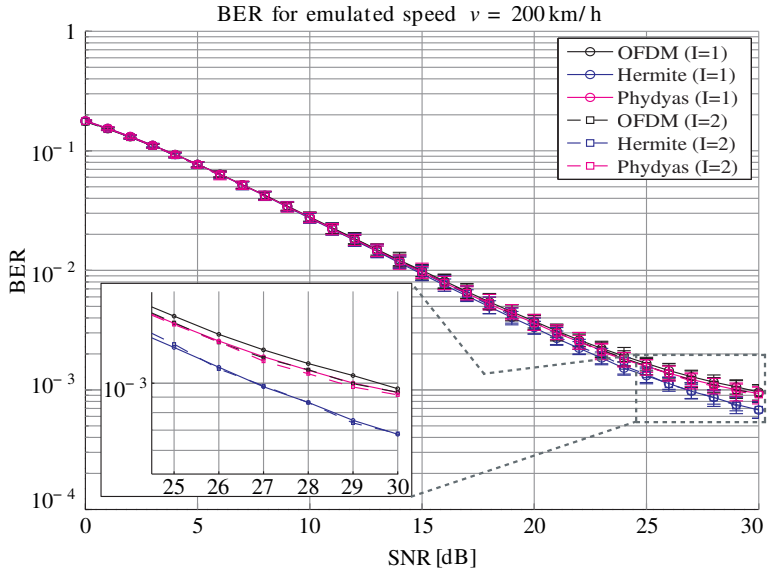

Figure 5.20: Measurements in the controlled environment. BER versus SNR, OFDM and FBMC (Hermite and PHYDYAS) modulations, $I = 1, 2$ and for an emulated speed of 200 km/h. Curves corresponding to different interpolation factors almost overlap, showing the accuracy of the proposed technique. FBMC with Hermite prototype filter performs slightly better in the high SNR regime.

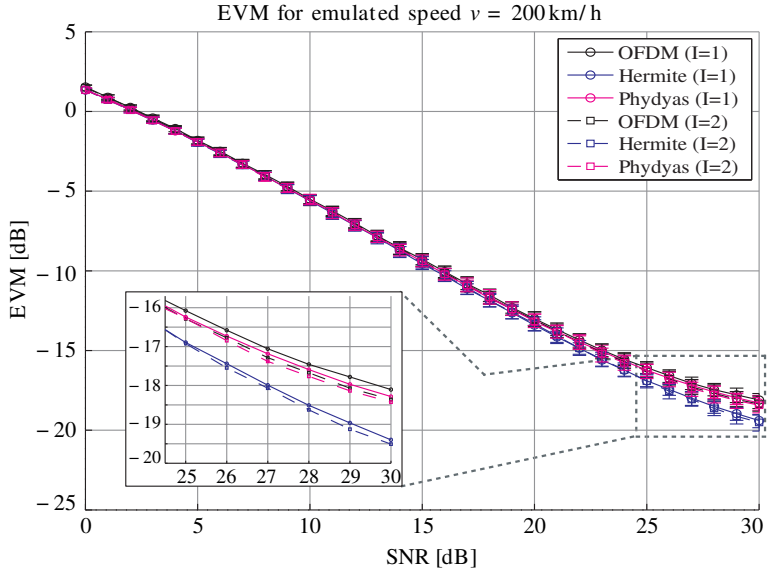

Figure 5.21: Measurements in the controlled environment. EVM versus SNR, OFDM and FBMC (Hermite and PHYDYAS) modulations and $I = 1, 2$. Curves corresponding to different interpolation factors almost overlap, showing the accuracy of the proposed technique. FBMC with Hermite prototype filter performs slightly better in the high SNR regime.

between the three different schemes considered, which is in accordance with the aforementioned results from simulations and measurements in the controlled environment. However, for 420 and 500 km/h, FBMC with the Hermite prototype filter performs the best, specially at 500 km/h, in which the difference is clearly noticeable.

Fig. 5.25 shows the corresponding results when EVM is the figure of merit instead of

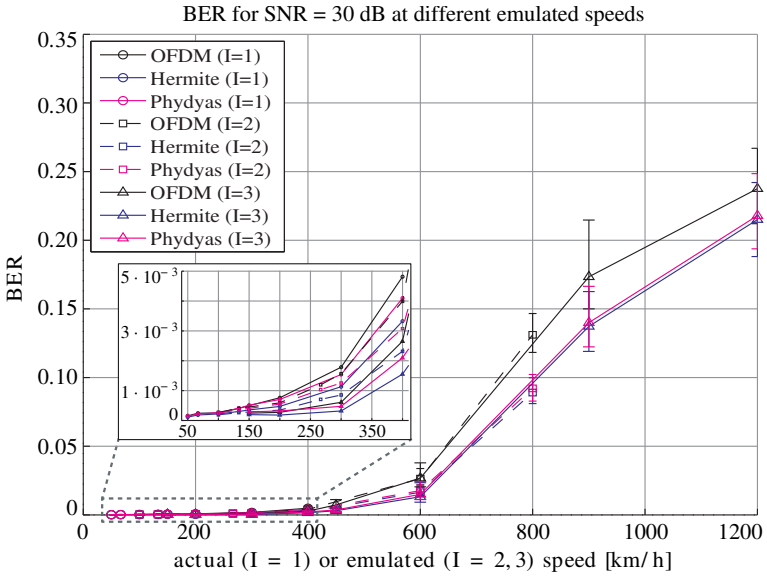

Figure 5.22: Measurements in the controlled environment. BER versus emulated speed for OFDM and FBMC (Hermite and PHYDYAS) modulations and $I = 1, 2, 3$. Curves corresponding to different interpolation factors almost overlap, showing the accuracy of the proposed technique. FBMC with both prototype filters performs better than OFDM for speeds above 300 km/h, whereas negligible performance differences are appreciated for lower speeds.

BER. The results show that when SNR is the dominant factor (200 km/h) the three modulation schemes perform very similar. Interestingly, for 300 km/h the PHYDYAS prototype filter performs slightly better than the Hermite one, whereas OFDM is the worst, although the differences are not large. For higher speed values (i.e. 420 and 500 km/h), the performance of the PHYDYAS prototype filter approaches that of the OFDM, whereas FBMC with the Hermite pulse performs the best. Notice that as ICI becomes the dominant distortion factor with respect to noise, the performance of OFDM and that of FBMC with the PHYDYAS prototype filter becomes very similar. However, this is not the case when the Hermite prototype filter is employed, hence showing the superior performance of the Hermite prototype filter with respect to the PHYDYAS one for time dispersive channels. In any case, the performance differences are not very large, hence the theoretical advantages of FBMC waveforms (such as its better bandwidth efficiency and the minimization of multiple-access interference in the uplink) can be exploited without additional performance losses. In fact, what we can safely conclude from the results is that FBMC schemes do not exhibit any a priori performance degradation in terms of BER versus SNR with respect to OFDM.

5.5 Conclusions

In this chapter we showed that the technique introduced in Section 3.2 to induce the effects caused by highly time-varying channels while conducting measurements (or evaluations) at

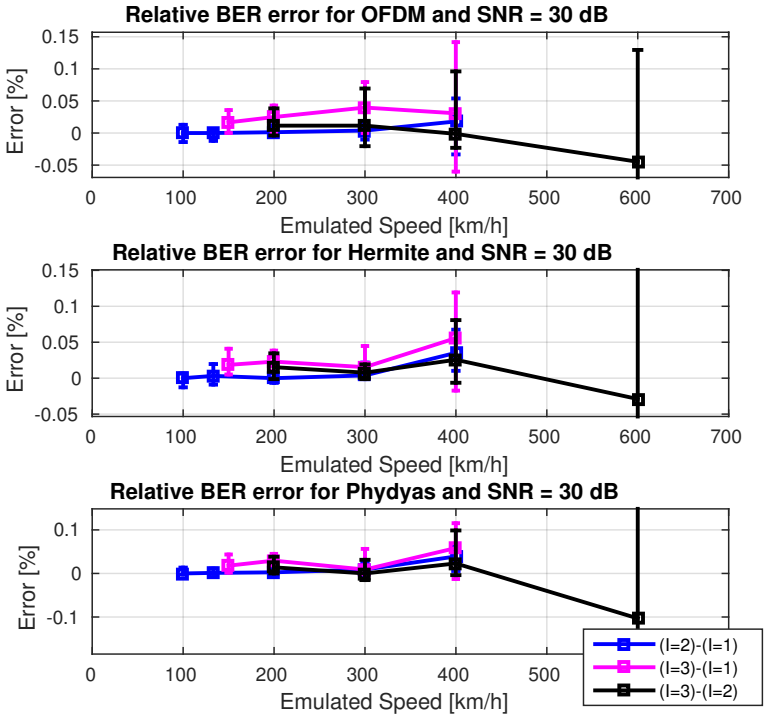

Figure 5.23: Measurements in the controlled environment. Relative error curves for BER evaluations. An excellent agreement can be appreciated. Notice that the confidence interval for the case labeled as "$(I = 3)$ - $(I = 2)$" is not completely shown in the graphs. The lower bounds of such an interval are approximately $-0.16\,\%$, $-0.22\,\%$ and -0.29% for the OFDM, FBMC (Hermite) and FBMC (PHYDYAS) cases, respectively. The respective upper bounds of the confidence interval are approximately $0.13\,\%$, $0.19\,\%$ and $0.23\,\%$.

much lower velocities can also be applied to FBMC-modulated signals. This allows for reducing the complexity, cost, and safety constraints of measurement campaigns for 5G systems in HST scenarios. The proposed technique was evaluated by means of simulations as well as measurements both in terms of BER and EVM versus SNR, and considering two FBMC prototype filters: the one proposed in the context of the PHYDYAS project and the so-called Hermite pulse. The good behavior and superb accuracy of the high speed emulation technique was validated by means of simulations considering different channel models as well as by measuring in a controlled (and also repeatable) measurement environment. From the excellent agreement exhibited by the performance results corresponding to both simulations and measurements, it can be concluded that the proposed technique is valid for inducing high-speed effects in FBMC-based systems.

Furthermore, the high speed emulation technique was used for assessing the downlink performance of future 5G systems for emulated speeds from 200 to $500\,$km/h, being typical in HST scenarios. The obtained performance results were also compared to those exhibited by OFDM. The obtained results show, on the one hand, that the main performance degradation sources are the SNR of the link and the speed of the mobile receiver. It was shown that for

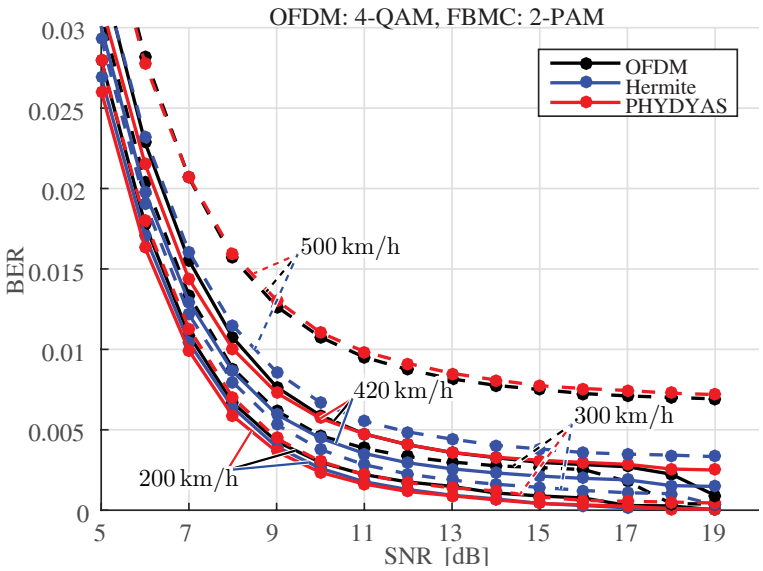

Figure 5.24: Measurements in the uncontrolled environment. BER versus SNR for OFDM and FBMC (Hermite and PHYDYAS prototype filters), and emulated speeds of 200, 300, 420 and 500 km/h. For speeds higher than 300 km/h the performance obtained by FBMC with the Hermite prototype filter is noticeable better than that of the other modulation schemes, whereas for lower velocities the difference is negligible.

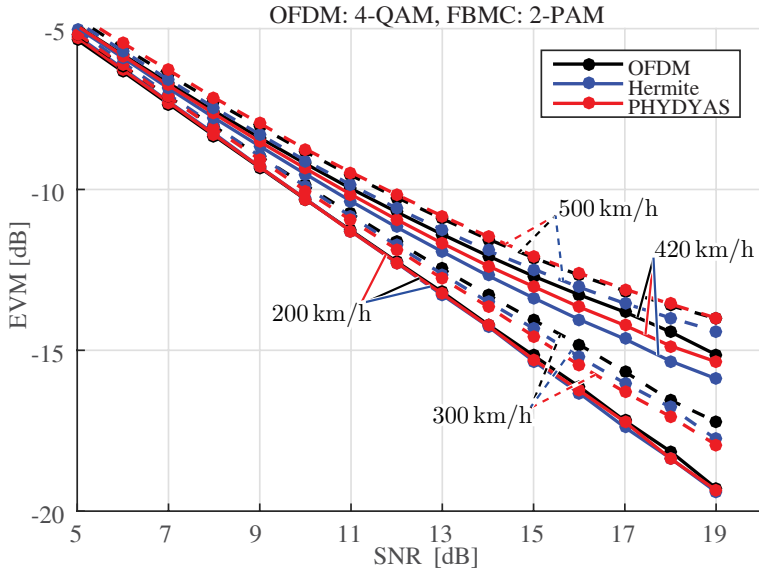

Figure 5.25: Measurements in the uncontrolled environment. EVM versus SNR for OFDM and FBMC (Hermite and PHYDYAS prototype filters), and emulated speeds of 200, 300, 420 and 500 km/h. For speeds higher than 300 km/h the performance obtained by FBMC with the Hermite prototype filter is noticeable better than that of the other modulation schemes, whereas for lower velocities the difference is negligible.

high speeds (exceeding 300 km/h), FBMC can be a much better choice than OFDM, specially when well localized prototype filters, both in time and in frequency, are employed, e.g. the Hermite pulse. However, for practical HST velocities (around 300 km/h) the performance

difference is not very significant. It is worth noting that we considered an isolated point-to-point link which does not exploit all the potential advantages of the FBMC schemes, mainly their better bandwidth efficiency. Such a bandwidth efficiency is very important for the co-existence between current GSM-R and new broadband wireless systems as well as to avoid multiple-access interference in the uplink. The obtained results confirm that FBMC advantages can be exploited in HST environments without additional performance losses.

Chapter 6

Conclusions and Future Work

Along this work we presented a complete study on the performance of high-capacity broadband wireless communication systems (e.g., fourth generation (4G) and fifth generation (5G) ones) for high speed environments (e.g., high speed trains). Special attention was devoted to the case of Long Term Evolution (LTE) for high speed trains. To finalize the study, this chapter presents the main conclusions derived from this work and proposes study lines to further continue it. Section 6.1 details the main conclusions, whereas Section 6.2 proposes future extensions to the work.

6.1 Conclusions

In order to be competitive with respect to other transportation means such as cars and airplanes, trains had to modernize themselves both regarding transportation speed as well as with respect to other aspects such that efficient resources usage and provision of services to passengers. While communication systems play a key role regarding the latter aspects, the transportation speed will severely impact on their performance. Nowadays, the most widely used communication system between trains and the elements involved in operation, control, and intercommunication within the railway infrastructure, is based on the Global System for Mobile Communications (GSM), as detailed in Chapter 2. This technology, namely the GSM for Railways (GSM-R), is not well suited for supporting advanced services such as automatic pilot applications or provisioning broadband services to the train staff and passengers. Taking into account the evolution of the mass market, 4G communication systems seem to be good candidates to substitute GSM as the fundamental technology for railway communications, being LTE the most successful 4G technology.

However, railway communications, specially when high speed environments are considered, pose a big challenge for communication systems. On the one hand, specific services are required in railway communications [Lam+12; Fra+15]. Moreover, as the communication

systems are also in charge of train control signaling and safety-related communications, the Quality of Service (QoS) must be satisfied with testability, controllability, reliability, effectiveness, maintainability, safety and security [10; Rod+12]. On the other hand, knowledge of the wireless channel characteristics is the fundamental basis for the planning of wireless communication networks and the design of transceivers [Ai+14]. Different channel models were proposed for moving networks (e.g., see [ITU97; Sie05; Kyo+07; ITU09a; Wei+10a; GZA11; Liu+12b; Par+08; Lua+13; HZA10; LZA10; He+11b; Liu+12a; Wei+10b; He+13e; Ai11; Ai+14; He+13a; He+13b; He+11a; LZB11; He+13c; BCA07; AGV98; CZW96; Zha+16b; HZB11; He+13d; Gua+12; Gua+13a; Gua+13b; Gua+14; He+12a; He+12b]), but high speed train environments demand for specific scenarios such as rural macro cell, hilly terrain, viaducts, cuttings, tunnels or crossing bridges, among others. Moreover, for very high speeds (above $300\,\text{km/h}$), non-stationary features of the channel arise [Ai+14] and the Wide-Sense Stationary Uncorrelated Scattering (WSSUS) assumption is no longer valid, whereas high Doppler frequency shifts and spreads are also introduced. This motivated the need of channel model characterizations based on measurement campaigns in realistic environments. However, measuring in the high speed train environment is complex, challenging and costly, whereas it usually demands for specific hardware and software solutions [Rod+13a]. In order to address such problems, a technique to induce the effects caused by highly time-varying channels in multicarrier systems signals while conducting the measurements at low speeds [Rod+14] was proposed in Chapter 3. By time-interpolating the transmitted signal before its transmission, the bandwidth of the whole multicarrier signal is scaled down, leading to an artificial reduction of the subcarrier spacing similar to what would have happened if the measurements were conducted at high speeds. After showing analytically that the same level of Inter-Carrier Interference (ICI) could be generated both by increasing the actual speed of the mobile receiver or by time interpolating the transmitted signals [Rod+16e], we supported our findings by means of simulations, showing that the proposed technique is accurate enough when inducing the ICI inherent to mobile scenarios for different channel models.

Next, we validated our technique both by means of measurements and simulations by transmitting actual LTE signals over the air in high speed environments. For the case of the measurements, a specific methodology for validating the technique in a controlled environment and under repeatable conditions was designed. For the simulations, we considered channel models specifically designed for modeling high speed scenarios. In both cases, the basic idea consists of evaluating different figures of merit (Error Vector Magnitude (EVM), coded and uncoded Bit Error Ratio (BER), and throughput) for a certain range of actual speeds and to compare them with emulated speeds of the same magnitude under the same conditions. The results based on all the figures of merit showed an excellent agreement between actual and emulated speeds for all the interpolation factors considered, hence validating the proposed technique as a good candidate to be considered not only for the assessment of the physical

layer, but also for higher layer ones. Moreover, it can be concluded that the high speed emulation technique is valid for inducing high speed effects at any point in the signal processing chain at the receiver. Furthermore, we showed theoretically that the same level of ICI can be generated both by increasing the actual speed of the mobile receiver or by time interpolating the transmitted Orthogonal Frequency-Division Multiplexing (OFDM) signals regardless of the channel frequency selectivity. These analytical findings were supported by simulation results, where it was shown that the proposed technique is accurate enough when inducing the ICI inherent to mobile scenarios for different channel models, including those that can be found in high speed train environments.

We also employed the high speed emulation technique to shed light on the effects caused by high and even extremely high speeds on OFDM signals. It could be observed that the received signals suffer a similar degradation (in terms of EVM, and uncoded and coded BER) when the Signal to Noise Ratio (SNR) decreases or when the speed (and correspondingly the ICI level) increases. However, low SNR values can conceal the effects due to high speeds as the noise becomes the main contributor of the signal distortion. It was also shown that lower Channel Quality Indicators (CQIs) provide more robustness at high speeds, although reducing the maximum achievable throughput. Even for not so low SNR levels, the performance can be increased by considering lower CQI values for the high speed train environment. Notice that, as expected, the higher the constellation size, the higher the sensitivity it exhibits with respect to the speed. Moreover, a reliable and low-latency link at very high speeds demands for small-size constellations like 4-QAM, making adaptive modulation and coding schemes less attractive in these scenarios since a potential throughput increment when increasing the constellation size yields a high-BER with a very high probability, thus requiring retransmissions and impacting on both the delay and the jitter of the link.

The main drawback of the proposed technique is that the signal bandwidth reduces proportionally to the time interpolation factor, therefore potential inaccuracies could arise due to the loss of frequency diversity. However, the frequency diversity reduction inherent to the bandwidth decrease does not seem to affect to the simulation or measurement results. It is expected to affect more in channels exhibiting a very high frequency selectivity, which is unlikely in high speed conditions in which the channel response changes fast. Moreover, alternative proposals which have the main advantage of not changing the spectral properties of the signal have been also considered. However, the technique for high speed emulation based on time interpolating the signals has proven to be much simpler than the other alternatives, being transparent for the transmitter and receiver processing chains.

When focusing on the provision of services to the users of high-speed trains, the Mobile-Relay technique [3GP12] might be considered as a way to provide coverage to passengers based on a relaying scheme. Moreover, not only high speed trains are the scenarios of interest, but also metro transportation in which both train control and video surveillance take advantage

of the high throughput exhibited by the 4G systems. It is also becoming more common to provide data access to users of buses, taxis or even cars by means of relaying schemes. This motivated not only the study of the Base Transceiver Station (BTS)-train channel (i.e., the outdoor-to-oudoor link between a BTS and the outdoor antennas of a train), but also the BTS-mobile one (i.e., the outdoor-to-indoor link between a BTS and a user mobile inside of a train), hence the gain achieved when deploying a Mobile-Relay scheme with respect to the case in which each user connects directly to the BTS was evaluated. Consequently, the performance of the 4G communication systems for both the outdoor-to-outdoor and the outdoor-to-indoor links in vehicle-to-infrastructure scenarios was experimentally assessed by means of several measurement campaigns detailed in Chapter 4. In order to achieve this goal, the so-called GTEC Testbed was designed, developed, and successfully used in different scenarios. More specifically, high-speed car-to-infrastructure scenarios (high speed conditions emulated by time interpolation), subway-to-infrastructure in tunnel scenarios, and high-speed-train-to-infrastructure in rural area scenarios were assessed, whereas both Worldwide Interoperability for Microwave Access (WiMAX) and LTE standard-compliant signals were transmitted and/or acquired over the air.

Time interpolation was successfully employed to emulate high speeds from measurements in car-to-infrastructure scenarios carried out at low velocities. From the results, it can be concluded that the main performance degradation sources are the link SNR and the mobile receiver speed.

From the comparison of the results for BTS-to-vehicle and BTS-to-mobile links in different environments (e.g., subway stations or high-speed trains crossing rural areas), it can be concluded that wireless communications directly with passengers inside the vehicles are still a challenge due to the strong attenuation introduced by the vehicle structure. This results in a noticeable reduction of the cell radius when indoor antennas are used with respect to the case where outdoor antennas are employed. This definitely motivates the study of communication architectures based on relay schemes. Moreover, the results obtained from the measurements in subway-to-infrastructure scenarios showed the importance of choosing an adequate placement of the receive antennas on the train to minimize the blockage of the signal by the train structure. Due to its importance for practical Mobile-Relay architectures, the performance of the BTS-train link in rural area environments deserved more attention. From Power Delay Profile (PDP) estimates at different speeds, it could be observed that the channel exhibited a low delay spread regardless of the train speed. Therefore, the time selectivity of the channel due to the high speeds achieved by the train was the limiting factor for the system performance. This finding was supported by the estimates of the channel capacity bounds obtained from the measurements at different speeds when considering the frame structure of LTE.

One should consider that the requirements and expectations regarding mobile communication systems grow day by day. In order to fulfill the increasing capacity demanded

by users, the LTE standard evolved and new versions arose during the development of this work. Moreover, nowadays we are in the beginning of a new era for mobile communications, since the so-called 5G communication systems are currently under definition. One of the most remarkable proposals for the definition of 5G is the utilization of Filter Bank Multicarrier (FBMC) modulation techniques instead of the well-known OFDM. FBMC offers significant advantages with respect to OFDM in the context of railway communications, such as higher bandwidth efficiency, improved multiple-access facilities in the uplink, and its suitability for doubly dispersive channels. Bandwidth efficiency is critical in railway environments due to the scarce spectrum available and facilitates the coexistence with legacy systems such as GSM-R. The use of close-to-perfect subcarrier filters in FBMC avoids multiple-access interference between different trains without requiring sophisticated synchronization methods since the subcarriers are well frequency-localized. Regarding doubly dispersive channels, FBMC allows for achieving a compromise between channel response spreading in time (multipath effect) and in frequency (due to the Doppler shift in different multipaths) by means of a proper prototype filter design [Far11]. In this sense, since OFDM is defined by means of a rectangular window in time, each OFDM symbol appears unbounded in the frequency domain, hence becoming a poor choice for doubly selective channels. FBMC waveforms perform much better for doubly selective channels with respect to OFDM because such prototype filters can be designed specifically for minimizing both time and frequency dispersion [FAB95; Ala01; HB97; SB03; Ami+10].

With the aim of drastically increasing the value of this work and to check the validity of the findings regarding the latest advances in wireless communication systems, proposals for 5G communication systems were also considered in Chapter 5. Hence, the aforementioned technique for the emulation of high speed conditions was shown to be accurate for FBMC-modulated signals with different prototype filters, such as the one defined by the PHYDYAS project [Bel+10] and the so-called Hermite pulse [HB97]. Following the same procedure proposed for the validation of the technique for the OFDM case, the good behavior and superb accuracy of the high speed emulation technique was shown by means of simulations considering different channel models as well as by measuring in a controlled (and also repeatable) measurement environment. From the excellent agreement exhibited by the performance results in terms of BER and EVM versus SNR, both for simulations and measurements, it can be concluded that the proposed technique is valid for inducing high-speed effects when FBMC-based systems are considered.

With the aid of the high speed emulation technique, we assessed the downlink performance of future 5G systems for emulated speeds from 200 to 500 km/h, being typical in High-Speed Train (HST) scenarios. It was shown that for very high speeds (exceeding 300 km/h), FBMC can be a much better choice than OFDM, specially when well localized prototype filters, both in time and in frequency, are employed, e.g. the Hermite pulse. However, for practical

HST velocities (around 300 km/h) the performance difference is not very significant. It is worth noting that an isolated point-to-point link was considered, which does not exploit all the potential advantages of the FBMC schemes, mainly their better bandwidth efficiency. Such bandwidth efficiency is very important for the co-existence between current GSM-R and new broadband wireless systems as well as to avoid multiple-access interference in the uplink. The obtained results confirmed that the advantages offered by FBMC can be exploited in HST environments without additional performance losses.

6.2 Future Work

When a work focuses on a wide topic it is difficult to establish the boundaries of its future extensions. Moreover, as wireless standards are continuously evolving, together with the requirements and expectations regarding mobile communication systems, this work could be extended indefinitely. However, in this section the most likely future extensions are considered, being most of them already under development.

Section 6.2.1 details the proposed future work lines in relation to channel modeling, whereas Section 6.2.2 considers the high speed emulation. Section 6.2.3 proposes future evaluations in vehicle-to-infrastructure environments, and Section 6.2.4 deals with future extensions in the scope of 5G communication systems. Section 6.2.5 presents the main proposals to extend the so-called GTEC Testbed and Section 6.2.6 concludes the section by considering the collaboration with standardization entities.

6.2.1 High Speed Train Channel Modeling

For the moment, only a small percentage of the recorded data (i.e., acquired signals that were transmitted over the air) was analyzed. As one of the most valuable parts of this work are the measurement results, we plan to derive channel models from the measurements for the different environments considered. More measurement campaigns to assist in the analysis of some of the observed phenomena is expected to be required, in particular for Doppler modeling. Once a set of channel models is derived, they could be used, for example, in network-level simulators. Some work in this direction has been already done.

6.2.2 High Speed Emulation

As mentioned above, the accuracy exhibited by the high speed emulation technique is superb. However, its main drawback is the potential loss with respect to the frequency diversity of the channel. Some alternatives were proposed to cope with this problem, being the most relevant conclusion that no perfect technique to emulate high speeds is found among the considered

methods. Currently, we are working on different alternatives to restore the lost frequency diversity in measurements carried out by time interpolating the signals.

The good accuracy of the high speed emulation technique for the case of FBMC signals has also been assessed. However, a theoretical analysis of the effects of interpolating FBMC signals is still missing. Contrarily to the OFDM case with a sufficiently long Cyclic Prefix (CP), one cannot assume the absence of Inter-Symbol Interference (ISI) in FBMC signals. Hence, a deep theoretical study will shed light on the implications of the presence of ISI in the signals for the time interpolation technique. The high speed emulation technique could be then modified accordingly, if necessary.

6.2.3 Vehicle-To-Infrastructure Communications

For our evaluations regarding vehicle-to-infrastructure communications, we always considered the links BTS-vehicle and BTS-mobile in an isolated way. Moreover, we did not consider the link between the Access Point (AP) and the mobile for the Mobile-Relay based architectures. Even more, we did not consider the potential interference effects between the aforementioned links as well as the performance of a complete communications system based on a relaying scheme. Works on the evaluation of the AP-mobile link considering APs located inside the same or a different train carriage (the so-called intra-car and inter-car links, respectively, in Section 4.1) are being performed. The assessment of the interference arising between the links involved in the communication for different Mobile-Relay schemes is also planned.

It is also worth noting that we always considered downlink communications. However, uplink communications are sometimes as challenging as their downlink counterpart. Moreover, in communication systems such as LTE noticeably differences in the physical layer definition for the downlink and the uplink are considered. Hence, assessing uplink communications is still an open topic.

6.2.4 5G Communication Systems

As the definition of 5G communication systems evolves, experimental evaluations will be required. For the scope of this work, we only considered low order modulations and isolated point-to-point links which do not exploit all the potential advantages of FBMC schemes for the high speed railway environment. On the one hand, measurements for higher order modulations are already scheduled. On the other, considering scenarios with more than a single user in high speed conditions is one of our major concerns. Experimental assessment of the advantages of FBMC schemes with respect to those based in OFDM in high speed multi-user scenarios has been also planned.

Regarding 5G proposals, although FBMC is very successful within the academia, it is

being discarded by the industry, at least for the moment. Conversely, other alternatives such as Filtered OFDM (fOFDM) are attracting more interest. Taking this into account, we also plan to experimentally assess the achievable performance for other modulation schemes different than FBMC and being also proposed for 5G.

6.2.5 The GTEC Testbed

Although it is something definitely undervalued by the academia, there is a common aspect in relation to all of the further work proposals. Since we are focusing on the experimental evaluation of communication systems, a way to perform such evaluations is required. In this sense, it is absolutely clear for the author of this work that the design and further development of the so-called GTEC Testbed [Dom+16b] (see Section 4.2) was one of the key points for achieving the proposed goals. Currently, the GTEC Testbed is an advanced set of hardware and software components which provides full flexibility to perform several kinds of evaluations for different wireless communication techniques. In order to perform any of the further work proposals detailed above, it is first required to extend the GTEC Testbed to support the necessary capabilities. Moreover, taking into account that the code of the GTEC Testbed has been made publicly available under the GPLv3 license [Tea] to assist other research groups or the industry in the evaluation of wireless communication systems, its evolution has never stopped. As the main ongoing improvements, we can highlight the development of a flexible Forward Error Correction (FEC) scheme, which will allow performing realistic throughput evaluations, increase the flexibility in the definition of different data frames to evaluate several modulations schemes in a single measurement, and the implementation of even more modulation techniques such as fOFDM.

6.2.6 Contribution to Standardization Proposals

A goal of this work is to provide some benefit to the society by increasing the quality and efficiency of wireless communications in high speed environments, specially high speed trains. This will enable more efficient and much safer transportation of passengers and load, while providing passengers with a more pleasant journey by means of different services. We think that one of the best ways of providing such a benefit is to collaborate with the standardization entities in the definition of new releases of the wireless communication standards. In this sense, collaboration with the standardization entities based on the obtained results and gained expertise during the development of this work is one of our main concerns.

Appendix A

Resumo da Tese

A.1 Introdución

Ao longo dos últimos anos o uso de servizos multimedia e, en xeral, baseados no acceso a información contida "na nube", experimentou un auxe sen precedentes. A diferencia respecto do pasado, os usuarios non soamente acceden aos servizos dende unha ubicación estática; por contra, navegan libremente entre distintos lugares ao tempo que acceden, dende os seus dispositivos móbiles, a servizos na nube con fins laborais, de entretemento ou de interactividade en redes sociais [SR16]. Asemade, outro tipo de usuarios entra en xogo: cada vez máis máquinas e dispositivos autónomos en xeral están provistos de conexión á rede e continuamente intercambian información.

Debido ao ritmo de vida actual, o tránsito entre zonas rurais e cidades tamén se incrementou de modo notable, ao ubicarse a maior parte dos lugares de traballo nas cidades ou nas súas respectivas contornas. A Axencia Europea do Medio Ambiente concluíu en 2013 que os tempos de tránsito típicos no núcleo das grandes cidades poden exceder unha hora, mentres que o acceso ás propias cidades dende zonas urbanas pode requirir tempos de tránsito meirandes na maior parte dos casos [SR16]. Durante os períodos de transporte, cada vez máis, os pasaxeiros empregan os seus dispositivos móbiles para traballar, acceder a redes sociais ou como ferramenta de entretemento. O factor común da maior parte dos servizos típicamente empregados é a súa dependencia do acceso á rede. Mentres, nalgúns casos, a transmisión duns poucos octetos de información pode ser suficiente, noutros requírese unha conexión permanente que posibilite a transmisión dun fluxo de datos multimedia en tempo real. Asemade, unha porción importante da información transmitida é creada por dispositivos autónomos. No eido do transporte, algúns exemplos poden ser o tráfico necesario para a monitorización do estado dos vehículos, os servizos de entretemento conectados á nube ou o intertroco de información entre vehículos autónomos ou semiautónomos. As aplicacións relacionadas co campo da seguridade merecen unha mención especial por impoñeren uns estritos requirimentos en termos de latencia

e dispoñibilidade do enlace de comunicacións.

Os trens representan un eficiente medio de transporte para diversas aplicacións [Dev89; AG84; Pro95]. A idea de mover vagóns sobre raís está xa presente en antigas civilizacións, tales como os Gregos ou os Romanos [AG84; Dev89; Pro95]; sen embargo, é ao longo dos últimos séculos cando acada os seus máximos niveis de desenvolvemento. A base do transporte ferroviario é o movemento guiado sobre raís de metal en contacto directo coas rodas dos vagóns. Este medio de desprazamento dos vagóns reduce moi drásticamente a resistencia ao arrastre [Pro95]. Ademais, habida conta da capacidade de unir diversos vagóns [Pro95], os trens posiciónanse como unha alternativa altamente competitiva para o transporte dun número elevado de toneladas de carga, así como de centos de pasaxeiros, dun xeito eficiente en termos de consumo enerxético [AM84; UIC93] e polución [UIC93; Pro95]. Non obstante, a medida que o transporte aéreo, así como o propio automóbil, comezaron a introducirse a grande escala na sociedade, os trens tiveron que modernizarse para tornarse competitivos en relación aos novidosos medios de transporte así xurdidos. Esta modernización non consistiu soamente no incremento das velocidades máximas acadables, senón tamén na mellora en aspectos organizativos e na eficiencia, de cara a reducir os custos de operación. Asemade, tamén as posibilidades ofertadas aos usuarios durante o seu transporte haberán de proporcionarlles un servizo de valor engadido [Pro95]. Así, os modernos trens de alta velocidade, con velocidades máximas darredor dos $500\,\mathrm{km/h}$, entraron en escena. A evolución ferroviaria afectou, por suposto, tamén ás comunicacións ferroviarias. Lonxe quedaron xa os primeiros sistemas de comunicación deseñados para asistir á sinalización óptica en condicións de baixa visibilidade, xurdidos xa no século XIX, baseados nun primitivo telégrafo [GFR98; AH11]. Logo de diversas melloras, os telégrafos empezaron a ser complementados cun servizo telefónico básico, xa entrado o século XX [GFR98]. Os sistemas de comunicación sen fíos atoparon tamén o seu lugar, sempre en relación a comunicacións de carácter non crítico, tales como aspectos loxísticos ou asistencia en tarefas de mantemento. Foi xa anos máis tarde, na década dos setenta, cando se estableceu unha conexión de tipo permanente entre o maquinista e un operador en terra; a base tecnolóxica que sustentaba este enlace de comunicacións foi a predecesora do denominado GSM for Railways (GSM-R).

Na actualidade, GSM-R é o sistema de comunicacións máis empregado entre os trens e o resto dos elementos involucrados na infraestrutura ferroviaria. GSM-R, á súa vez baseado no xa vetusto Global System for Mobile Communications (GSM), proporciona unha conexión permanente entre os maquinistas e os operadores terrestres que proporciona servizos como a transmisión de sinais de emerxencia, chamadas de voz selectivas e inclusive a transmisión de datos cunha taxa limitada. O enlace de comunicacións establécese entre o propio tren e a estación base máis próxima, mentres tódalas estacións base se conectan, con enlaces cableados, a unha estación central. Habida conta de que GSM-R transmite información relativa á sinalización de control do tren, así como a aspectos de seguridade, a calidade de servizo debe

manterse cuns altísimos niveis de fiabilidade [Lam+12; Fra+15; Rod+12; 10]. Os requirimentos operativos e funcionais para a contorna ferroviaria impoñen, deste xeito, uns niveis de esixencia superiores aos habituais en sistemas de comunicación típicos, especialmente en canto ao tempo necesario para o establecemento dunha conexión e á probabilidade de fallo do servizo.

Sen embargo, GSM-R non é axeitado para proporcionar servizos de carácter máis avanzado, como o control de piloto automático, así como para sustentar transmisións de banda ancha aos operadores ferroviarios. Botando unha ollada ao mercado de dispositivos de comunicacións de ámbito xeral, a explosión de usuarios e servizos multimedia dos últimos anos motivou a migración, primeiro ás redes de terceira xeración e, seguidamente, ás de cuarta, con Long Term Evolution (LTE) á cabeza. Así, parece natural plantexar LTE como a tecnoloxía candidata para a substitución de GSM-R no ámbito ferroviario. Non obstante, cómpre facermos un exhaustivo estudo da viabilidade do emprego de LTE para comunicacións ferroviarias, habida conta dos requisitos operativos e funcionais mencionados con anterioridade. Aínda máis, a crecente demanda do emprego de teléfonos móbiles, ordenadores portátiles e outros dispositivos dotados de conectividade sen fíos por parte dos pasaxeiros de trens de alta velocidade abriu unha nova posibilidade de negocio aos operadores ferroviarios. Non soamente as novas tecnoloxías de conectividade son de interese para os trens de alta velocidade, tamén os sistemas de control e vixilancia empregados polo metro se poden beneficiar das elevadas taxas de transmisión acadables. Finalmente, é cada vez máis común dotar aos usuarios de autobuses, taxis ou inclusive automóbiles privados de conectividade sen fíos. Simultaneamente a esta necesidade ou oportunidade de negocio, comezaron a propoñerse esquemas de conectividade sen fíos para os viaxeiros baseados en arquitecturas de retransmisión montadas nos propios vehículos [3GP12]. A conxunción de todos estes factores motivou a crecente interese no estudo e caracterización da propagación electromagnética en contornas ferroviarias, co fin de proporcionar sistemas de comunicacións de banda ancha a bordo [Bri+14a; Ai+14].

A literatura recolle distintos modelos de canle para contornas con movemento relativo entre os transmisores e receptores, tales como [ITU97; Sie05; Kyo+07; ITU09a; Wei+10a; GZA11; Liu+12b; Par+08; Lua+13; HZA10; LZA10; He+11b; Liu+12a; Wei+10b; He+13e; Ai11; Ai+14; He+13a; He+13b; He+11a; LZB11; He+13c; BCA07; AGV98; CZW96; Zha+16b; HZB11; He+13d; Gua+12; Gua+13a; Gua+13b; Gua+14; He+12a; He+12b]. Sen embargo, a contorna ferroviaria comprende escenarios específicos coma contornas rurais cunha clara liña de visión directa entre os extremos da comunicación, terreos montañosos, viadutos, transmisión entre altas paredes paralelas ao carón das vías, túneles ou pontes de cruce de vías, entre outros. Ademais, para desprazamentos a altas velocidades (meirandes que $300\,\mathrm{km/h}$), poden empezar a apreciarse características non estacionarias da canle de transmisión [Ai+14] e a hipótese de dispersión incorrelacionada estacionaria en sentido amplo perde a súa validez; ao tempo, os sinais quedan fortemente afectados por desprazamentos e ancheamentos Doppler. Estes feitos motivan a necesidade do desenvolvemento de novos modelos de canle baseados en campañas

de medidas levadas a cabo en contornas realistas. Sen embargo, realizar medidas en trens ferroviarios de alta velocidade é todo un reto, ademais de complexo e caro; ao tempo require de equipamentos de medida hardware e software específicos [Rod+13a].

No presente traballo lévase a cabo un completo estudo das prestacións de sistemas de comunicacións sen fíos de banda ancha en vehículos de alta velocidade, baseado en campañas de medidas levadas a cabo en contornas realistas de alta velocidade. Estudouse especialmente o caso de comunicacións LTE en trens de alta velocidade. Propóñense técnicas de redución de custo e complexidade en relación ás avaliacións en contornas de alta velocidade e próbase o seu funcionamento de xeito empírico. Tamén no eido da presente tese deseñouse, desenvolveuse e usouse o denominado "GTEC Testbed", que permitiu a realización de distintos tipos de avaliacións sobre diversos sistemas de comunicacións sen fíos en contornas de alta velocidade.

A evolución en canto aos sistemas de comunicacións sen fíos segue o seu camiño de forma imparable. As expectativas dos usuarios seguen aumentando día tras día. De cara a proporcionar a necesaria base tecnolóxica para satisfacer as necesidades dos usuarios, así como o volume daqueles, a especificación de LTE foi evolucionando durante o desenvolvemento deste traballo. Ademais, actualmente atopámonos no inicio dunha nova era para as comunicacións móbiles, marcada polos denominados sistemas de comunicación de quinta xeración, actualmente en fase de definición. Moitas das propostas para sistemas de comunicacións de quinta xeración están enfocadas en usuarios quasi-estáticos; por contra, pouca consideración se tivo en conta en relación aos efectos da alta mobilidade nas novas propostas xurdidas [SR16]. De cara a comprobar a validez dos desenvolvementos presentados nesta tese en relación aos últimos desenvolvementos para sistemas de comunicacións, consideráronse tamén as propostas para sistemas de quinta xeración. Máis concretamente, evaluáronse as prestacións de modulacións Filter Bank Multicarrier (FBMC) en contornas de alta velocidade. FBMC ofrece vantaxes significativas en relación a Orthogonal Frequency-Division Multiplexing (OFDM) no contexto das comunicacións ferroviarias, tales como unha meirande eficiencia espectral, máis facilidades para a compartición da canle de subida por varios usuarios e maior capacidade de adaptación a canles dobremente dispersivas. A eficiencia espectral toma un papel clave nas comunicacións ferroviarias debido ao limitadísimo espectro dispoñible e de cara a facilitar a coexistencia con outros sistemas de comunicacións actualmente en uso, tales como o GSM-R. Asemade, o emprego de subportadoras moi localizadas en frecuencia evita efectos de interferencia entre distintos trens que comparten un mesmo enlace ascendente sen necesidade de implementar complexos sistemas de sincronización. En relación ás canles dobremente dispersivas, FBMC permite establecer un compromiso entre a dispersión da resposta da canle en tempo (propagación multitraxecto) e en frecuencia (desprazamentos Doppler para os distintos camiños involucrados na transmisión do sinal) mediante un coidadoso deseño dos filtros prototipos empregados [Far11; FAB95; Ala01; HB97; SB03; Ami+10].

A.2 Principais Contribucións

A presente tese conforma un estudio das prestacións de sistemas de comunicación de banda ancha e sen fíos (tales como sistemas de comunicacións de cuarta e quinta xeración) para vehículos de alta velocidade (como trens de alta velocidade), baseado en campañas de medidas realizadas en contornas de alta mobilidade.

As principais contribución da tese poden sintetizarse nos vindeiros puntos:

- Estudo das características particulares das comunicacións ferroviarias. Máis concretamente, introdúcense tanto os requirimentos operativos como os servizos típicamente establecidos na contorna ferroviaria e estúdase a viabilidade de LTE para dar soporte a tales servizos. Estúdanse en detalle, asemade, as particularidades dos modelos de canle para a contorna ferroviaria de alta mobilidade.
- Proposta, análise teórica e verificación mediante medidas e simulacións dunha técnica deseñada para induci-los efectos causados por canles altamente variables en tempo en sinais OFDM, pero realizando as medidas a baixas velocidades. Propóñense métodos alternativos á citada técnica e realízase unha comparativa entre os mesmos.
- Deseño, desenvolvemento e emprego do denominado GTEC Testbed, un completo conxunto hardware e software que proporciona unha alta flexibilidade na realización de distintos tipos de avaliacións para diversos sistemas de comunicacións sen fíos.
- Avaliación das prestacións para as canles estación base-vehículo e estación base-móbil dentro do vehículo para sistemas de comunicacións de cuarta xeración. O estudo foi levado a cabo vía campañas de medidas realizadas mediante receptores instalados en automóbiles, metros e trens de alta velocidade en contornas reais.
- Estudo teórico das vantaxes que as propostas relativas a sistemas de quinta xeración, tales como o emprego de modulacións FBMC, poden proporcionar á contorna ferroviaria de alta velocidade. Aplicación da técnica de emulación de altas velocidades mencionada con anterioridade para modulacións propostas en sistemas de comunicacións de quinta xeración e avaliación das prestacións de tales esquemas de comunicación en condicións de alta mobilidade mediante simulacións e medidas.

A.3 Principais Conclusións

De cara a mante-lo nivel de competitividade respecto ás súas alternativas, os trens experimentaron unha profunda modernización nas derradeiras décadas. Esta modernización non se basea únicamente no incremento das velocidades de operación, senón que tamén inclúe a eficiencia no uso de recursos e o deseño de servizos de valor engadido para os viaxeiros. Mentres as comunicacións poden xogar un papel clave nos últimos aspectos, a alta

velocidade pode impactar drásticamente nas prestacións de calquera sistema de comunicacións. A tecnoloxía de comunicacións actualmente dominante no mercado ferroviario, GSM-R, xa se queda curta para sustentar servizos que precisan da transmisión dun volume de datos elevado. Tendo en conta a evolución do mercado actual, LTE plantéxase como unha alternativa para a substitución de GSM-R.

Sen embargo, tal como foi detallado no segundo capítulo da tese, as comunicacións ferroviarias, especialmente a alta velocidade, supoñen un reto para calquera sistema de comunicacións. Por unha banda, deben proporcionarse certos servizos inherentes ao entorno ferroviario [Lam+12; Fra+15]; por outra, as comunicacións involucradas en sistemas de control e seguridade deben satisfacer uns estritos requirimentos de calidade de servizo [10; Rod+12]. Finalmente, aínda que existen diversos modelos de canle deseñados para comunicacións con movemento relativo entre os transmisores e os receptores (por exemplo, véxanse [ITU97; Sie05; Kyo+07; ITU09a; Wei+10a; GZA11; Liu+12b; Par+08; Lua+13; HZA10; LZA10; He+11b; Liu+12a; Wei+10b; He+13e; Ai11; Ai+14; He+13a; He+13b; He+11a; LZB11; He+13c; BCA07; AGV98; CZW96; Zha+16b; HZB11; He+13d; Gua+12; Gua+13a; Gua+13b; Gua+14; He+12a; He+12b]), as comunicacións ferroviarias implican escenarios específicos coma contornas rurais cunha forte liña de visión directa entre os extremos da comunicación, terreos montañosos, viadutos, transmisión entre altas paredes paralelas ao carón das vías, túneles ou pontes de cruce de vías, entre outros. Ademais, para desprazamentos a altas velocidades (meirandes que $300\,\mathrm{km/h}$), poden empezar a apreciarse características non estacionarias da canle de transmisión [Ai+14] e a hipótese de dispersión incorrelacionada estacionaria en sentido amplo perde a súa validez; ao tempo, os sinais quedan fortemente afectados por desprazamentos e ancheamentos Doppler. Estes feitos motivan a necesidade do desenvolvemento de novos modelos de canle baseados en campañas de medidas levadas a cabo en contornas realistas. Sen embargo, realizar medidas en trens ferroviarios de alta velocidade é todo un reto, ademais de complexo e caro; ao tempo, require de equipamentos de medida hardware e software específicos [Rod+13a]. De cara a lidiar con estes inconvenientes, no terceiro capítulo da presente tese propúxose unha técnica que permite induci-los efectos causados por canles altamente variantes no dominio temporal en sistemas multiportadora, aínda realizando as medidas a baixas velocidades [Rod+14]. Así, interpolando o sinal a transmitir no dominio do tempo antes da transmisión, o ancho de banda do sinal redúcese, decrementándose, asemade, o espaciado entre subportadoras. Deste xeito, é posible xerar interferencia inter-portadoras de magnitude semellante á que se observaría se as medidas fosen realizadas a velocidades meirandes. Despois de amosar a validez do plantexamento de xeito analítico [Rod+16e], a eficacia da técnica é corroborada mediante simulacións, amosando que resulta precisa con independencia do nivel de selectividade en frecuencia do modelo de canle considerado. Seguidamente, validouse a técnica de emulación de altas velocidades mediante medidas e simulacións mediante a transmisión de sinais LTE en contornas de alta velocidade. Para o caso das medidas, desenvolveuse unha

metodoloxía que posibilita a validación da técnica en condicións controladas e repetibles. Para o caso das simulacións, consideráronse modelos de canle específicamente deseñados para contornas de alta mobilidade. A avaliación de diversas figuras de mérito corroborou a excelente correlación entre os resultados obtidos empregando a técnica de emulación de altas velocidades e medindo a velocidades reais equivalentes ás emuladas para a mesma contorna.

Unha vez validada, a técnica de emulación de altas velocidades foi empregada para estudalos efectos de canles altamente variables en tempo sobre sinais OFDM. Pode observarse unha degradación das prestacións tanto cando se reduce a relación sinal a ruido como cando se incrementa a velocidade. Para baixos valores de relación sinal a ruido, o efecto da velocidade queda enmascarado pola dominancia do ruido. Aínda para valores de velocidade non demasiado elevados pode resultar máis eficaz a transmisión empregando modulacións de orde baixa, posto que incrementan a robustez, pese a reduciren a taxa máxima acadable. Dados os requirimentos de baixa latencia nas transmisións, os esquemas de modulación e codificación adaptativos perden o seu atractivo na contorna ferroviaria de alta velocidade.

Posto que a técnica de emulación de altas velocidades proposta presenta a desvantaxe de reducir a selectividade en frecuencia da canle experimentada polos sinais, propuxéronse métodos alternativos. Sen embargo, a técnica orixinal resulta moito máis simple e a exactitude nos resultados acadados debería soamente verse mermada en canles cunha alta selectividade en frecuencia, que non é o caso das canles altamente variantes, como as inherentes aos escenarios considerados.

A dotación de cobertura aos usuarios mediante esquemas de retransmisión [3GP12] foi xa motivada non soamente para trens de alta velocidade, senón tamén para comunicacións en metro ou en automóbiles e derivados daqueles. Así, unha parte importante deste traballo foi a avaliación experimental dos enlaces de comunicación estación base-vehículo (empregando as propias antenas situadas no exterior do vehículo) e estación base-dispositivo móbil no interior do vehículo (enlace que experimentaría un pasaxeiro do vehículo de conectares o seu dispositivo, situado no interior do vehículo, directamente á estación base). Así, puido avaliarse a ganancia das arquitecturas de retransmisión en relación aos esquemas clásicos onde cada usuario se conecta á estación base de forma individual. Para isto, no cuarto capítulo da presente tese considerouse a avaliación experimental en distintos escenarios, como son *(a)* automóbiles en condicións de alta velocidade (emulada mediante a técnica proposta anteriormente), *(b)* medidas en metro en túneles e estacións e *(c)* medidas en trens de alta velocidade en contornas rurais. Para as avaliacións deseñouse, desenvolveuse e empregouse o denominado GTEC Testbed. Consideráronse tanto sinais Worldwide Interoperability for Microwave Access (WiMAX) como LTE. Como principal resultado das campañas de medidas pode concluirse que a comunicación directa cos usuarios no interior de vehículos segue a supoñer un reto, debida a alta atenuación introducida pola estrutura do propio vehículo. Deste xeito, o emprego de arquitecturas baseadas en estratexias de retransmisión amósase como

unha alternativa moito máis eficiente. Asemade, observouse a importancia de optimiza-lo emprazamento das antenas do vehículo de cara a evitar efectos de bloqueo do sinal en contornas tales como túneles ou estacións. Finalmente, foi analizada a capacidade do enlace estación base-vehículo a partires das estimas de canle obtidas durante as medidas en tren de alta velocidade. Puido observarse que o factor limitante das prestacións do sistema de comunicacións é a selectividade en tempo da canle, causada polo movemento do vehículo.

Xa foron comentadas as vantaxes das técnicas de modulación propostas para sistemas de comunicación de quinta xeración, tales como FBMC, para a contorna ferroviaria de alta velocidade. De cara a incrementar o valor da presente tese e comprobar a aplicabilidade dos resultados obtidos para as modulacións propostas en sistemas de comunicacións de quinta xeración, no quinto capítulo da presente tese considerouse a avaliación de sistemas baseados en modulacións FBMC en contornas de alta mobilidade. En primeiro lugar amosouse, mediante simulacións e medidas en condicións controladas e repetibles, a aplicabilidade da técnica de emulación de altas velocidades para o caso de modulacións FBMC. Seguidamente, empregouse a devandita técnica para a avaliación experimental de sistemas de comunicacións baseados en modulacións FBMC en contornas de alta mobilidade. Mentres para velocidades moi altas (superiores a $300\,\mathrm{km/h}$) as prestacións de sistemas baseados en FBMC son notablemente superiores ás correspondentes a sistemas OFDM, para velocidades inferiores a ganancia en prestacións é moi reducida. Non obstante, ha de tomarse en consideración que nos experimentos realizados non se explotaron as potenciais vantaxes dos sistemas baseados en FBMC respecto daqueles que empregan OFDM, tales como a súa meirande eficiencia espectral. Así pois, pódese concluir que, ao non apreciarse unha mingua nas prestacións dos sistemas baseados en FBMC respecto daqueles que consideran OFDM, é posible aproveitar as vantaxes brindadas por FBMC para a contorna ferroviaria de alta velocidade sen incurrir en perda de prestacións.

O código fonte do GTEC Testbed e do GTEC 5G Simulator está dispoñible públicamente baixo a licenza GPLv3 en https://bitbucket.org/tomas_bolano/gtec_testbed_public.git.

Appendix B

List of Acronyms

1G first generation

2G second generation

3G third generation

3GPP 3rd Generation Partnership Project

3GPP2 3rd Generation Partnership Project 2

4G fourth generation

5G fifth generation

ADC Analog-to-Digital Converter

ADIF Spanish Railway Infrastructure Administrator

AMPS Analogue Mobile Phone System

AP Auxiliary Pilot

AP Access Point

AWGN Additive White Gaussian Noise

BCa Bias-Corrected and accelerated

BEM Basis Expansion Model

BER Bit Error Ratio

BS Base Station

BSS Base Station Subsystem

BTS Base Transceiver Station

CAP Coded Auxiliary Pilot

CCDF Complementary Cumulative Distribution Function

CDMA Code-Division Multiple Access

CP Cyclic Prefix

CQI Channel Quality Indicator

DAC Digital-to-Analog Converter

DC Direct Current

DFT Discrete Fourier Transform

DMI Driver-Machine Interface

EDGE Enhanced Data Rates for Global system for mobile communications Evolution

EIRENE European Integrated Railway Radio Enhanced Network

eNodeB Evolved NodeB

EPC Evolved Packet Core

EPS Evolved Packet System

ERTMS European Rail Traffic Management System

ERTMS/ETCS European Rail Traffic Management System/European Train Control System

ETCS European Train Control System

ETSI European Telecommunications Standards Institute

EVC European Vital Computer

EV-DO EVolution-Data Optimized

EVM Error Vector Magnitude

FBMC Filter Bank Multicarrier

FDD Frequency Division Duplex

FEC Forward Error Correction

FFT Fast Fourier Transform

FLoS Far Line-of-Sight

FMT Filtered MultiTone

fOFDM Filtered OFDM

FRS Functional Requirement Specification

GFDM Generalized FDM

GPRS General Packet Radio Service

GPS Global Positioning System

GSM Global System for Mobile Communications

GSM-R GSM for Railways

GTIS GTEC Testbed Interface Software

HST High-Speed Train

IBx Indoor Office B

ICI Inter-Carrier Interference

IEEE Institute of Electrical and Electronics Engineers

IFFT Inverse Fast Fourier Transform

IMT International Mobile Telecommunications

IP Internet Protocol

ISI Inter-Symbol Interference

ITU International Telecommunication Union

ITU-R ITU Radiocommunication Sector

J-TACS Japanese Total Access Communication System

KP Kilometric Point

LEU Lineside Electronic Units

LoS Line-of-Sight

LS Least Squares

LTE Long Term Evolution

LTE-A LTE-Advanced

MAC Medium Access Control

MCS Modulation and Coding Scheme

MIMO Multiple-Input Multiple-Output

MMSE Minimum Mean Squared Error

MORANE Mobile Radio for Railways Networks in Europe

MRCN Mobile Radio Center

MS Mobile Station

NGMN Next Generation Mobile Networks

NLoS Non-Line-of-Sight

NMT Nordic Mobile Telephone

NSS Network Switching Subsystem

OFDM Orthogonal Frequency-Division Multiplexing

OFDMA Orthogonal Frequency-Division Multiple Access

PA Public Address

PAPR Peak-to-Average Power Ratio

PC Personal Computer

PDP Power Delay Profile

PRCN Portable Radio Center

QoS Quality of Service

RAx Rural Area channel model

RBCN Radio Block Center

RCC Radio Control Center

RENFE Red Nacional de los Ferrocarriles Españoles

RMS Root Mean Square

RF Radio Frequency

SAE System Architecture Evolution

SAGE Subspace-Alternating Generalized Expectation-Maximization

SC-FDMA Single Carrier Frequency-Division Multiple Access

SIM Subscriber Identity Module

SIR Signal-to-Interference Ratio

SMT Staggered Multitone

SNCF Société Nationale des Chemins de Fer Français

SNR Signal to Noise Ratio

SRS System Requirement Specification

TACS Total Access Communication System

TBM Tunnel Boring Machine

TDD Time Division Duplex

TD-LTE Time-Division LTE

TUx Typical Urban channel model

UHD USRP Hardware Driver

UIC Union Internationale des Chemins de Fer

UMTS Universal Mobile Telecommunications System

USRP Universal Software Radio Peripheral

UTRAN Universal mobile telecommunications system Terrestrial Radio Access Network

VehA Vehicular A

WCDMA Wideband Code-Division Multiple Access

WiMAX Worldwide Interoperability for Microwave Access

WSSUS Wide-Sense Stationary Uncorrelated Scattering

ZF Zero-Forcing

References

[10] **ETCS/GSM-R Quality of Service – Operational Analysis**. ERTMS Std. 04E117. 2010.

[3GP04] 3GPP. **3GPP TR 25.943: 3GPP; Technical Specification Group Radio Access Network; Univerlsal Mobile Telecommunications System (UMTS); Deployment aspects**. Tech. rep. ETSI, Dec. 2004.

[3GP12] 3GPP. **Technical Specification Group Radio Access Network; Mobile Relay for E-UTRA**. Tech. rep. 3GPP TR 36.836. 3GPP, 2012.

[AG84] Jean Alias and P Gentil. **La voie ferrée: techniques de construction et d'entretien**. Eyrolles, 1984.

[AGV98] Pauli Aikio, Ralf Gruber, and Pertti Vainikainen. **Wideband radio channel measurements for train tunnels**. In: *Vehicular Technology Conference, 1998. VTC 98. 48th IEEE*. Vol. 1. IEEE. 1998, pp. 460–464.

[AH11] José María Muñiz Aza and Víctor Reviriego Hernández. **Las Telecomunicaciones y el Ferrocarril**. In: *Vía Libre* (June 2011). Colección Cuadernos Técnicos, Fundación de los Ferrocarriles Españoles.

[Ai11] Bo Ai. **Interview**. In: *Electronic Letters* 47.21 (Oct. 2011), p. 1158.

[Ai+14] Bo Ai, Xiang Cheng, T. Kurner, Zhang-Dui Zhong, Ke Guan, Rui-Si He, Lei Xiong, D.W. Matolak, D.G. Michelson, and C. Briso-Rodriguez. **Challenges Toward Wireless Communications for High-Speed Railway**. In: *IEEE Transactions on Intelligent Transportation Systems* 15.5 (Oct. 2014), pp. 2143–2158. ISSN: 1524-9050. DOI: 10.1109/TITS.2014.2310771.

[al14] N. Michailow et al. **Generalized Frequency Division Multiplexing for 5th Generation Cellular Networks**. In: *IEEE Transactions on Communications* 62.9 (Sept. 2014), pp. 3045–3061.

[Ala01] Michel Alard. **Construction of a multicarrier signal**. US Patent 6,278,686. Aug. 2001.

[AM84] Liviu Leonard Alston and Banco Mundial. **Railways and energy**. Tech. rep. 1984.

[Ami+10] Pooyan Amini, Chung Him Yuen, Rong-Rong Chen, and Behrouz Farhang-Boroujeny. **Isotropic filter design for MIMO filter bank multicarrier communications**. In: *Sensor Array and Multichannel Signal Processing Workshop (SAM), 2010 IEEE*. IEEE. 2010, pp. 89–92.

[And+12] Jørgen Bach Andersen, Kin Lien Chee, Martin Jacob, Gert Frølund Pedersen, and Thomas Kürner. **Reverberation and absorption in an aircraft cabin with the impact of passengers**. In: *IEEE Transactions on Antennas and Propagation* 60.5 (2012), pp. 2472–2480.

[BCA07] Cesar Briso-Rodríguez, Javier M Cruz, and Jose I Alonso. **Measurements and modeling of distributed antenna systems in railway tunnels**. In: *Vehicular Technology, IEEE Transactions on* 56.5 (2007), pp. 2870–2879.

[Bel+10] M Bellanger, D Le Ruyet, D Roviras, M Terré, J Nossek, L Baltar, Q Bai, D Waldhauser, M Renfors, T Ihalainen, et al. **FBMC physical layer: a primer**. Tech. rep. PHYDYAS FP7 Project Document, 2010.

[Bri+14a] César Briso-Rodríguez, Carlos F. López, Jean R. Fernández, Sergio Pérez, Drasko Draskovic, Jaime Calle-Sánchez, Mariano Molina, José I. Alomso, Carlos Rodríguez, Carlos Hernández, Juan Moreno, José Rodríguez-Piñeiro, José A. García-Naya, and Luis Castedo. **Broadband Access in Complex Environment: LTE on Railway**. In: *IEICE Transactions on Communications* 97.8 (2014). Special Section on EU's FP7 R&D Project Activities on Future Broadband Access Technologies. Online access: http://dx.doi.org/10.1587/transcom.E97.B.1514, pp. 1514–1527.

[Bri+14b] César Briso-Rodríguez, Carlos F. López, Jean R. Fernández, Sergio Pérez, Drasko Draskovic, Jaime Calle-Sánchez, Mariano Molina, José I. Alomso, Carlos Rodríguez, Carlos Hernández, Juan Moreno, José Rodríguez-Piñeiro, José A. García-Naya, and Luis Castedo. **Broadband Access in Complex Environment: LTE on Railway**. In: *IEICE Transactions on Communications* 97.8 (2014). Special Section on EU's FP7 R&D Project Activities on Future Broadband Access Technologies. Online access: http://dx.doi.org/10.1587/transcom.E97.B.1514, pp. 1514–1527.

[Cab+11] S. Caban, A. Disslbacher-Fink, J. A. Garcia-Naya, and M. Rupp. **Synchronization of Wireless Radio Testbed Measurements**. In: *Proc. International Instrumentation and Measurement Technology Conference*

(I2MTC 2011). Binjiang, Hangzhou, China, May 2011. DOI: 10.1109/IMTC.2011.5944089.

[Cab+15] David Caballero, Federico Gavilán, Raúl Gregor, Jorge Rodas, Sergio Toledo, and José Rodríguez-Piñeiro. **MBPC Power Control in Three-phase Inverters for Grid-connected Applications**. In: *2015 IEEE PES Innovative Smart Grid Technologies Latin America (ISGT LATAM)*. Uruguay, Sept. 2015, pp. 817–821.

[Cas15] Pedro Suárez Casal. "Design and evaluation of OFDM radio interfaces for high mobility communications". PhD thesis. Faculty of Computer Engineering, University of A Coruña, 2015.

[CGR11] Sebastian Caban, Jose A. Garcia-Naya, and Markus Rupp. **Measuring the physical layer performance of wireless communication systems: Part 33 in a series of tutorials on instrumentation and measurement**. In: *IEEE Instrumentation and Measurement Magazine* 14.5 (Oct. 2011), pp. 8–17. ISSN: 1094-6969. DOI: 10.1109/MIM.2011.6041377.

[Che+13] L. Chen, Y. Huang, F. Xie, Y. Gao, L. Chu, H. He, Y. Li, F. Liang, and Y. Yuan. **Mobile relay in LTE-advanced systems**. In: *IEEE Communications Magazine* 51.11 (Nov. 2013), pp. 144–151. ISSN: 0163-6804. DOI: 10.1109/MCOM.2013.6658666.

[Che84] Union Internationale des Chemins de Fer. **Prescriptions Techniques pour les Systèmes Analogues Radio Sol-Train en Service International (UIC 751-3)**. 3rd edition. June 1984.

[Co] Huawei Technologies Co. **Developing the World's First Metro LTE Network for Train**.

[CRG11a] S. Caban, J. Rodas, and J. A. Garcia-Naya. **A Methodology for Repeatable, Off-line, Closed-loop Wireless Communication System Measurements at Very High Velocities of up to 560 km/h**. In: *Proc. International Instrumentation and Measurement Technology Conference (I2MTC 2011)*. Binjiang, Hangzhou, China, May 2011. DOI: 10.1109/IMTC.2011.5944019.

[CRG11b] S. Caban, J. Rodas, and J.A. Garcia-Naya. **A methodology for repeatable, off-line, closed-loop wireless communication system measurements at very high velocities of up to 560 km/h**. In: *2011 IEEE Instrumentation and Measurement Technology Conference*. May 2011, pp. 1–5. DOI: 10.1109/IMTC.2011.5944019.

[Cui+15] W. Cui, D. Qu, T. Jiang, and B. Farhang-Boroujeny. **Coded Auxiliary Pilots for Channel Estimation in FBMC-OQAM Systems**. In: *IEEE Transactions on Vehicular Technology* PP.99 (2015), pp. 1–1. ISSN: 0018-9545. DOI: 10.1109/TVT.2015.2448659.

[CZW96] Dieter J Cichon, Thomas Zwick, and Werner Wiesbeck. **Ray optical modeling of wireless communications in high-speed railway tunnels**. In: *IEEE VEHICULAR TECHNOLOGY CONFERENCE*. Vol. 46. INSTITUTE OF ELECTRICAL ENGINEERS INC (IEEE). 1996, pp. 546–550.

[DA] Beman Dawes and David Abrahams. **Boost C++ Libraries**.

[Dev] Analog Devices. **Analog Devices AD9361 RFIC**.

[Dev89] Pierre Devaux. **Les chemins de fer**. Presses universitaires de France, 1989.

[Día06] Xosé Carlos Fernández Díaz. **El ferrocarril en Galicia: Pasado, Presente, Futuro**. ISBN: 9788476805862. Ir indo, 2006.

[Dom+16a] Tomás Domínguez-Bolaño, José Rodríguez-Piñeiro, José A. García-Naya, and Luis Castedo. **Experimental Evaluation of 5G Modulation Schemes in Quasi-Static Scenarios**. In: *ITG Workshop on Smart Antennas (WSA 2016)*. Munich, Germany, Mar. 2016.

[Dom+16b] Tomás Domínguez-Bolaño, José Rodríguez-Piñeiro, José A. García-Naya, and Luis Castedo. **The GTEC 5G Link-Level Simulator**. In: *International Workshop on Link- and System Level Simulations (IWSLS2 2016)*. Vienna, Austria, July 2016.

[Don+10] Weihui Dong, Guangyi Liu, Li Yu, Haiyu Ding, and Lianhua Zhang. **Channel properties of indoor part for high-speed train based on wideband channel measurement**. In: *Proc. of 5th International ICST Conference on Communications and Networking in China (CHINACOM 2010)*. IEEE. Aug. 2010, pp. 1–4.

[EH94] Bradley Efron and D. V. Hinkley. **An Introduction to the Bootstrap (CRC Monographs on Statistics & Applied Probability)**. First. United States: Chapman & Hall, 1994. ISBN: 0412042312.

[ETSa] ETSI. **3GPP TS 36.101. User Equipment (UE) Radio Transmission and Reception. 3rd Generation Partnership Project; Technical Specification Group Radio Access Network; Evolved Universal Terrestrial Radio Access (E-UTRA).**

[ETSb] ETSI. **ETSI TS 136 211: LTE; E-UTRA; Physical channel and modulation**.

[FAB95] Bernard Le Floch, Michel Alard, and Claude Berrou. **Coded orthogonal frequency division multiplex [TV broadcasting]**. In: *Proceedings of the IEEE* 83.6 (1995), pp. 982–996.

[Far11] Behrouz Farhang-Boroujeny. **OFDM versus filter bank multicarrier**. In: *Signal Processing Magazine, IEEE* 28.3 (2011), pp. 92–112.

[Fei+16] Dan Fei, José Rodríguez-Piñeiro, José A. García-Naya, Luis Castedo, and Lei Xiong. **TD-LTE Downlink Performance Assessment in High Speed Scenarios**. In: *2016 IEEE 83rd Vehicular Technology Conference (VTC2016-Spring)*. Track "2nd International Workshop on Wireless Communications for High Speed Railways (HSRCom2016)". Nanjing, China, May 2016.

[FKB09] G. Fettweis, M. Krondorf, and S. Bittner. **GFDM – Generalized Frequency Division Multiplexing**. In: *2009 IEEE 69th Vehicular Technology Conference (VTC2009-Spring)*. Barcelona, Spain, 2009.

[Fra+15] Paula Fraga-Lamas, José Rodríguez-Piñeiro, José A. García-Naya, and Luis Castedo. **Unleashing the Potential of LTE for Next Generation Railway Communications**. In: *8th International Workshop on Communication Technologies for Vehicles (Nets4Cars / Nets4Trains / Nets4Aircraft 2015)*. Online access: http://dx.doi.org/10.1007/978-3-319-17765-6_14. Sousse, Tunisia, May 2015, pp. 153–164.

[Gar+13] José A. García-Naya, José Rodríguez-Piñeiro, Ángel Carro-Lagoa, and Luis Castedo. **Demostrador para la Evaluación Experimental de LTE en Entornos Ferroviarios de Alta Velocidad**. In: *XXVIII Simposium Nacional de la Unión Científica Internacional de Radio (URSI 2013)*. Sept. 2013.

[GFR98] Francisco Cayón García, Rafael González Fernández, and Miguel Muñoz Rubio. **El Camino del Tren. 150 Años de Infraestructura Ferroviaria**. ISBN: 84-88675-57-7. Fundación de los Ferrocarriles Españoles, 1998.

[Gre+14] Raúl Gregor, Guido Valenzano, José Rodríguez-Piñeiro, and Jorge E. Rodas Benítez. **FPGA-based Real-Time Simulation of a Dual Three-Phase Induction Motor**. In: *16th European Conference on Power Electronics and Applications (EPE'14-ECCE)*. Online access: http://dx.doi.org/10.1109/EPE.2014.6911031. Lappeenranta, Finland, Aug. 2014, pp. 1–8.

[Gre+16] Raúl Gregor, Guido Valenzano, Jorge Rodas, José Rodríguez-Piñeiro, and Derlis Gregor. **Design and Implementation of an FPGA-based Real-time Simulator for a Dual Three-Phase Induction Motor Drive**. In: 16.2 (Mar. 2016). Online access: http://dx.doi.org/10.6113/JPE.2016.16.2.553, pp. 553–563.

[Gua+12] Ke Guan, Zhangdui Zhong, José I Alonso, and Cesar Briso-Rodríguez. **Measurement of distributed antenna systems at 2.4 GHz in a realistic subway tunnel environment**. In: *Vehicular Technology, IEEE Transactions on* 61.2 (2012), pp. 834–837.

[Gua+13a] Ke Guan, Zhangdui Zhong, Bo Ai, Ruisi He, and Cesar Briso-Rodriguez. **Five-zone propagation model for large-size vehicles inside tunnels**. In: *Progress In Electromagnetics Research* 138 (2013), pp. 389–405.

[Gua+13b] Ke Guan, Zhangdui Zhong, Bo Ai, Ruisi He, Binghao Chen, Yuanxuan Li, and Cesar Briso-Rodriguez. **Complete propagation model structure inside tunnels**. In: *Progress In Electromagnetics Research* 141 (2013), pp. 711–726.

[Gua+14] Ke Guan, Zhangdui Zhong, Bo Ai, and Thomas Kurner. **Propagation measurements and modeling of crossing bridges on high-speed railway at 930 MHz**. In: *Vehicular Technology, IEEE Transactions on* 63.2 (2014), pp. 502–517.

[GZA11] Ke Guan, Zhangdui Zhong, and Bo Ai. **Assessment of LTE-R Using High Speed Railway Channel Model**. In: *2011 Third International Conference on Communications and Mobile Computing (CMC)*. Apr. 2011, pp. 461 –464. DOI: 10.1109/CMC.2011.34.

[Har+13] Fredrik Harrysson, Jonas Medbo, Torbjorn Hult, and Fredrik Tufvesson. **Experimental investigation of the directional outdoor-to-in-car propagation channel**. In: *IEEE Transactions on Vehicular Technology* 62.6 (2013), pp. 2532–2543.

[Hat80] Masaharu Hata. **Empirical formula for propagation loss in land mobile radio services**. In: *Vehicular Technology, IEEE Transactions on* 29.3 (1980), pp. 317–325.

[HB97] Ralf Haas and Jean-Claude Belfiore. **A time-frequency well-localized pulse for multiple carrier transmission**. In: *Wireless Personal Communications* 5.1 (1997), pp. 1–18.

[He+11a] Ruisi He, Z Zhong, Bo Ai, and J Ding. **Propagation measurements and analysis for high-speed railway cutting scenario**. In: *Electronics Letters* 47.21 (2011), pp. 1167–1168.

[He+11b] Ruisi He, Zhangdui Zhong, Bo Ai, and Jianwen Ding. **An empirical path loss model and fading analysis for high-speed railway viaduct scenarios**. In: *Antennas and Wireless Propagation Letters, IEEE* 10 (2011), pp. 808–812.

[He+12a] Ruisi He, Zhangdui Zhong, Bo Ai, and Jianwen Ding. **Measurements and analysis of the directional antenna bottom area in high speed rail**. In: *Antennas and Propagation Society International Symposium (APSURSI), 2012 IEEE*. IEEE. 2012, pp. 1–2.

[He+12b] Ruisi He, Zhangdui Zhong, Bo Ai, Jianwen Ding, and Yaoqing Yang. **Propagation measurements and analysis of fading behavior for high speed rail cutting scenarios**. In: *Global Communications Conference (GLOBECOM), 2012 IEEE*. IEEE. 2012, pp. 5015–5020.

[He+13a] Ruisi He, Andreas F Molisch, Zhangdui Zhong, Bo Ai, Jianwen Ding, Ruifeng Chen, and Zheda Li. **Measurement based channel modeling with directional antennas for high-speed railways**. In: *Wireless Communications and Networking Conference (WCNC), 2013 IEEE*. IEEE. 2013, pp. 2932–2936.

[He+13b] Ruisi He, Z Zhong, Bo Ai, Ke Guan, and R Chen. **Simplified analytical propagation model for railway environments based on uniform theory of diffraction**. In: *Electronics Letters* 49.6 (2013), p. 1.

[He+13c] Ruisi He, Zhangdui Zhong, Bo Ai, Jianwen Ding, Yaoqing Yang, and Andreas F Molisch. **Short-term fading behavior in high-speed railway cutting scenario: Measurements, analysis, and statistical models**. In: *Antennas and Propagation, IEEE Transactions on* 61.4 (2013), pp. 2209–2222.

[He+13d] Ruisi He, Zhangdui Zhong, Bo Ai, Ke Guan, Binghao Chen, Jose I AIonso, and Cesar Briso. **Propagation channel measurements and analysis at 2.4 GHz in subway tunnels**. In: *Microwaves, Antennas & Propagation, IET* 7.11 (2013), pp. 934–941.

[He+13e] Ruisi He, Zhangdui Zhong, Bo Ai, Gongpu Wang, Jianwen Ding, and Andreas F Molisch. **Measurements and analysis of propagation channels in high-speed railway viaducts**. In: *Wireless Communications, IEEE Transactions on* 12.2 (2013), pp. 794–805.

[HH03] B. Hassibi and B.M. Hochwald. **How much training is needed in multiple-antenna wireless links?** In: *IEEE Transactions on Information Theory* 49.4 (Apr. 2003), pp. 951–963. ISSN: 0018-9448. DOI: 10.1109/TIT.2003.809594.

[HR09] H. Hijazi and L. Ros. **Polynomial Estimation of Time-Varying Multipath Gains With Intercarrier Interference Mitigation in OFDM Systems**. In: *IEEE Trans. Veh. Technol.* 58.1 (Jan. 2009), pp. 140 –151. ISSN: 0018-9545. DOI: 10.1109/TVT.2008.923653.

[HZA10] Ruisi He, Zhangdui Zhong, and Bo Ai. **Path loss measurements and analysis for high-speed railway viaduct scene**. In: *Proceedings of the 6th International Wireless Communications and Mobile Computing Conference*. ACM. 2010, pp. 266–270.

[HZB11] Ruisi He, Zhangdui Zhong, and Cesar Briso. **Broadband channel long delay cluster measurements and analysis at 2.4 GHz in subway tunnels**. In: *Vehicular Technology Conference (VTC Spring), 2011 IEEE 73rd*. IEEE. 2011, pp. 1–5.

[Ito+11] Toshio Ito, Naoki Kita, Wataru Yamada, Ming-Chien Tseng, Yuichi Sagawa, Mamoru Ogasawara, Masashi Nakatsugawa, and Takatoshi Sugiyama. **Study of propagation model and fading characteristics for wireless relay system between long-haul train cars**. In: *Proc. of the 5th European Conference on Antennas and Propagation (EUCAP 2011)*. IEEE. Apr. 2011, pp. 2047–2051.

[ITU09a] ITU-R. **Guidelines for evaluation of radio interface technologies for IMT-Advanced, Report ITU-R M.2135-1**. Dec. 2009.

[ITU09b] ITU-R. **Requirements related to technicalk performance for IMT-Advanced radio interface(s), Report ITU-R M.2134**. Dec. 2009.

[ITU97] ITU-R. **Guidelines for evaluation of radio transmission technologies for IMT-2000. ITU-R Recommendation M.1225**. 1997.

[JLR03] Jean-Philippe Javaudin, Dominique Lacroix, and Alexandre Rouxel. **Pilot-aided channel estimation for OFDM/OQAM**. In: *Vehicular Technology Conference, 2003. VTC 2003-Spring. The 57th IEEE Semiannual*. Vol. 3. IEEE. 2003, pp. 1581–1585.

[JW08] Tao Jiang and Yiyan Wu. **An Overview: Peak-to-Average Power Ratio Reduction Techniques for OFDM Signals**. In: *Broadcasting, IEEE Transactions on* 54.2 (June 2008), pp. 257–268. ISSN: 0018-9316. DOI: 10.1109/TBC.2008.915770.

[KM98] W. Kozek and A. Molisch. **Nonorthogonal pulseshapes for multicarrier communications in doubly dispersive channels**. In: *IEEE Journal on Selected Areas of Communications* 16.8 (Oct. 1998), pp. 1579–1589.

[Kyo+07] Pekka Kyosti, Juha Meinila, Lassi Hentila, Xiongwen Zhao, Tommi Jamsa, Christian Schneider, Milan Narandzic, Marko Milojevic, Aihua Hongand Juha Ylitalo, Veli-Matti, Holappa, Mikko Alatossava, Robert Bultitude, Yvo de Jong, and Terhi Rautiainen. **IST-4-027756 WINNER II D1.1.2 V1.1: WINNER II Channel Models**. July 2007.

[Lam+12] Paula Fraga Lamas, José Rodríguez-Piñeiro, José A. García-Naya, and Luis Castedo. **A survey on LTE networks for railway services**. In: *IEEE Congreso de Ingeniería en Electro-Electrónica, Comunicaciones y Computación ARANDUCON 2012*. Nov. 2012.

[LC01] Ye Li and L.J. Cimini. **Bounds on the interchannel interference of OFDM in time-varying impairments**. In: *IEEE Transactions on Communications* 49.3 (2001), pp. 401–404. ISSN: 0090-6778. DOI: 10.1109/26.911445.

[Ler+14] Martin Lerch, Sebastian Caban, Martin Mayer, and Markus Rupp. **The Vienna MIMO Testbed: Evaluation of Future Mobile Communication Techniques**. In: *Intel Technology Journal* 18.3 (2014), pp. 58–69.

[Ler+16] Martin Lerch, José Rodríguez-Piñeiro, José A. García-Naya, and Luis Castedo. **Methods to Perform High Velocity LTE Experiments at Low Velocities**. In: *2016 IEEE 83rd Vehicular Technology Conference (VTC2016-Spring)*. Nanjing, China, May 2016.

[Liu+12a] Liu Liu, Cheng Tao, Jiahui Qiu, Houjin Chen, Li Yu, Weihui Dong, and Yao Yuan. **Position-based modeling for wireless channel on high-speed railway under a viaduct at 2.35 GHz**. In: *Selected Areas in Communications, IEEE Journal on* 30.4 (2012), pp. 834–845.

[Liu+12b] Liu Liu, Cheng Tao, Tao Zhou, Youping Zhao, Xuefeng Yin, and Houjin Chen. **A highly efficient channel sounding method based on cellular communications for high-speed railway scenarios**. In: *EURASIP Journal on Wireless Communications and Networking* 2012.1 (2012), pp. 1–16.

[Lua+13] Fengyu Luan, Yan Zhang, Limin Xiao, Chunhui Zhou, and Shidong Zhou. **Fading characteristics of wireless channel on high-speed railway in hilly terrain scenario**. In: *International Journal of Antennas and Propagation* 2013 (2013).

[LZA10] Jinghui Lu, Gang Zhu, and Bo Ai. **Radio propagation measurements and modeling in railway viaduct area**. In: *Wireless Communications Networking and Mobile Computing (WiCOM), 2010 6th International Conference on*. IEEE. 2010, pp. 1–5.

[LZB11] Jinghui Lu, Gang Zhu, and Cesar Briso-Rodríguez. **Fading characteristics in the railway terrain cuttings**. In: *Vehicular Technology Conference (VTC Spring), 2011 IEEE 73rd*. IEEE. 2011, pp. 1–5.

[Mar+13] Andrea Mariscotti, Attilio Marrese, Nicola Pasquino, and Rosario Schiano Lo Moriello. **Characterization of the radio propagation channel aboard trains for optimal coverage at 2.45 GHz**. In: *Proc. of IEEE International Workshop on Measurements and Networking Proceedings (M&N 2013)*. IEEE. Oct. 2013, pp. 195–199.

[Meh+11] C. Mehlführer, J. Colom Ikuno, M. Simko, S. Schwarz, M. Wrulich, and M. Rupp. **The Vienna LTE Simulators - Enabling Reproducibility in Wireless Communications Research**. In: *EURASIP Journal on Advances in Signal Processing* 2011 (2011), pp. 1–13.

[MKP07] Michele Morelli, CC Jay Kuo, and Man-On Pun. **Synchronization techniques for orthogonal frequency division multiple access (OFDMA): A tutorial review**. In: *Proceedings of the IEEE* 95.7 (2007), pp. 1394–1427.

[Mol05] Andreas F. Molisch. **Wireless Communications**. John Wiley & Sons Ltd., 2005.

[Mor+09] Techniques Nektarios Moraitis, Philip Constantinou, Fernando Perez Fontan, and Pavel Valtr. **Propagation measurements inside different civil aircrafts and comparison with EM techniques**. In: *Proc. of 3rd European Conference on Antennas and Propagation (EuCAP 2009)*. IEEE. Mar. 2009, pp. 887–891.

[NGM06] NGMN. **Next Generation Mobile Networks Beyond HSPA & EVDO – A white paper**. http://www.ngmn.org/. Dec. 2006.

[Par+08] Roope Parviainen, Pekka Kyösti, Y Hsieh, P Ting, J Chiou, and Muhrong Yang. **Results of high speed train channel measurements**. In: *European Cooperation in the Field of Scientific and Technical Research* (2008).

[Pro85] Vassilios Profillidis. **High-Speed Trains**. In: *Technika Chronika (Scientific Journal of Greek Engineers)* 5.3 (1985).

[Pro95] Vassilios Profillidis. **Railway Engineering**. ISBN: 0 291 39828 6. Cambridge University Press, 1995.

[PS09] G. Palou and M. Stojanovic. **Underwater acoustic MIMO OFDM: An experimental analysis**. In: *OCEANS 2009*. Oct. 2009, pp. 1–8.

[Resa] Ettus Research. **Ettus USRP B210**.

[Resb] Ettus Research. **Ettus USRP Hardware Driver (UHD)**.

[RK99a] Patrick Robertson and Stefan Kaiser. **The effects of Doppler spreads in OFDM (A) mobile radio systems**. In: *IEEE Vehicular Technology Conference, Fall*. Vol. 1. IEEE. 1999, pp. 329–333.

[RK99b] P. Robertson and S. Kaiser. **Analysis of the loss of orthogonality through Doppler spread in OFDM systems**. In: *Global Telecommunications Conference, 1999. GLOBECOM '99*. Vol. 1B. 1999, 701–706 vol. 1b. DOI: 10.1109/GLOCOM.1999.830152.

[RL11] M. Rahman and S. et al Latif. **The Study of OFDM ICI Cancellation Schemes in 2.4 GHz Frequency Band Using Software Defined Radio**. In: *WiCOM 2011*. Sept. 2011, pp. 1–6. DOI: 10.1109/wicom.2011.6040059.

[Rod+12] José Rodríguez-Piñeiro, Paula Fraga Lamas, José A. García-Naya, and Luis Castedo. **LTE security analysis for railway communications**. In: *IEEE Congreso de Ingeniería en Electro-Electrónica, Comunicaciones y Computación ARANDUCON 2012*. Nov. 2012.

[Rod+13a] José Rodríguez-Piñeiro, José A. García-Naya, Ángel Carro-Lagoa, and Luis Castedo. **A Testbed for Evaluating LTE in High-Speed Trains**. In: *16th Euromicro Conference on Digital System Design (DSD 2013)*. Online access: http://dx.doi.org/10.1109/DSD.2013.27. Sept. 2013, pp. 175–182.

[Rod+13b] José Rodríguez-Piñeiro, José A. García-Naya, Pedro Suárez-Casal, and Luis Castedo. **LTE under the High-Speed-Train Channel Model**. In: *XXVIII Simposium Nacional de la Unión Científica Internacional de Radio (URSI 2013)*. Sept. 2013.

[Rod+14] José Rodríguez-Piñeiro, Pedro Suárez-Casal, José A. García-Naya, Luis Castedo, César Briso-Rodríguez, and J. Ignacio Alonso-Montes. **Experimental Validation of ICI-Aware OFDM Receivers under Time-Varying Conditions**. In: *Eighth IEEE Sensor Array and Multichannel Signal Processing Workshop*. Online access: http://dx.doi.org/10.1109/SAM.2014.6882411. A Coruña, Spain, June 2014, pp. 341–344.

[Rod+15a] José Rodríguez-Piñeiro, Martin Lerch, José A. García-Naya, Sebastian Caban, Markus Rupp, and Luis Castedo. **Emulating Extreme Velocities of Mobile LTE Receivers in the Downlink**. In: *EURASIP Journal on Wireless Communications and Networking* 2015.106 (Apr. 2015). Special Issue on Experimental Evaluation in Wireless Communications. Online access: http://dx.doi.org/10.1186/s13638-015-0343-0.

[Rod+15b] José Rodríguez-Piñeiro, Martin Lerch, Pedro Suárez-Casal, José A. García-Naya, Sebastian Caban, Markus Rupp, and Luis Castedo. **LTE Downlink Performance in High Speed Trains**. In: *2015 IEEE 81st Vehicular Technology Conference (VTC2015-Spring)*. Glasgow, United Kingdom, May 2015.

[Rod+16a] José Rodríguez-Piñeiro, Tomás Domínguez-Bolaño, José A. García-Naya, and Luis Castedo. **Performance Assessment of 5G-Candidate Waveforms in High Speed Scenarios**. In: *27th Annual IEEE International Symposium on Personal, Indoor and Mobile Radio Communications (PIMRC 2016)*. Accepted for publication. Valencia, Spain, Sept. 2016.

[Rod+16b] José Rodríguez-Piñeiro, Tomás Domínguez-Bolaño, Pedro Suárez-Casal, José A. García-Naya, and Luis Castedo. **Affordable Evaluation of 5G Modulation**

Schemes in High Speed Train Scenarios. In: *ITG Workshop on Smart Antennas (WSA 2016)*. Munich, Germany, Mar. 2016.

[Rod+16c] José Rodríguez-Piñeiro, José A. García-Naya, Pedro Suárez-Casal, César Briso-Rodríguez, J. I. Alonso-Montes, and Luis Castedo. **Assessment of Channel Propagation Conditions for FDD LTE Transmissions in the Spanish High-Speed Railways**. In: *10th European Conference on Antennas and Propagation (EuCAP 2016)*. Davos, Switzerland, Apr. 2016.

[Rod+16d] José Rodríguez-Piñeiro, Martin Lerch, Tomás Domínguez-Bolaño, José A. García-Naya, Sebastian Caban, and Luis Castedo. **Experimental Assessment of 5G-Candidate Modulation Schemes at Extreme Speeds**. In: *Ninth IEEE Sensor Array and Multichannel Signal Processing Workshop (SAM 2016)*. Río de Janeiro, Brazil, July 2016.

[Rod+16e] José Rodríguez-Piñeiro, Pedro Suárez-Casal, Tomás Domínguez-Bolaño, José A. García-Naya, and Luis Castedo. **Emulation of High Mobility Scenarios in Wireless Broadband OFDM Communications**. In: *Submitted to the IEEE Transactions on Vehicular Technology.* (2016).

[Rou85] P Roumeguere. **Les installations fixées du TGV deux ans après la mise en service**. In: *Rail international* 16.8 (1985), pp. 5–15.

[Rou94] Philippe Roumeguere. **Le schéma directeur français des liaisons à grande vitesse**. In: *Revue générale des chemins de fer* 6-7 (1994), pp. 17–25.

[RST16] Markus Rupp, Stefan Schwarz, and Martin Taranetz. **The Vienna LTE-Advanced Simulators: Up and Downlink, Link and System Level Simulation**. 1st ed. Signals and Communication Technology. Springer Singapore, 2016. ISBN: 978-981-10-0616-6. DOI: 10.1007/978-981-10-0617-3.

[SB03] Thomas Strohmer and Scott Beaver. **Optimal OFDM design for time-frequency dispersive channels**. In: *Communications, IEEE Transactions on* 51.7 (2003), pp. 1111–1122.

[S C+14] S. Caban, R. Nissel, M. Lerch, and M. Rupp. **Controlled OFDM Measurements at Extreme Velocities**. In: *Proc. of 6th Extreme Conference on Communication and Computing (ExtremeCom)*. San Cristobal, Galapagos, Ecuador, Aug. 2014.

[SC97] Timothy M Schmidl and Donald C Cox. **Robust frequency and timing synchronization for OFDM**. In: *Communications, IEEE Transactions on* 45.12 (1997), pp. 1613–1621.

[SGA14] A. Sahin, I. Guvenc, and H. Arslan. **A Survey on Multicarrier Communications: Prototype Filters, Lattice Structures, and Implementation Aspects**. In: *IEEE Communications Surveys & Tutorials* 16.3 (2014), pp. 1312–1338.

[Shi+14] Masami Shirafune, Takashi Hikage, Toshio Nojima, Motoharu Sasaki, Wataru Yamada, and Takatoshi Sugiyama. **Propagation characteristic estimations of 2 GHz inter-car wireless links in high-speed train cars in a railway tunnel**. In: *Proc. of International Symposium on Antennas and Propagation (ISAP 2014)*. IEEE. Dec. 2014, pp. 215–216.

[Sie05] Siemens. **High speed environment channel models (R4-050388)**. 3GPP TSG-RAN Working Group 4 (Radio) meeting #35. May 2005.

[Sim+11] M. Simko, C. Mehlführer, T. Zemen, and M. Rupp. **Inter-Carrier Interference Estimation in MIMO OFDM Systems with Arbitrary Pilot Structure**. In: *IEEE VTC Spring 2011*. May 2011. DOI: 10.1109/VETECS.2011.5956126.

[SM13] Ruoyu Sun and D.W. Matolak. **Characterization of the 5-GHz Elevator Shaft Channel**. In: *IEEE Transactions on Wireless Communications* 12.10 (Oct. 2013), pp. 5138–5145. ISSN: 1536-1276. DOI: 10.1109/TWC.2013.090413.122016.

[SR16] Stefan Schwarz and Markus Rupp. **Society in motion: challenges for LTE and beyond mobile communications**. In: *IEEE Communications Magazine* 54.5 (2016), pp. 76–83.

[STB11] Stefania Sesia, Issam Toufik, and Matthew Baker, eds. **LTE The UMTS Long Term Evolution from theory to practice**. 2nd. John Wiley & Sons, 2011.

[Sti+10] Tobias Hidalgo Stitz, Tero Ihalainen, Ari Viholainen, and Markku Renfors. **Pilot-based synchronization and equalization in filter bank multicarrier communications**. In: *EURASIP Journal on Advances in Signal Processing* 2010 (2010), p. 9.

[Suá+13] Pedro Suárez-Casal, José A. García-Naya, Luis Castedo, and Markus Rupp. **KLT-based Estimation of Rapidly Time-Varying Channels in MIMO-OFDM Systems**. In: *IEEE SPAWC 2013*. 2013.

[Suá+14a] Pedro Suárez-Casal, José Rodríguez-Piñeiro, José A. García-Naya, and Luis Castedo. **Experimental Evaluation of the WiMAX Downlink Physical Layer in High-Mobility Scenarios**. In: *EURASIP Journal on Wireless Communications and Networking* 2015.109 (Dec. 2014). Special Issue on Experimental Evaluation in Wireless Communications. Online access: http://dx.doi.org/10.1186/s13638-015-0339-9.

[Suá+14b] Pedro Suárez-Casal, José Rodríguez-Piñeiro, José A. García-Naya, Luis Castedo, César Briso-Rodríguez, and J. Ignacio Alonso-Montes. **Experimental Assessment of WiMAX Transmissions under Highly Time-Varying Channels**. In: *Eleventh International Symposium on Wireless Communication Systems (ISWCS)*. Online access: http://dx.doi.org/10.1109/ISWCS.2014.6933447. Barcelona, Spain, Aug. 2014, pp. 717–721.

[TAG03] C. Tepedelenlioglu, A. Abdi, and G.B. Giannakis. **The Ricean K factor: estimation and performance analysis**. In: *IEEE Transactions on Wireless Communications* 2.4 (July 2003), pp. 799–810. ISSN: 1536-1276. DOI: 10.1109/TWC.2003.814338.

[Tan+07] Zijian Tang, R.C. Cannizzaro, G. Leus, and P. Banelli. **Pilot-Assisted Time-Varying Channel Estimation for OFDM Systems**. In: *IEEE Trans. Signal Process.* 55.5 (May 2007), pp. 2226 –2238. ISSN: 1053-587X. DOI: 10.1109/TSP.2007.893198.

[Tas06] Luis García Tassias. **Telecomunicaciones ferroviarias en las líneas de alta velocidad**. In: *Bit* 157 (2006), pp. 34–39.

[Tea] The GTEC Testbed Project Development Team. **GTEC Testbed Project**. https://bitbucket.org/tomas_bolano/gtec_testbed_public.git.

[tea] The Vienna LTE-A Simulators development team. **The Vienna LTE-A Simulators**. URL: http://www.nt.tuwien.ac.at/ltesimulator/.

[Tec02] Technical Specification Group Radio Access Network. **High Speed Downlink Packet Access: UE Radio Transmission and Reception**. Tech. rep. TR 25.890. 3rd Generation Partnership Project (3GPP), May 2002.

[TLB06] Zijian Tang, G. Leus, and P. Banelli. **Pilot-Assisted Time-Varying OFDM Channel Estimation Based on Multiple OFDM Symbols**. In: *IEEE SPAWC 2006*. 2006. DOI: 10.1109/SPAWC.2006.346364.

[UIC12a] UIC. **EIRENE Functional Requirements Specification**. Version 7.3.0. Mar. 2012.

[UIC12b] UIC. **EIRENE System Requirements Specification**. Version 15.3.0. Mar. 2012.

[UIC93] UIC, ed. **The Railways: An Indispensable Part of the European Transport System**. 1993.

[Wai87] Francisco Wais. **Historia de los ferrocarriles españoles**. 3rd. Fundación de los Ferrocarriles Españoles, Madrid, 1987.

[Wei+10a] Hong Wei, Zhangdui Zhong, Ke Guan, and Bo Ai. **Path loss models in viaduct and plain scenarios of the High-speed Railway**. In: *2010 5th International ICST Conference on Communications and Networking in China*. Aug. 2010, pp. 1 –5.

[Wei+10b] Hong Wei, Zhangdui Zhong, Ke Guan, and Bo Ai. **Path loss models in viaduct and plain scenarios of the high-speed railway**. In: *Communications and Networking in China (CHINACOM), 2010 5th International ICST Conference on*. IEEE. 2010, pp. 1–5.

[WG00] Zhendao Wang and G.B. Giannakis. **Wireless multicarrier communications**. In: *IEEE Signal Process. Mag.* 17.3 (May 2000), pp. 29–48. ISSN: 1053-5888. DOI: 10.1109/79.841722.

[Wik] Wikipedia contributors. **Santiago de Compostela derailment**. Published at Wikipedia, The Free Encyclopedia. https://en.wikipedia.org/w/index.php?title=Santiago_de_Compostela_derailment&oldid=695821645.

[YG06] Taesang Yoo and A. Goldsmith. **Capacity and power allocation for fading MIMO channels with channel estimation error**. In: *IEEE Transactions on Information Theory* 52.5 (May 2006), pp. 2203–2214. ISSN: 0018-9448. DOI: 10.1109/TIT.2006.872984.

[ZC14] Yonghong Zeng and Meng Wan Chia. **Joint time-frequency synchronization and channel estimation for FBMC**. In: *Personal, Indoor, and Mobile Radio Communication (PIMRC), 2014 IEEE 25th Annual International Symposium on*. IEEE. 2014, pp. 438–442.

[Zha+15] X. Zhang, M. Jia, L. Chen, J. Ma, and J. Qiu. **Filtered-OFDM – Enabler for Flexible Waveform in the 5th Generation Cellular Networks**. In: *2015 IEEE Global Communications Conference (GLOBECOM)*. San Diego, CA, 2015, pp. 1–6.

[Zha+16a] Lei Zhang, José Rodríguez-Piñeiro, Jean R. Fernández, José A. García-Naya, David W. Matolak, César Briso, and Luis Castedo. **Propagation Modeling for Outdoor-to-Indoor and Indoor-to-Indoor Wireless Links in High-Speed Train**. In: *Submitted to the Measurement journal.* (2016).

[Zha+16b] Lei Zhang, Pedro Suárez-Casal, Jean Fernández, José Rodríguez-Piñeiro, Jaime Calle-Sánchez, José A. García-Naya, Luis Castedo, C. Rodríguez-Sánchez, J. Moreno, César Briso-Rodríguez, and J. I. Alonso-Montes. **Experimental Evaluation of 4G Technologies in Metro Tunnel Scenarios**. In: *10th European Conference on Antennas and Propagation (EuCAP 2016)*. Davos, Switzerland, Apr. 2016.

[ZM05a] T. Zemen and C.F. Mecklenbräuker. **Time-Variant Channel Estimation Using Discrete Prolate Spheroidal Sequences**. In: *Signal Processing, IEEE Transactions on* 53.9 (Sept. 2005), pp. 3597–3607. ISSN: 1053-587X. DOI: 10.1109/TSP.2005.853104.

[ZM05b] T. Zemen and C.F. Mecklenbräuker. **Time-Variant Channel Estimation Using Discrete Prolate Spheroidal Sequences**. In: *IEEE Transactions on Signal Processing* 53.9 (Sept. 2005), pp. 3597 –3607. ISSN: 1053-587X. DOI: 10.1109/TSP.2005.853104.

[ZX03] Yahong Rosa Zheng and Chengshan Xiao. **Simulation models with correct statistical properties for Rayleigh fading channels**. In: *IEEE Transactions on Communications* 51.6 (June 2003), pp. 920 –928. ISSN: 0090-6778. DOI: 10.1109/TCOMM.2003.813259.